



LAWRENCE
LIVERMORE
NATIONAL
LABORATORY

Proceedings of the Workshop on Accelerator Driven High Energy Density Physics

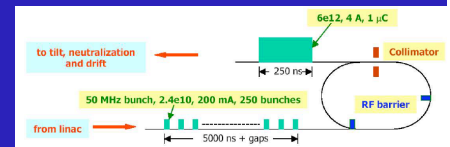
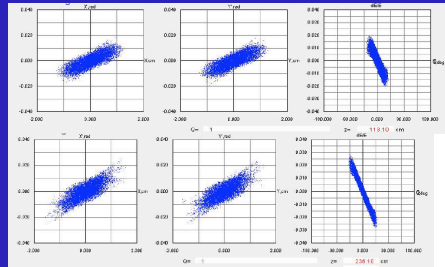
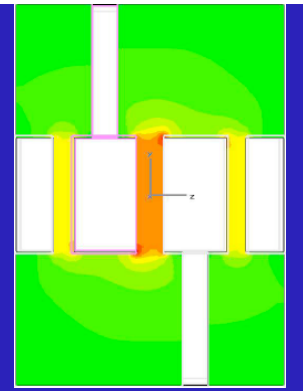
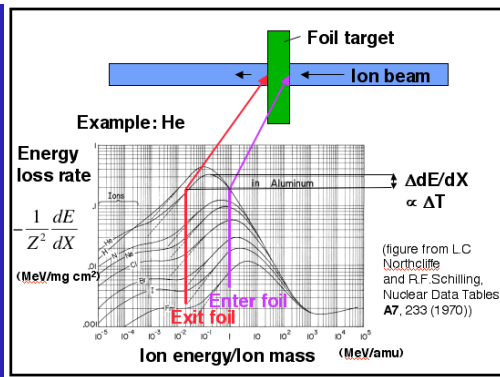
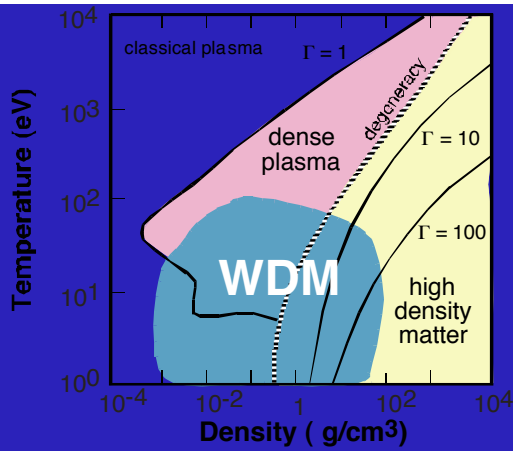
J. J. Barnard

May 5, 2005

Proceedings of the Workshop on Accelerator Driven High
Energy Density Physics
Berkeley, CA, United States
October 26, 2004 through October 29, 2004

Disclaimer

This document was prepared as an account of work sponsored by an agency of the United States Government. Neither the United States Government nor the University of California nor any of their employees, makes any warranty, express or implied, or assumes any legal liability or responsibility for the accuracy, completeness, or usefulness of any information, apparatus, product, or process disclosed, or represents that its use would not infringe privately owned rights. Reference herein to any specific commercial product, process, or service by trade name, trademark, manufacturer, or otherwise, does not necessarily constitute or imply its endorsement, recommendation, or favoring by the United States Government or the University of California. The views and opinions of authors expressed herein do not necessarily state or reflect those of the United States Government or the University of California, and shall not be used for advertising or product endorsement purposes.

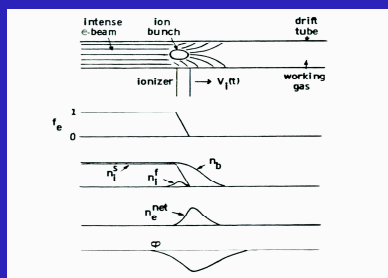
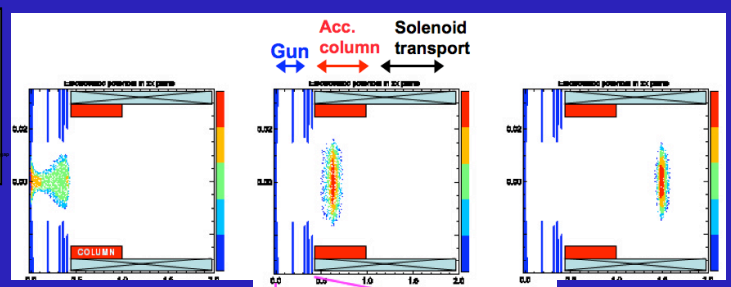
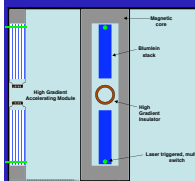
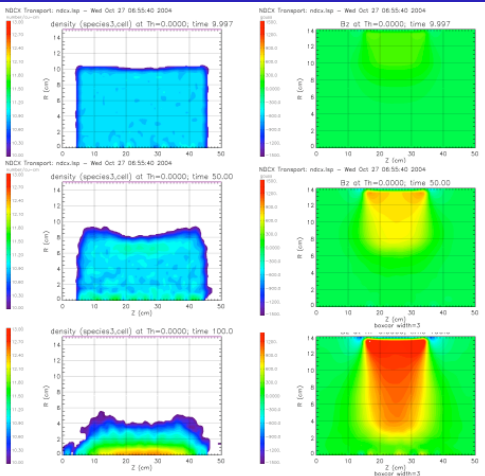


Proceedings of the Workshop on Accelerator Driven High Energy Density Physics

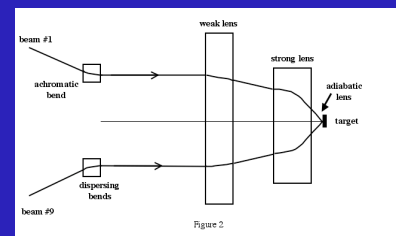
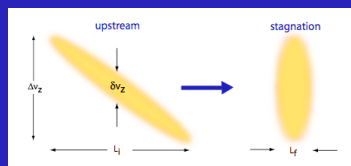
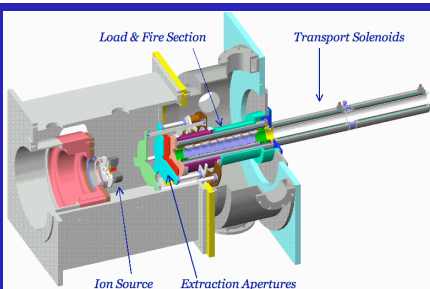
Lawrence Berkeley National Laboratory

October 26-29, 2004

LBNL-57518 UCRL-xxxxxx



$$\frac{\epsilon_f^2}{R_j^2} = \frac{2I}{\beta M c^3 / Ze}$$



Sponsored by the Heavy Ion Fusion Virtual National Laboratory



Proceedings of the Workshop on
Accelerator Driven High Energy Density Physics
Lawrence Berkeley National Laboratory
October 26-29, 2004
LBNL-xxxxxx UCRL-xxxxxx

proceedings editor: J. J. Barnard
workshop chairmen: E. P. Lee and J. J. Barnard
program/organizing committee: J. J. Barnard, R. J. Briggs,
A. Faltens, A. Friedman, E. P. Lee, R. W. Lee, B. G. Logan,
J. N. Marx, L. L. Reginato, A. M. Sessler, J. W. Staples,
W. L. Waldron, J. S. Wurtele, S. S. Yu
administrative support: S. L. Buckley, T. G. Gallant
L. C. Heimbucher, W. W. Tabler

sponsored by the Heavy Ion Fusion Virtual National Laboratory*
(Lawrence Berkeley National Laboratory,
Lawrence Livermore National Laboratory,
Princeton Plasma Physics Laboratory)

*Work performed under the auspices of the U.S. Department of Energy under University of California contract W-7405-ENG-48 at LLNL, University of California contract DE-AC03-76SF00098 at LBNL, and contract DEFG0295ER40919 at PPPL.

Table of Contents:
 Proceedings of the Workshop on
 Accelerator Driven High Energy Density Physics
 Held October 26-29, 2004
 Lawrence Berkeley National Laboratory

I. Workshop Overview

Cover and title page	1
Executive Summary	5

II. Working Group Reports

1. High Energy Density Science, Experiments and Diagnostics	
1.1 The science and context of accelerator driven HEDP -- Richard Lee	8
1.2 Overview of discussions held in working group 1 -- John Barnard and Richard Lee	26
1.3 Accelerator requirements -- John Barnard	32
2. RF- accelerator options	
2.1 RF group overview -- John Staples	42
2.2 Linac plans -- John Staples	45
2.3 Ion source -- Roderick Keller	47
2.4 Linac -- Peter N. Ostroumov	51
2.5 Ring -- Weiren Chou	60
2.7 Alternate Structures -- John Staples	64
2.8 Future development -- John Staples	66
2.9 Appendices A-H: Presentations -- John Staples, Peter Ostroumov, and Wieren Chou (included on CD's only)	
3. Pulsed power accelerator options	
3.1 Report from working group 3: Multi-gap pulsed power -- Alex Fredman and Richard Briggs	68
3.2 Report from the working group on Single-Gap Pulsed Power -- Craig Olson, Paul Ottinger, and Tim Renk.....	82
3.3 Pulsed Drift Tube Accelerator -- Andy Faltens	93
3.4 Phase space considerations -- Roger Bangerter	113

3.5	High gradient induction cell -- George Caporaso.....	118
4.	Drift compression and final focus	
4.1	Final Focus and Drift Compression Working Group Overview -- Edward Lee	121
4.2	Strong Solenoidal Final Focus Lens for HEDP -- Edward Lee	127
4.3	Issues for Neutralized Drift Compression and Focusing of Heavy Ion Beams for HEDP -- Dale R. Welch	129
4.4	Ne Charge State Distributions In Gaseous And Solid Targets -- Igor Kaganovich	140
4.5	Constraint on longitudinal velocity spread for beams undergoing neutralized drift compression -- William Sharp	142
4.6	Using Pulsed Lens to Compensate Tilt -- Yu-Jiuan Chen	144
4.7	Adiabatic Plasma Lens -- A current density booster -- Simon Yu	148

IV. Appendices

A1	A Unique U.S. Approach for Accelerator-Driven Warm Dense Matter Research--Preliminary Report -- Grant Logan, Ron Davidson, John Barnard, Richard Lee	151
A2.	Workshop Agenda	179
A3.	Workshop Attendee List	181
A4.	Workshop Objectives	183
A5.	National Task Force Report on HEDP (included on CD's only)	
A6.	Workshop Photos -- John Staples	185

V. [Talks held at the plenary sessions](#) (included on CD's only)

Executive Summary

Grant Logan, John Barnard, Edward Lee, and Christine Celata

On October 26-29, 2004, the Heavy Ion Fusion (HIF) Virtual National Laboratory (VNL) hosted a workshop at Lawrence Berkeley National Laboratory (LBNL) on "Accelerator-Driven High Energy Density Physics (HEDP)." The workshop was attended by sixty five researchers, from the VNL (the HIF/HEDP groups of LBNL, Lawrence Livermore National Laboratory (LLNL), and Princeton Plasma Physics Laboratory (PPPL)) as well as LBNL's Center for Beam Physics, and LLNL's X-and V-Divisions, Sandia National Laboratory, University of Maryland, Fermilab, Argonne National Laboratory, SLAC, Mission Research Corporation, SAIC, Tech X Corp, University of Nevada, Reno, and the University of Electrocommunication, Tokyo, who, together, gave representation to accelerator-, laser-, high energy density-, and computational- physics.

The objectives of the meeting were to 1. explore options and possibilities for a staged experimental program in Warm Dense Matter (WDM)/HEDP that utilizes ion accelerator sources as they become available, from early machines that can be developed at modest cost beginning with existing equipment, to later machines that reach well into the HEDP regime. The goals included defining physics regimes and scientific objectives to be explored, requirements for targets and diagnostics, and the scientific program that can be carried out using the ion beam drivers under consideration. The objectives were also to study various accelerator approaches, including conceptual designs of three types of accelerators: pulse-power-driven single-stage diodes; pulse-power-driven multi-stage accelerators; and rf-accelerators. In addition, options for pulse compression and final focus were to be studied.

Prior to the meeting some initial parameters were specified. Target characteristics that fall within a broad range in temperature and density, were specified as goals: Temperature between 0.1 and 30 eV, and density between 10^{-3} to 30 g/cm^3 . The temperature must be constant over a hydrodynamic expansion time, and the volume must be sufficiently large to be able to diagnose the state of the properties with minimal ($\sim 5\%$) variations over the volume being diagnosed. Additionally, the energy deposition over the volume must result in similarly small ($< 5\%$) variation in the volume being diagnosed. As a specific example, a Ne+1 beam, entering a 50 micron thick Aluminum foam target (mass density $\rho = 0.1$ solid density), with ion central energy entering the foam at 19 MeV, and exiting at 4.4 MeV. The combination $N_{\text{ions}}/(r_{\text{spot}}/1\text{mm})^2 > 1.4 \times 10^{13}$, where N_{ions} is the number of ions in the pulse and r_{spot} is the equivalent pulse radius if the intensity were uniformly distributed over a circle of radius equal to r_{spot} . If the pulse duration is less than 1 ns, these beam parameters have been estimated to result in a 15 eV plasma, with mean ionization state of ~ 2.7 , and mean energy density $1.3 \times 10^{11} \text{ J/m}^3$.

The first day of the workshop consisted primarily of talks, reporting on what had previously been learned about the possibilities for using heavy ion beams to heat matter

to "Warm Dense Matter (WDM)" conditions. WDM studies would be relevant, for example, to both the interiors of planets and the early stages of capsule implosion for inertial fusion energy. Talks were presented on the WDM science to be obtained, the experiments needed to figure out the science, and the requirements needed to carry out the experiments. Talks were also given on the status of injector and drift compression/final focus.

Prior to the workshop, four working groups were established: 1. science, experiments and diagnostics; 2. rf-accelerator concepts, 3. Pulsed-power accelerator concepts, and 4. drift compression and final focus. On the first day representatives from the working groups gave summaries and status reports of previous work and gave goals for the workshop. The working groups met separately for the next two days to explore concepts and estimate parameters for different architectures. Although, the groups nominally met separately, there was a great deal of communication between groups, as some meetings were held jointly, and some members "floated" between groups. The final half-day consisted of plenary summary sessions.

Group 1 held wide-ranging discussions, including the impact of HEDP diagnostics on the final focus and chamber design (and whether to incorporate multiple chambers in the design of the accelerator); repetition rate requirements; ion stopping and equation of state tutorials; recent warm dense matter experiments in Japan using lasers, capabilities of short pulse lasers for diagnosing accelerator-driven WDM experiments, and accelerator flexibility. Discussions also occurred on the current state of uncertainty in the equation of state (see figure 1), and the implications for this uncertainty in designing WDM experiments.

Group 2 examined several options for the rf-accelerator approach including a multiple-beam 50 MHz linac that incorporated interdigital H-mode cavities with drift tubes, and 15 T superconducting solenoids for focusing. Multiple-beam options (16 beams) with different beamline geometries and single beam options with storage rings were considered.

Group 3 looked at both single gap and multiple gap architectures using pulsed power to provide the acceleration voltage. The single gap architectures would rely on existing diodes, at Sandia, NRL, or elsewhere. A unique "ionization front accelerator" using the potential of an electron beam to accelerate ions along an ionization path created by a laser (and previous experiments of this concept) were described. Multiple gap accelerators that were considered included the novel Broad Band Traveling Wave Accelerator, and a multiple beam, electrostatic-quadrupole focused, drift tube linac.

Group 4 examined the drift compression and final focus sections, including issues of switchyards, focusing, and interface. Finding a background which strips ions to the desired state while providing sufficient electrons for neutralization is a key issue for drift compression. There were discussions on various "tools" in the toolbox including neutralized drift compression, large solenoids for final focus, dipoles to stop electrons

(among other purposes), solenoids to suppress instabilities, pulsed lenses to compensate tilt-induced chromatic problems, and adiabatic funnels close to the experiments.

The results of the workshop identified several workable accelerators that could meet the set of given HEDP target drive requirements, (although costs and critical issues such as phase space constraints and development R&D requirements and pathways were not uniformly addressed). Much more future work is required to uniformly evaluate the costs of the various approaches and development requirements, and much of that work is already in progress.

The science and context of accelerator driven HEDP

Richard W. Lee, LLNL

I. Introduction

The recent increase in interest in the regime of High Energy Density (HED) Science witnessed by three broad-based scientific reports (a) *Connecting Quarks with the Cosmos: Eleven Science Questions for The New Century* (National Academies Press, 2003); b) *Frontiers in High Energy Density Physics - The X-Games of Contemporary Science* (National Academies Press, 2003); and c) *Frontiers For Discovery In High Energy Density Physics* (prepared for National Science and Technology Council's Interagency Working Group on the Physics of the Universe, see http://www.sc.doe.gov/production/henp/np/program/docs/HEDP_Report.pdf, 2004) provides the impetus to explore the potential for the heavy ion beam community to participate in the generation of HED matter with the express purpose of improving our fundamental knowledge in this exciting regime.

The discussion below sets the stage for the proposed heavy ion beam studies that are considered. First we will provide a general background describing the regimes and physical processes of interest. This is meant to be a simple explanation of the problems of interest included for completeness and, as such, should not be considered exhaustive. Next in keeping with the goal of providing the backdrop for the proposed heavy-ion beam experiments and facilities we will outline the various aspects of HED science that are being performed currently on existing facilities. The plans for experiments on current facilities, in a general sense will also be outlined to indicate the direction of the activity in the field. Finally, we will look at the future proposed facilities to examine where a heavy ion beam proposal would be placed.

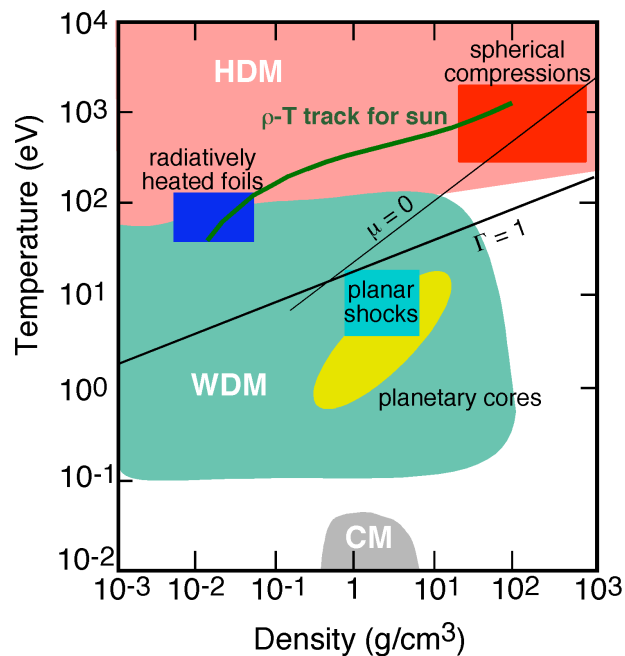


Figure 1: Hydrogen phase diagram indicating the high energy density regime separated into the hot dense region (pink) and the warm dense region (green). Various states found in nature are indicated on the graph. The above the line $\mu = 0$ is the region where degeneracy is unimportant, while above the line $\Gamma = 1$ strong coupling effects are unimportant. The condensed matter phase is indicated by the gray region. The data is taken from a compilation of data from the NRL Plasma Formulary (Huba, 2000)

The general definition of the HED regime can be illustrated by reference to the hydrogen temperature-density phase space graph in Fig. 1. Here we show the temperature–density phase space of hydrogen. The HED regime can be separated into the hot dense matter (HDM) region shown in pink and the warm dense matter (WDM) region shown in green. HDM occurs in astrophysical plasmas in supernovas, accretion disks, and stellar interiors –in Fig.1 the temperature-density track relevant to the sun is shown. Further, HED matter can be produced in laboratory-based plasma generation devices such as laser-produced plasmas and pulsed power machines, e.g., Z-pinchs. In Fig. 1 we roughly note the phase space in the HDM region occupied by the plasma produced in inertial fusion compression and foils irradiated by x-ray created at these laboratory-based facilities.

The WDM matter region, on the other hand, is a more complex object of study and will be discussed in more detail below. WDM occurs in the cores of large planets where the pressures become immense. The WDM region is accessed by all laboratory experiments that starts out as solid and end up in the plasma states; thus exploding wire arrays or laser-matter produced plasmas all transit the WDM region. Further, high-pressure shocks where the temperature becomes substantial – for shocks that is- access the WDM region. Finally, it is worth noting that in indirectly driven inertial fusion the desire to remain on a low temperature adiabat during the early phase of the compression indicates that on the run-in phase of the implosion the compressing material is in the WDM state.

It is important to understand that the usual condensed matter (CM) phase is not of interest in the HED regime. We schematically illustrate the CM matter region with the gray area at low temperature near normal density.

We will show that as a result of our analysis we believe that the heavy ion beam capability is of interest and important as it provides an alternative method to reach interesting states of matter in the HED regime. Particularly important are the contributions that such a capability will play in the Warm Dense Matter part of the HED phase space. Indeed we think that the heavy ion beams have a decided advantage in creating WDM due to several considerations: The ion beams can provide relatively large sample sizes (mm^3); more uniform conditions; achieve high entropy at high density; the extreme conditions persist for long times; and, the repetition rates can be high. In contrast, optical laser-based experiments in WDM regime tend to have: smaller volumes; larger gradients; shorter lifetimes; and, lower repetition rates.

II. Background

Since the late 1960's research into the regime of finite temperature matter has moved toward higher density regimes. The advent of laser-produced plasmas and laser-based plasma diagnostics has fueled interest in the formation of plasmas at densities nearing solid density. There are two separate areas where the proposed next generation sources can play a critical role in moving these fields substantially forward. The first is in the area of warm dense matter research, where X-ray Free Electron Lasers (XFEL) and the next generation of Heavy Ion Beam sources, will provide major improvements over the current state of the field. The second is in the area of techniques relevant to hot dense matter production and diagnostics, where the role of the 4th generation light sources, which are in this regard essentially x-ray lasers, will provide substantive improvements. For more information on these facilities see the website <http://www-ssl.slac.stanford.edu/LCLS/> for information on the LCLS facility, the website <http://www-hasylab.desy.de/facility/fel/> for information on the TESLA facility and the TESLA Test Facility (TTF) a soft x-ray FEL facility), and the website http://hifweb.lbl.gov/public/papers/US_accelerator_HEDP.12.pdf for information on the ion

beam sources. <http://www-aix.gsi.de/~plasma/> for information on the GSI ion beam sources

For the 4th generation sources, whether we are interested in creating warm dense matter, performing Thomson scattering, or probing a plasma the XFEL capability, will provide a major advance on any capability that exists with 3rd generation sources. The key to the advance is the tunable, narrow band x-ray source with very short pulse duration. Since the individual bunch photon intensity is the essential quantity for all the plasma-based research, comparing peak spectral brightness best summarizes the comparison of the XFEL to current synchrotron sources – see the Source Table in Fig. 18. Indeed, one finds an enhancement of 10 orders of magnitude will make the XFEL most promising source for plasma-based research. The utility of the high repetition rate of other sources, *e.g.*, APS or ESRF, are not useful here since we require a single photon pulse to either heat, scatter, or probe matter that is transient. Indeed, to create solid matter that is at a temperature greater than 1 eV temperature while not expanding on x-ray light sources will require the capability of the XFEL.

For the next generation of ion beam sources the high intensity upgrade of the heavy ion beam accelerator facilities will lead to energy densities greater than 10^{11} ergs/cm³ and temperatures between 1 and 10 eV at solid-state densities, enabling interesting experiments in the regime of non-ideal plasmas, *e.g.*, in the interior of the Jovian planet. (Tahir, 2001) These experiments are similar to those that may be performed on the 4th generation light sources; however, the energy will potentially provide heating of larger samples. This, then, will create WDM samples that have gradients that are small when compared to the size of the warmed volume. Further, the coupling of an intense short pulse laser source at the future heavy ion facility can provide an x-ray absorption source. It is important to point out that the approach taken here is quite distinct from that taken in the SIS-100 facility proposed for GSI, Darmstadt. In the GSI approach the ion beam heating is achieved by using substantially larger amounts of beam energy, with the beam passing through the sample before reaching the Bragg peak. This requires substantially larger facilities. In the approach proposed here we use the favorable energy deposition associated with the Bragg peak to enhanced energy transfer from the heavy ion beam to the sample. This will allow a more efficient coupling of the beam energy and permit the construction of a heavy ion beam facility in a more cost-effective manner

A. Warm Dense Matter

With a short duration pulse containing a substantial number of high-energy photons or ions one can generate solid matter at temperatures of ≤ 10 eV, *i.e.*, warm dense matter. The interest in the warm dense matter regime arises because in dense plasmas the atoms and/or ions will start to behave in a manner that is intrinsically coupled to the plasma. That is, the plasma starts to exhibit long- and short-range order due to the correlating effects of the atoms/ions. This intriguing regime where the plasma can no longer be considered a thermal bath and the atoms are no longer well described by their isolated atom behavior provides a tremendous challenge to researchers. In the limit of dense cool plasmas one obviously arrives at the threshold of condensed matter. Here the problem has changed from a perturbative approach to ground-state methods where complete renormalization of the atom/ion and its environment is essential.

From the perspective of plasma studies the defining quantity is the coupling parameter Γ , *i.e.*, the ratio of the inter-atomic potential energy to the thermal energy given in Eq. 1:

$$\Gamma = \frac{Z^2 e^2}{r_0 k T} \quad \text{with} \quad r_0 = \left(\frac{3Z}{4n_e} \right)^{1/3} \quad 1)$$

here Z is the ion charge and r_0 is the interparticle spacing given in terms of the electron density n_e . The regions of interest span the density-temperature phase space going from modestly coupled ($\Gamma \leq 1$) to strongly coupled ($\Gamma > 1$), while bridging the transition regimes between solid to liquid to plasma. This is schematically represented in Fig. 2 .

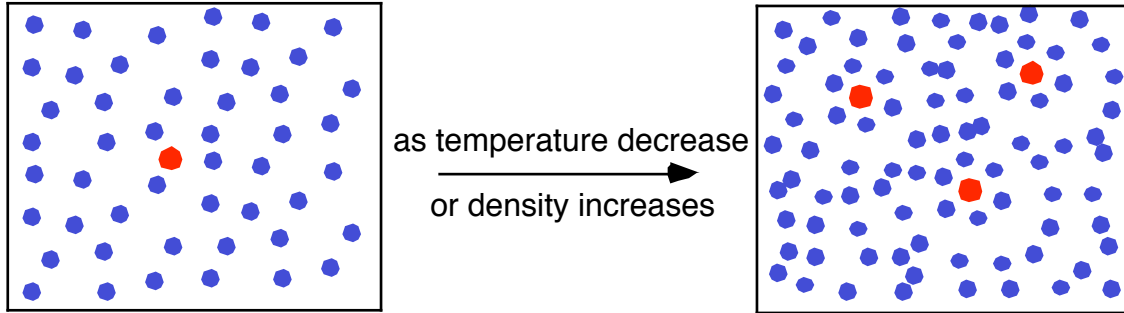


Figure 2. Schematic of the effect of increasing the coupling parameter, Γ , in a plasma. As indicated in Eq. 1 the coupling will occur with increasing density and/or decreasing temperature.

On the other hand, from the point of view of a solid the temperature of the system relative to its Fermi energy defines the WDM regime. The Fermi energy E_{Fermi} is the maximum energy level of an electron in cold (essentially $T = 0$) condensed matter and thus when the temperature $T \ll E_{\text{Fermi}} = T_{\text{Fermi}}$ then the standard tools of condensed matter are applicable. However, when the temperature $T \geq T_{\text{Fermi}}$ one gets excitation of the core level and potentially ionization leading to a complex mixture of species. In this latter case the ion-electron correlations change and the ion-ion correlations yield distinct short and long-range order, when compared to the $T=0$ solid. This is illustrated in the Fig. 3 where we show for the case of aluminum the changes in the electronic density localization and the band structure of solid aluminum at $T=0$ and the band structure at finite $T > T_{\text{Fermi}}$. The calculation of the structure becomes substantially more complex due to the number of band required to describe the system and due to the fact that there are several ionization stages present.

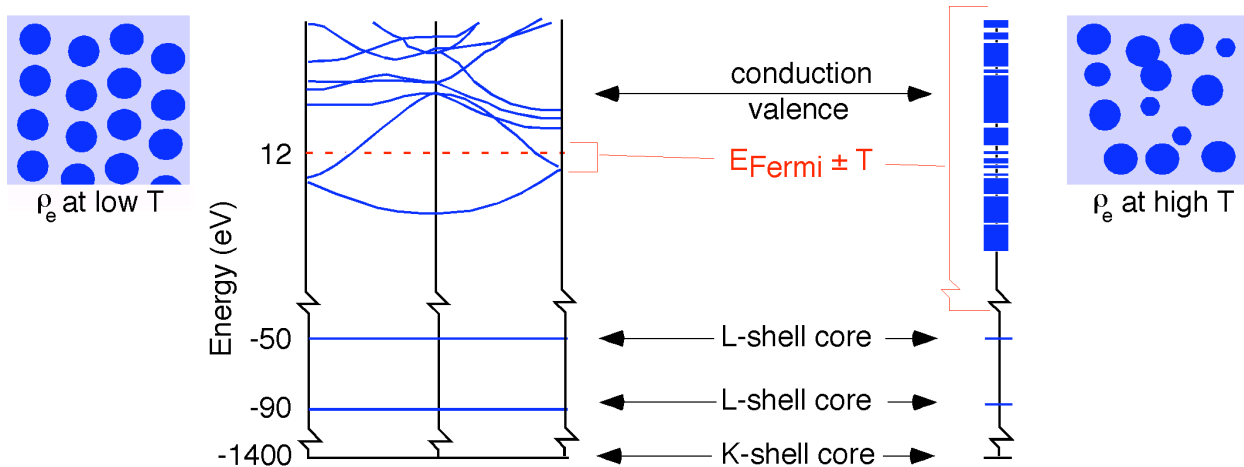


Figure 3. The warm dense regime is defined from the point of view of condensed matter. The increase of the

temperature toward the Fermi temperature while keeping the density at normal solid density creates a more complex band structure as well as numerous possibilities for more random placement of the electron charge density

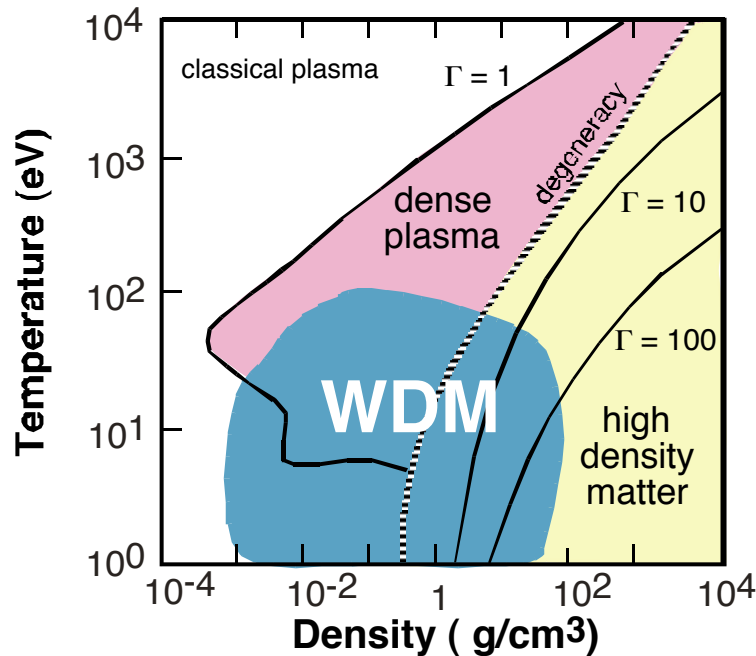


Figure 4 The temperature-density phase diagram for aluminum. The relevant regimes are noted, as are the various values of the coupling Γ . The region of greatest uncertainty is roughly noted by the teal area. Also indicated is the region where degeneracy will become important: it is the region to the right of the line where the chemical potential $\mu = 0$. The aluminum data is derived from the QEOS formalism (More, 1988)

In Fig. 4 above we show the region of the temperature-density plane where warm dense matter studies are important. Here we show the temperature (T) in eV versus the density (ρ) in g/cm^3 both for aluminum, a moderate Z element. The various values of the strong coupling parameter defined in Eq. 1 are shown as well as the region where degeneracy plays a role. The region where the theoretical uncertainties are largest are those where the standard theoretical approaches fail and experiments are exceedingly difficult; the WDM region indicates this. The difficulty arises theoretically from the fact that this is a regime where there are no obvious expansion parameters, as the usual perturbation expansions in small parameters used in plasma phase theories are no longer valid. Further, there becomes an increased importance on density-dependent effects, *e.g.*, pressure ionization, as the surroundings starts to impinge on the internal structure of the ion or atom. Experimentally the study of warm dense matter is difficult, as the isolation of samples in this regime is complicated. Indeed, although the plasma evolution of every ρ - T path that starts from the solid phase goes through this regime and plays an important role in its evolution, trying to isolate warm dense matter remains a major challenge.

B. Studying Warm Dense Matter in the Laboratory

It has been exceedingly difficult to perform experiments in the warm dense matter regime, which is, simply, why we know so little about it. As a first step, one must create a well-characterized warm dense matter state; the second is to gain information on the state through experiments. The first step has been the problem: warm dense matter is not a limiting case of matter, *e.g.*, high- or low-temperature. When created in a laboratory environment, it does not tend to remain in a specified thermodynamic state for very long, making characterization difficult. The various methods suggested to produce the kind of warm dense matter of interest are the proposed x-ray free electron laser, the heavy ion beams of interest here, and with a sub-30-fs visible laser pulse on sub-100-Å-thick foils and perform thermodynamic measurements on a few-fs timescale over extremely small spatial dimensions. As we will discuss the heavy ion beam approach presents a very interesting option.

One finds that the problem is not that WDM is difficult to create as it occurs widely; but, to create it in a manner that is conducive to quantitative examination. The problem is that the deposition of substantial energy in a short time leads to large gradients in both temperature and density. If the energy is deposited slowly so that hydrodynamics expansion dominates the system then the difficulties in isolating a well-defined state is further compounded. The effort in most WDM experiments to date has been in creating matter that can be diagnosed. Then diagnostics must define the state of the matter: there must be a measurement of the temperatures (ion, electron and radiation) and densities (the electron, ion and possibly the mass density); measurements of the pressure, flow velocities and the uniformity must be undertaken; and, one needs to consider the effect of shocks, turbulence, and material mixing. These requirements have been difficult to meet and indeed have been achieved in very few cases. One is attempting to measure the equation of state (EOS) of the system. The equation of state is a formula describing the relationship between various macroscopically measurable properties of a system, usually the temperature-density-pressure.

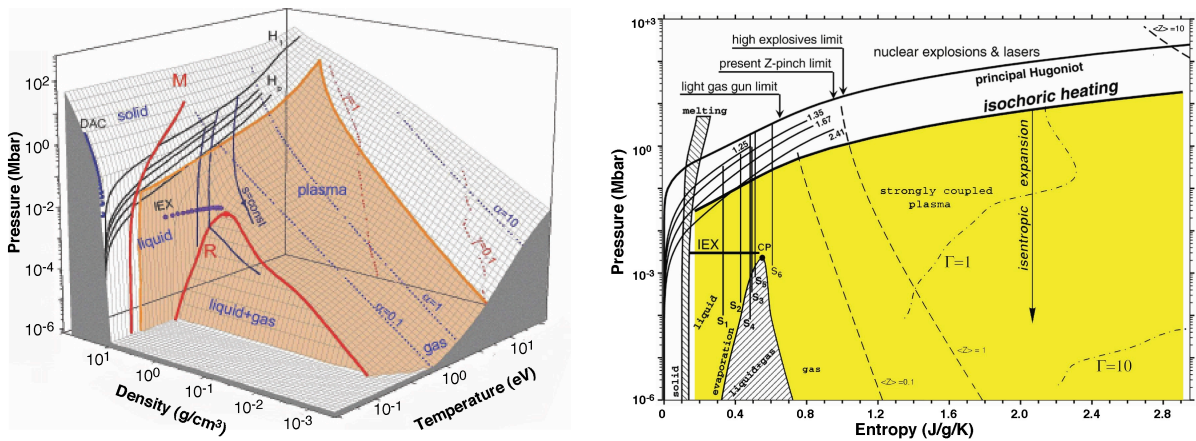


Figure 5. The phase-space diagram of Pb with experimental data and various phases. shown a) the Pressure-Density- Temperature phase diagram. b) The Pressure-Entropy diagram showing the isochoric heating/isentropic release curves.

The best examples of WDM studies performed to the level indicated are found in the literature on shock generation with the largest part of these coming from experiments employing single strong shocks. As an indication of the possibilities we show a phase diagram of lead, a much studied material, in Fig. 5 a and b. The Fig. 5a shows the pressure-density-temperature phase space with curves generated by difference experiments. The H₁ and H_p are the shock Hugoniot for the principal and porous Pb. The Hugoniot is the locus of states reached by single strong shocks, one point for each shock. As is clear these Hugoniot represent the largest

contributions to the data set. The diamond anvil cell (DAC) measurement are done at very low temperature and form a limiting case not of interest to WDM studies. There is one isobaric expansion experiment (IEX). These represent the experiments in the region of interest, illustrating the paucity of data. The one additional curve that is shown is noted as by $s=\text{const}$ and represents the isochoric, constant density, heating of a sample and the isentropic, constant entropy (S), release. Indeed, the ion-beams capability will attempt to access this regime by providing uniform bulk heating and then isentropic expansion. This is shown in Fig. 5b where the phase space representation has been converted to Pressure-Entropy space. In Fig 5b the same experiments are shown as on Fig. 5a with the isochoric heating/isentropic expansion more clearly indicated.

The understanding to be gleaned from Fig 5 is that there are: 1) little data in the WDM, even for a well studied material; 2) there are few extant methods that can access the regime of interest, and 3) the potential of volumetric heating possible with heavy ion beams can play an important role. Indeed the concept for ion-beam heating is straightforward and is illustrated in Fig. 6

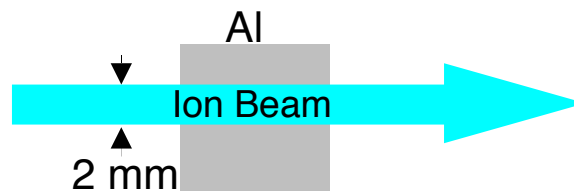


Figure 6. Schematic of the ion beam heating experiment

Figure 6 schematically illustrates an experiment of this nature. The Al phase diagram of Fig 4 illustrates the parameter space of such an experiment. In Fig. 7 the phase space diagram has been annotated, to show the trajectory of the isochoric heating and the subsequent release along the isentrope, by red and pink lines, respectively. Note that the entire trajectory maps out a set of states in the WDM regime that, if each of those states is in thermodynamic equilibrium, provide a large set of data. Further, the use of a foam or porous target, indicated by the trajectory displaced to lower than normal solid density allows one to collect data across a wide swath of the WDM region.

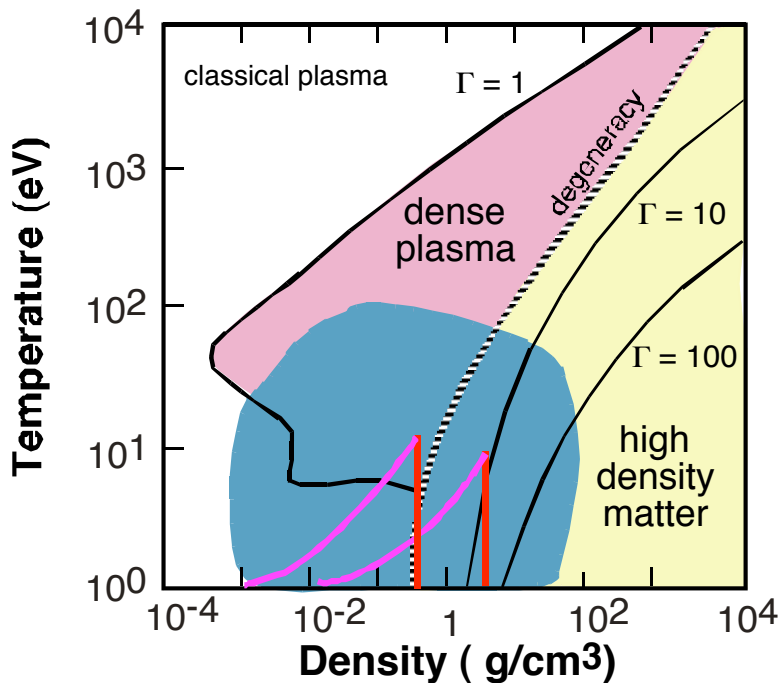


Figure 7 The temperature-density phase diagram for aluminum. As Fig. 4 with the inclusion of the schematic isochoric heating (red) trajectory and the subsequent isentropic (pink) trajectory. Note that underdense material, e.g., foams, allows multiple trajectories to be studied.

III. Current State WDM studies

In the past few methods have been used to study the WDM regime, as indicated by the discussion above; however, currently more experimental techniques are being employed. We will attempt to outline the state of the art specific to WDM studies. The methods we will cover include experiments using Short pulse Laser experiments in their various forms, High-energy lasers, 3rd generation light sources, and large and small pulse power machines. The main purpose is to provide an understanding of the fact that although an ion beam facility does not exist the field is far from crowded with viable options.

A) Short pulse lasers

Over the past few decades as visible laser have become prevalent the number of application to the production of exotic states of matter have increased. More recently the move toward ever shorter pulse lasers systems have made for exciting new possibilities in the generation of these novel states. However, the number of experiments directed toward studies of the detailed nature of either HDM or WDM is quite small. The overarching reason for this paucity of experiments is the difficulty faced when one has a visible laser and attempts to directly heat dense matter, as the visible laser can not penetrate effectively beyond the critical electron density, which as function of the laser wavelength, λ_{laser} (Ångstroms), given by

$$n_{critical} \approx 10^{29} / \lambda_{laser}^2 \text{ (cm}^{-3}\text{)} \quad 2)$$

This indicates that the primary interaction of the short pulse laser will be with a region of small depth, $\leq 1000 \text{ \AA}$, and leads to substantial gradient formation on the time scales of the laser irradiation, which lead to hot dens plasma studies. This is the case for the overwhelming majority of laser-matter experiments to date. In contrast to this are two examples of potentially interesting experimental setups that could lead to WDM matter experimental interest.

The first type of experiment uses of a short pulse laser with diagnostic capability to record information on the state of the heated system on the time scale of the laser irradiation (Widmann et PRL 92, 125002 (2004)). The concept is shown schematically in Fig. 8 where the short pulse laser is split into a beam that will be converted to 2 μm to heat the target and one that will be used as a probe. The part to be used as a probe is put through a Michelson interferometric setup. The resultant two probe beams impinge on the sample surface, one before the heating beam arrives and one after, and are afterwards recombined in a spectrometer creating a one-dimensional image of the surface at various times relative to the heating pulse. This information about the surface motion together with the energy of the incident, reflected, scattered and transmitted beams provides a best effort to date at bracketing the equation of state.

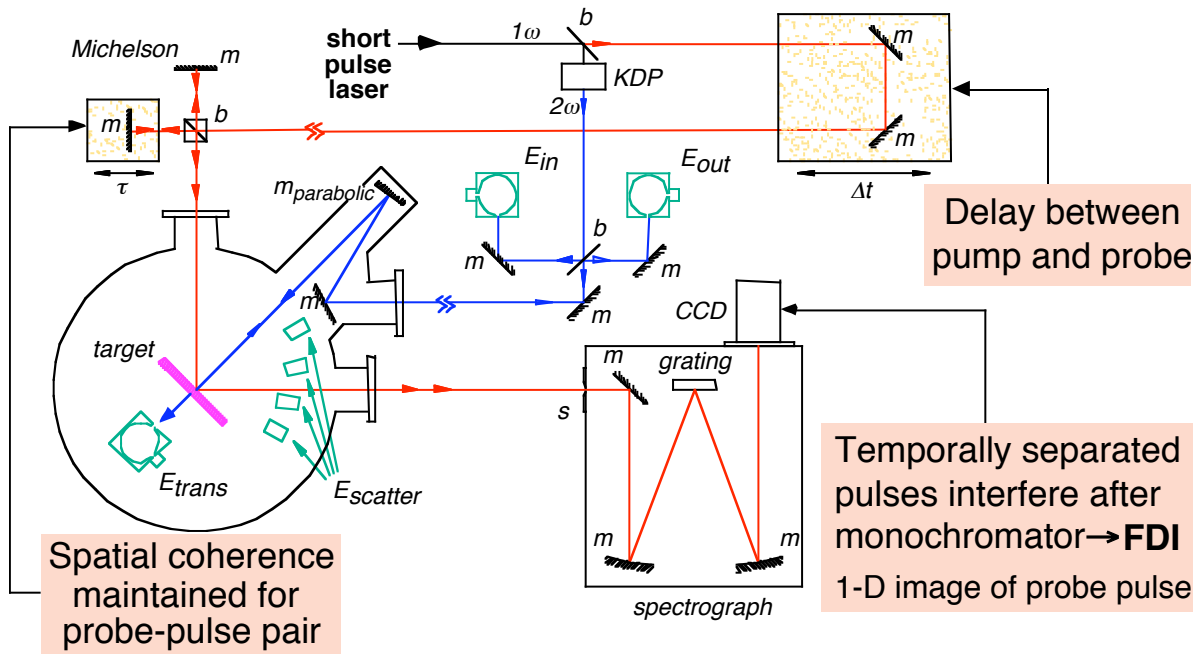


Figure 8. Set up of a short pulse laser experiment to measure the states of a heated sample as a function of time.

The results from this experimental setup have proved interesting but there remains the problem the sample is undergoing hydrodynamic motion and has substantial gradients during the time of the experiments. The lack of sample uniformity cannot be ameliorated due to the fact that the heating occurs non-uniformly.

The second type of experiment would be quite similar to the one shown in Fig. 8 except one would use a slightly longer pulse and overcoat the thin sample with a large layer of lower Z material (Davidson et al., JQSRT, **65**, 151 (2000)). For example, one could have a 100 Å layer of Fe embedded in a sandwiched configuration with 1500 Å of CH on either side. The object would be to heat the Fe layer via electron conduction from the laser irradiated surfaces and wait until the Fe layer was uniform. This would, were simulations to prove correct, form a very uniform Fe layer at times long compared to the laser pulse. The simulations show, in Fig. 9, that at 5 ps, the Fe sample is at 0.2 of normal density and at an elevated temperature of 150 eV. This, if true, would allow one to study the WDM regime also.

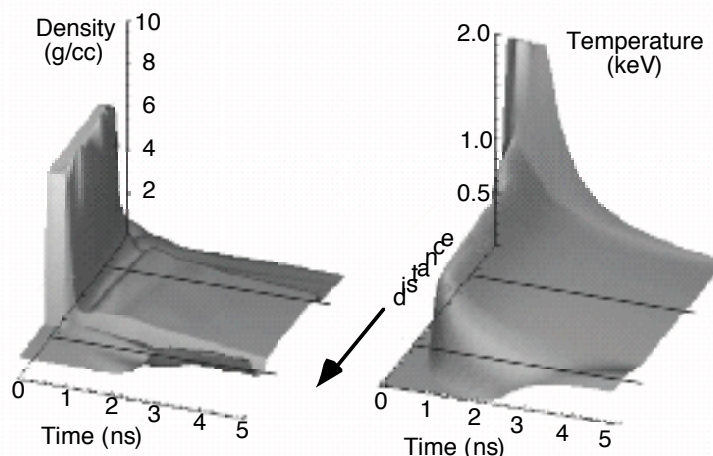


Figure 9. A simulation showing the temperature and density history of a one dimensional sample irradiated

from the far side with a 700 ps short pulse laser at 10^{17} W/cm². The sample starts as a 100 Å Fe layer sandwiched between 1500Å of CH.

The fact that this experiment has never been performed may be due to one or more of several factors. Two of these factors are: 1) Simulations are more alluring than the experimental program needed to achieve them; 2) The interest in creating a test bed for WDM using a higher energy short pulse laser is of low priority compared to the number of exotic states that can be produced more simply.

B. 3rd Generation X-ray Light Sources

Experiments on current x-ray light sources are limited by the fact that these light sources have low intensity per bunch and have relatively long pulse durations, ≥ 50 ps. Thus to study WDM states one needs to couple a short pulse laser as a heating source with a beamline at the light source. This has been done at the Advanced Light Source, Advanced Photon Source, and the European Synchrotron Radiation Facility. At all these sources similar experiments have been performed which are schematically illustrated in Fig. 10. The basic idea is to use the short pulse laser to create a perturbation at a crystal surface and use the x-rays from the light source to probe the disturbance. The experiments have proved extremely fruitful but are limited by the fact that signal levels per bunch are small so that the perturbed sample must be probed repeatedly to gather data. This is overcome by ensuring that the sample perturbation is small so that the crystal returns to its original state between pulses, which with current technology is limited by the short pulse laser repetition rate of ~ 1 kHz. An example of the results is shown on the right-hand side of the Fig. 10 where the diffracted signal is shown as a function of time after the short-pulse laser perturbation. This form of data has been used to measure the phonon dispersion relations under non-equilibrium conditions, providing a measure of the electron-phonon coupling, and observation of order-disorder laser-induced phase transitions.

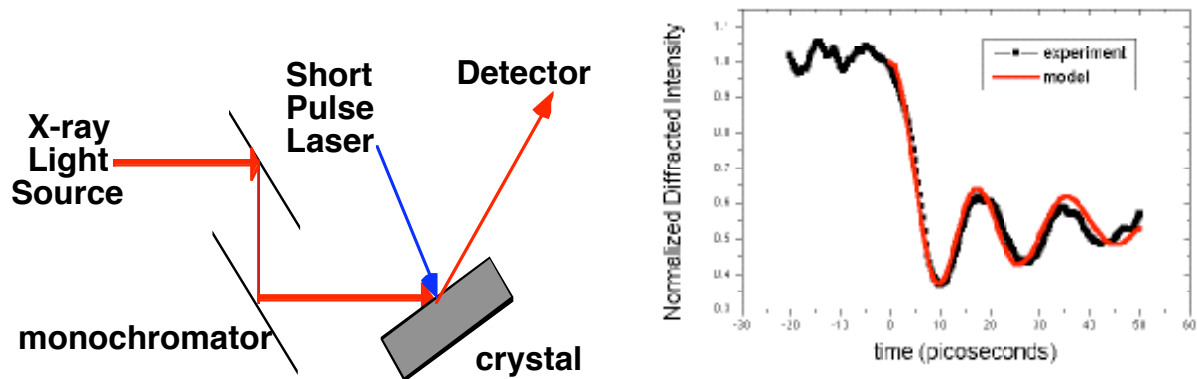


Figure 10. The left-hand side shows a schematic of the short pulse laser coupled to a 3rd generation x-ray light source. The laser is synchronized to the RF signal from the light source to provide ~ 1 ps timing. The time resolution of the experiment depends on the detector as the light source has ≥ 50 ps time duration. The right-hand side shows the diffracted signal as a function of time measured from the laser irradiation.

C. High-Energy Lasers

The use of high energy lasers -for the purposes of discussion here we take laser with energies greater than > 50 J- to produce WDM is predominantly associated with using the high energy laser to drive a strong shock for the purposes of using the Hugoniot relations to measure the equation of state along the principle single shock Hugoniot (see for example: L. B. Da Silva et al., Phys. Rev. Lett. **78**, 483 (1997); and, G. W. Collins et al., Phys. Plasmas **5**, 1864 (1998)). Next, one finds that in the run-in phase of a radiatively driven inertial fusion capsule implosion

the desire to remain on a low adiabat leads to WDM conditions. Although this is not a case where fundamental measurements can be made concerning the WDM state one could ideally use the detailed measurement of the hydrodynamics of the run-in to infer the state of the imploding capsule. Finally, we show the one set of experiments performed on high-energy lasers where the laser provides an x-ray source to warm matter and also provides an x-ray source that allows the probing of the warmed matter by Thomson Scattering.

The use of the high-energy laser to create shocks has been perfected over the past decade and provides a method of reaching very high pressures (≥ 10 Mbar) in the laboratory. The schematic is straightforward and shown in Figure 11 together with the data where the image of the shock and the pusher interfaces are shown as a function of time. The latter data provides the pusher and shock velocities that together with the Hugoniot relations provide the equation of state for the shock pressure induced by the laser.

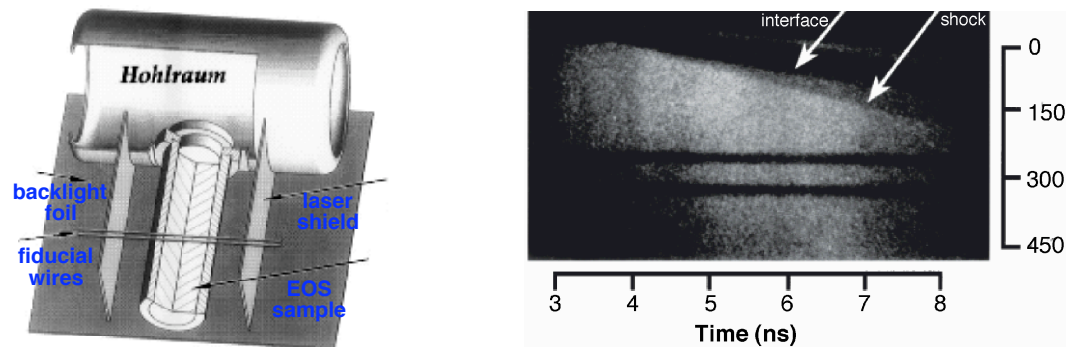


Figure 11. The use of a hohlraum, left-hand side, an enclosure that is irradiated by a high-energy laser to convert the visible light to x-ray that then drive a shock into the sample appended. Another laser beam impinges on the backlight foil to create a long duration x-ray source to observe the shock transit. This is imaged on a x-ray streak camera and produces, right-hand side, a record of the shock and pusher positions as a function of time.

The result of each of these experiments is a point on the Hugoniot an example of which is shown in Fig. 12 where several sets of experimental data are shown.

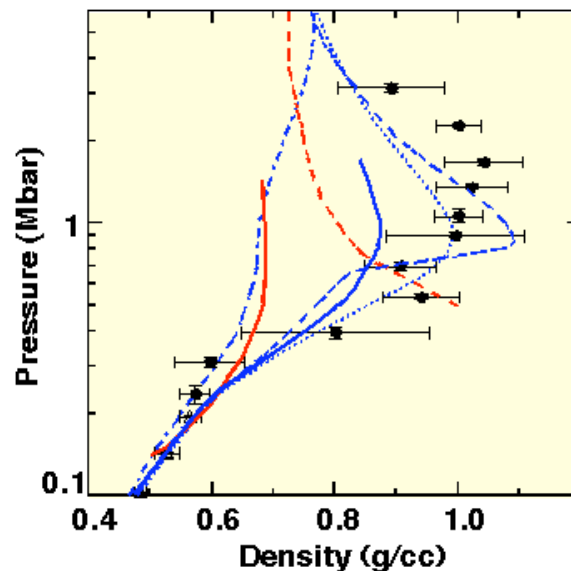


Figure 12. Gas gun data (triangles) are shown. The blue curve indicate models based on fits to extant data while the red line are physical model base on *ab initio* methods. The EOS model is shown as the dotted blue line. The widely used SESAME tabular EOS is shown as a dot-dashed blue line. The remaining curves are newer attempts to model the data.

The accessing of the WDM regime occurs much more frequently as an integral part of experiment where the end result is some aspect of the HDM regime. One excellent example of this is the run-in phase of indirectly driven inertial fusion capsules. To best keep the pressure of the inflowing material at low pressures one designs the driving pulse to keep the pusher (shell of the capsule) on a low adiabat. This then allows the pusher to compress the gas (fuel inside the capsule) more efficiently. In Fig. 13, the schematic configuration of the experiment is shown. On the left-hand side is the radiation enclosure, hohlraum, into which laser beams are focused. The lasers impinge on the high-Z wall and through laser-matter interaction the laser light is converted to x-rays that then irradiate the capsule in the center of the hohlraum. The capsule is shown in diameter on the right-hand side where the pusher is composed of Cu, to block the x-ray from heating the DT fuel, and Be. The simulated temperature-density paths for a representative volume of the Be pusher and the volume of the DT fuel are shown in Fig. 14 where we see that for large parts of the run-in the fuel and the pusher are in the WDM regime. The light yellow areas indicate the WDM regime. Detailed diagnosis of the WDM, in a configuration as complex as this, is beyond the current scope of any experimental program. However, the hydrodynamics of an experiment of this kind can be measured, e.g., the timing of the shocks and the imaging of the compressing core, and that would provide indirect evidence of the WDM models used in the simulations.

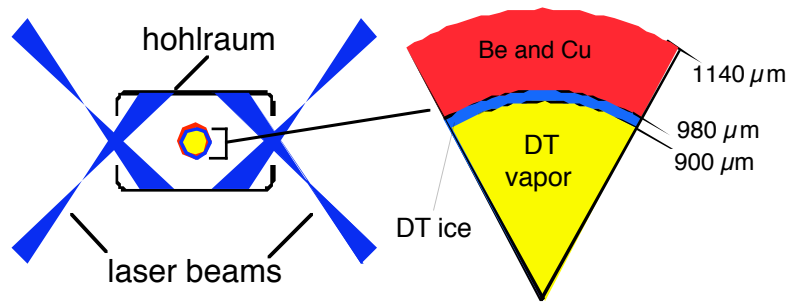


Figure 13. Schematic of the indirectly driven ICF capsule experiment on the left and an enlarged view of the capsule, right, showing the pusher and the fuel regions

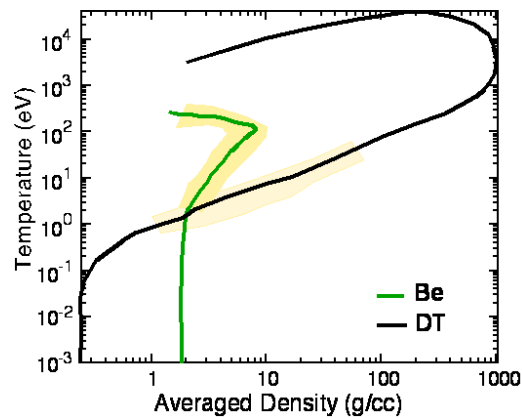


Figure 14. Temperature and density track of representative regions of the pusher and the fuel are shown in green and black, respectively. The yellow highlighting indicates the WDM regime. Further, the fuel can be seen reaching extreme condition, e.g., 1000 g/cc and 10^4 eV at peak compression.

Finally, there is one particular experiment on high-energy lasers where the main focus is the WDM regime. In Fig. 15 we see on the left the target configuration: here a plug of Be surrounded is by a Rh layer. The Rh layer is irradiated with 15 laser beams to create x-rays that heat the sample. These beams are 1 ns in duration and after they turn off 30 beams irradiate the Ti layer to create x-ray from the He-like Ti resonance lines that are then pass through the heated Be. The Ti x-rays are scattered from the heated Be sample and recorded on a spectrometer. The

Compton shifted scattering, shown in the data on the right-hand side, as the green area represent the free electrons scattering from the Be sample. The lower plot shows the measurement with no x-ray heating beams and represents the $T = 0$ case. The upper curve shows that the number of free electrons per Be atom, z_f , increases due to the heating. The sensitivity of the measurement of the temperature using this technique is quite accurate with differences in 10 eV easily discernible.

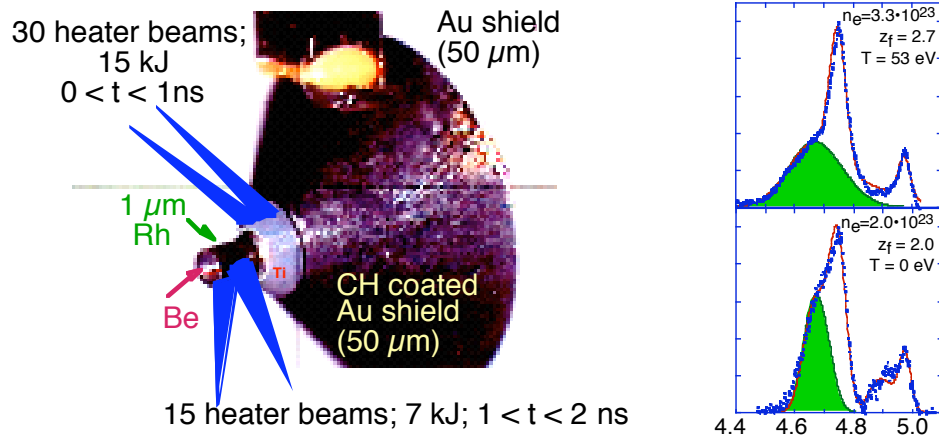


Figure 15. On the right target configuration of a high energy laser experiment specifically design to create and probe the WDM regime. The experiment has 15 beams creating an x-ray source that heats a Be sample, and 30 beams that create an x-ray probes to be scattered from the heated sample. The Thomson Scattering signal is on the right with the green area indicating the unbound electrons contribution. The bottom right plot show the data with no heating and the top shows the data from a sample that is heated.

D. Large Pulse Power Technology

The recent improvements in efficiently delivering the vast amounts of energy generated by pulsed power technology to loads have created an important avenue for research into the generation of WDM via shocks. The researchers at the Sandia Z facility have perfected a technique to launch cold, high velocity (to 28 km/s) flyer plates and have obtained results at 1-Mbar in D_2 . The effort began in the year 2000 with results in the 0.3-0.8 Mbar range reached in 2001. Shown in Fig. 16, the pressure and density relationship (shock Hugoniot) agrees with the SESAME EOS model (used in most hydrodynamics simulation codes) and with *ab initio* molecular dynamics calculations, but disagrees with the greater compressibility in Nova data and the Ross model (see Fig. 12). These data contribute to the controversy about the D_2 data and have implications for inertial confinement fusion (ICF) and for stellar and planetary models. The fact that there is a disagreement is not of immediate importance here; however, it brings two important points to the forefront: 1) There is in the study of new regimes a real need for alternative methods to perform experiments in the same parts of phase space and 2) the large energy of the new pulse power machine will be an important resource in the future for the study of WDM. Indeed, the relatively new interest in the WDM regime should spark this interest.

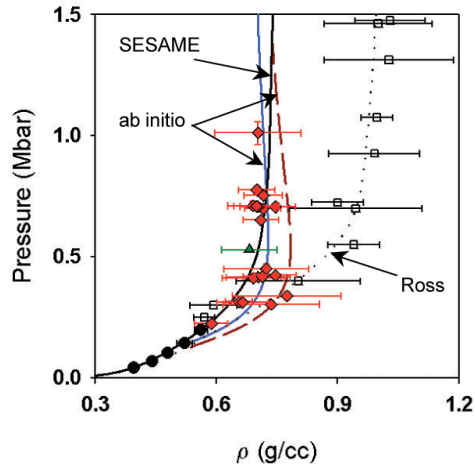


Figure 16. EOS data from the Z Pulsed Power machine (red diamonds), gas gun (solid circles), and Nova (open squares) data for D_2 compared with *ab initio* calculations and the SESAME and Ross models. The disagreement with the laser-based shock Hugoniot data remains a subject of discussion (See Fig. 12 for reference)

E. Smaller Pulse Power Technology

Due to the rather low temperatures that are of interest to the WDM regime it is not surprising to find that alternative methods using relatively simple pulse power plasma generators have made inroads into the stuff of WDM. In these examples presented here measurements are made of a transport property that are of interest in the WDM regime. However, there are no direct measurement of both the temperature and density of the system. These conditions tend to be inferred by plausibility arguments and/or simulations. Indeed the experimental setups are modest, at least by the usual high-energy laser facility or large pulsed power facility standards and efforts to perfect the methods may prove cost-effective.

All these pulsed power concepts are variations of exploding/evaporating wires with the added feature of tamping the wires in various ways to retain the density. First, there is the work of Benage et al. (Phys. Rev. Lett. **83**, 2953 (1999)) in which the electrical transport properties of dense aluminum are measured in the disordered liquid-like phase using a well-tamped, thermally equilibrated, exploding wire z pinch. Direct measurements of the electrical conductivity were made using voltage and current measurements. These measurements span the minimum conductivity regime and found generally good agreement with theory, in contrast to other experiments performed in similar regimes that indicated poor agreement. Here the range of ion densities and temperatures inferred were from $n_i \sim 5.1 \times 10^{22} \text{ cm}^{-3}$ at $T \sim 0.85 \text{ eV}$ to $n_i \sim 1.5 \times 10^{21} \text{ cm}^{-3}$ at $T \sim 25 \text{ eV}$, with strong coupling values Γ_{ii} from 15 to 2. Krisch and Kunze (Phys Rev. E **58**, 6557 (1998)) also studied aluminum wires rapidly vaporized in small glass capillaries by means of a short pulse current from an electrical discharge converting the aluminum into a non-ideal plasma at high density. For a short period of time, the inner wall of the rigid glass capillary confines the homogeneous plasma until the induced pressure pulse disintegrates the capillary. During this part of the discharge, no instabilities occur, and the transient plasma covers a range of inferred conditions: the density ranges from 0.001 to 1.0 g/cm^3 , the temperature from 0.6 to 2.1 eV and the electron density from 2×10^{18} to $3 \times 10^{19} \text{ cm}^{-3}$. Plasma conductivity was deduced by simply applying Ohm's law to the measured voltage drop across the wire and to the measured current through the wire. On the other hand, DeSilva and Katsouras (Phys Rev. E **57**, 5945 (1998)) measured of electrical conductivity of copper and aluminum plasmas in the temperature range 0.85-2.6 eV with densities from 0.3 to 0.02 g/cm^3 . Plasmas were created by rapid vaporization of metal wires in a water bath. At temperatures below about 1.3 eV, as density decreases from the highest values measured, the conductivity falls roughly as the cube of density,

reaches a minimum, and subsequently rises to approach the Spitzer prediction at low density. Finally, in the work of Renaudin et al. (Phys. Rev. Lett. **88**, 215001 (2002)) the electrical resistivity, pressure, and internal energy variation of warm dense titanium (density 0.2 g/cm^3) and aluminum (density 0.1 g/cm^3) are measured inside a closed-vessel. The temperature range, which is inferred from equation of state tables, varies from 1.3 to 2.6 eV, and it is assumed that the vaporized wire is homogeneous and thermally equilibrated.

IV. The Near Future

In the next five years there will be few new capabilities that come on line to address the physics of the WDM regime. These fall into three broad categories: the upgrading of existing facilities to include intense short pulse laser systems, in particular the addition of petawatt lasers; the implementation of a sub-picosecond on a 3rd generation x-ray sources light sources; and, the first 4th generation x-ray light source, a free electron laser will open.

A. Petawatt lasers as Facility Upgrades

Since the primary interaction with optical lasers is limited to the surfaces due to the limitation to the propagation of light to electron densities $\ll n_{cr}$ (see Eq. 2) we find that there is an keen interest in having very high intensity laser system associated with large scale facilities to provide a method of probing the HED matter that is produced. Further, in stand-alone configuration the petawatt laser may provide a source of intriguing plasma generation mechanism as well as being able to produce intense protons beams that have durations of $\sim 5 \text{ ps}$. The number of facilities proposed and funded petawatt lasers is substantial and the map of lasers in the US on a graph of laser energy versus pulse duration is presented in Fig. 17.

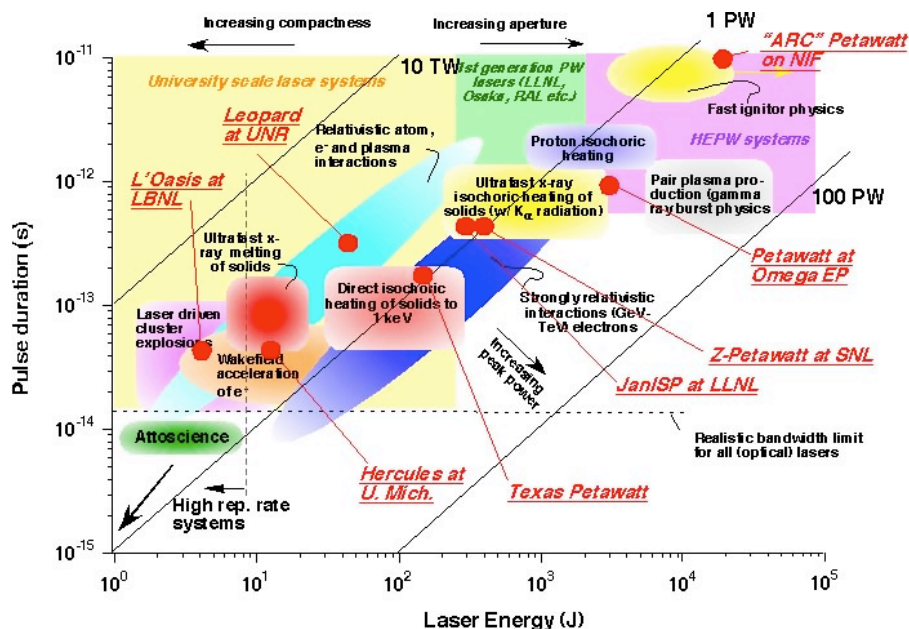


Figure 17. Laser capabilities in the USA. The various facilities are called out in red on a graph of Laser energy in Joules versus pulse duration in seconds. The Petawatt systems at Omega EP, Z-Petawatt, and ARC all have as a central application the generation of short pulse intense x-rays for probing the dense matter generated. The facility Jan/SP is functioning currently and producing proton beam for various purpose.

The wealth of facilities and those that will come on line within the next few years indicate the interest in the use of petawatt systems. However, these are largely not devoted to WDM studies. Meanwhile at the Jan/SP facility intense short pulses (5 ps) of protons have been reported and there will clear be progress in the effort to develop this source for WDM matter studies in the near future.

B. Subpicosecond 3rd generation X-ray Light sources

There are two possible venues where sub-picosecond x-ray light sources can be used. The first is the SPPS (Short Pulse Photon Source) in operation at SSRL and second is the “Slicing Source” at the ALS (Advanced Light Source) to be in operation in 2005 at LBNL. The SPPS as can be seen from the Source Table in Fig. 18 is in operation; however, SPPS will have a short life as the LCLS facility construction will require its space. With particular respect to the 3rd generation sources the study of WDM will be restricted predominantly to the type of experiments that have already been performed, see section III.B.

	SPPS (SSRL)	Slicing (ALS)	VUV-FEL (DESY)	LCLS (SSRL)
Energy range (keV)	8	0.2-10	0.04- 0.2	0.08 8.0
Photons/pulse/0.1%BW	1×10^8	8×10^2	2×10^{12}	2×10^{12}
Pulse length (fs)	80	200	50	100
Bandwidth (%)	0.1	0.1	0.3	0.3
Repetition rate (Hz)	10	4×10^4	50	120
Start date	2004	2005	2005	2009

Figure 18. The newer X-ray Light Sources that could play a role in WDM research in the near future.

C. Subpicosecond 4th generation X-ray Light sources

The advent of free-electron laser source should provide an important advance for WDM, and also HDM, research. These new light sources are laser-like in that there are high intense, small bandwidth, short pulses and they will be tunable. As such the fist of these to start, the VUV-FEL at DESY (see the Source Table in Fig. 18) will allow studies of the interaction of laser and matter where the laser penetration will go beyond the surface, see Eq. 2. These sources are to be used for a series of experiment starting in 2005 that will assist in the understanding of the WDM matter regime. They include: The creation of WDM and the measurement of the equation of state of the matter; absorption spectroscopy of laser heated matter, and surface studies of femtosecond irradiated material.

V. The Future

It is beyond the next four or five years that the capabilities of several facilities will come to fruition. The facility can be simply grouped into large-scale lasers –the National Ignition Facility (NIF at LLNL), and the petawatt enhancement to the Omega Laser (Omega EP at LLE)–, the up grade to the Z Pulsed Power Facility (ZR at Sandia), and the first x-ray Free electron laser (LCLS at SSRL). Each of these facilities will have related capabilities build up overseas. The potential for discovery becomes enormous particularly in a field as fertile at that of WDM. It is worth noting that of all these new facilities the only one that is dedicated to scientific use is the LCLS. All the other facilities are devoted largely to programmatic use and have small amounts (~10%) of their experimental time dedicated to users

However, the one capability that is missing is heavy ion beams. The SIS100 upgrade (proposed at GSI, Darmstadt) will be an important advance but will not come online until well after 2010. Thus, the prospect for volumetric and shockless heating using heavy ion beams is not on the horizon.

VI. Advantages of the Ion Beam Approach

In summary it would appear that the development of a Heavy Ion Beam user capability would be timely. The case is clear that the heavy ion beams would provide a unique method to study HED matter as the heating will occur in a shockless manner, so that the creation of high pressures will be done in manner that is alternative to the standard approaches. Further, the long time scales and larger volumes obtainable will be unique for the WDM regime. In addition, the heating can be achieved by deposition at the Bragg range or shorter distances thus changing the deposition process. We can summarize the advantages of using the heavy ion beam approach by highlighting them here. First, the ion beams will be able to heat matter on a shockless manner, which is distinct from other approaches. This will permit distinct experimental techniques to access states in the WDM regime, a necessary condition for independent evaluation of both transport properties and the equations of state. Second, the state reached is achieved by volumetric energy deposition providing several related benefits: sample heating uniformity within a few percent; relatively large volumes essential for diagnostic access; reduced gradients within the sample; and, access to high entropy matter at high density. Third, the nature of the ion beams will lead to time scales that are long enough for equilibrium conditions to be established. Fourth, the ion beams parameters can be precisely controlled to provide variations in sample conditions and these beam parameters are measurable.

The basic configuration of the experiment is shown in Fig.6 is straightforward but does not represent the complexity necessary for the fielding of the experiment. There are several areas where the discussion above provides insight into the technical requirements for the experiment. First, it is clear that *in situ* measurement of the heated matter is essential. The probing of a warmed solid will require x-ray sources with duration shorter than the heavy ion beam source. In fact, the ideal situation would be to have an absorption source, i.e., a backlight, be sufficiently short in duration so that the changes in the state of the matter are extremely small. Currently the most efficient manner to produce intense short-pulse x-rays is with a high intensity, ≥ 10 TW, short pulse laser. Indeed coupling a short pulse laser to the ion beam capability will allow the x-ray probe to provide data that is essentially static. Thus, the coupling of a heavy ion beam facility with an intense short pulse laser capability is appropriate. Further, there are additional advantages to the coupling of the short pulse laser and the heavy ion beam, e.g., the laser can provide the sample pre-ionization so that the heavy ion beam can be used in dense finite temperature plasma-related studies

The simultaneous measurement of a set of physical parameters in an experiment where all the data must be obtained on each pulse necessitates the implementation of numerous diagnostics. This implementation, in turn, requires that the samples be fabricated in a manner that allows diagnostic access and that precise measurements are performed to define the sample characteristics. This is essential to ensure that each aspect of the experiment (beam deposition, spectrometers, time resolved radiography, *in situ* scattering and/or absorption measurements) can obtain uncompromised data. This will, in turn, necessitate that shielding of the various components of the sample as an integral part of the preparation. Next, the accuracy required for equation of state measurements is highly dependent on the measurement of, for example, the expansion velocities that in turn are dependent on accurate distance versus time diagnostics. In those cases where one uses x-radiography to measure the expansion uniformity of the sample, alignment and diagnostic calibration (e.g., in a streak camera this translates to the uncertainty in the sweep speed and its linearity) combine to make 10% accuracies difficult to attain. Third, the variation of the heavy ion beam focus, the variation in beam total energy, and the variation in the

beam spectrum (in heavy ion beam experiments this translates to details of the velocity profile) requires that one be able to generate a series of reproducible experiments to evaluate a single data point in the equation of state. Fourth, the need for reproducibility requires additional pulses. All these considerations lead to an estimated repetition rate for the heavy ion beam that is on the order of a minute. This repetition rate will be needed to account for the experiment preparations, calibrations, and accelerator variability.

VII. Conclusion

In conclusion the unique aspects of shockless and volumetric heating, long duration pulses, and a user facility dedicated to the study of intriguing area of warm dense matter with heavy ion beams makes a five year plan an aggressive competitor with other planned and extant facilities.

Overview of Discussions Held in Working Group 1: HEDP Science, Experiments
Diagnostics

John J. Barnard and Richard W. Lee

1. Moveable chambers versus moveable beams?

Considering the large forest of diagnostics and wires that sprout from a chamber it seems unlikely that moving the chambers in and out of the ion beam line makes much sense. It seemed more likely that either a beam switchyard is built which redirects the beam along a number of beamlines just prior to drift compression, or the accelerator and drift is built upon a large, railroad-like turntable, which could direct the beamlines physically to one of a number of chambers. A third option was mentioned which places the chambers on colinear or nearly colinear paths, with the velocity tilt determining where the maximum compression is reached. Since the maximum beam intensity varies with velocity tilt, this option would mean the closer chambers could achieve the highest particle intensities, and so flexibility is limited in this option.

2. Are solenoids consistent with diagnostics?

If the target is placed in the middle of a solenoid, diagnostic access becomes problematic. It is better if the beam is focused onto a target which is a few cm (5 to 20 cm seem possible) past the edge of the solenoid. (Here we were considering solenoids with bores of ~ 6 cm radius, fields of ~ 10 T). There are some diagnostics which are sensitive to magnetic fields (CCD's and fast X-Ray streak cameras) so those situations would require shielding the diagnostic. More often the constraint will be having line of site access to the target, which would be highly constrained if the target were deep within the solenoid. Many lines of site to probe the target are preferred.

3. What is the spatial and temporal resolution of diagnostics?

Typically, short pulse lasers, can diagnose samples in the 50 micron regime, and some experiments have been proposed to resolve down to 10 microns using laser based backlighting probes. Typical time scales of ~ 50 ps should be easily achievable with lasers. Synchronicity may be the biggest issue, i.e. how does one trigger the accelerator pulse and the probe laser pulse with 50 ps resolution? How does one control the jitter in the accelerator firing mechanism to achieve such resolution?

4. How important are multiple chambers?

One approach is to have a single chamber with a comprehensive set of diagnostics, so diagnostics are not duplicated. For each experiment perhaps only a small subset of the diagnostics could be used. However, Dick Lee thought it is obvious that you will start with one chamber, but almost certainly that chamber could be completely devoted to facility experiments. Ultimately more chambers are required to satisfy users and develop

user interest. Thus we must do the research, to incorporate switching to allow for more than one chamber. It is clear the chamber radius itself need only be about 20 or 30 cm, but that the the diagnostics and particular the shielding between chambers will lead to footprints which are $\sim 2\text{-}3$ m in radius. The shielding is needed because the short pulse lasers used for diagnostics will produce MeV electrons (which can result in X-ray emission, which must be shielded with \sim a few feet of concrete or somewhat less than a few feet of lead), whereas the HEDP ion accelerators may produce $\sim 1\text{MeV/amu}$, which does not require such thick shielding. The shielding would be required around each chamber, if experimenters are allowed to be present in one chamber area, while experiments are occurring in another, deemed to be a very important attribute. Thus the shielding itself may be the driver that determines how closely the chambers can be spaced, which in turn helps set the bending angle needed for the beams.

5. How flexible in energy, ion mass, and ion current, should facility be?

It should be flexible enough so that as much of the rho-T plane in WDM regime can be explored as possible. Further, for measuring dE/dX a range in ion energy, and ion mass is desirable. Simulations and analytical calculations should continue to be carried out which explores possible operating regimes.

6. What should the rep rate be?

There will be a large fraction of time for setting up the diagnostics for the experiment. The rep rate will be largely for setting up and aligning the diagnostics, and for scanning some diagnostics, for example, taking spectra on device that measure a small range of wavelengths, and the wavelengths must be scanned. It is likely that accelerators operating at the 1 Hz level, would be useful for both setting up the experiments and scanning type experiments.

7. What equation of state questions will be studied?

Simple equations of state, such as the QEOS of Lee and More will be adequate to get into the ball park to design experiments. But the experiments should be flexible enough so that parameters can be varied. Many of the questions will be material science motivated, and colleagues at LLNL and LBNL should be consulted as to how measurements in the .1 to 10 eV range may be of interest. Many of the detailed measurements of quantities such as energy levels and energy bands, and transport parameters will require very sophisticated EOS models, and this comparison of the data with detailed theories will be the scientific bounty.

8. What is the time scale for equilibrium to occur?

This is not well known, but it is thought that it may take a few ps for local thermodynamic equilibrium (LTE) to be established. This is an area where the longer

length scales of ion-driven HEDP may be a big advantage over lasers. For ion driven HEDP on the 1 ns timescale, states will be more likely to have achieved LTE.

9. Ion stopping; is range shortening significant?

The energy loss rate of an ion, dE/dX , is proportional to the charge of the projectile squared, over the velocity squared times a logarithmic term given by $\ln(m_e v^2/I_p)$ for bound electrons or $\ln(m_e v^2/[\hbar \omega_p])$ for unbound electrons. (The velocity dependence of $1/v^2$ is in the high energy limit; at low energy the dE/dX is proportional to v . The peak occurs roughly where the electron velocity in the target medium equals the ion projectile velocity). Here, m is the electron mass, v is the ion velocity, I_p is the ionization potential, ω_p is the electron plasma frequency. Since for aluminum, at room temperature the number of free electrons, is already \sim a few, increasing the target temperature to a few eV, will not significantly change the range, so cold dE/dX is not a bad estimate for rough scoping of experiments. For detailed experimental comparisons of data with theory the details will matter, and stopping power will be temperature dependent.

10 Targets

Tamping of targets. It was found by D. Callahan that initial scoping of target tamping did not show dramatic improvement of solid density experiments. That is, targets a few microns thick which are bombarded with $\sim 10^{13}$ 20 MeV Ne ions per square mm in a ns, would reach temperatures of order a few eV, if the target did not disassemble before a ns is reached. The question Debbie explored was whether tamping (by sandwiching layers of tamping material (such as gold) about the material to be studied) could help change this conclusion. Debbie found that since the range was limited, only a small fraction of the target could be of the material under investigation. Further, waves were generated at the boundaries of the materials. Further, the equation of state of the tamping material complicates the hydro motion, so Debbie did not believe this was a significant improvement although factors of \sim two might be achieved. Others felt there was more to be tried including using plastics as tamping material, which would have a tendency to apply pressure to the central slice. Further as experiments progressed the uncertainties in the tamping material would be reduced, and comparing motion as a function of material composition might be a sensitive experimental tool. Again it was advised that talking to material scientists to find out the interest of their community, would help design target experiments for particular measurements (such as finding maximum strain rates of the heated materials, and for looking at dislocation dynamics as a function of strain).

11. What diagnostic tools will be available?

The GSI collaboration HEDGEHOB letter of intent document outlines a number of diagnostics which they are considering for use on the GSI HEDP experiments. The current plans for the GSI upgrade include two target chambers: one for materials (such as metals) initially at room temperature, and one for cryostatic targets (such as solid hydrogen). The plans call for \sim 12 M Euros per beamline for experiments.

The diagnostics include: VISAR (a laser interferometry technique) ; a fast multi-channel pyrometer; proton radiography; a laser for making X-rays for backlighting the target and imaging it; spectroscopic methods (measuring K-alpha shifts, Stark broadening of lines, level depressions, and other line shifts), contact pressure measurements, electrical conductivity measurements, and a Thomson X-ray scattering diagnostic.

12. Can Thompson scattering experiments be used to study density and temperature of matter in the WDM regime?

There are two experimental methods where Thompson scattering is used as part of the experiment. One of them, is to use an accelerator and a laser to upscatter the laser photons to X-ray energy, and use the scattered photons to illuminate a target sample. The accelerator can be a traditional accelerator (as in experiments with a rf accelerator at LLNL) or a laser based accelerator.

The second method uses Thompson scattering as the diagnostic within the target sample. Here laser generated X-ray line radiation is scattered in the heated material, and the Thompson scattered line width and intensity give temperature and density information.

13. What scientific areas will benefit by the study of Warm Dense Matter?

The oft-cited areas of Warm Dense Matter studies, are equation of state of closely coupled matter, including transport properties (electrical and heat) conductivities , dielectric constant, and wave properties (sound speed and shock speeds). The most direct application appears in the interior of giant planets and low mass stars. But material scientists may also have an interest in understanding yield strengths of materials at these temperatures and densities. Other possibilities offered by R. More include: Magnetic transient phenomena, ionic and electronegative plasmas, refractory metals (such as Tungsten), switching transistors, lasers, and possibly electromechanical devices. Stopping power of ions in this regime is also of interest from a fundamental physics point of view. X-ray diffraction experiments, gives the density structure $S(k)$ and the ion structure factor. MHD behavior may also be studied in this regime. Ion beam heating has the potential of yielding high resolution data, due to the ability to volumetrically heat samples.

14. What happens if the pulse duration is too long, even if the intensity is satisfactory? (Can one perform meaningful experiments during heating of the material?)

Difficult question to answer a-priori. Simulations are needed for definitive answers.

15. What simulations and analysis should be done?

There are three types of targets:

- a). Solids (tamped and untamped) H, Al, and Cl
- b). Foams (Aluminum at manufacturable densities)
- c). Gas (e.g. Neon at $10^{20}/\text{cm}^3$)

There are a number of ions that should be explored (both low Z and high Z, e.g. H, He, Ne, Ar). Particles per pulse: 10^{10} - 10^{13} , Pulse durations of 100 ps (a very demanding possibility for the accelerator); 1 ns (achievable) and 10 ns (perhaps achievable near term).

Ion energies should explore both Bragg peak heating, and energies well beyond Bragg peak (as in the GSI regime). Particles such as Hydrogen could, in principle reach the higher energy regime where dE/dX is nearly constant, (but will be utilizing the energy gained in the pulse to a far lesser extent than experiments at the Bragg peak.)

So to order of magnitude there are 9 targets by 4 ion species by 4 ion intensities, by 3 ion times by 2 ion energies or ~ 1000 simulations or analyses to carry out.

16. What new capabilities needed in the experimental path towards a user facility?

In answering this question a list of new experiments as well as existing facilities which could play a role was generated. The list included:

X-Ray diagnostic development (Source development; ~ 6 keV broad band source/spectrometer; Proton source to evaluate HIB/HED experiments; Cluster/gas jets-diagnostic development; 1020 H inverse bremsstrahlung heating (extendable to Ne, Ar, Kr);

Wire array development (to study initial dynamics of wire arrays, and also for a stand-in for foam experiments);

X-ray heating on the ns timescale (Bunch of ps bursts over ns timescale, heating matter to a few eV. Nevada Terrawatt Facility (NTF) (Zebra + laser). Will develop techniques at this facility);

NTF magnetized laser target (volumetric heating by electrons, Z pinch induced B-field);

Ionization Front Accelerator (IFA) concerning possibly building an IFA at LBNL's L'Oasis facility.

Sandia/Naval Research Laboratory Experiments; rf experiments; other pulsed power experiments

17. What plans are needed for the near term (by \sim Jan 1, 2005)?

a) A plan for what facility is to be defined. Need the flexibility to achieve the ion mass, energy, and intensity as determined by the analysis and simulations indicated above.

b) A plan to develop the experimental techniques (diagnostics) necessary to perform the experiments.

c) A plan to improve and develop a local computer and theory capability, so that simulations can be carried out in a rapid and unclassified environment.

Accelerator Requirements for HEDP

John Barnard

In order to set the requirements on an ion accelerator for heating a target to Warm Dense Matter conditions, a number of accelerator and target parameters must be understood. Scaling relations between the ion energy loss rate (dE/dX), and the ion energy and mass; at least a rough understanding of the equation of state for the matter that is to be studied, and an understanding of the relation between the achievable pulse duration and focal spot on accelerator and beam parameters are needed. In this note, we try to connect some of these basic parameters to help search the extensive parameter space (including ion mass, ion energy, total charge in beam pulse, beam emittance, target thickness and density, to name a few of the parameters) and obtain a sensible set of accelerator and beam parameters which can achieve interesting Warm Dense Matter conditions.

We first examine dE/dX , where E is the ion energy and $X \equiv \int \rho dz$ is the integrated range of the ion. This quantity has been displayed graphically for a number of different ions, in ref [1], and scaling to other target materials is also given.

For heating solid aluminum (at room temperature) over a range of ion mass from 4 amu (Helium) to 126 amu (Iodine), the energy loss at the peak of the dE/dX curve (dE/dX_{max}) may be parameterized approximately as:

$$(1/Z^2)dE/dX_{max} \approx 1.09 \text{ (MeVcm}^2\text{/mg)} A^{-0.82} \quad (1)$$

where Z and A are the ion nuclear charge and atomic mass, respectively. Expressing dE/dX_{max} as a function of A only yields:

$$dE/dX_{max} \approx 0.35 \text{ (MeVcm}^2\text{/mg)} A^{1.07}. \quad (2)$$

Thus, the peak energy loss rate increases (nearly linearly) with ion atomic mass.

Similarly, the energy at the peak increases with ion nearly quadratically with A :

$$E \text{ (at } dE/dX_{max}) \approx 0.052 \text{ MeV } A^{1.803}. \quad (3)$$

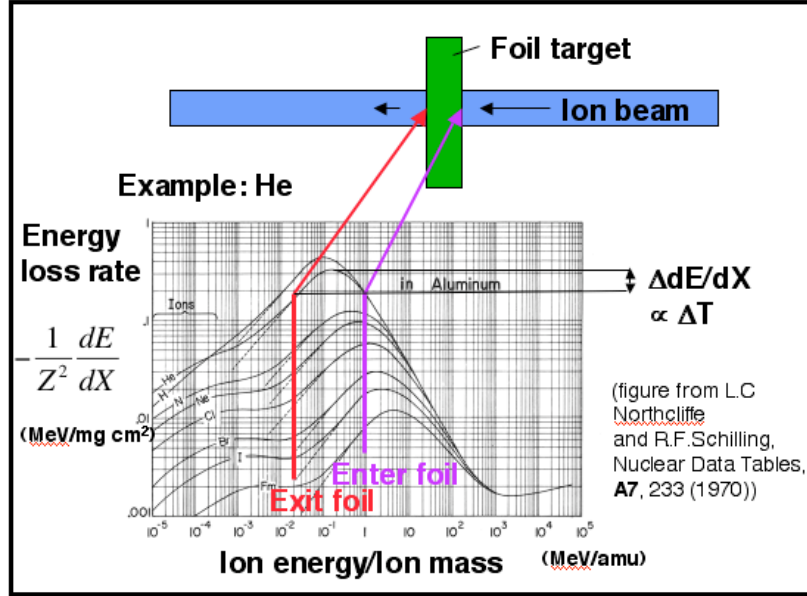


Figure 1. Temperature variations in an ion-beam heated foil can be minimized by choosing an ion and energy such that the peak in dE/dX occurs in the center of the foil (ref. [2]).

Target uniformity is another important consideration. In ref. [2] it was pointed out that target temperature uniformity can be maximized in simple planar targets if the particle energy reaches the maximum in the energy loss rate dE/dX when the particle has reached the center of the foil (see figure 1). For any specified fractional deviation in target temperature (assuming the energy is deposited in a time short so that no hydrodynamic, radiative, or other cooling has occurred) one can determine the energy at which the ion must enter and exit the foil. From the dE/dX curves of ref. [1] we find that for the entrance and exit energies to have a 5% lower energy loss rate relative to the peak in dE/dX , $\Delta E/E \approx 1.2$, where ΔE is the difference in ion energy between entering and exiting the foil, and E is the energy at which dE/dX is maximum. Note the large (>1) fractional range in energy relative to peak energy is expected for a broad peak in a log-log representation. The spatial width of the foil Z , for a 5% temperature non-uniformity is then given by:

$$Z = \Delta E / (\rho dE/dX) \approx 0.77 \mu A^{0.733} (\rho_{al} / \rho) \quad (4)$$

Here we have used $\rho_{al} = 2.7 \text{ g/cm}^3$ to convert the range into a physical distance. So by using materials of low density such as metallic foams, for example, the width of the foil can be large, which can be advantageous as will be shown. The total energy density U , calculated from the total energy deposited over the course of the pulse and neglecting losses is thus:

$$U = N_{ions} E / \pi r^2 Z = 3.7 \times 10^9 \text{ (J/m}^3\text{)} (N_{ions} / 10^{12}) (1 \text{ mm/r})^2 (\rho / \rho_{al}) A^{1.07} \quad (5)$$

Here N_{ions} is the number of ions in the pulse, and r is the equivalent radius of the focal spot, defined such that the beam is assumed to have uniform density within r , and has zero intensity outside of r . So to achieve high energy density, large particle number, small spot radius, and higher target densities must be attained. In addition, to realize the

energy density given by eq. (5), the hydrodynamic expansion timescale Z/c_s must be much shorter than the pulse duration Δt .

Hydrodynamic disassembly time:

The sound speed c_s is given by $c_s = (\gamma P/\rho)^{1/2} = (\gamma[\gamma-1]U/\rho)^{1/2}$. Here γ is the ratio of specific heats, P is the pressure and ρ is the mass density. For estimating purposes, we take γ to be 5/3, although more refined estimates below will relax this assumption. For a ‘‘shock tube,’’ that at a finite longitudinal distance z , has a discontinuous drop to zero pressure at some initial time, an analytical solution exists (ref. [3]; see fig.2) in which a rarefaction wave propagates inward at speed c_s , and a plasma front flows outward at $2 c_s$. For the case of isochoric heating, when the pulse duration $\Delta t \ll \Delta z/ c_s$, where Δz is the width of the foil, the dynamics will be the same as the shock tube solution. For times $\Delta t \sim \Delta z/ c_s$, we expect that, since the sound speed is increasing over the course of the pulse, the position of the rarefaction wave z_r will be somewhat less than would be expected if calculated on the basis of the final heated plasma:

$$z_r = \int_0^t c_s dt = \frac{2}{3} c_{s*} \Delta t \left(\frac{t}{\Delta t} \right)^{3/2} . \tag{6}$$

Here $c_{s*} = c_s(T_*)$ and we assume $\frac{T}{T_*} = \frac{t}{\Delta t}$, where T_* is the temperature achieved at the end of the ion pulse; we also assume $c_s \propto T^{1/2}$.

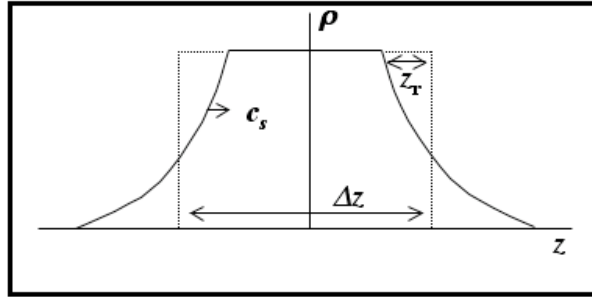


Figure 2. Schematic representation of rarefaction wave propagating inward at sound speed c_s , and plasma front moving outward at speed c_s . As material is heated over course of pulse c_s increases. The original density distribution of the foil is indicated by dotted line, and location of the rarefaction wave by z_r .

We envision isochorically heating a target foil, and taking measurements with various optical or beam diagnostics. If our diagnostic is unable to resolve a volume smaller than the volume heated by the ion beam, and if we want to distinguish equations of state with 5% accuracy, then the sample volume cannot consist mostly of blow off material (i.e. material that is part of the rarefaction wave). If we demand that the blow off material is less than 5% of the total mass, that implies $2z_r/\Delta z < 0.05$, or

$$\Delta t < 3\Delta z/(80 c_{s*}). \tag{7}$$

If on the other hand, the diagnostic has resolution z_{min} such that it can sample a fraction of the target ($z_{min} < \Delta z$), then, as long as the central part of the target has not been

"contaminated" by the rarefaction wave, useful data can be obtained by just observing the central (heated) part of the foil. In this latter case, the pulse duration must satisfy

$$\Delta t < 3(\Delta z - \Delta z_{\min}) / (4 c_{s^*}). \quad (8)$$

If $\Delta z \gg \Delta z_{\min}$, this can be a significantly longer time, but in any case, the longer of the two timescales above (eq. 7 and eq. 8) should be taken. For our examples to be discussed below, we have used Δz_{\min} to be 40 μ , which may be achievable using a K- α diagnostic generated by a short pulse laser.

In order to calculate more accurately the sound speed, one needs to understand the response of the target to the energy deposited by the ion beam. In particular, the pressure and temperature will depend on the ionization state of the plasma. For our estimating purposes, we use a model developed by Zeldovich and Raizer and summarized in ref. [4]. The basic idea of the model is to calculate the average ionization state Z^* by approximately solving the Saha equation and accounting for the ionization energy of each ion in the energy density U (where $U = (3/2)nkT + Q(Z^*)\rho/Am_h$), and to include contributions to the pressure P (where $P = nkT = kT(Z^* + 1)\rho/Am_h$) from the electrons and partially ionized target atoms. Here $Q(Z^*) = \sum_{i=1}^{Z^*} I_i$, where I_i is the (known) ionization energy of the i^{th} level of the target material, n is the total number density of ions, atoms, and electrons, and ρ is the mass density. Other more detailed equation of state models, including degenerate effects, correlation effects, and more exact treatment of the Saha equation, may have an impact on various transport and thermodynamic properties. These details are not to be minimized; after all that is why there is an experimental interest in this regime. For our purposes, however, the Zelodovich-Raizer equation of state allows approximate calculation of Z^* (see fig. 9), T , and the coupling parameter Γ_{ii} .

A second model for equation of state uses the Thomas Fermi model for calculating the distribution of electrons within an atom (see ref. [5], and reference therein for a description). Results of both models for the mean ionization state Z^* are displayed in Figure 3.

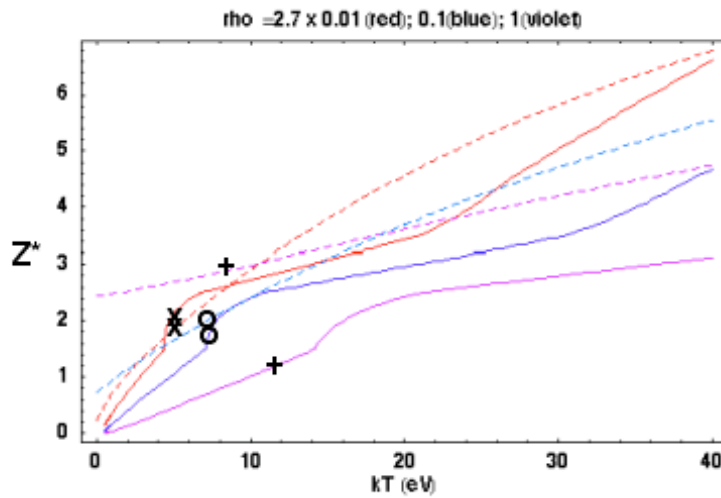


Figure 3. Calculation of ionization state, as a function of temperature for three different densities

(0.01:red, 0.10: blue, 1.00:violet) time solid density Al, using Zeldovich-Raizer equation of state(dashed) or Thomas Fermi model (solid). The x,o, and + would correspond to the conditions of reached in accelerator described by the central column of each of the 1%, 10%, and 100% solid density cases in Table 1.

Examples of accelerator requirements:

Using the model described in the previous section for ion beam stopping, the time scale for hydrodynamic expansion and the equation of state we are able to make estimates of the required beam parameters for exploring the Warm Dense Matter regime. Tables 1 and 2 give examples of requirements for two different ion energy and mass, Neon⁺¹ (A=20.17) at foil entrance energy (E_{max}) of 19 MeV, and Chlorine⁺¹ (A=35.453) at E_{max} =52.4 MeV. The energy at the center of the foil (E_{center}) and the energy at the exit of the foil (E_{min}) are listed in the captions to the tables. For each ion, three different mass densities of Aluminum target are given: Solid density (2.7 g/cm³) and 10% and 1% of solid, which can be produced by making an aluminum "foam." In turn for each target density, three target temperatures are shown. Both tables are based on a minimum diagnosable length scale Z_{min} of 40 μ . It is clear from the tables that solid density, although resulting in the highest energy density, requires vary short pulse durations, because the foil width is smaller than Z_{min} and so only a small rarefaction wave propagation distance is allowed. But for the 1% and 10% cases, the foil is larger than Z_{min} , so that the rarefaction wave propagation distance can be 10's or 100's of microns, with concomitantly longer pulse duration times. In all cases the plasma temperature is in the few to tens of eV, and the required number of particles is in the order of 10^{12} to 10^{13} particles, for equivalent focal spot radii of 1 mm.

$\rho(\text{g/cm}^3)\%$ solid	0.027 (1%)			0.27 (10%)			2.7 (100%)		
Foil length (μ)	480			48			4.8		
kT (eV)	3.1	4.8	15	4.2	7.3	18	5.9	12	22
Z*	1.1	2.1	2.7	0.56	1.7	2.6	0.56	1.2	2.5
$\Gamma_{ii}=Z^{*2}e^2n_i^{1/3}/kT$	0.45	1.1	0.95	0.30	0.63	1.4	0.30	0.70	1.6
$N_{ions}/(r_{spot}/1\text{mm})^2/10^{12}$	1	3	10	1	3	10	1	3	10
Δt (ns)	84	48	27	3.8	2.2	1.2	0.04	0.03	.014
U (J/m³)/10¹¹	.015	.045	0.15	0.15	0.45	1.5	1.5	4.5	15

Table 1. Neon beam: $Z=10$, $A=20.17$, $E_{min}=7.7$ MeV, $E_{center}=12.1$ MeV, $E_{max}=20.1$ MeV, and $\Delta z_{min}=40 \mu$

$\rho(\text{g/cm}^3)(\% \text{solid})$	0.027 (1%)			0.27 (10%)			2.7 (100%)		
Foil length (μ)	1050			105			10.5		
kT (eV)	3.8	6.5	20	5.2	8.5	25	7.6	14	31
Z^*	1.3	2.5	3.5	1.1	2.2	3.2	0.75	1.5	2.8
$\Gamma_{ii} = Z^2 e^2 n_i^{1/3} / kT$	0.45	1.1	0.71	0.61	1.5	1.1	0.42	0.77	1.5
$N_{ions} / (r_{spot} / 1\text{mm})^2 / 10^{12}$	1	3	10	1	3	10	1	3	10
Δt (ns)	96	56	30	6.2	3.5	2.0	0.050	0.028	.012
U (J/m ³)/10 ¹¹	.022	.065	0.22	0.22	0.65	2.2	2.2	6.5	22

Table 2. Chlorine beam: $Z=17$, $A=35.453$, $E_{\min}=21.1$ MeV, $E_{\text{center}}=48.8$ MeV, $E_{\max}=68.5$ MeV, and $\Delta z_{\min}=40 \mu$.

Beam Ion	Z	A	Energy at Bragg Peak (MeV)	dE/dX at Bragg Peak (MeV-mg/cm ²)	Foil Entrance Energy (app) (MeV)	Delta z for 5% T variation (10% solid Al) (microns)	Beam Energy for 10 eV (J/mm ²)	t _{hydro} =delta z/(2 cs) at 10 eV (ns)	Beam Power per sq. mm (GW/mm ²)	Beam current for 1 mm diameter spot (A)
Li	3	6.94	1.6	2.68	2.4	22.1	3.3	0.5	6.1	1990.6
Na	11	22.99	15.9	11	23.9	53.5	8.0	1.3	6.1	200.3
K	19	39.10	45.6	18.6	68.4	90.8	13.6	2.2	6.1	69.8
Rb	37	85.47	158.0	39.1	237.0	149.7	22.4	3.7	6.1	20.2
Cs	55	132.91	304.0	59.2	456.0	190.2	28.5	4.7	6.1	10.5

Table 3. Parameters for five different ion beam species such the central temperature of a 10% solid density Aluminum foil reaches 10 eV,

Tolerance on Velocity Spread:

Several different types of accelerators are being considered to produce the very short ($< \sim$ ns) pulses required for HEDP studies. But one common thread in all of the approaches, has been the need to invoke neutralized drift compression, to overcome the limit imposed by space-charge. Neutralized drift compression is a departure from the more traditional approach of non-neutral drift compression that allows the longitudinal space charge to cause the beam velocity to "stagnate," thereby removing the velocity tilt, just as the beam is passing through the final focusing magnets, thus minimizing any potential chromatic aberrations that arise in the final focusing process. Using neutralized drift compressions achieves shorter pulses, but the various longitudinal parts of the beam that have different longitudinal velocities maintain those velocities through to the end, including the final focus. So, not only do the final focusing optics have to be tolerant of velocity spread, but target heating uniformity must be maintained as different parts of the beam (with different longitudinal velocities) will have different stopping powers (dE/dX) and which in principal lead to a temperature variation larger than that of a single particle near the Bragg peak.

To investigate the effect of velocity spread we integrated the dE/dX curves of ref. [1]. As an example we investigated the evolution of a Ne ion beam propagating through 4.8 μ foil of aluminum (see figs. 4 and 5). To represent the effect of a velocity spread we chose a number of different ion energies and averaged the energy loss rate at each point

in the foil (corresponding to a energy distribution that is uniform between a lower and upper energy cutoff), and then calculated the maximum change in energy loss rate and normalized to the average energy loss rate in the foil ($= \Delta T/T$). In the 4.8μ foil case, for Neon with energy centered about 20 MeV and with zero energy spread, there was a 5.4% fractional spread in dE/dX through the foil. (So $\Delta T/T=0.054$ for this example, and is defined as the difference between the maximum and minimum energy loss rate divided by the average energy loss rate). As we increased the energy spread of the He beam, the calculated $\Delta T/T$ did not significantly increase until the velocity spread $\Delta v_{\text{spread}}/v=(1/2)\Delta E_{\text{spread}}/E$ is of order the fractional energy change of a single particle through the foil $\Delta E_{\text{single_particle}}/E$. Here ΔE_{spread} is the half width of the uniform particle distribution in energy and Δv_{spread} is the corresponding velocity spread. The general conclusion, would appear to be that if $\Delta E_{\text{spread}} \ll \Delta E_{\text{single_particle}}$ then there is no appreciable degradation of the uniformity. On the other hand, there does not appear to be a significant advantage in a small but finite energy spread. Both statements need to be verified over a broad range of foil thickness and particle energy spreads, and the dependence on particle distribution function needs to be explored. If confirmed the temperature uniformity variations in the target may not be the most severe limitation to the allowed energy spread from velocity tilt, but more likely final optics considerations.

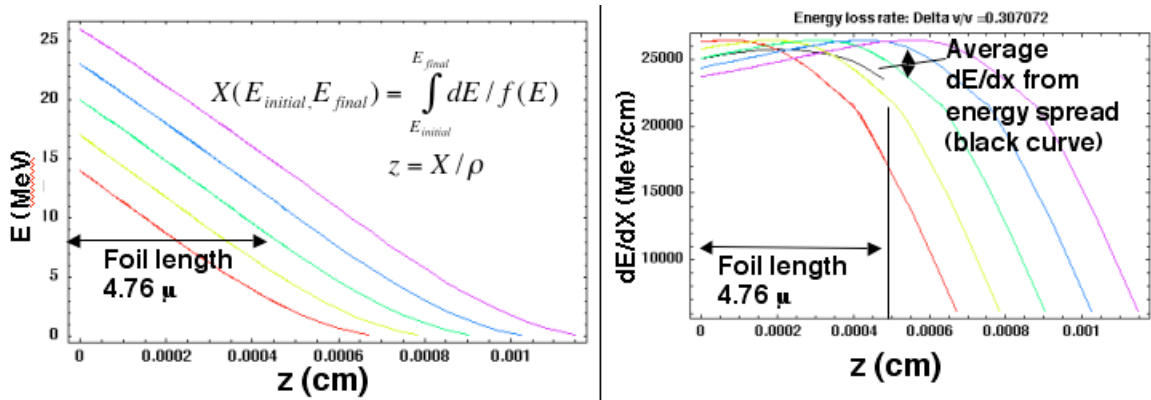


Figure 4. Energy vs. distance and dE/dX vs. distance, for a Ne ion propagating in cold aluminum, for five different energies ranging from 14 to 26 MeV. The black curve in the right hand figure is the average of the five colored curves and represents the total average energy loss rate for an ion distribution function that is uniform in energy.

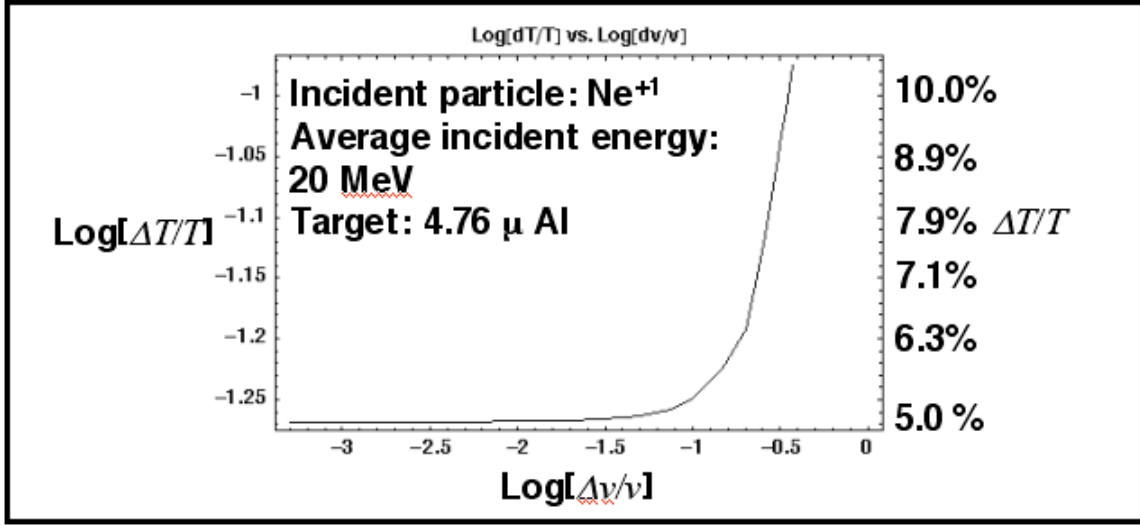


Figure 5. Temperature uniformity vs. velocity spread, for a Ne beam with central energy 20 MeV, propagating through a 4.8 μ cold aluminum foil.

Not only do HEDP experiments require uniform deposition but they also require high intensity, which means both short pulse and small beam radius. We may make simple estimates for the contribution to the spot size from chromatic effects (i.e. for the effects of a velocity spread) from a number of optical systems. For example, for a "thick" solenoidal lens in which a beam enters a solenoid with zero convergence angle and focuses to a spot within the solenoid, it can be shown to have a radius from emittance and chromatic effects r_{spot} to be approximately:

$$r_{\text{spot}}^2 \approx (\pi r_0 / 2)^2 (\Delta v_{\text{spread}}/v)^2 + (2 \epsilon f / \pi r_0)^2 \quad (9)$$

where r_0 is the radius of the beam at the entrance to the solenoid, f is the focal length, i.e., the distance from the entrance of the solenoid to the focal spot, and ϵ is the beam emittance. The quantity r_{spot} is minimum when $r_0^2 = (2/\pi) \epsilon f / (\Delta v_{\text{spread}}/v)$ and has the value

$$r_{\text{spot}}^2 = 2 \epsilon f \Delta v_{\text{spread}}/v \quad (10)$$

At minimum pulse duration the velocity tilt is converted to a velocity spread, so achieving high beam intensity will limit the velocity tilt. A system which is less sensitive to velocity tilt has also been proposed, such as the adiabatic plasma lens, but the dynamic range of these types of lens are generally limited to a reduction in spot size to a factor of around 2 or less, so these will most likely be used as a final "after burner" optic, with the bulk of the focusing being carried out by a conventional, solenoid optic, for which equations (9) and (10) provide limits.

It is apparent from equation (10) that a large velocity spread has deleterious effects in the focusing. Thus a larger velocity tilt will allow a shorter pulse but will yield a large overall spot. But if the longitudinal emittance is small, a larger velocity tilt is not needed to achieve the short pulse duration. Thus one is in obtaining a small spot there are tradeoffs that can be made between longitudinal and transverse emittance, which can be made if one is easier to obtain than the other. This may be made more explicit by

expressing equation (10) in terms of the transverse and longitudinal normalized emittances:

$$r_{\text{spot}}^2 = \varepsilon_{nx} \varepsilon_{nz} f / (\sqrt{3} \beta^3 c \tau) \quad (11)$$

Here ε_{nx} is the normalized x emittance ($= 4\beta(\langle x^2 \rangle \langle x'^2 \rangle - \langle xx' \rangle^2)^{1/2}$) and ε_{nz} is the normalized z (longitudinal) emittance ($= 2\sqrt{3}\beta(\langle z^2 \rangle \langle z'^2 \rangle - \langle zz' \rangle^2)^{1/2}$), f is the final focal length, β is the final velocity in units of c and τ is the final pulse duration. Prime indicates derivative with respect to the path length s , and non-relativistic velocities are assumed. Table 4 lists a number of parameters for possible 23 MeV Na beams, with final pulse duration τ of 1 ns, total charge of 0.1 mC, and final spot radius of 1 mm. The table illustrates some of the tradeoffs that can be made involving pulse duration before drift compression, velocity tilt and requirement on longitudinal and transverse emittance. It is apparent (and obvious) that the larger compression required during final neutralized drift compression the more constrained the normalized emittance will be.

Pulse duration (before drift compression) (ns)	Velocity tilt (Head to tail) dvlv_tilt	Maximum rms velocity spread dp/p_rms (befor drift comp)	Maximum emittance unnormalized 4 rms (mm-mrad)	Maximum normalized emittance 4 rms (mm-mrad)	Beam radius at solenoid entrance Ro (m)	Neutralized Drift length (m)	Maximum rms velocity spread dp/p_rms (at injector)	Normalized Long. Emittance (m-rad)
20	0.05	7.22E-04	49.5	2.3	0.031	5.34	1.98E-03	3.29E-05
20	0.1	1.44E-03	24.7	1.2	0.016	2.67	3.97E-03	6.58E-05
20	0.2	2.89E-03	12.4	0.6	0.008	1.34	7.93E-03	1.32E-04
50	0.05	2.89E-04	49.5	2.3	0.031	13.77	1.98E-03	3.29E-05
50	0.1	5.77E-04	24.7	1.2	0.016	6.89	3.97E-03	6.58E-05
50	0.2	1.15E-03	12.4	0.6	0.008	3.44	7.93E-03	1.32E-04
100	0.05	1.44E-04	49.5	2.3	0.031	27.83	1.98E-03	3.29E-05
100	0.1	2.89E-04	24.7	1.2	0.016	13.91	3.97E-03	6.58E-05
100	0.2	5.77E-04	12.4	0.6	0.008	6.96	7.93E-03	1.32E-04
250	0.05	5.77E-05	49.5	2.3	0.031	69.99	1.98E-03	3.29E-05
250	0.1	1.15E-04	24.7	1.2	0.016	35.00	3.97E-03	6.58E-05
250	0.2	2.31E-04	12.4	0.6	0.008	17.50	7.93E-03	1.32E-04
250	1	1.15E-03	2.5	0.1	0.002	3.50	3.97E-02	6.58E-04

Table 4. Comparison of requirements on a 23 MeV Na beam with final pulse duration of 1 ns, and final focal spot radius of 1 mm, assuming neutralized drift compression and solenoidal final focus, satisfying equations (9) and (11). The injected beam has energy 1 MeV and pulse duration 171 ns.

References

1. I.C. Northcliffe and R. F. Schilling, "Range and Stopping Power Tables for Heavy Ions," Nuclear Data Tables, **A7** 233-463 (1970).
2. L. R. Grisham, *Moderate Energy Ions for High Energy Density Physics Experiments*, Physics of Plasmas, **11**, 5727 (2004).
3. L.D. Landau and E.M. Lifshitz, Fluid Mechanics, [Pergamon Press, Oxford], Chapter 10, Section 92, problem 2. (1959).
4. R. J. Harrach and F.J. Rogers, J. Appl. Phys. **52**, 5592 (1981).
5. S. Atzeni and J. Meyer-ter-Vehn, "The Physics of Inertail Fusion," [Clarendon Press, Oxford], (2004).

2.0 *RF Group Presentations*

- 2.0 Staples This page
- 2.1 Staples RF Linac-Based Ion Acceleration: Overview
- 2.2 Staples Multiple-beam RF Linac Scenario
- 2.3 Keller Ion Source for an RF-Accelerator Based HEDP Experiment
- 2.4 Ostroumov Linac
- 2.5 Chou An Accumulator/Compressor Ring for Ne⁺ Ions
- 2.6 (Deleted)
- 2.7 Staples Alternate Structures
- 2.8 Staples Areas of Future Research & Development
- 2.9 Appendices
 - A: Staples: Introductory talk to RF Group (25 viewgraphs)
 - B: Staples: Status Report – Linac RF Group (32 viewgraphs)
 - C: Staples: RF Approach to HEDP (8 viewgraphs)
 - D: Staples: Update on Ne+1 pulse and RF acceleration (19 viewgraphs)
 - E: Staples: Loose Ends
 - F: Ostroumov: Trace3d simulations of linac (10 viewgraphs)
 - G: Ostroumov: Buncher Simulations (6 viewgraphs)
 - H: Chou: Ring Simulations (3 viewgraphs)

2.1 *RF Linac-Based Ion Acceleration: Overview*

John Staples, LBNL

The RF linac group was charged to find methods of using RF-based acceleration to provide a beam that matched the target requirements.

The members of the group were

John Staples	LBNL	co-chair
Andy Sessler	LBNL	co-chair
Joe Kwan	LBNL	
Rod Keller	LBNL	
Paul Schloessow	Tech-X	
Peter Ostroumov	ANL	
Weiren Chou	FNAL	
Bill Herrmannsfeldt	SLAC	

Motivation and Challenges

Short, intense beams of light heavy ions can be accelerated in induction linac cells, but at what cost? Can RF acceleration techniques be used to produce a less expensive machine that will meet the technical challenges of producing beams that satisfy the demands of the experimental requirements of the beam conditions on the target. Can RF-based techniques be competitive with other acceleration techniques?

RF accelerators have not been known for accelerating amperes of beam with masses in the so-called light heavy ion range, typically neon through argon. Typical accelerating cavity structures are better impedance matched to low current beams, providing high accelerating gradients with modest stored energy in the cavity immediately available to transfer to the beam.

RF accelerators to date use either Alvarez or Sloan-Lawrence Interdigitated H-mode resonant structures to accelerate a bunched beam usually with strong focusing quadrupoles located in the drift tubes, or between cavities with one or more accelerating gaps. The gap-to-gap spacing in Alvarez structures is an even multiple of 180 degrees RF phase advance, and an odd multiple of 180 degrees RF phase advance in Sloan-Lawrence machines. In both structures the phase velocity of the accelerating wave is much slower than c , and varies synchronously with particle velocity along the accelerator.

Technical limitations on quadrupole gradient and length available in drift tubes for quadrupole limits the focusing available at the low-energy end of an RF accelerator, setting a lower limit of the injection energy. New ideas using high-strength superconducting solenoids allow substantial currents of heavy ions to be accelerated and focused.

Strawman Reference Parameters

The beam conditions on target selected to provide a point of reference are:

Ion	Ne ⁺¹	
Total kinetic energy	20	MeV
Total charge	1	microcoulomb
Pulse length at target	1	nanosecond
Beam radius at target	1	mm

Staples presented two linac scenarios, a 100 MHz Alvarez linac with conventional quadrupole focusing in the drift tubes and a pulsed drift tube design that accelerated a single beam pulse at the same time starting the compression process. Neither of these structures was developed further at the workshop and are summarized in section 2.7.

Recent advances in superconducting solenoid technology opens up a new parameter space where very strong, azimuthally-symmetric focusing can contain high space-charge heavy-ion beams. The important breakthrough was the realization that very high field (15T) superconducting solenoids are available and are able to focus large currents of Ne⁺¹ in an RF structure. An RF-based linear accelerator scenario using these high-field solenoids and multi-gap accelerating cavities is described in sections 2.2 and 2.4.

The 1 nanosecond, 1 microcoulomb beam pulse at the target implies a 1 kA beam current, which is the product of a significant longitudinal compression in the HEBT. The degree of the compression is dependent on the energy spread resulting from the bunching and acceleration process in the linac and is limited to the range of 100:1 or so, implying a linac output of a few amperes.

Even with the help of high-field superconducting solenoid focusing, currents of several amperes are probably not feasible in a single beam, so in one scenario (1) the linac designs uses multiple parallel beams, which would be recombined in the HEBT/final beam transport. An alternative, scenario (2), is to use a single-beam linac and load an accumulator (stacker) ring, building up transverse phase space by painting, and kick a short beam pulse out and further compress it. This will be discussed further in section 2.5.

The linac requires a high injection energy, and multiple parallel beams in scenario (1). An ion source is described in section 2.3 which includes a 2 MV column with a number of parallel beams and multiaperture extraction geometry for each of the beams. Only one beam is required for the stacker ring concept of scenario (2).

High-field superconducting solenoids may open up new opportunities in the development of high-current linear accelerators for heavy ions. Substantial fractions of an ampere may

be accelerated, but to satisfy HEDP target requirements of 1 nsec, 1 kA type beams, further beam manipulation beyond the linac is still required. Parallel-beam structures or accumulator rings may be used to provide the total charge and, and some sort of ballistic compression, probably with the use of an induction core, will be needed.

It appears that an RF linac scenario may be feasible. No obvious show-stoppers were identified during the workshop, and subsequent calculations done in more detail have not identified any. Areas recommended for future technology development are discussed in section 2.8.

2.2 Multiple-beam RF Linac Scenario

John Staples, LBNL

Generating amperes of Ne^{+1} in an RF linac exceeds the capability of any RF-based linac now in existence. An important new idea introduced at the workshop by P. Ostroumov is to use very-high-field superconducting solenoids as focusing elements, separated physically from the accelerating cavities. Calculations showed that for a 50 MHz frequency that currents of 300-500 mA of Ne^{+1} could be accelerated.

The beam conditions on target selected to provide a point of reference are:

Ion	Ne^{+1}	
Total kinetic energy	20	MeV
Total charge	1	microcoulomb
Pulse length at target	1	nanosecond
Beam radius at target	1	mm

To generate amperes, required to produce 1 microcoulomb of charge in a few hundred nanoseconds, requires multiple parallel beam to be accelerated and combined at the target. The energy spread of the linac after debunching limits the longitudinal ballistic compression attainable to meet the 1 nanosecond target requirement to 100 or so to 1.

The frequency of 50 MHz is selected but not optimized. It is characteristic of the low-frequency superconducting cavities on ATLAS and proposed for RIA, although the cavities proposed here are normal conducting, not superconducting.

The use of high-field superconducting solenoids extends significantly the focusing strength needed in the first part of conventional drift tube linacs. With quadrupole focusing located in the drift tubes, the entrance drift tubes are the shortest, with gap-to-gap center spacing $\beta\lambda$, limiting the length of the quadrupole and its integrated strength. The technological limit of quadrupole strength in the range of 2T/cm establishes the injection energy and was typically 750 keV in 200 MHz proton linacs of the last generation.

Superconducting solenoids operating in the 15 T range provide significantly larger focusing strengths, needed for ion with low charge-to-mass, such as Ne^{+1} than quadrupoles can, and have the added benefit of significantly reduced envelope flutter for better aperture utilization and wider momentum bandwidth.

A linac lattice was assembled (see section 2.4 for more details) comprising approximately 25 cm long accelerating cavities interspersed with 15 cm long 15 T superconducting solenoids with a 2 cm bore radius. Each cavity, modeled on a three-gap interdigital H-mode (IH) structure, provides an energy gain of approximately 1 MV. Twenty cavities accelerate the 2 MeV Ne^{+1} beam to 20 MeV total energy.

The space charge limit of this arrangement is estimated at several hundred mA per beam, and therefore approximately 16 beams at 300 mA per beam are required to produce a 200 nanosecond pulse at the end of the linac, 4.8 amperes total, to be ballistically compressed by introducing an energy ramp over the 200 nsec with an induction linac core.

The 16 parallel beams may be arranged either in a circle or in a linear array, constraining the shape of the drift tube. (The voltage distribution on the drift tube, a not insignificant fraction of a wavelength, must be compensated for in the cavity design so not to increase the energy spread of the accelerated beam.)

The large area of the drift tubes will result in a rather low cavity shunt impedance due to the high displacement current in the drift tube stems, but the high inter-gap capacitance will also allow a high stored energy in the cavity, as 16 parallel beams will remove nearly 1 joule of stored energy from each accelerating cavity, which stores 10-20 Joules.

More detailed calculations (see section 2.4a) indicate that at 300 mA, the 1-times normalized rms transverse emittance at the exit is on the order of 0.9π mm-mrad. With an input emittance of the same order, the transverse emittance growth is essentially zero, but remains almost constant as the input emittance is reduced, due to space charge.

The 1-rms longitudinal output emittance is on the order of 1π MeV-degree, about a factor of three larger than an optimized, idealized longitudinal input emittance (waterbag, not what a realistic prebuncher will produce). A debuncher cavity following the linac reduces the 1-rms energy spread from 350 keV to about 55 keV, a factor of six.

The center-to-center spacing of the multiple beams is dictated by the superconducting solenoids. Commercial 15 T units can be packed with a 12 cm center-to-center spacing of the bores, which would result in the beams, if arranged in a circle, to have a radius of 30 cm. Arrangements of 1 by 16 or 2 by 8 are also possible. The even number of beams is associated with alternating field polarities of the superconducting solenoids, which will tend to reduce the extent of the fringe field, as field clamping is not feasible at the 15 T level. Some fringe field penetrating the normal-mode cavities may be a benefit, reducing tendency of multipactoring.

As the linac itself is fundamentally a constant-velocity device, but it is possible to vary the output energy continuously by turning off cavities, starting from the high-energy end, and adjusting the timing of the induction linac core following the linac, used to impose the energy ramp needed for ballistic compression. The energy ramp required of the induction core is more than the energy gain of one linac accelerating cavity.

2.3 Ion Source for an RF-Accelerator Based HEDP Experiment

R. Keller, LBNL

The primary goal for the ion source is to deliver a Ne^{1+} beam of 8 A current through 16 parallel channels to the main rf accelerator at 2 MeV energy, with a pulse length of 200 ns. The ion optical aspects of this problem had been discussed in depth in Ref. [1], leading to three basic formulae for the maximum beam current I_1 fully transported in one channel with 20 mrad divergence half-angle in the waist; extraction gap width d as a function of gap voltage; and un-normalized, encompassing r/r' emittance ϵ_r . Note that the formulae given here have already been converted to directly apply to Ne^{1+} beams. Further, it is common experience that for a pulse duration of about 200 ns, the extraction gap width can be significantly reduced as compared to the d. c. case, and the fairly conservative reduction factor already incorporated into to Eq. (2) amounts to 0.7.

$$I_1 = 0.4243 S^2 / (1 + 1.7 S^2) U^{1.5} \quad [\text{mA/kV}^{1.5}] \quad (1)$$

with $S = R/d$ being the aspect ratio of the extraction gap with an outlet aperture radius R

$$d = 0.009898 U^{1.5} \quad [\text{mm / kV}^{1.5}] \quad (2)$$

$$\epsilon_r = 10 r \quad [\pi \text{ mrad}] \quad (3)$$

For Ne^{1+} , the normalized 1-rms x/x' emittance is calculated from a given value of ϵ_r by:

$$\epsilon_{x,, \text{norm}} = 0.125 \epsilon_r \beta_{\text{rel}} \quad (4)$$

$$\text{with } \beta_{\text{rel}} = 0.00146 (U/20)^{0.5} \quad [\text{kV}^{-0.5}] \quad (5)$$

While direct, single gap, extraction of a neon beam at a voltage of 2 MV would in principle lead to the required single-channel beam current of 500 mA, the price to pay lies in having to deal with the exorbitantly large outlet-aperture radius of 106 mm (even with a rather low aspect ratio of 0.12). It would be rather challenging to uniformly fill such a large aperture with plasma in a very short pulse time, and likewise to control the gas load in the MV-type extraction column, and the starting emittance for this beam would be very high as well.

A more practical way consists in inserting an intermediate extractor electrode into the 2-MV gap and utilizing a 7-aperture extraction system for each of the 16 beam channels. For 100 kV primary extraction voltage and an aspect ratio $S = 0.5$, each beamlet now carries 74.4 mA of current according to Eq. 1, and the aperture radius is reduced to 4.95 mm. The effective configuration radius R_7 for this 7-aperture system relevant for calculating the starting emittance is three times larger than that of a single hole, assuming half a radius as material thickness between inner and out hole and another half aperture radius for the outer envelope of the outer beamlet near its waist:

$$R_7 = 3 R_1 = 14.85 \text{ mm} \quad (6)$$

With an initial divergence half-angle of 20 mrad, this leads to an un-normalized r/r' emittance of $297 \pi \text{ mm mrad}$ and a normalized 1-rms x/x' emittance of

$$\varepsilon_{7,n} = 0.121 \pi \text{ mm mrad} \quad (7)$$

The current density necessary to yield 74.4 mA of beamlet current is 96.7 mA/cm^2 , well in range for many filament-sustained plasma discharges. The arrangement of the 16 beam channels is entirely dictated by the needs of the subsequent rf accelerator structure; a schematic layout is given in Fig. 1. In case a single-channel accelerator structure with attached stacking ring is chosen, the configuration is reduced to just of one of these beam channels.

The extension of the 100-kV multi-aperture extraction system to a full-energy 2-MV accelerating column is straightforward, and there is ample space available to insert more intermediate electrodes of suitable shapes to divide the column into manageable segments, each about 100 mm long, and achieve matching input beam-parameters for injection into the rf accelerator. The detailed electrode contours have still to be designed; several simulation codes are available for this task.

For the plasma generator, a large discharge chamber is chosen, lined with permanent cusp magnets, see Fig. 2. A pulsed gas valve feeds neon into the chamber from the backside, and a diverter speeds up the establishment of uniform pressure across the chamber. 8 thermionic filaments (Ta or W) are inserted into the chamber backside and operated in d. c. mode to best avoid the effects of temperature shocks. A low-power pre-ionization discharge of about $5 \mu\text{s}$ duration is ignited to facilitate a fast rise time of the main discharge pulse that will have a duration of about 250 ns to offer a sufficiently long flat-top time for beam-pulse generation. With the extremely low duty factors involved, the design of cooling channels is straightforward.

Beams are extracted from the discharge chamber by applying high-voltage pulses to the 100-kV extraction gap as well as to the main 1.9-MV injection column; the circuitry needed to generate these pulses has still to be designed.

Reference

- [1] R. Keller, 'Ion Extraction,' in I. G. Brown, ed., "The Physics and Technology of Ion Sources," John Wiley & Sons, New York, 1st edition, pp. 42 - 43 (1989)

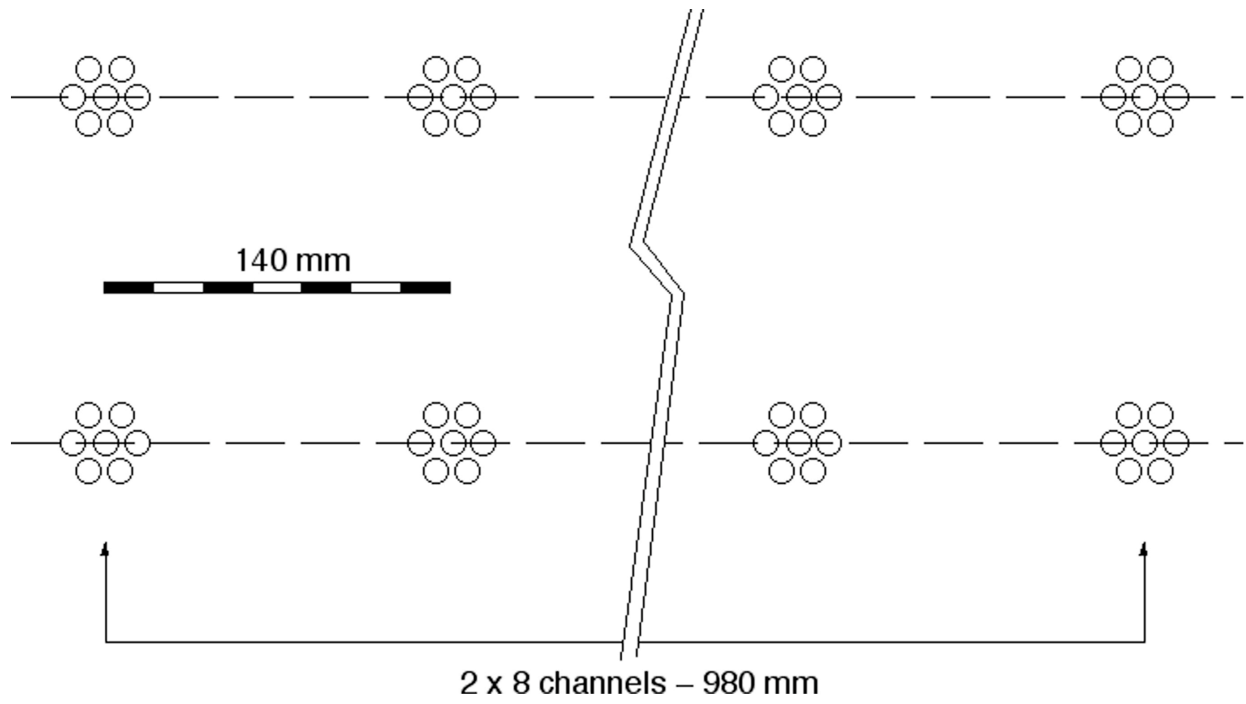


Fig. 1. Beam Channel Pattern for RF Linac Scenario

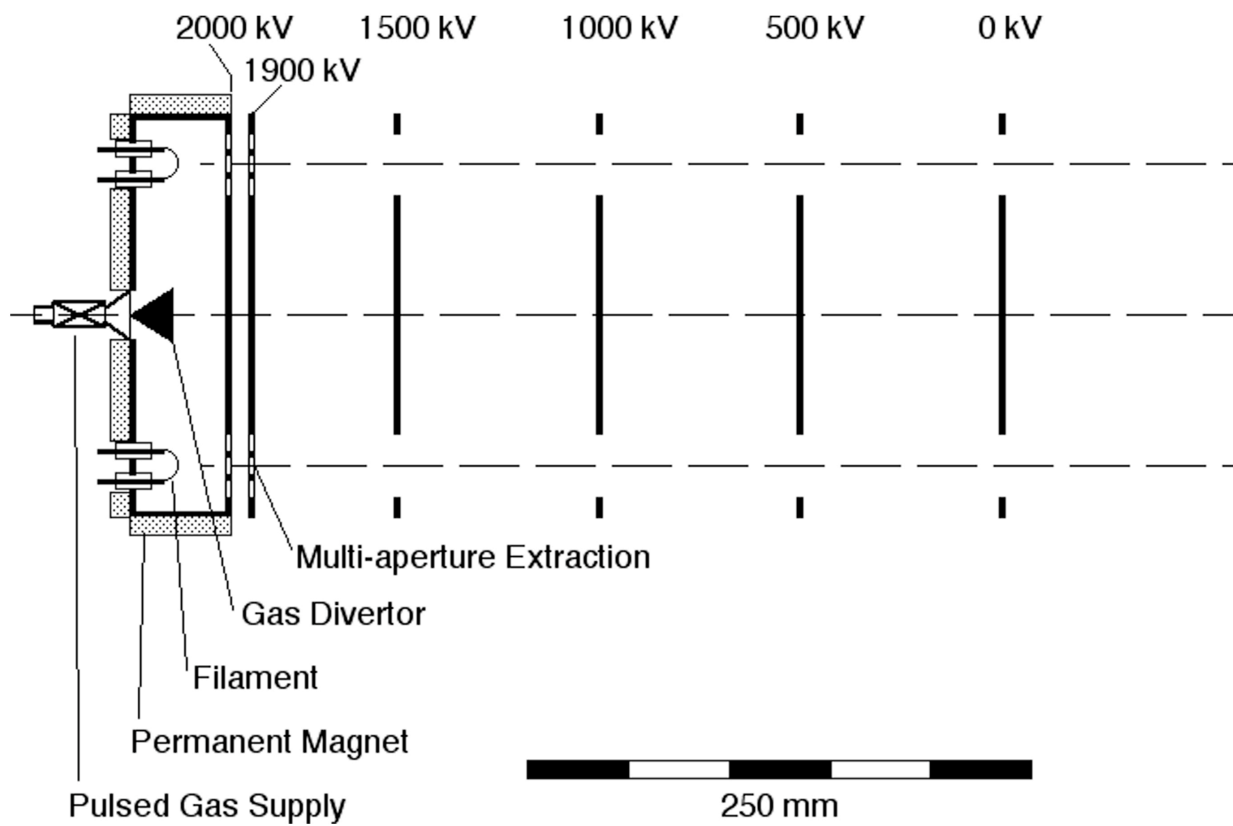


Fig. 2. Schematic of a multi-cusp ion source with multi-aperture, multi-gap extraction system. There is a total of 112 beamlets, grouped into 2x8 channels of 7 beamlets, each. The illustration shows a section of the narrow side view, with two beam channels.

2.4 Linac

*P.N. Ostroumov, Physics Division, ANL
November 8, 2004*

Accelerating cavities

Experiments with IH resonator at CERN show the possibility of obtaining high electric fields in IH resonators [1]. At 200 MHz operating frequency the maximum effective accelerating gradient was 10.7 MV/m. This corresponds to a local field maximum of 75 MV/m, and to fields in excess of 50 MV/m (3.5 times the Kilpatrick limit) on large portions of the drift tube surfaces. The average field in the accelerating gap was 30 MV/m. The pulse length in this experiments was in the range from 100 μ s to 1 ms.

For the HEDP driver application a 50 MHz 3-gap IH-resonators can be effectively applied. The accelerating gap length depends on the beam velocity and will be in the range of \sim 2-5 cm. At low frequency the Kilpatrick limit only slightly depends upon the gap length and it is 9.5 MV/m for 50 MHz and gap length \sim 2 cm. The CERN IH resonator has small diameter drift tubes therefore the total surface area under high electric field is small. In the HEDP driver resonator the surface area is much larger due to the multi-channel feature. From other side, the pulse length can be very short and close to the resonator filling time which is \sim 20 μ s for $Q_0 = 3000$. We assume peak surface field in the HEDP resonators less than \sim 3.2 Kilpatrick limit which is slightly lower than in the CERN IH resonator. This assumption results in a peak surface field 30 MV/m and average field in the gap \sim 18 MV/m. However, there is no need to operate all resonators at the highest possible fields because the field level can be limited by beam loading.

A more reasonable scenario is to operate all resonators to provide equal voltage gain \sim 1MV. In this case the energy transferred to the beam is less than 10% of the stored energy as is seen from Table 1. The electrodynamic calculations of the resonators have been performed by the CST MWS code. Figure 1 and 2 show some views of the IH resonator designed for 100 keV/u and 1 MeV/u ion beam. Large-surface drift tubes are suitable to locate 16 beam apertures in two rows (only one aperture hole at the center of the cavity is shown in Fig. 1). For simplicity of the design and simulations a rectangular cross-section has been assumed. The surface area of the drift tube is 90x18 cm² which is sufficient to locate 2 rows of aperture holes, 8 holes in each row. Figure 2 shows the intensity of the electric field in the accelerating gaps of the resonator at the high-energy end of the linac. The distribution of the E_z field in the first resonator is shown in Fig. 3.

Table 1

Input energy	0.1 MeV/u	0.95 MeV/u
Q (copper)	3588	6950
Stored energy	16 J	\sim 16 J
Power to achieve total voltage gain 1 MV	160 kW	80 kW
Energy transferred to beam with the pulse length 200 nsec and current 5 A	1.0 J	1.0 J

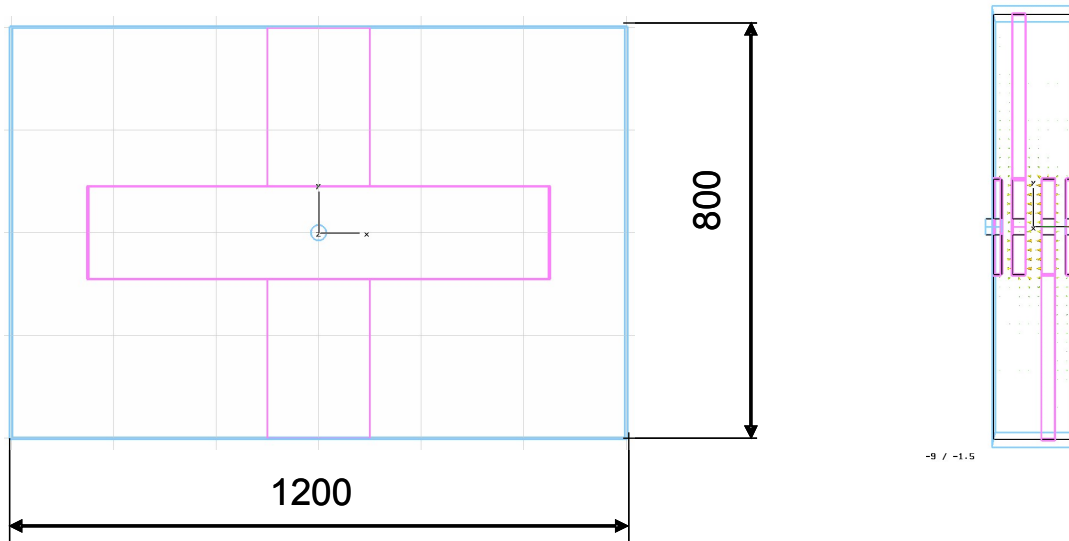


Figure 1. Plane and side views of the 3-gap IH resonator. The dimensions are in mm.

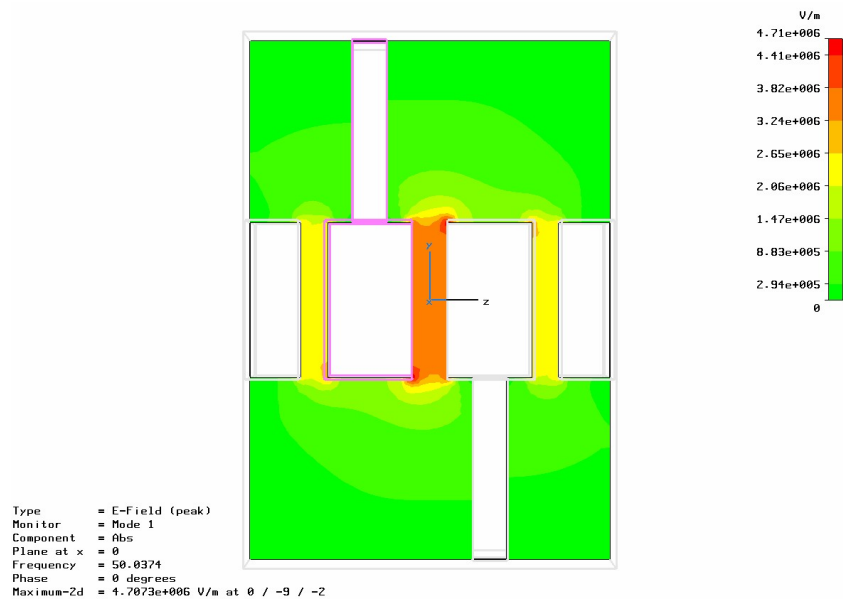


Figure 2. Side view of the 3-gap IH resonator designed for $\beta=0.01465$.

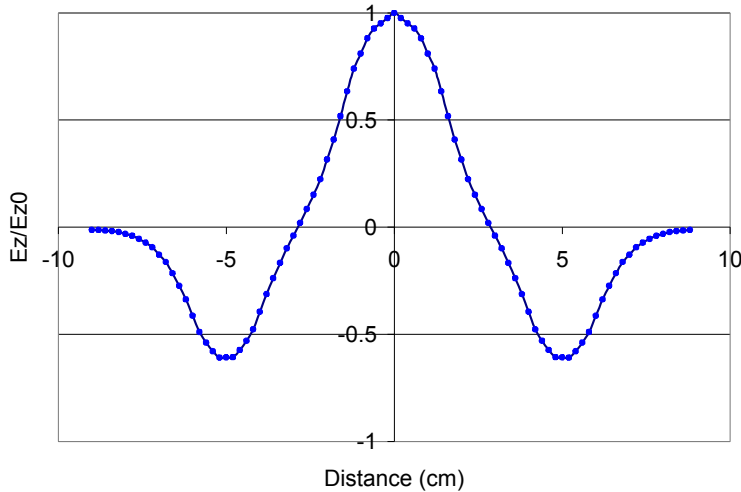


Figure 3. E_z along the resonator #1.

Design of the linac

The linac has been designed using TRACE-3D [2]. The main assumptions are:

- 1) Focusing by ~ 15 Tesla solenoids following each resonator;
- 2) Total voltage gain in each resonator is 1.2 MV. The voltage is limited by the peak surface field in the first resonator and beam loading in all other resonators;
- 3) Synchronous phase is $\varphi_s = -30^\circ$ except in the first two resonators where $\varphi_s = -40^\circ$.
- 4) For each of 16 beamlet the normalized transverse emittance (5σ) is 5π mm·mrad. Longitudinal emittance (5σ) is 5000 keV·deg.

Main parameters of the linac are given in Table 2

Table 2. Main parameters of the linac.

Beam	$^{20}\text{Ne}^{1+}$
Input energy	2 MeV, 0.1 MeV/u
Output energy	20 MeV, 1 MeV/u
Current	300 mA
Frequency	50 MHz
Length	8.6 m
Number of resonators	17
Voltage per gap	400-500 kV
Type of resonator	3-gap IH
Field in the solenoids	15 Tesla
Effective length of the solenoids	15 cm

Figure 4 shows TRACE-3D screen of the $^{20}\text{Ne}^{1+}$ beam simulation in the linac. Beam current is 300 mA. The input file for TRACE-3D is attached. The solenoids provide strong focusing with small beam envelope modulation. Beam radius is less than 15 mm. According to the TRACE-3D calculations 600 mA neon beam can be accelerated in the linac with the same setting of

solenoids. To obtain smooth beam envelopes the initial Twiss parameters should be slightly changed with respect to 300 mA case as is seen from Fig. 5.

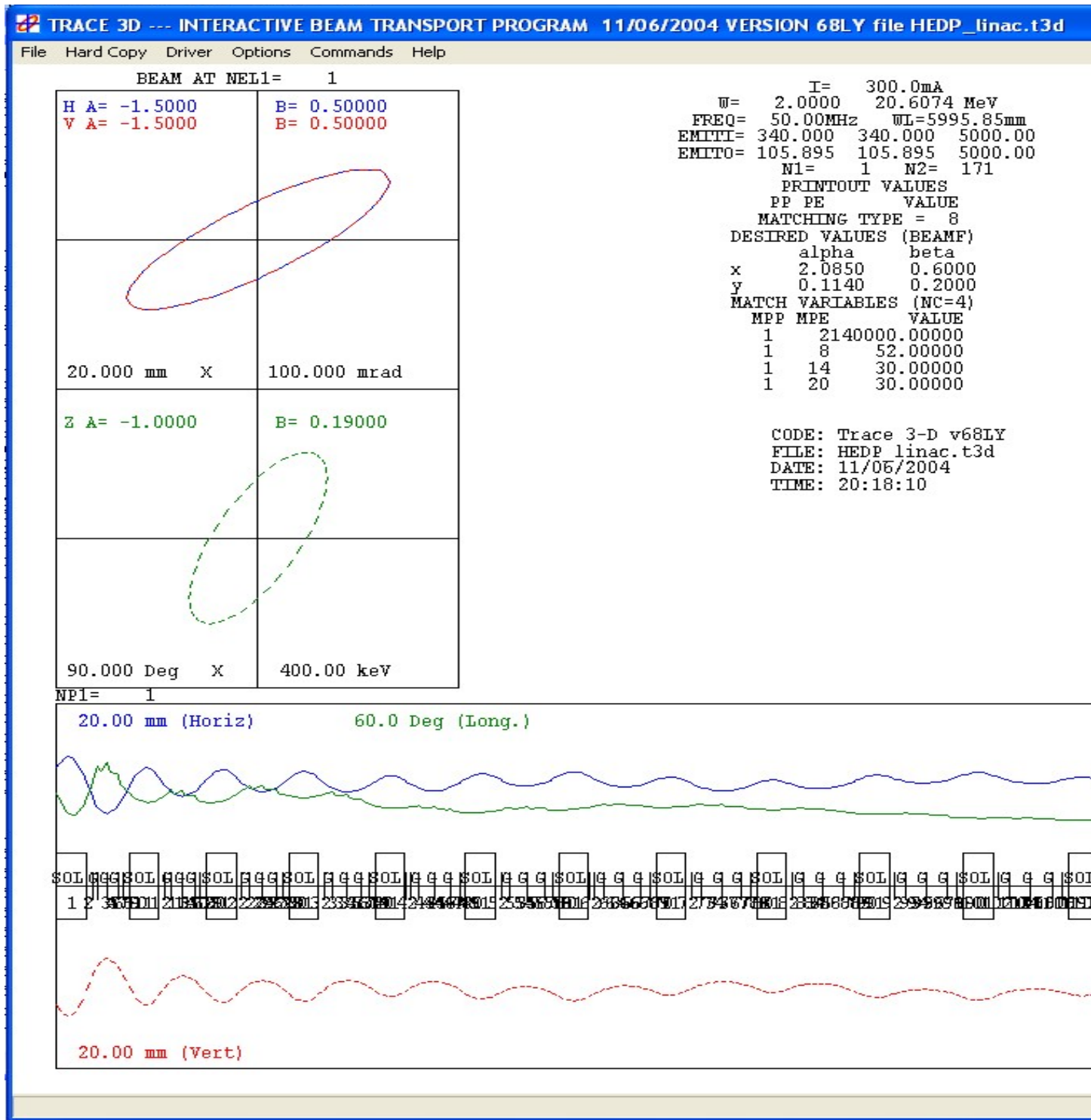


Figure 4. TRACE-3D screen of the linac lattice. Beam current is 300 mA. The blue curves show X-envelope, the red curves – Y-envelope and the green curves are the phase envelope.

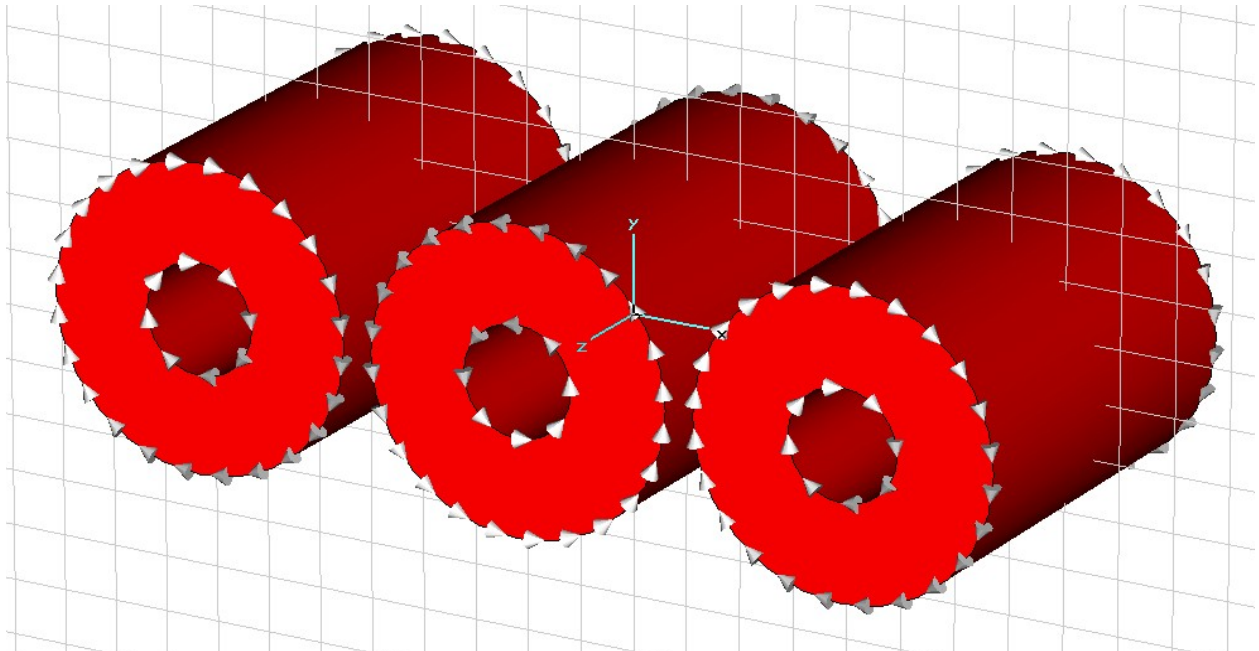


Figure 6. CST EM studio models of the solenoids.

Beam bunching

Bunching of high-current beam prior to injection into the linac can be performed using a standard “klystron” buncher technique. The buncher is a 3-gap IH resonator with total voltage 100 kV and located ~70 cm upstream of the first accelerating cavity. Beam dynamics simulations have been carried out for 100 keV/u 500 mA singly-charged neon beam. Fig. 7 shows evolution of the phase space plots along the buncher and drift space. Beam space charge prevents the effective bunching. However, 63% of a dc beam can be bunched into a phase width 100° as is shown in Fig. 8.

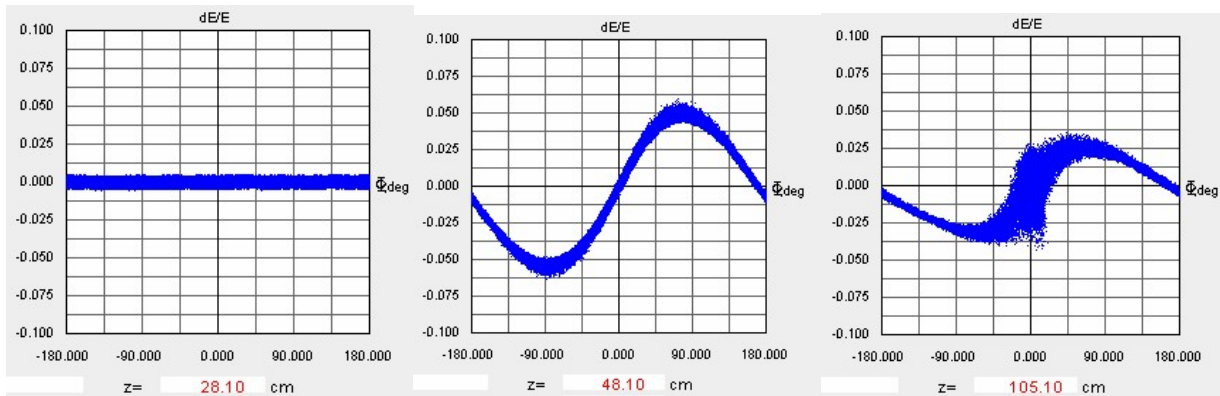


Figure 7. Longitudinal phase space plots of the beam during the bunching.

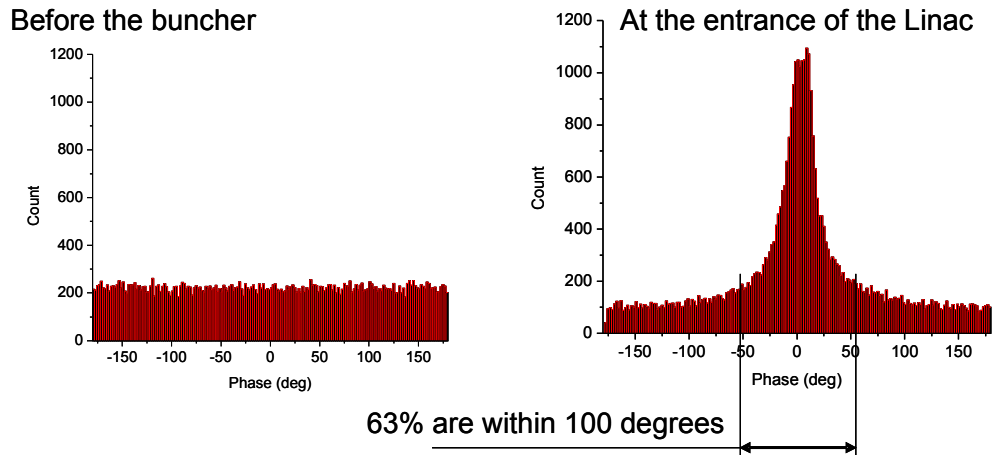


Figure 8. Bunch phase spectrum before the buncher and at the entrance of the linac.

Beam debunching

At the exit of the linac the beam pulse length is 200 nsec and consists of 10 short bunches. The time width of each bunch is ~ 2.2 nsec. The dynamics of the neon beam debunching in the drift space downstream of the linac has been simulated by the TRACK code [3]. The simulation has been performed using full 3D external and space charge fields. The solenoids were represented by 3D fields obtained from CST EM-Studio code. Figure 9 shows the phase space plots of the beam exiting the linac and post-linac 4.46 m transport system containing solenoids and debuncher. The energy spread of the beam is $\pm 1\%$. Due to strong space charge forces the beam energy spread increases in the drift space upstream of the debuncher. The debuncher is a 3-gap IH resonator with the voltage 0.7 MV. In this simulation the debuncher is a single-harmonic resonator operating at 50 MHz. Therefore the beam phase space plots show strong nonlinear shape of the beam longitudinal phase space plots as is seen from the bottom plots in Fig. 10. These non-linearity can be minimized using second and third harmonic debuncher resonators.

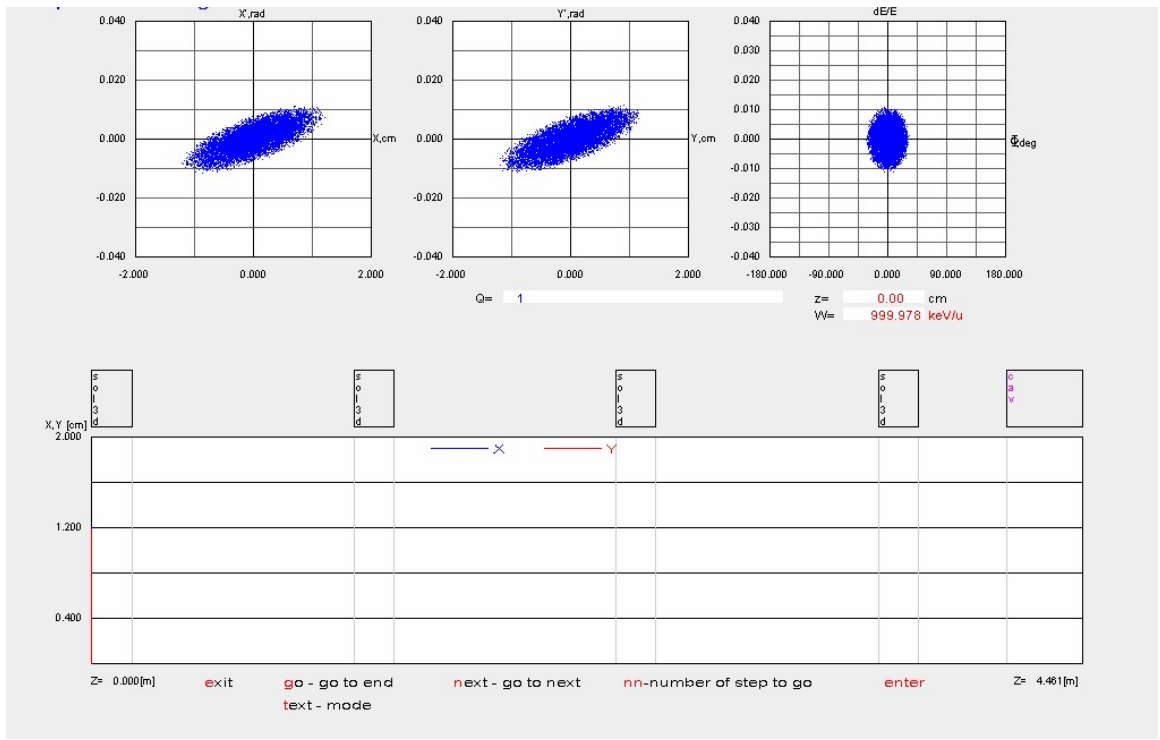
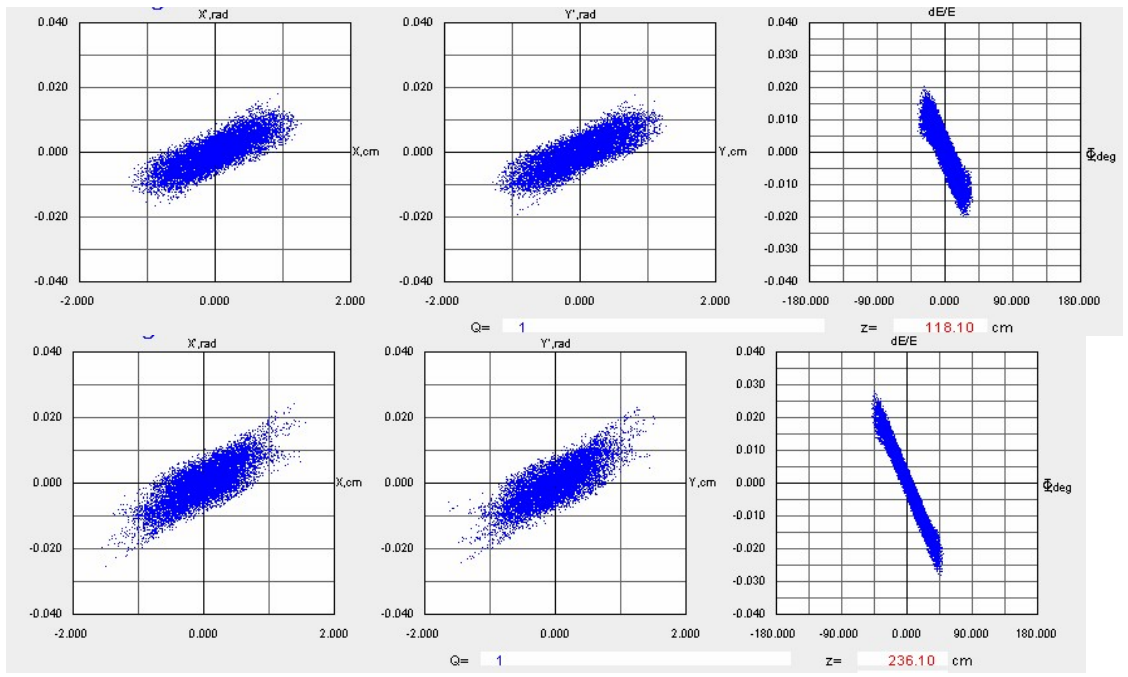


Figure 9. Beam phase space plots at the exit of the linac and transport line to the debuncher.



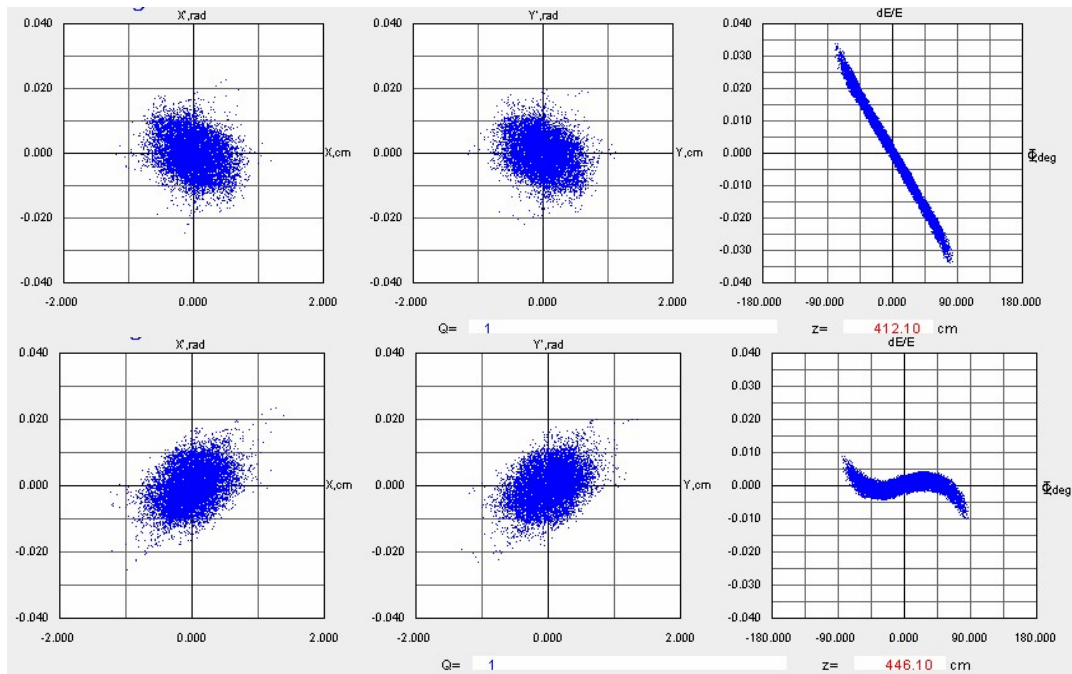


Figure 10. Evolution of bunched beam phase space plots in the drift space and effect of the debuncher.

Attachments

1. TRACE-3D input files for the linac (300 mA and 600 mA)
2. EXCEL file of the electric field distribution in the gap.

References

1. J.Broere et al. High Power Conditioning of the 202 MHz IH Tank 2 at the CERN Linac3. Proc. of the LINAC-98, p. 771.
2. K.R. Crandall, *TRACE 3-D Documentation*, Report LA-11054-MS, Los Alamos, 1987.
3. Ostroumov, P.N., Aseev, V. N., Mustapha, B., *Phys. Rev. ST. Accel. Beams*, Volume 7, 090101 (2004).

2.5 *An Accumulator/Compressor Ring for Ne⁺ Ions*

Weiren Chou

Fermilab, November 8, 2004

1. Observations

The primary goal of the High Energy Density Physics (HEDP) program is to create an extremely bright ion beam at low duty cycle. For example, a typical set of parameters is:

Particle type = Ne⁺

Ion energy = 20.1 MeV

One ion pulse = 1 μC, 1 ns, 1 mm²

Repetition rate = 1 Hz

This would give a volume density of $\sim 10^{12}$ particles/mm³, which is several orders of magnitude higher than any existing proton machines (typically $10^8 - 10^9$ particles/mm³, see reference [1]). On the other hand, however, the beam power is very low. At 20.1 MeV, 1 μC and 1 Hz, one has:

Beam power = 20.1 W

This leads to the following observation: *In an HEDP machine, beam loss is a non-issue.* This has important implication in the machine design. The machine is fundamentally different from those high power (\sim MW) proton machines such as PSR, ISIS, SNS, RIA, GSI and JPARC.

A second observation is that, as it stands now, the HEDP program has limited funds (several \$M). The hardware design needs to be as simple and as realistic as possible.

2. An accumulator/compressor ring for Ne⁺ ions

Rather than using an RF linac with 16 beam channels as suggested in an alternative design, we propose to use a ring that would require a linac with only one beam channel as the injector. It would accumulate a long linac beam pulse and compress it to a short pulse prior to extraction (just like in a conventional accumulator ring). The layout is shown in Figure 1.

The linac is assumed to be 50 MHz and a beam current 200 mA. The beam intensity is 2.4×10^{10} per bunch, which is similar to that of existing proton linacs. The beam normalized rms emittance is 1π mm-mrad. A train of 250 bunches for a total pulse length of 5000 ns (plus gaps) is injected into the ring in 20 turns. The beam is debunched and confined by two RF barriers.

The beam length in the ring is 250 ns, corresponding to a compression ratio of 20:1. After 20 turns, the beam would accumulate 6×10^{12} particles or about $1 \mu\text{C}$. The beam current is 4 A. It is then extracted from the ring and injected into an induction linac for an energy tilt, followed by neutralization and drift compression to about 1 ns in beam length. A straw man's ring parameters are listed in Table 1.

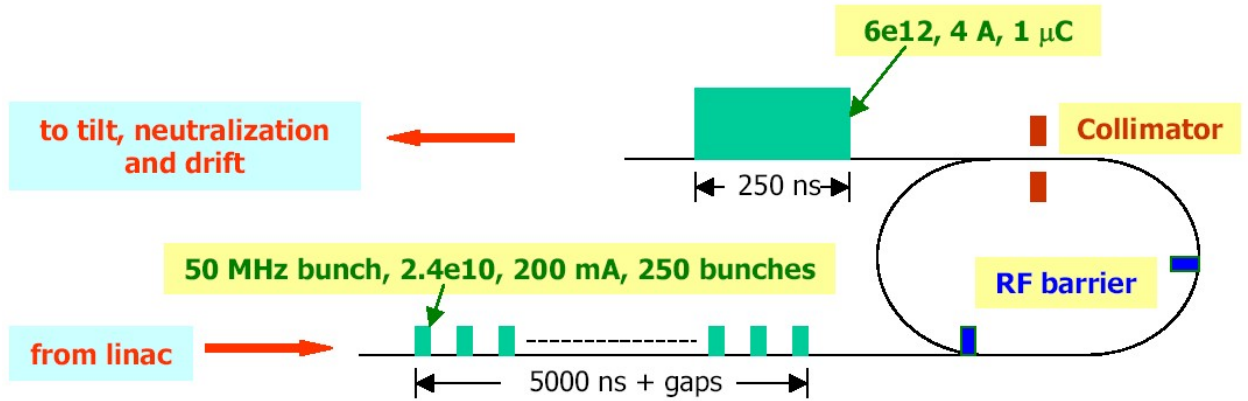


Figure 1. Layout of the accumulator/compressor ring

Table 1. Parameters of the accumulator/compressor ring

Particle	Ne ⁺
Mass number	20.17
Kinetic energy	20.1 MeV
Total energy	18.945 GeV
Momentum	0.872 GeV/c
β	0.046
γ	1.001
$B\rho$	2.91 T-m
Magnet	superconducting, combined-function
Bending field	4 T
Bending radius	0.73 m
Total magnet length	4.57 m
Ring circumference	8 m
Beam occupancy	3.45 m (250 ns)
Momentum spread	$\pm 0.2\%$
Debunching rate	± 0.5 ns per turn
Injection turns	20

Injected beam emittance	1π mm-mrad (normalized rms)
Accumulated beam emittance	6π mm-mrad (normalized rms)
Total number of ions	6×10^{12}

3. Discussions

The followings are a number of issues discussed at the workshop concerning the ring option:

1) Vacuum requirement:

Sessler and Yu estimated that a vacuum of 10^{-7} torr would be required for beam lifetime in the ring. This looks trivial when compared with the GSI storage ring, in which the vacuum reaches 10^{-11} torr.

2) Outgassing from lost ions:

Logan pointed out the lost ions could lead to outgassing from the pipe wall and shorten beam lifetime. This problem could be solved by installing a collimator (as shown in Fig. 1) for beam loss control.

3) Space charge:

The Laslett tune shift can be expressed as:

$$\Delta\nu = -\frac{r_p}{4m\beta^2} \frac{N}{\epsilon} B_f$$

in which r_p is the classical proton radius, m the particle mass relative to proton, β and γ the relativistic factors, N the total number of particles, ϵ the normalized rms emittance, B_f the bunching factor (peak current/average current). The tune shift is inversely proportional to the product of $m\beta\gamma^2$. For a 20.1 MeV Ne^+ ion, β is low. But this is largely compensated by the value of m , which is 20 times higher than a proton. Table 2 is a comparison of 20.1 MeV Ne^+ ion and Fermilab Booster 400 MeV proton.

Table 2. Comparison of 20.1 MeV Ne^+ ion and Fermilab Booster 400 MeV proton

	Ne^+	Fermilab Booster Proton
Kinetic energy (MeV)	20.1	400
m	20.17	1
β	0.046	0.713
γ	1.001	1.426
$m\beta\gamma^2$	0.93	1.45

N	6×10^{12}	6×10^{12}
ε (mm-mrad, norm. rms)	6π	3π
B_f	2.3	2.5
Δv	0.3	0.4

It is seen the space charge effect in the Ne⁺ ring is comparable to that in the Fermilab Booster. However, the duration of Ne⁺ in the ring is much shorter (20 turns, or about 10 μ s) than the protons in the Booster (19500 turns, or 33.3 ms). Therefore, the emittance dilution and beam loss should not be a problem.

4) Intrabeam scattering:

The emittance growth due to intrabeam scattering is slow and usually takes many turns. During a 20-turn circulation, this effect is negligible.

5) Energy tilt for drift compression:

To compress the beam longitudinally from 250 ns to 1 ns by drifting, the required energy tilt from the beam head to tail is $\pm 14\%$. This can be achieved by using an induction linac downstream from the ring.

References

1. W. Chou, O. Bruning, M. Giovannozzi and E. Metral, “*Summary Report of Session VI,*” Proc. ELOUD’02, CERN, Geneva, 15-18 April 2002, CERN-2002-001, p. 307.

2.7 *Alternate Structures*

John Staples, LBNL

Two alternate structures were presented to the workshop and subsequently not followed up as they were clearly inferior to the scenario developed using high-field superconducting solenoids and multigap accelerating structures. The two rejected scenarios are outlined here and further presented in Appendix A.

Structure 1: Conventional Alvarez Linac

This structure was developed as the tools for constructing a conventional Alvarez linac are well known and documented.

A 100 MHz frequency was selected for a Ne^{+1} structure ($q/A = 1/20$) with an electrical beam current of 200 mA to be accelerated. Focusing is provided through magnetic quadrupoles located in the drift tubes.

The linac generation parameters were:

Frequency	100	MHz
E_0	2.0	MV/m
aperture radius	2	cm
Quad length	0.5	drift tube length

In order to keep the quadrupole strengths down, a FFFDDD focusing sequence was assumed, and a 2 MeV injection energy (100 keV/n) was chosen, but even then, the quadrupole strengths at the beginning of the linac are 20 kG/cm, about a factor of 2 higher than obtainable with the best permanent-magnet quadrupoles.

The calculated length is 13 meters, containing 143 cells to accelerate the Ne^{+1} to 20 MeV total energy, for an average energy gain of 1.4 MeV/meter. The fraction of 200 mA input beam current surviving to the exit is 83%.

This rather conventional design is seen as inefficient, producing less than 200 mA at the end of a large (100 MHz), 13 meter long structure, requiring a high injection energy and very high gradient quadrupoles.

Structure 2: Single-bunch pulsed drift tube linac

This is essentially a very low-frequency structure where a single bunch is accelerated through a series of drift tubes, each pulsed by a trapezoidal-shaped voltage waveform, timed to provide a field in the gap between adjacent drift tubes as the single bunch

traverses the gap.

As this was entirely a study of longitudinal beam dynamics, no transverse beam dynamics, space charge or focusing systems were considered.

A high-voltage injector, 1 MV in this case, injects a Ne^{+1} pulse 100 nsec long into the first drift tube. As the bunch travels through the drift tube, its potential is raised by 500 kV, so the voltage across the following gap is 500 kV, which accelerates the bunch. After the bunch enters the second drift tube, its potential is raised by 500 kV and the acceleration process continues in the same way, through all the gaps in the structure until the final energy of 20 MeV is reached. Five centimeter gaps are assumed between each drift tube, for a gap gradient of 10 MV/m.

As the bunch is accelerated, longer drift tubes are required to contain the entire bunch. In addition, a 100 nsec risetime of the potential is assumed (5MV/microsecond pulser slew rate), which is added to the time the bunch must be contained in each drift tube. This risetime is a major contributor to the overall length of the accelerator.

It is possible to compress the bunch in the accelerator by applying a few percent tilt to the voltage pulse of each drift tube, which introduces a correlation between the bunch energy and position along the bunch. A reasonable scenario can achieve a compression of a factor of 5, producing a 20 nsec, 20 MeV beam at the end of the structure.

In Appendix A a spreadsheet design of such an accelerator is presented which comprises 30 drift tubes, each with its own 500 kV pulser that occupies a length of 57.7 meters. This length is dominated by the 100 nsec risetime of the pulsers, where the bunch must be contained within each drift tube, with the 5cm gaps and the total length of the bunch itself a lesser contributor.

Since this was only an exercise in longitudinal beam dynamics, the space charge limit of this scheme is unknown. The sheer length of the structure renders this approach undesirable, although it may be employed just after the gun, or prior to injecting into an IH-structure accelerator module.

2.8 *Areas of Future Development*

John Staples, LBNL

High-field superconducting solenoids may open up new opportunities in the development of high-current linear accelerators for heavy ions. Substantial fractions of an ampere may be accelerated, but to satisfy HEDP target requirements of 1 nsec, 1 kA type beams, further beam manipulation beyond the linac is still required. Parallel-beam structures or accumulator rings may be used to provide the total charge and, and some sort of ballistic compression, probably with the use of an induction core, will be needed.

Several areas of future development emerged from the preliminary strawman design:

Accelerator

A 0.2 ampere, 1 microsecond beam macrobunch extracts about 1 Joule from a 500 keV cavity, which is up to 10% of the stored energy of the cavity. IH-mode cavities have a relatively small stored energy to start with, as the fields are concentrated in the gap region. This may lead to stability or energy spread problems which must be addressed.

The large gap capacitance in the multi-gap structures considered require a large RF power and geometric factors may result in an uneven distribution of potential across the gaps of a multi-beam structure. Recent calculations by Ostroumov (private communication) show that in the 16-beam scenario, the potential across the drift-tube structure may vary by as much as 8%.

Engineering issues of compact high-field superconducting solenoids and issues of placing them close together. Even with alternating polarities, asymmetry of the field across the apertures may cause emittance growth in each beam.

The sheer number of components, particularly focusing elements in a multiple beam structure, is a drawback. Multiple-aperture solenoids may be a partial solution, if feasible.

Beam Compression and Transport

The beam dynamics in the ballistic compression region must be clarified.

Combining multiple beams at the target will be a challenge.

Beam Dynamics

What is the ultimate current limitation of such RF-linac devices? Optimization, including careful study of space-charge effects, needs to be done to determine if one can reduce the number of beams below 16 in the multiple-beam scenario.

Summary

In the near-term, theoretical studies of highly space-charge beam transport through the accelerating and focusing structures is needed. The longitudinal emittance growth issues that limit the ultimate compression ratio at the target must be addressed.

In the one-beam scenario with the stacker ring, growth of the energy spread of the bunches due to space charge and stacking scenarios must be addressed.

In the longer term, hardware modeling of appropriate injector, accelerator structures and focusing solenoids in multiple-beam arrays needs to be carried out.

Report from working group 3: multi-gap pulsed power

Alex Friedman and Richard Briggs

Introduction

This large working group discussed a wide range of topics, including a number of accelerator architectures that fall under the general heading of multi-gap pulsed power; general physics issues and constraints; and the interfaces to both injector systems and final compression/focusing systems. In addition, the group met with the Final Compression and Focusing group, organized a more detailed presentation by Craig Olson on the Ionization Front Accelerator (held jointly with the Experiments group), and enjoyed the participation of group members knowledgeable about single-gap diodes (a working group that had met separately, in advance of the main workshop).

This overview begins with a brief description of concepts for the injection of a beam with high line charge density. The approach currently being explored for near-term experimental tests on the NDCX facility at LBNL is the “accel-decel / load-and-fire” principle; a diode that uses magnetic insulation to forestall electron backflow across the gap is another possibility. Two accelerator concepts were examined in some detail. These were the Broad-Band Traveling Wave Accelerator (BBTWA) and the Drift Tube Linac (DTL). Two other approaches that have received recent study, the Multi-Pulse Induction Linac and the High-Gradient Induction Accelerator, were also considered in brief, but did not receive detailed examination during the workshop. This overview describes the first two of these approaches, and (more briefly) the latter two. Finally, a brief summary of a discussion on physics constraints is presented. The reader is referred to the summaries of many of these topics, to be found elsewhere in these Proceedings.

Injection at high line charge density

(Presentations were made by Enrique Henestroza and, as part of his plenary talk, Joe Kwan)

Two concepts for injection at high line charge density were presented during the opening day’s talk by Joe Kwan: a magnetically-insulated short-pulse diode and the “accel-decel / load-and-fire” principle. An illustration of one possible configuration for a magnetically insulated diode is shown in Fig. AAA.

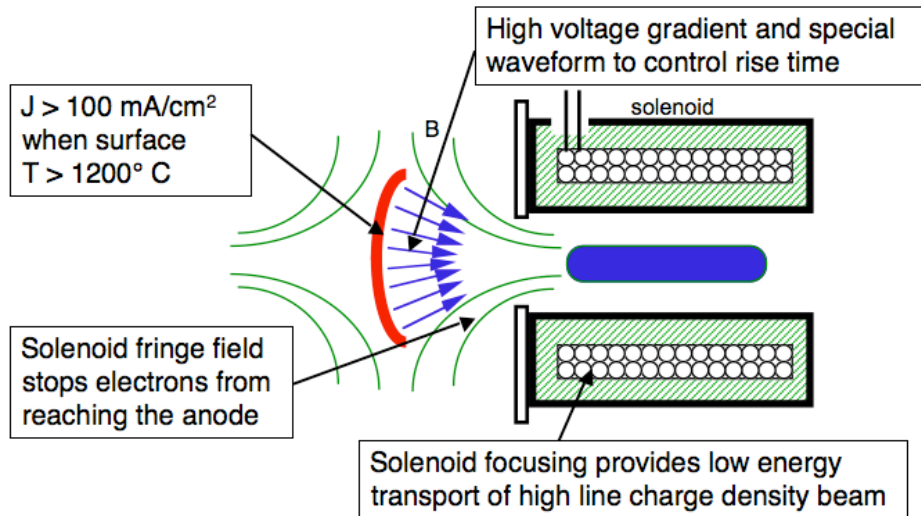


Fig. AAA. One concept for a short-gap diode employing magnetic insulation.

In the accel-decel / load-and-fire concept, a beam is accelerated in a high-voltage diode to obtain a large current; decelerated to a slow speed to obtain a high line charge density (in steady flow, the current is constant along the beam line); “loaded” into a solenoid; and finally “fired” downstream as a bunched beam, that is, accelerated all at once in a resistively graded column. A different load-and-fire approach, based on the helical-line traveling wave principle as described herein, was suggested at the workshop by Dick Briggs as an alternative worth analyzing in more detail. Additional analysis done after the close of the workshop proper indicates this option may have a number of advantages. By varying the waveform applied to the helix, a variety of initial pulse compression “tilts” may be imposed and tested experimentally, and more aggressive “early bunching” carried out.

The NDCX-1 experimental program at LBNL is intended to explore the physics of neutralized drift compression (in phase 1a, beginning concurrently with this writing), solenoid transport (1b, beginning in June of 2005), and accel-decel / load-and-fire injection (1c, beginning in October of 2005). The configuration of NDCX-1c as currently envisioned (it is still evolving) is shown schematically in Fig. AA, and a CAD rendering is shown in Fig. BB.

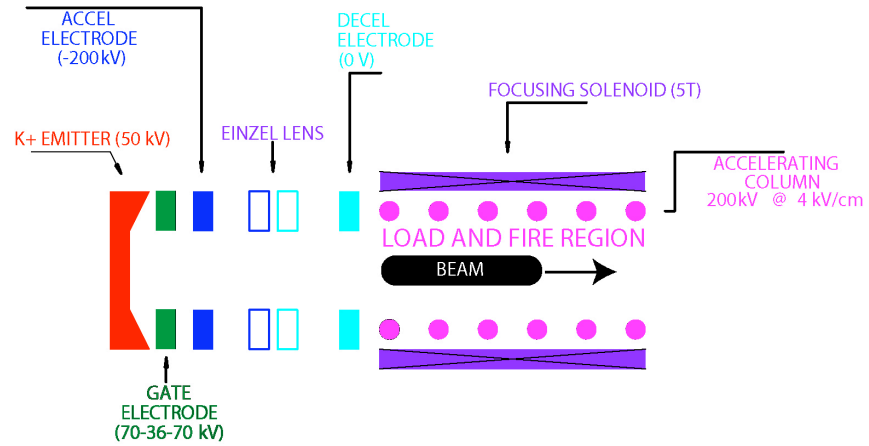


Fig. AA. Schematic of accel-decel / load-and-fire injector experiment on NDCX.

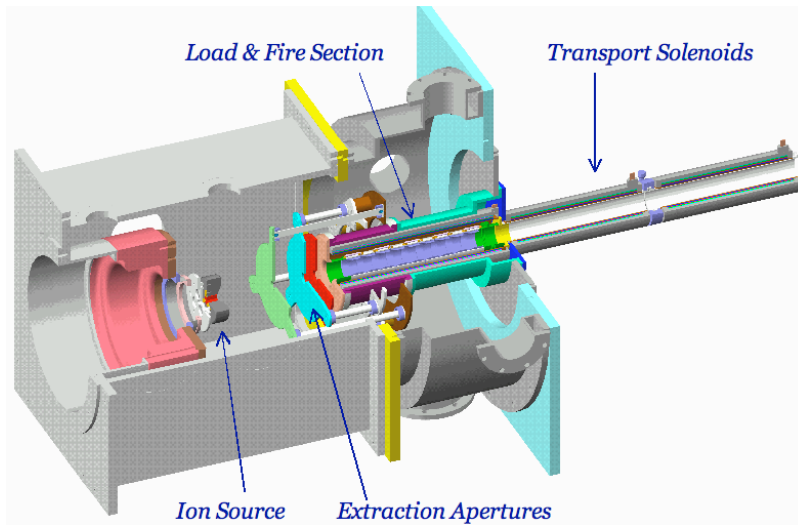


Fig. BB. CAD rendering of accel-decel / load-and-fire injector experiment on NDCX.

Simulations of the accel-decel / load-and-fire experiments are being carried out using WARP, and these were discussed during the working group's sessions. An example of such a simulation is shown in Fig.~CC.

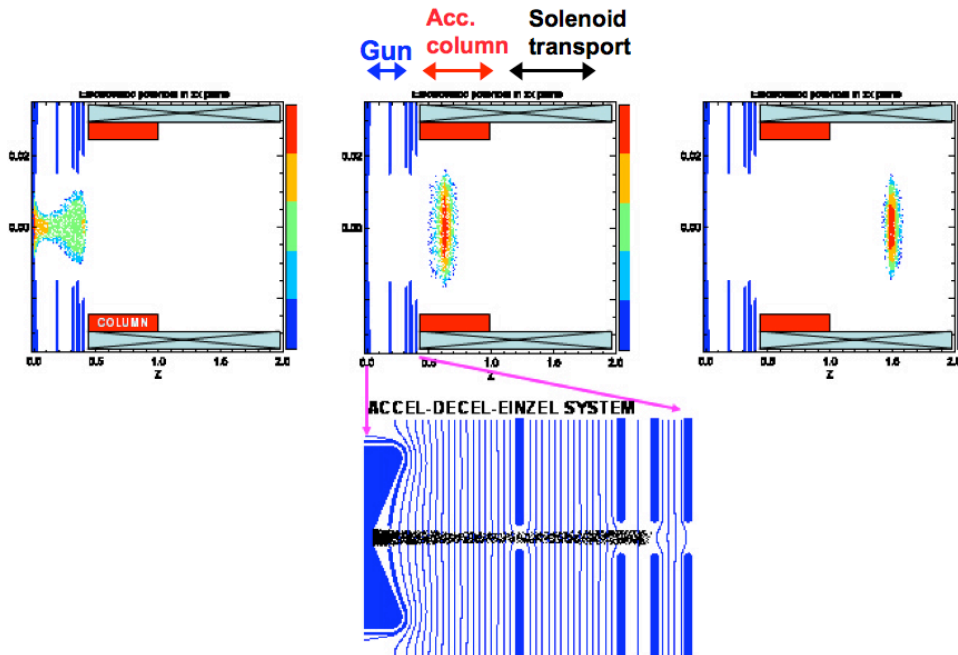


Fig. CC. WARP simulation of a possible NDCX-1c accel-decel/load-and-fire experiment

A topic of some concern to the working group was the question of how well matched transversely the beam head could be given that, in the ideal 1D case solved by Lampel-Tieffenback and independently by Caporaso, the beam head rises as a step function, so that particles at the head should experience half the transverse space charge defocusing force experienced by those in the body. Nonetheless, simulations indicate a well-behaved beam head. The resolution seems to be that the converging diode geometry and the unequal transit times of particles at different transverse positions conspire to generate a rounded beam head that is in approximate force balance. This is evident in the simulations, and can be seen in Fig. DD.

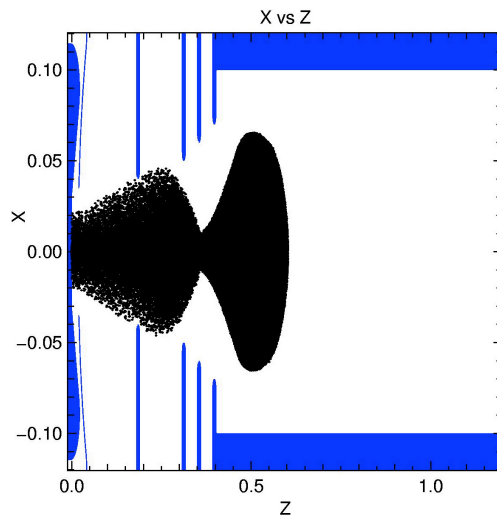


Fig. DD. WARPrz simulation of accel-decel process in possible NDCX-1c configuration with perveance $Q \sim 0.05$, 500 ns duration, 140 mA peak current, 50 keV K^+ , 0.05 μC , showing benign behavior of beam head.

Informal goals for NDCX-1c are: $Q = 0.05$; $I = 140$ mA peak; beam energy after accel-decel 50 keV; K^+ , $\lambda = 1/4 \mu C/m$; $\tau_{pulse} = 1/2 - 1 \mu s$ ($q_{tot} = 0.05 - 0.1 \mu C$). A resistive column 50 cm (5 T solenoid 60 cm) imparts (mostly) tilt; for the 200 kV column case, two cases were identified: (1) 180 keV head, 250 keV tail ($1/2 \mu s$, beam= 25 cm); (2) 50 keV head, 250 keV tail ($1 \mu s$, beam=50 cm).

Broad-Band Traveling Wave Accelerator concept

(Presentations were made by Dick Briggs, Scott Nelson, and Alex Friedman; the subgroup working on this topic consisted of Alex Friedman (chair), Dick Briggs, George Caporaso, Enrique Henestroza, Ned Birdsall, Will Waldron, and Yu-Juan Chen)

This concept is also referred to as a "Pulse-Line Ion Accelerator," as well as by other names. It is based upon the idea of launching a voltage pulse into a broad band slow-wave structure. If the line is sufficiently non-dispersive, a voltage pulse with a segment that rises linearly in time at the input end will become a linear ramp in space, corresponding to a region of constant accelerating field. The voltage pulse travels down the line with minimal deformation, and has the appearance of a solitary wave (though the governing equations of this system are linear). The beam pulse "surfs" on the traveling wave, experiencing a total energy gain that can greatly exceed the applied voltage. The current favorite for this slow-wave structure consists of a helical wire, inside a metal tube and embedded in dielectric material. The applied voltage waveform can be shaped so as to afford longitudinal confinement of the beam against its own space charge forces, and indeed to impart an inward compression to the beam in anticipation of neutralized drift compression. In the first stage, the pulse (and beam) may be moving as slowly as 1% of the speed of light.

A possible configuration is shown in Fig. EE, and one possible layout for an HEDP facility based on this principle is shown in Fig. FF.

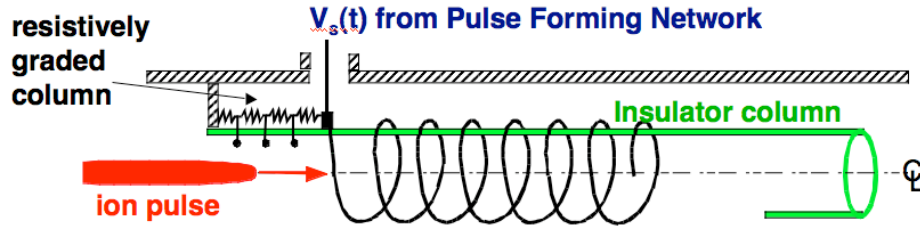


Fig. EE. A possible configuration for a Pulse Line Ion Accelerator.

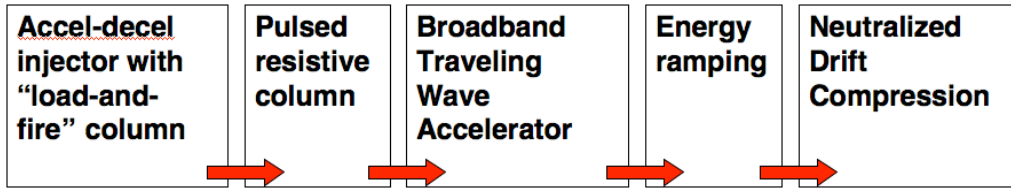


Fig. FF. One layout for a Pulse Line Ion Accelerator HEDP facility.

Success on NDCX-1 and on BBTWA helix tests now under way would offer a new opportunity for the NDCX-2 experiments, planned for the 2009 time-frame, to heat matter significantly. A BBTWA might be appended to NDCX-1, which could continue to use K^+ or could use Na^+ , instead of the He^+ considered for the induction-based nominal "reference design" HEDP/WDM user facility. The final energy of 20 MeV is less than that of the Bragg peak (~ 50 MeV), but the energy deposition at that lower energy is only down by 10-15%. Target heating to ~ 1 eV is estimated, for a focal spot radius less than but of order a millimeter.

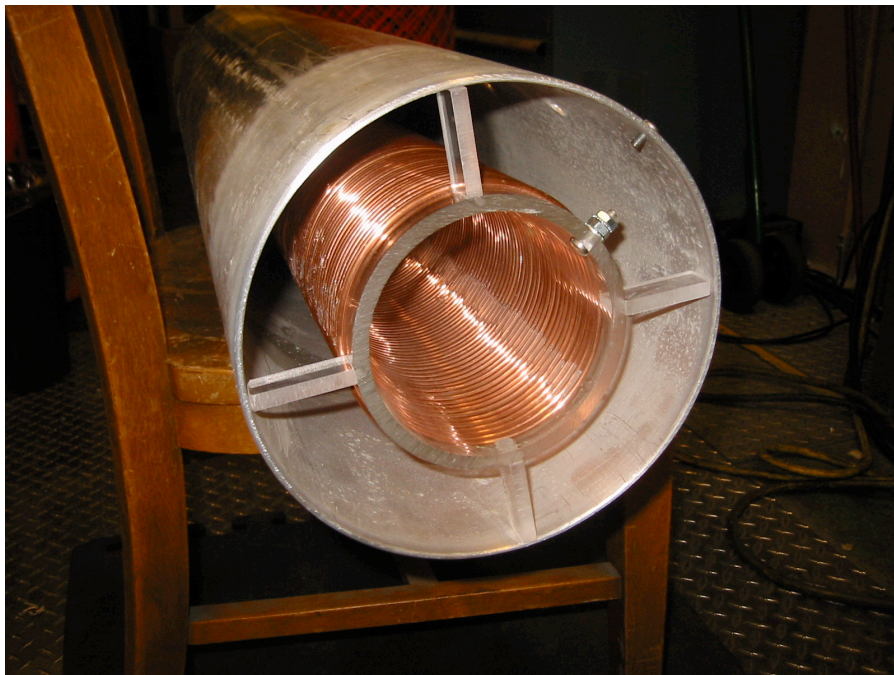
Such a system might use three segments of helix, each with a "tapered" line designed to track a factor-of-two gain in velocity. Other parameters are: $r_{beam} = 2$ cm, $a_{helix} = 4$ cm, $b_{wall} = 10$ cm, ± 450 kV drive (not all usable for beam), $l_{beam} = 15-20$ cm, voltage ramp over 30 cm (implying acceleration at 3 MV/m). Note that the voltage waveform can impart "tilt" in the helix (in addition to any imparted by the upstream system); longitudinal space-charge blow-up is controlled by this "tilt" as well as by "inertia" (the rapid acceleration implies a short residence time). The system would be ~ 8 m long, and the cost appears to be attractive; helices are inexpensive, and commercial solenoids are available at $\sim \$2M$ for a 5-T system of the required length.

For the "reference" HEDP facility itself that would follow, one possibility is a 20 MeV Ne^+ beam with total charge of $1 \mu C$, in a parabolic-profile bunch with length constant at 30 cm, and a peak line charge density of $5 \mu C/m$. The beam radius would be 3 cm, and 9-T solenoids would afford transverse confinement. The helix radius would be 6 cm, leading to peak voltages of ± 750 KV, and a peak radial stress of 125 KV/cm in a bore tube of diameter 30 cm. The peak axial space charge field would be ± 0.8 MV/m, and the acceleration gradient (and vacuum stress along the insulator column) 5 MV/m.

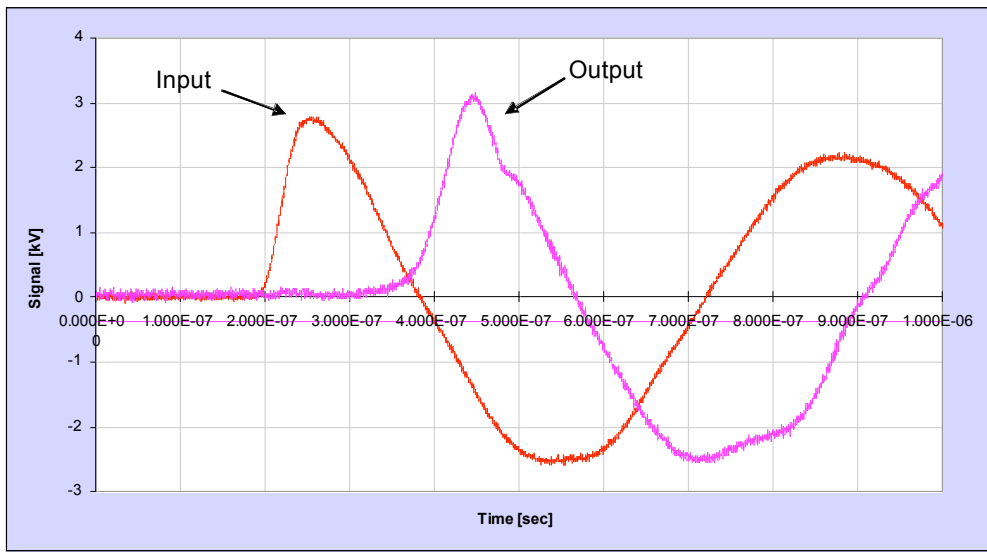
Several final bunch compression and focusing options can be considered for a Pulse Line Ion Accelerator based system. In such a system, the final tilt is imposed by the last helix segment; the 30-cm pulse implies a short neutralized drift compression section a few meters in length. The perveance at the 20 MeV output end is of order 2×10^{-3} . Three options (roughly in increasing order of aggressiveness) are: (1) Helix -> Strong Solenoids -> Dipole -> Stripper to +7 -> Neutralized Drift Compression (NDC) at 1 T (match from ~ 3 cm to ~ 1 cm radius for NDC) -> 15 T Solenoid -> Target; (2) Helix -> Dipole -> Optional Stripper -> Graded-solenoid NDC (beam radius reduced gradually during NDC, no matching section) -> 15 T Solenoid -> Target; and (3) Helix -> Graded-solenoid NDC (plasma builds up along line, gradually) -> 15 T Solenoid -> Target.

Both experimental and theoretical / simulation studies of helical-line ion acceleration principles are underway. Low voltage models have been constructed to test the propagation of ramped pulses, and to measure the dispersion in the frequency domain.

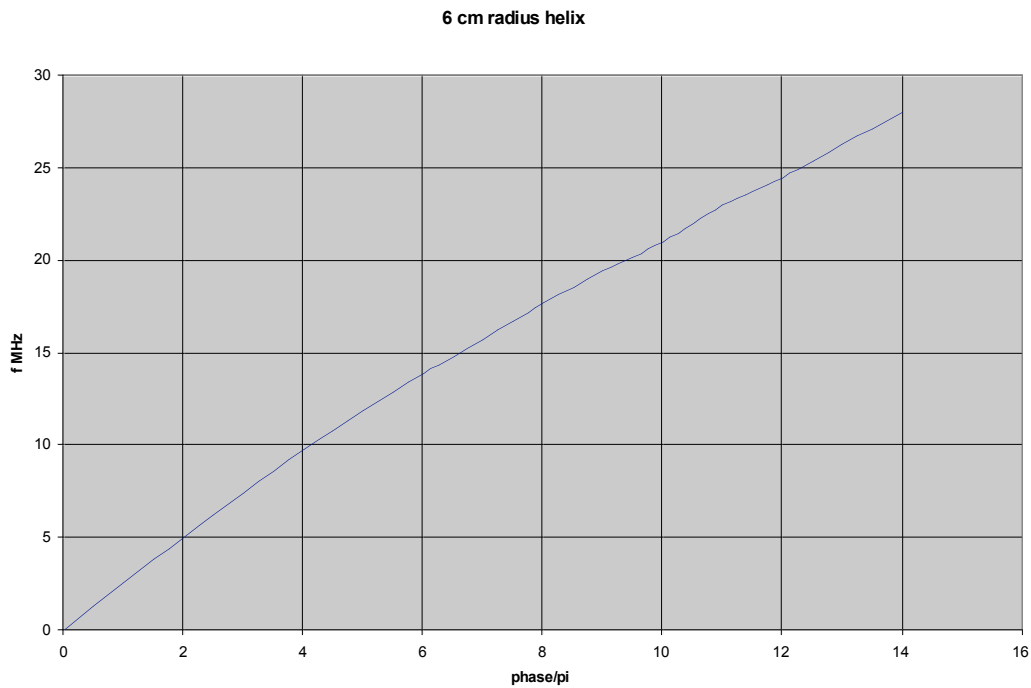
The first model constructed is shown in the picture below. The 6 cm radius, 0.9 meter long helix is wound using copper wire with a diameter of 0.1" and a spacing of 0.1" between the wires (wire to wire period of 0.2"). The helix is mounted on a plastic cylinder centered inside a 10 cm radius metal cylinder, with air as the dielectric media. It was terminated in a resistor that was varied to get what looked like the best match, which was about 1.5 K ohm vs a calculated characteristic impedance of about 1.9 K ohm.



The propagation of a pulsed voltage ramp through the 0.9 meter long helix is shown in the figure below. The delay time from input to output is as expected with a propagation velocity $\sim 4.6 \times 10^6$ m/sec.



To more accurately quantify the dispersion properties of the helix, measurements were made in the frequency domain with a network analyzer of the phase difference between the output voltage and input voltage vs frequency.



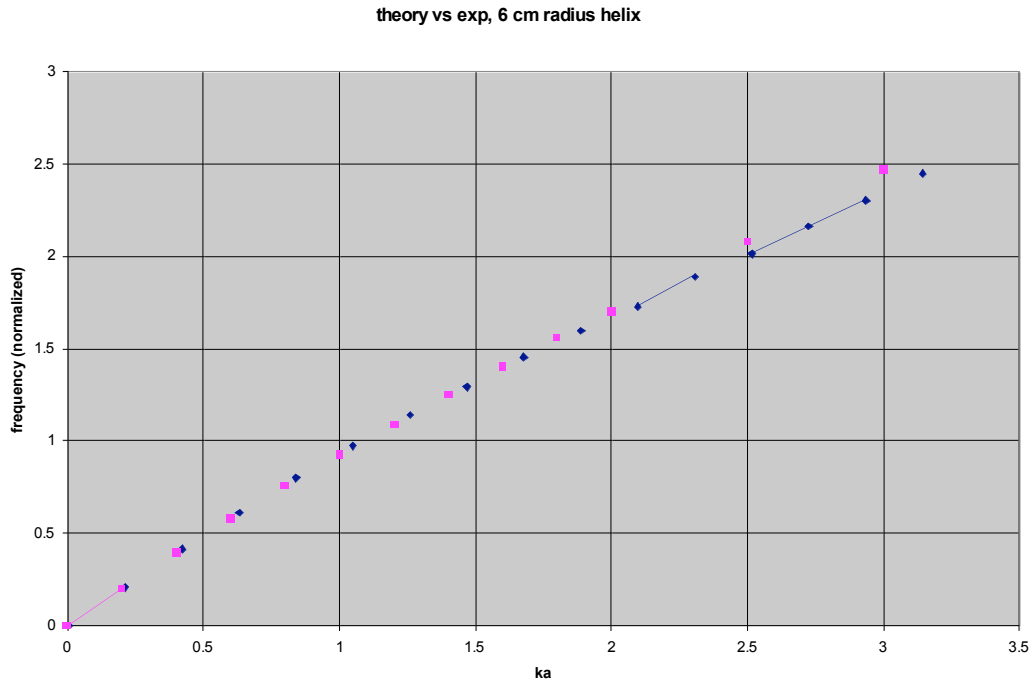
To compare with a sheath helix model, we normalize the frequency as $\omega a / v_0$, where from the measurements of the slope at low frequency the low frequency phase velocity is

$$v_0 = 4.6 \times 10^6 \text{ m/sec}$$

We then plot this frequency vs ka , where

$$ka = \left(\frac{\phi}{\pi}\right)\left(\frac{\pi a}{\text{helix length}}\right)$$

The results are shown below, where the data is blue, and the theoretical prediction of the dispersion using a sheath helix model for this configuration is red.



On the modeling front, Scott Nelson is using a 3D Finite-Difference Time-Domain code package to solve for the electromagnetic fields in a helical line via a “first principles” solution of Maxwell’s equations. Another, by Alex Friedman, is using a circuit model to compute the response to an applied voltage waveform, then tracking marker particles to quantify the output energy spread. The plan is to use these methods in tandem, cross-validate them and validate them versus experimental measurements, then to feed the resulting accelerating fields into WARP for fully self-consistent simulations including space charge effects (the influence of the beam back on the circuit is minimal in these small systems).

Drift-Tube Linac concept

(A presentation was made by Andy Faltens; the subgroup working on this topic consisted of Andy Faltens (chair), Peter Seidl, and Steve Lund)

This concept is among the first that had been considered for the Heavy Ion Fusion application, and has a rich history. Indeed, one of the earliest experiments carried out used three “tanks” of a DTL to generate a 2MV, 1A, Cs⁺ beam with line charge densities of 0.5-1 $\mu\text{C}/\text{m}$. Various transverse focusing schemes were considered, and the configuration evolved from solenoid focusing, to aperture focusing, to aperture focusing with grids to short the defocusing fields at the gap exits, to a similar concept with shaped grids, to electrostatic quadrupole focusing, to multiple-beam electrostatic quadrupole focusing. It is noteworthy that, when grids were employed, copious electrons added to the focusing significantly. This experiment is depicted in Fig. A.

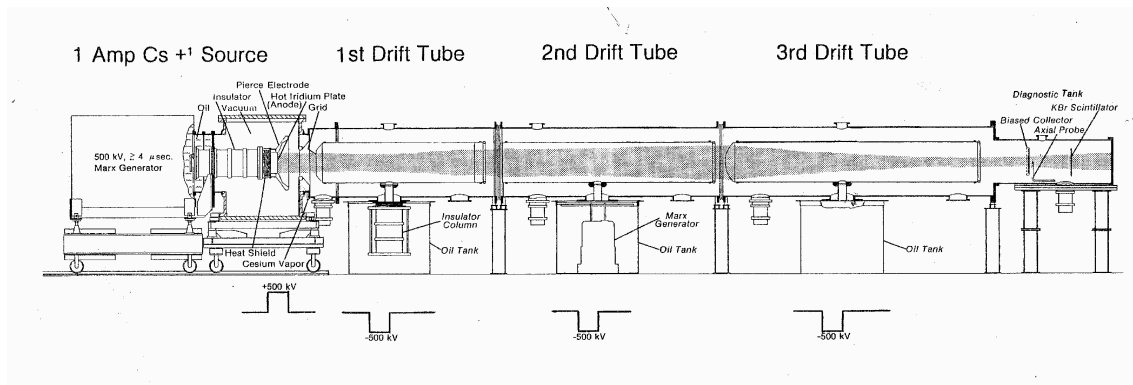


Fig. A. Layout of original drift-tube linac based experiment at LBNL.

The “baseline” HIF concept employs a long initial pulse of ten microseconds or more to obtain the requisite number of ions for target implosion, implying that such a DTL-based fusion system would use long electrodes and so offer a low accelerating gradient; indeed, that consideration led the program toward DC injector architectures such as the Electrostatic Quadrupole (ESQ) injector now used on HCX. For the HEDP accelerator application, which requires only a short pulse, the concept may be especially attractive, with shorter tanks and a larger gradient.

A number of variations are possible, ranging from a system with multiple compact beams launched by multi-beamlet injectors, to one with much larger sources. Since the voltage pulses do not require that ferromagnetic cores surround the beams, the system cost is expected to be quite insensitive to the transverse cross-sectional area of the beam transport system, in marked contrast to a multi-beam induction linac.

One variation of an HEDP accelerator uses multiple beams inside each drift tube, injected initially from compact sources at 750 keV and transversely confined by electrostatic quadrupoles. See Fig. B. This system uses transport lines similar to those of HCX: $L_{\text{half-period}} \sim 50 \text{ cm}$; $L_{\text{electrodes}} \sim 30 \text{ cm}$; $\lambda \sim 1/4 \mu\text{C}/\text{m}$; beam semi-axes $\sim 1 \text{ cm}$ and 1.5 cm ; $I_{\text{beam}} \sim 1 \text{ A}$; $J_{\text{source}} \sim 100 \text{ mA} / \text{cm}^2$; 100 ns flat-top, 100-200 ns beam head, and 100-200 ns beam tail; drift tube switching time 100-200 ns; drift tubes 1-2 m long.

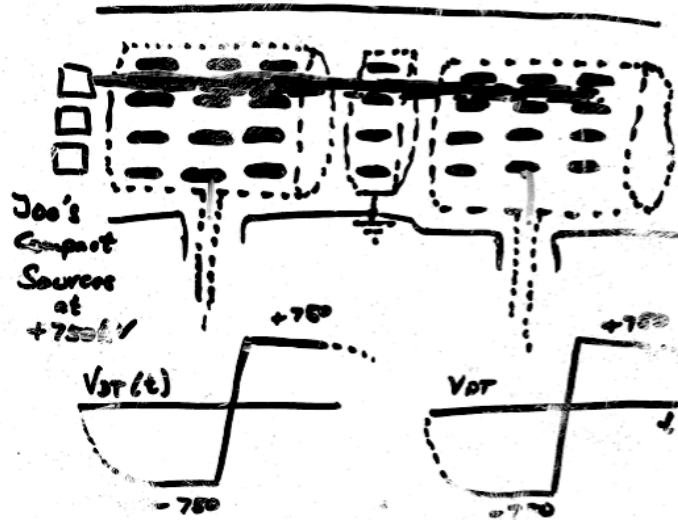


Fig. B. Multi-beam DTL configuration

For final compression, a velocity “tilt” is imparted by the final drift tube. For a constant bunch length scenario, T_p has decreased as $1/E^{1/2}$. Also, $T_p \approx 30$ ns, *e.g.* $\Delta V/V \approx (1 \text{ MeV})/(10 \text{ MeV})$, $\Delta v/v \approx 1/20$, and a longitudinal focus in 20 bunch lengths, or 6 meters. The large tilt would imply a significant chromatic variation of the focal spot with time. This can be avoided by deflecting the beam using time-dependent dipole fields imparted by a pulsed high-voltage deflector; it could be tapped off of the same pulser that imparts the tilt. See Fig. C.

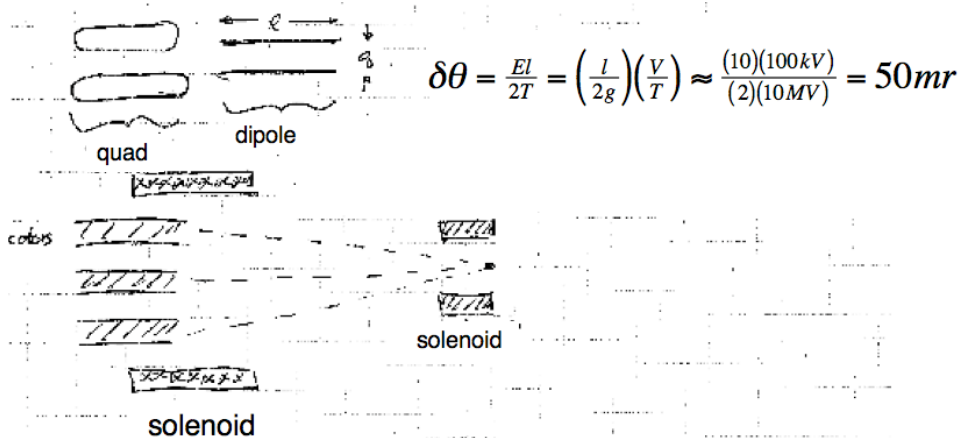


Fig. C. Focusing for DTL example.

The group also discussed briefly a related concept, the resistively-graded column. In such a system, and in contrast with a DTL, the beam spends very little time “coasting.” The ESQ injector is of this nature, as might be the column in a load-and-fire system.

High-Gradient Induction Accelerator concept

(A presentation was made by George Caporaso)

In this concept, a planar stack of blumleins inside a ferromagnetic core functions as a voltage adder. The concept takes advantage of newly available technologies: strip-line materials with dielectric constants up to 45 and high-gradient insulators. The goal is an accelerating gradient of 3-5 MV/m. At present, it appears that the accelerating waveform will be set by the geometry (it is not tunable), and the existing concept is limited to pulses of 20-40 ns duration; the latter may be stretched somewhat by the use of spiral lines. The fast switches needed for this concept are still in development.

Multi-Pulse Induction Linac concept

(A presentation was made by Grant Logan)

Replace long injected bunch with many short pulses into load and fire section, drive induction cores with smaller volt-seconds repetitively with fast-reset pulse-forming networks (PFNs). Tailor $\lambda(z)$ and waveforms for continuous acceleration and compression to desired pulse train with velocity tilts into neutralized drift region for longitudinal merging. See Fig. X.

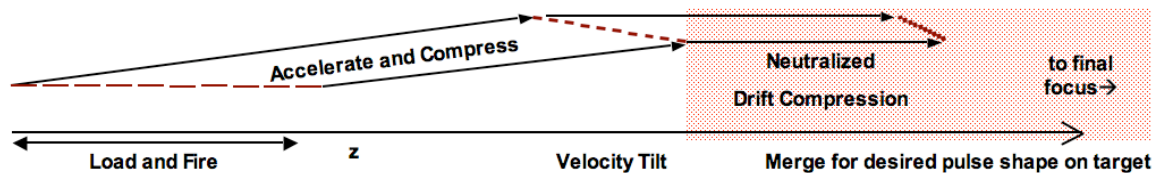


Fig. X. Multi-pulse induction accelerator with a sequence of high line charge density beam pulses, using solenoid focusing

Constraints: For any linac, minimum length for last pulse to catch up to first pulse. Longitudinal invariant limits input pulse train length for acceptable momentum spread on target. Achromatic focusing (Lee) or assisted pinches (Yu) accept higher momentum spreads \rightarrow longer input pulse trains allowed.

Potential Benefits: For any linac, multi-pulsing reduces upstream λ , perveance. Allows more pulse shaping and data sampling on target per shot. *For induction linacs, multi-pulsing increases acceleration gradients (due to shorter pulses). Lower core mass (volt-seconds) savings offset higher pfn network costs.*

Preliminary conclusions from the multi-pulse study were:

- Multi-pulsing up to 5-20 pulses appears feasible under “conventional” (but still-to-be-determined) longitudinal momentum spread limits, and induction gradient limits.
- For reasonable maximum core radial builds (V-s/m limits) minimum induction linac lengths for tail pulse to catch up to the head pulse will likely be $\sim 2-3$ x longer than for single pulse cases for short pulse HEDP cases, *but comparable for longer pulse IFE cases.*
- Multi-pulsing can lower total linac core volt-seconds and peak line charge densities by a factor roughly $\sim N_p^{1/2}$, for the same total delivered beam energy.

- Fast-reset pfn network costs need to be evaluated. If future fast switching costs go down, multi-pulsing is likely to reduce total costs, while enhancing target pulse shape capability.
- Gas and electron cloud effects for multi-pulses need to be evaluated. (Total beam charge \sim same, load-in times longer, peak line-charge densities lower with multi-pulses compared to single pulse)

Physics Constraints

(Presentations were made by Roger Bangerter and Steve Lund)

For all these concepts, both the transverse and longitudinal phase-space “budgets” must be carefully monitored. For one HIF driver case using neutralized drift compression, LSP simulations to date show a 20 MeV energy spread acceptance in compression and focusing; thus, with a 5 ns pulse length, the longitudinal admittance is of order 0.1 eV-s. The source temperature of order 1 eV, when boosted and multiplied by the 20 microsec initial pulse duration, gives an emittance of order 0.1 eV-s, so that this case is on the edge of feasibility. A similar estimate for the BBTWA HEDP case described above shows that the parameters are within the acceptable range based on this one consideration, but without a large safety factor. Waveform errors of \sim 1% can be significant.

In addition, beam mismatch must be kept to acceptable limits; this constrains the rapidity with which energy “tilt” can be applied, and other transitions effected. Recent work has clarified these constraints.

List of Participants in Working Group 3

(Not all were present at the same time)

Dick Briggs (co-chair)

Alex Friedman (co-chair)

Roger Bangerter

Santiago Bernal

Frank Bieniosek

Ned Birdsall

George Caporaso

Christine Celata

Yu-Jiuan Chen

Shmuel Eylon

Andy Faltens

Enrique Henestroza

Bill Herrmannsfeldt

Igor Kaganovich

Joe Kwan

Grant Logan

Steve Lund

Scott Nelson

Craig Olson

Lou Reginato

Tim Renk

Prabir Roy

Peter Seidl

Will Waldron

**Workshop on Accelerator Driven High Energy Density Physics
LBNL October 26-29, 2004**

Report from the working group on Single-Gap Pulsed Power

Craig Olson, Paul Ottinger, and Tim Renk

Introduction

A Pre-Workshop was held at SNL on October 19, 2004 to discuss the use of Single Gap Pulsed Power to produce ion beams for accelerator driven HEDP. Many who participated in this Pre-Workshop could not attend the main Workshop, so this was a valuable mechanism to get input from the "Single-Gap Pulsed Power" community. In the following, a summary of the results of this Pre-Workshop is given - including general comments on single-stage ion diodes, possible facilities for single-stage ion diode experiments, and an introduction to the Ionization Front Accelerator (IFA). Then, proposals are given for (1) possible single-stage ion diode experiments for HEDP, and (2) possible IFA experiments for HEDP.

Summary of the Pre-Workshop on Single-Gap Pulsed Power

The Pre-Workshop at SNL on October 19, 2004 included input from the following:

SNL	NRL	ATK-MRC	UNM	Cornell
Craig Olson	Paul Ottinger	Dave Rose	Stan Humphries	John Greenly
Tim Renk	Jess Neri	Dale Welch		(by telephone)
John Maenchen	Bruce Weber			
Steve Slutz	Frank Young			
Mike Desjarlais				

The purpose of the meeting was to review the HEDP requirements as per the HIF-VNL documents, and then assess the utility of various pulsed power, single-gap accelerators to reach the HEDP goals. Possible accelerators considered were:

- (1) Gamble II at NRL
- (2) Mercury facility at NRL
- (3) RITS facility at SNL
- (4) RHEPP/MAP facility at SNL
- (5) High impedance ion diode with no requirement on efficiency
- (6) IFA

(Note that Sabre at SNL and Cobra at Cornell were not considered because Sabre has been disassembled, and Cobra has been converted to a z-pinch driver.) Of course, any of these facilities might be used directly, or the accelerator concept could be developed into an accelerator that could be constructed at LBNL if desired.

First, it should be noted that pulsed power accelerators have been used for a long time for HEDP. In Table 1, a brief summary of HEDP examples from pulsed power facilities

is given. With these approaches, matter has been heated up to temperatures exceeding 200 eV. More importantly, the pulsed power community has developed considerable expertise in diagnosing hot dense matter in a harsh environment. Some of this diagnostic expertise may be useful for the HIF-VNL in developing accelerator driven HEDP.

Table 1. HEDP examples with Pulsed Power facilities

electron beam - rod pinch on Gamble II	25 eV
ion beam (D): PRD on Gamble II	15 eV
ion beam (p): (diode on Sabre)	30 eV
ion beam (Li): (barrel diode on PBFA II)	60 eV
ion beam (p): (short focus on Kalif)	several 10's eV
x-rays (double-pinch target on Z)	70 eV
x-rays (dynamic hohlraum on Z)	215 eV

Throughout our discussions, several questions arose concerning the charge to the group. Some of these questions were recurring, so we wanted to pose them to the entire group. These questions are:

1. If the first 1 ns of the ion pulse meets the requirements, can the actual ion pulse be longer? (i.e., is it acceptable to leave the beam on longer).
2. Why does it need to be repetitive? Why have multiple chambers? Aren't the HEDP experiments intrinsically single-shot experiments?
3. The neutralizing plasma near the target was listed as having a density requirement $\sim 10^{12}/\text{cm}^3$, but shouldn't it be much higher (since the ion beam density near the target will be $\sim 3 \times 10^{14}/\text{cm}^3$)?
4. Why have only 5 m total length (since this will require a huge velocity tilt)?
5. Is enhanced ion stopping being considered (since it was not mentioned in the paper)?

Lastly, the desired nominal ion beam parameters that we considered were:

$$\begin{aligned}
 &19 \text{ MeV Ne}^{+1}, \quad N \sim 1.4 \times 10^{13}, \quad t \sim 1 \text{ ns}, \quad r_{\text{spot}} \sim 1 \text{ mm.} \\
 &\text{energy/nucleon} \sim 1 \text{ MeV}, \quad I_{\text{particle}} \sim 2.2 \text{ kA}, \quad \beta \sim 0.05, \\
 &\text{ion pulse length} = \beta ct \sim 1.5 \text{ cm}, \quad \text{total ion bunch energy} \sim 36 \text{ J}
 \end{aligned}$$

For the ion diodes used in the light ion fusion program, high diode voltages and small anode-cathode gaps (required to maximize the ion current density possible) meant that there would always be electron emission from the cathodes. Therefore, the pulsed power ion diodes used for light ion fusion were all designed to minimize the electron current to the anode to achieve high efficiency. This was accomplished by preventing the electrons from reaching the anode for as long as possible. This led to several diode types [reflexing-electron diode, magnetically-insulated diode (with external magnetic field coils), and pinched electron beam diode]. For the "barrel-diode" geometry used on PBFA, several schemes were devised, including the radial applied B diode, the AMPFION diode, the hybrid diode, and the pinch reflex diode. This culminated in the applied B, extractor diode used on PBFA that produced 50 kJ of Li ions. A comparison of the beam from this PBFA-X diode with the parameters needed for a high-yield (HY)

fusion driver beam are summarized in Table 2. Note that the microdivergence required for the HY case was 6 mR (assuming ballistic transport) and 12 mR (assuming channel-like transport).

Table 2. Parameters achieved on PBFA-X, and parameters needed for a High-Yield Facility Li ion beam.

Parameter	PBFA-X	HY Li ion beam
Diode voltage	10 MV	30 MV
Ion current	0.3 MA	1 MA
Ion Power	3 TW	30 TW
Ion pulse length	15 ns	40 ns
Ion energy	50 kJ	1.2 MJ
Ion micro-divergence	22 mR	6-12 mR
Ion current density at source	0.6 kA/cm ²	1-2 kA/cm ²

The key issues that were uncovered in ion beam generation using high-power single-gap ion diodes in the light ion program were microdivergence, parasitic load, and impedance collapse. Microdivergence: if the transverse beam temperature associated with the microdivergence of 22 mR achieved with a passive ion source on PBFA-X held constant as the voltage increased from 10 MV to 30 MV, then the microdivergence would scale to 12 mR for a HY driver - exactly as needed. Therefore, it could be argued that the microdivergence was essentially within reach for a HY driver. Parasitic load: A more serious problem was that the desired Li beam was only the initial and small part of the total ion beam produced. Further work on creating a pure Li ion source was needed. Impedance collapse: The desired diode electrical behavior was to simultaneously have a rising voltage (for beam bunching) and a rising beam current. Typically, the current would rise (due to the parasitic load) and the voltage would drop - i.e., the impedance collapsed. It should be emphasized that all of these issues occurred for a magnetically-insulated ion diode in which a circulating electron cloud in the anode-cathode gap was present.

The voltage accuracy needed for ion bunching is a concern for all schemes that use drift compression of a voltage-ramped ion beam. The voltage accuracy needed, ϵ_{volt} , is given in Figure 1. Examples of the voltage accuracy needed for several relevant cases (IBX, HEDP, and an HIF driver) are given in Table 3.

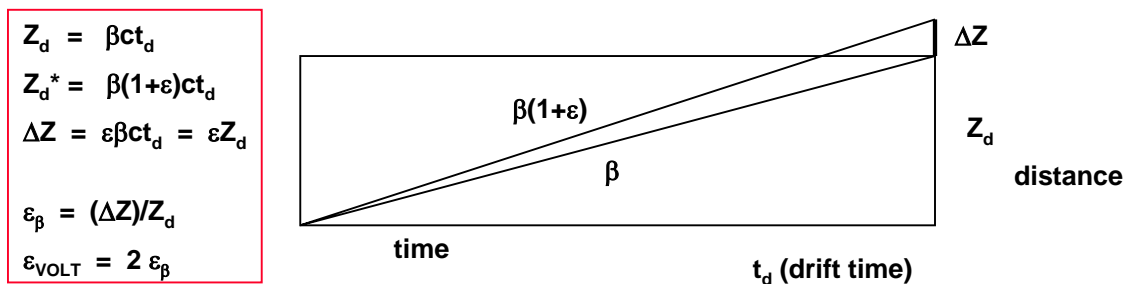


Figure 1. Voltage accuracy (ϵ_{volt}) needed for bunching.

Table 3. Examples of the voltage accuracy needed for bunching.

Examples:	IBX	HEDP	HIF Driver
	$\beta = 0.03$	$\beta = 0.05$	$\beta = 0.2$
“acceptance”	$\Delta t = 50 \text{ ns}$	$\Delta t = 1 \text{ ns}$	$\Delta t = 10 \text{ ns}$
($\Delta Z = \beta c \Delta t$)	$\Delta Z = 45 \text{ cm}$	$\Delta Z = 1.5 \text{ cm}$	$\Delta Z = 60 \text{ cm}$
	$Z_d = 30 \text{ m}$	$Z_d = 5 \text{ m}$	$Z_d = 400 \text{ m}$
	$\epsilon_\beta = 45/3000 = 1.5\%$	$\epsilon_\beta = 1.5/500 = 0.3\%$	$\epsilon_\beta = 60/40000 = 0.15\%$
	$\epsilon_{\text{VOLT}} = 3\%$	$\epsilon_{\text{VOLT}} = 0.6\%$	$\epsilon_{\text{VOLT}} = 0.3\%$

Note that the voltage accuracy needed for the HEDP case is getting close to that needed for the HIF driver case.

Based on discussions at the Pre-Workshop, several general comments were made concerning the utility of considering pulsed power single-gap ion diodes for accelerator driven HEDP. These comments were:

1. The shortest pulses in pulsed power accelerators are typically 10-20 ns (not 1 ns).
2. Ion beam transverse temperatures are sufficiently large so that for ballistic focusing, very short focal lengths are required to hit a small spot (e.g., 1 mm radius).
3. Therefore, for drift compression, the beam must be transported at a relatively large radius, and then focused radially near the target with a focusing cell.
4. The voltage accuracy needed for a single-stage, voltage-ramped, ion diode will typically limit the drift compression possible to factors much less than 100. (For the light ion program, bunching factors of only a few were needed, and the corresponding voltage accuracy needed was 20% - which could readily be achieved).
5. All past ion diode studied for fusion required high efficiency, whereas for HEDP, this is not a requirement. For example, the simple bi-polar diode offers the possibility of better beam quality.

Given these general comments on pulsed power ion diodes, the group then proceeded to consider several existing facilities as a possible facility for a single-stage ion diode for accelerator driven HEDP. The electrical parameters for these facilities are:

Gamble II at NRL: (1.5 MV, 1 MA, 50 ns)

Mercury at NRL: (6 MV, 350 kA, 50 ns, either + or - polarity: will be operational in FY05)

RITS at SNL: (Radiographic Integrated Test Stand accelerator, 5.5 MV, 150 kA, 60 ns, either + or - polarity: will be upgraded to 11 MV, 150 kA in FY05)

RHEPP/MAP at SNL: (0.5-0.75 MV, beams from H, He, N₂, O₂, Ne, Ar, Xe, etc.) (Sabre at SNL has been disassembled)

(Cobra at Cornell has been made into a z-pinch driver)

Based on all of the above considerations, the group proposed three possible single-gap diode options for accelerator driven HEDP:

Single-gap ion diode OPTION 1:

(Near-term) PRD (Pinch Reflex Diode) on Gamble II at NRL at 1.5 MV

The purpose of this option is to get started doing accelerator driven HEDP as soon as possible. This experiment would use a PRD on Gamble II at ~ 1.5 MV, and focus a proton beam to obtain the highest ion current density possible at the focus (~ 250 kA/cm²). Then, at the focus, a plate with a 1 mm radius hole would allow a 1 mm radius beamlet to pass. The beamlet current be ~ 7.5 kA. The beamlet energy per ns would be (7.5 kA)(1.5 MV)(1 ns) ≈ 10 J, which means 10 J/ns would go into a 1 mm radius spot.

The issues associated with this direct approach concern the pulse length. The ion beam pulse length is 50 ns, and the beam rise time is 25 ns. The question then is how to switch out a 1 ns portion of the beam at full power? For example, can the ion beam burn through a foil to steepen the pulse front? If steepened, can a pulse length longer than 1 ns be used?

The possible phases of this approach would be:

Phase 1. Set up an ion diode on Gamble II and create a 1 mm radius beamlet ASAP. This would take about 1-2 weeks on Gamble II at about \$45k/week (includes experimenter). Total cost for this phase: ~ \$100k.

Phase 2. Do experiments to steepen the pulse front (e.g., burn through a foil) and test HEDP diagnostics. Total cost for this phase: ~ \$100k.

Phase 3. Add a z-discharge focus cell ($\lambda/4$ or $\lambda/8$) to obtain even higher deposition for HEDP. Total cost for this phase: ~ \$150k.

The total cost for all phases would be ~ \$350k, and the experiments could be done on a time scale of less than a year.

Single-gap ion diode OPTION 2:

(Medium-term) MAP He Applied-B Diode on Mercury at 6 MV

The purpose of this option is to combine (1) the He MAP active ion source developed on RHEPP that produces a pure He⁺¹ beam, (2) the newly commissioned 6 MV Mercury voltage-adder accelerator at NRL that could be operated in positive polarity, and (3) applied-B ion diode expertise as developed at SNL during the light ion program:

(1) The He MAP source on RHEPP at 750 kV produces pure He⁺¹, as determined by TOF. Measurements are underway to confirm the ion composition with a Thompson Spectrometer. Faraday cup signals on RHEPP show an initial sharp rise, evidently due to voltage bunching. This maximizes energy delivery in the first part of the pulse.

Although the beam emittance on RHEPP is not yet known, beam quality measurements on RHEPP are on-going. The ion beam in RHEPP tends to diverge, as if from a line source in the diode. This could be caused by either (a) lack of a fixed magnetic field topology due to the fact that the MAP source in RHEPP has evolving field lines, or (b) beam blow-up due to excessively high space charge in spite of the co-emitted and co-moving electrons. The Russian group at Tomsk operates a MAP diode with a screen on the anode in place of an open hole, as used at SNL. The Russian group will be making both shadow-box and Thompson spectrometer measurements of beam quality to compare with similar data on RHEPP at SNL.

(2) The Mercury accelerator at NRL will operate at 6 MV with 350 kA. This relatively high impedance is in the right direction for a large gap, high-insulating field beam, which should tend to maximize beam quality.

(3) Magnetically-insulated ion diodes have been studied at SNL for about two decades, and operated at voltages up to ~ 10 MV with the PBFA-X extractor ion diode. This expertise would be used to design an applied-B diode for Mercury.

Combining He MAP, Mercury, and applied-B ion diode expertise should produce a 6 MeV He⁺¹ ion beam (1.5 MeV/nucleon). Assuming present estimates of beam brightness, a rough estimate of the beam power delivered to an HEDP target would be 2-10 J/cm² in the first 1 ns of the beam. In a 1 mm radius spot, this would be 0.06- 0.3 J in the first 1 ns (too small for HEDP). In a 2.5 mm radius spot, this would be 0.4-1.9 J in the first ns: radial focusing in a z-discharge cell might then be used to reduce the radius to 1 mm.

This single-gap diode option would require applied-B diode design and modeling, capacitor banks for the B field, subsystems for MAP, conversion of Mercury to positive polarity, machine time for bringing up hardware and optimizing the diode, etc. A rough estimate of the cost involved would be \$1M - \$2M, and the time scale would be 1-2 years.

Single-gap ion diode OPTION 3:

(Longer-term) High impedance ion diode with no requirement on efficiency

As mentioned earlier, all of the ion diodes developed for the light ion program use various means to prevent the electrons from crossing the anode-cathode gap and draining most of the power, i.e., the efficiency for ion production had to be high. The presence of the electrons in the diode led to instabilities that contributed to strong emittance growth of the ion beam. For HEDP, there is the possibility of developing a high impedance ion diode with no requirement on the efficiency - the ion beam so produced should show much better beam quality (lower emittance, etc.).

The simplest example of such a diode is the bi-polar diode in which both ions and electrons flow freely. A bi-polar diode might be investigated to see if such a diode would have a much improved ion beam emittance. For a planar bi-polar flow diode, the electron current must remain below the magnetic pinching limit. Paul Ottinger estimates that this means the diode impedance must be

$$Z(\text{Ohms}) > 30 (\gamma^{1/2} - 0.8471)^2 / (\gamma + 1)$$

(where γ is the usual relativistic factor for the electrons) to avoid pinching of the electron flow. For 1.5 MV, this is roughly 8 Ohms. The ratio of the ion current to the electron current for bi-polar flow is

$$I_i / I_e = (Zm_e / m_i)^{1/2} [(\gamma + 1)/2]^{1/2}$$

Therefore, at 1.5 MV for protons, $I_i \sim 7$ kA and $I_e \sim 190$ kA. At 4.5 MV for He⁺¹, the impedance must be greater than 15 Ohms, and $I_i \sim 8$ kA and $I_e \sim 300$ kA.

This option would need a high impedance driver and a bi-polar diode. If the ion beam emittance is significantly improved over that of magnetically-insulated ion diodes, then this approach may prove useful for HEDP. For initial tests to study the ion beam emittance for a 1.5 MV bi-polar, planar, proton diode on Gamble II, a rough funding estimate would be ~ \$200k, and the time scale would be less than a year. Further experiments with a focusing diode would then be needed to assess the utility of this concept for HEDP.

Ionization Front Accelerator OPTION:

Ion acceleration based on use of the collective fields of an intense, relativistic electron beam (IREB) were studied at length in the 1970's. A natural collective acceleration process that occurs when an IREB is injected into a low pressure neutral gas was demonstrated at many laboratories, and many theories were proposed to explain the effect. A theory developed by C. Olson showed that the mechanism was a space charge mechanism, and this theory was compared in great detail with all of the data that had accumulated. This understanding led to the concept of the Ionization Front Accelerator (IFA) which is a controlled collective ion accelerator that improves on the natural collective acceleration process to make a scalable high-gradient ion accelerator. A comprehensive summary of research in this field is in the book "Collective Ion Acceleration" by C. L. Olson (Collective Ion Acceleration with Linear Electron Beams) and U. Schmacher (Collective Ion Acceleration with Electron Rings), Springer Tracts in Modern Physics, Vol. 84, (Springer-Verlag, Berlin-Heidelberg-New York, 1979).

In the IFA, the ions are bunched radially and longitudinally into a compact ion bunch right at the start of the accelerator, and ion bunch pulse lengths less than 1 ns are typical. Two sets of experiments (IFA-1 and IFA-2) were successfully completed in the late 1970's and early 1980's. The IFE concept was scaled to an HIF driver (and for several other applications such as GeV protons, etc.). The IFE uses a pulsed power IREB and short-pulse high-power laser(s) to produce and control the motion of a strong potential well at the head of the beam that can trap and accelerate ions. What is new now is that high-power short-pulse laser technology, as well as pulsed power technology, has made great improvements over the last 20 years. This suggests that it is worth re-visiting the IFE concept, especially since the IFA may potentially be used for both HEDP and HIF.

The IFA concept is shown in Figure 2. An IREB with current typically above the space charge limiting current is injected into a drift tube that has "perfectly conducting walls." A special working gas at low pressure fills the tube. The pressure of the working gas is chosen to be low enough so that the IREB does not significantly ionize the gas on the time scale of interest. Then a swept photoionizing light source (a laser or lasers) is injected through the side of the drift tube. The gas is ionized by the light source to provide a fractional charge neutralization of $f_e = 1$ for the IREB (the background secondary electrons are quickly expelled radially). In this manner, the IREB will propagate through the $f_e = 1$ region, and then blow up just past the f_e front. In the front region, a deep electrostatic potential well is created that will synchronously follow the swept ionization front. Ions are trapped and accelerated in the deep potential well. Acceleration gradients of 100 MV/m and larger (above 1 GV/m) are possible.

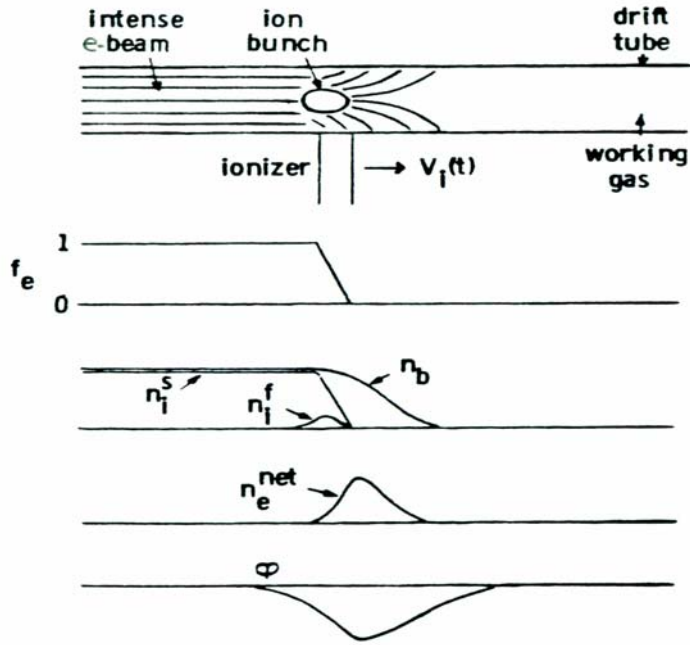


Figure 2. Ionization Front Accelerator (IFA).

The first set of experiments (IFA-1) used the configuration shown in Figure 3. The working gas was Cs at low pressure (30 mTorr). The ion source was a separate gas (such as hydrogen for protons) that was partially ionized by the IREB to provide some test ions. The ionization process was 2-step photoionization with a dye laser exciter (852.1 nm) that was swept by using a light pipe array. The "kicker" laser was a ruby laser frequency doubled. Self-breakdown oil switches on the IREB machine blumlein had a jitter of about 5 ns. The second set of experiments (IFA-2) used the configuration shown in Figure 4. The working gas was again Cs at low pressure (30 mTorr). The ion source was again a separate gas that was partially ionized by the IREB to provide some test ions. The ionization process was 2-step photoionization with a dye laser exciter (852.1 nm) that flooded the acceleration region, and a "kicker" laser that was a XeCl laser (308 nm) that was swept with a programmed fast electro-optic deflector. Laser-triggered switches were used on the ethylene glycol insulated blumlein to provide 1 ns jitter. Different sweep rates controlled the beam front velocity and test ion results showed that the ions were moving at the controlled beam front velocity [C.L. Olson, C.A. Frost, E.L. Patterson, J.P. Anthes, and J.W. Poukey, Phys. Rev. Lett. **56**, 2260 (1986)].

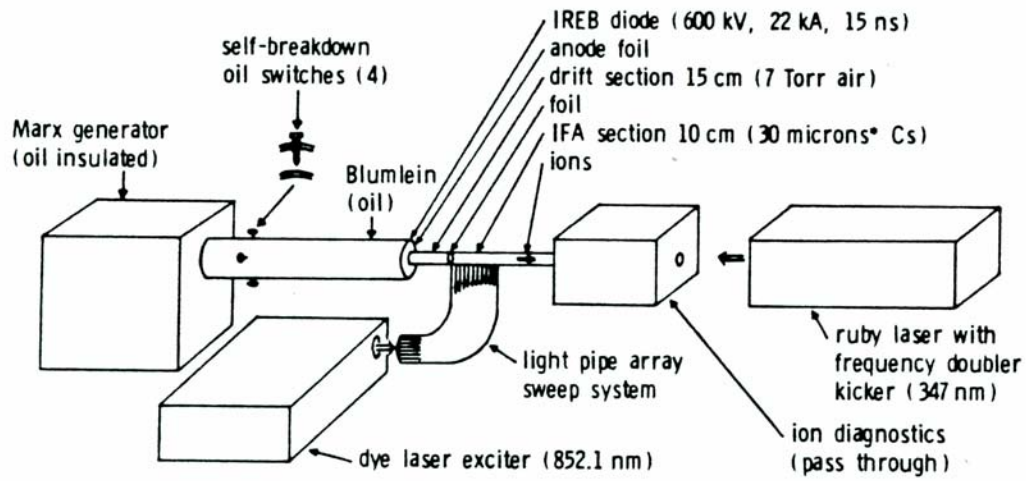


Figure 3. IFA-1.

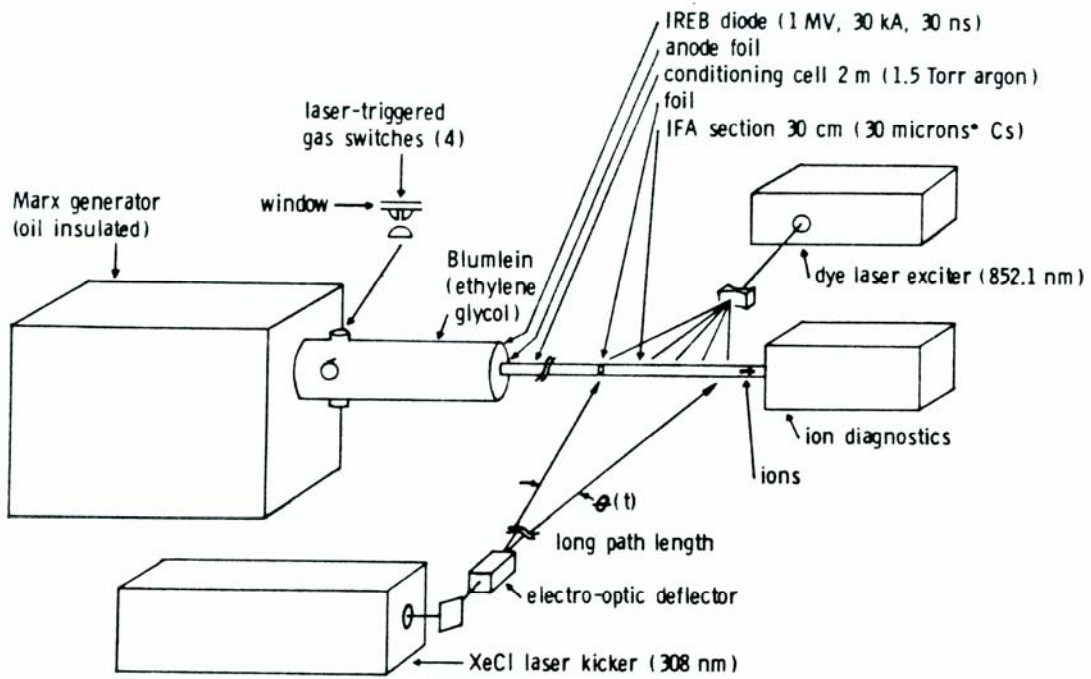


Figure 4. IFA-2.

The IFA intrinsically generates a sub-nanosecond ion pulse. Three examples of IFA parameters for 20 MeV p, 1 GeV p, and a 12 GeV U accelerators are given in Table 4. Note that the ion pulse lengths for the three cases are 100 ps, 30 ps, and 100 ps. All three cases also show the basic IFA scaling of (laser energy) < (ion energy) < (IREB energy). For HEDP, the ion energy for the third case would be reduced from 12 GeV to about 1.2 GeV, and the IFA accelerator length would be only 20 cm. The U ion source would be a laser-target ion source for this case.

Table 4. IFA examples for 20 MeV H, 1 GeV p, 12 GeV U

IFA Example: Feasibility (20 MeV Protons)			IFA Example: 1 GeV PROTON			IFA Example: 50 A MeV $^{238}_{92}\text{U}^{60+}$		
IREB	ϵ_e I_o τ r_b ρ ϵ_b	600 keV 20 kA > 10 nsec 0.5 cm $1.3 \times 10^{10} \text{ W}$ >130 J	IREB	ϵ_e I_o τ r_b ρ ϵ_b	2 MeV 30 kA 75 nsec 1 cm $6 \times 10^{10} \text{ W}$ 4.5 kJ	IREB	ϵ_e I_o τ r_b ρ ϵ_b	1 MeV 30 kA 50 nsec 1 cm $3 \times 10^{10} \text{ W}$ 1.5 kJ
DRIFT	l E_o P ϵ_{IONIZE}	20 cm 10^6 V/cm 0.003 Torr $6 \times 10^{-5} \text{ J}$	DRIFT	l E_o P ϵ_{IONIZE}	10 meters 10^6 V/cm 0.003 Torr 0.006 J	DRIFT	l E_o P ϵ_{IONIZE}	200 cm 10^6 V/cm 0.003 Torr 0.0012 J
LIGHT	J_1 τ_1 ϵ_1 J_2 τ_2 ϵ_2	10^7 W 1 nsec 0.01 J $1.5 \times 10^8 \text{ W}$ 10 nsec 1.5 J	LIGHT	J_1 τ_1 ϵ_1 J_2 τ_2 ϵ_2	10^9 W 1 nsec 1 J $1.5 \times 10^8 \text{ W}$ 75 nsec 11 J	LIGHT	J_1 τ_1 ϵ_1 J_2 τ_2 ϵ_2	$1.5 \times 10^8 \text{ W}$ 1 nsec 0.15 J $1.5 \times 10^8 \text{ W}$ 50 nsec 7.5 J
PROTONS	ϵ_i N ρ T E	20 MeV 10^{12} $3 \times 10^{10} \text{ W}$ 0.1 nsec 3 J	PROTONS	ϵ_i N ρ T E	1 GeV 3×10^{12} 10^{13} W 0.03 nsec 500 J	$^{238}_{92}\text{U}^{60+}$ IONS	ϵ_i/A $N\zeta$ ρ T E	50 MeV 3×10^{12} 10^{12} W 0.1 nsec 100 J

The parameters for a first example of an IFA for accelerator driven HEDP are summarized in Table 5. A 300 ps pulse of 10 J of 1.2 GeV U ions would be in a spherical bunch of radius 5 mm. About 4 J of U ions would be contained within a 2.5 mm radius, and this radius could be reduced to 1 mm radius with a z-discharge focusing cell. These parameters are close enough to those desired for HEDP that the IFA should be considered as a possibility for HIF-HEDP.

Table 5. Possible parameters for an IFA for HIF HEDP

IREB: 1 MeV, 30 kA, 20 ns, radius 1 cm, $3 \times 10^{10} \text{ W/cm}^2$, 600 J

Acceleration section: length 20 cm, acceleration gradient 10^6 V/cm ,
sweep velocity $0 \rightarrow 0.1c$ in $\sim 16 \text{ ns}$

Ions: 1.2 GeV U^{60+} , 5 MeV/nucleon, $N\zeta = 3 \times 10^{12}$, $N = 5 \times 10^{10}$, power 30 MW,
pulse length 300 ps, energy 10 J, spherical bunch radius 5 mm

An IFA accelerator consists of an IREB machine, lasers, a heated cell with the working gas (presumably Cs), an ion source (presumably a laser/target source), and diagnostics (for the ions, IREB, lasers, Cs, etc.). Command firing with low jitter (~ 1 ns) is required to ensure proper synchronization of the lasers with the IREB.

The IREB parameters listed in Table 5 are very similar to those used for IFA-2. The IFA-2 experiments were funded at about \$600k/year for several years in the late 1970s and early 1980s, and that did not include the costs of the major equipment (IREB machine, dye laser, XeCl laser, streak camera, etc.). A definitive IFA experiment today would require state-of-the-art equipment, dedicated laboratory space, and adequate funding. A very rough estimate for funding is \$1M - \$2M for equipment, and \sim \$1M/year or more for 1-2 years for building, operating, and optimizing the IFA accelerator.

Pulsed Drift Tube Accelerator

A. Faltens

October 31, 2004

The pulsed drift-tube accelerator (DTA) concept was revived by Joe Kwan and John Staples and is being considered for the HEDP/WDM application. It could be used to reach the full energy or as an intermediate accelerator between the diode and a high gradient accelerator such as multi-beam r.f. In the earliest LBNL HIF proposals and conceptual drivers it was used as an extended injector to reach energies where an induction linac with magnetic quadrupoles is the best choice. For HEDP, because of the very short pulse duration, the DTA could provide an acceleration rate of about 1MV/m.

This note is divided into two parts: the first, a design based on existing experience; the second, an optimistic extrapolation. The first accelerates 16 parallel K^+ beams at a constant line charge density of $0.25\mu C/m$ per beam to 10 MeV; the second uses a stripper and charge selector at around 4MeV followed by further acceleration to reach 40 MeV. Both benefit from more compact sources than the present 2MV injector source, although that beam is the basis of the first design and is a viable option.

A pulsed drift-tube accelerator was the first major HIF experiment at LBNL. It was designed to produce a $2\mu s$ rectangular 1Ampere C_s^+ beam at 2MeV. It ran comfortably at 1.6MeV for several years, then at lower voltages and currents for other experiments, and remnants of that experiment are in use in present experiments, still running 25 years later. The 1A current, completely equivalent to 1.8A K^+ , was chosen to be intermediate between the beamlets appropriate for a multi-beam accelerator, and a single beam of, say, 10A, at injection energies. The original driver scenarios using one large beam on each side of the reactor rapidly fell out of favor because of the very high transverse and longitudinal fields from the beam space charge, circa 1MV/cm and 250 kV/cm respectively, near the chamber and because of aberrations in focusing a large diameter beam down to a 1mm radius spot at a distance of 10m. Almost all subsequent work and the present concept have invoked multiple beams. For HEDP the major differences are that the focal distance can be centimeters instead of meters, provided strong-enough lenses exist and they do, thereby allowing much higher transverse and longitudinal emittances than driver concepts, and focusing parallel small beams is easier than one big beam.

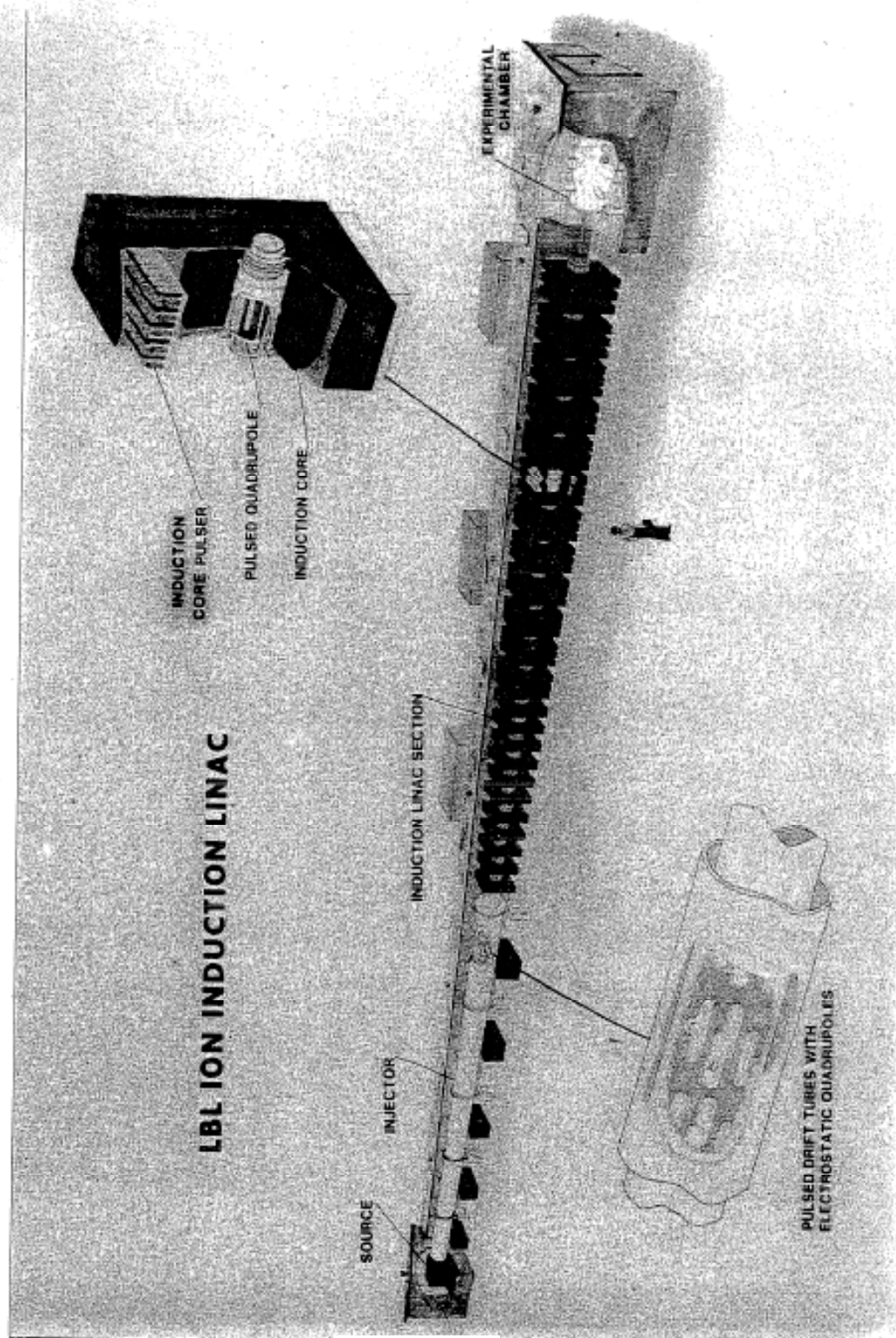
After and in parallel with the DTA experiment, the first two major LBNL HIF proposals, the 500J Ion Induction Linac [1], and the reduced cost 50J Ion Induction Linac [2] included pulsed drift tubes. The first proposal, in 1979, included two drift tubes with bipolar 750kV pulses to accelerate a 2.75A C_s^+ beam, equivalent to 5A K^+ . The second proposal, in 1980, included five unipolar 500kV drift tubes to accelerate a $5\mu s$, 1A C_s^+ beam. The second proposal's DTA was very similar to the 2MV, $2\mu sec$, 1A C_s^+ accelerator which was built, which used 3 drift tubes of 500kV and a 500kV gun to create a 1MV triode at the source and two 500kV acceleration gaps downstream. The first proposal's DTA required some development for the bipolar pulsing and the higher voltage whereas the second proposal's DTA had an experimental base. The drift tube concept is described in the second HIF Symposium

[3], at LBL in 1977, and in the above proposals. A schematic of the experiment is shown in Fig. 1.

The amount of charge that can be contained within a drift tube is a crucial parameter that depends on the size of the drift tube and the type of focusing employed. Grids, Einzel lenses in circular and ribbon beams, neutralization with electrons or thin wires, electric quads, magnetic quads, higher multi-poles, and solenoids have all been considered. The first conceptual drivers included a DTA section within a 4T superconducting solenoid. Shortly thereafter the solenoid was superseded by electrostatic quad focusing inside of the drift tube – similar to the magnetic quad focusing within the drift tubes of some Alvarez linacs. This configuration is shown in Fig.2. When the Test Bed proposals were set aside, work was in progress on multiple beam electrostatic quad arrays within the drift tubes, and it is that scheme, now enhanced by experiments in SBTE, MBE-4, and HCX which all used electric quads (singly or in arrays, and at reduced and full quad operating voltages), that we consider here for HEDP. In an electric quad channel the line charge density of a space charge dominated and space charge limited beam is directly proportional to the quad voltage. The voltages envisaged here are +/- 75 kV, which are well below those used in the HCX injector and matching section quads, and the same as the nominal operating voltages of the HCX electric quad transport line. The line charge density corresponding to this choice is a quarter microcoulomb per meter. The 16 beams carry a total of 4 $\mu\text{C}/\text{m}$, which is 4 times greater than was carried in the original experiment. As the number of beams in the array is increased, the number of electrodes tends toward one electrode per beam, as contrasted to 4 electrodes for a single beam, and the array packs more efficiently into a circular container, so there is an incentive to use a large number of beams. 16 was chosen as a case which exhibits some of these scaling features, but an economic analysis including the cost of sources and acceleration might find a better optimum.

Much of the experimental work alluded to above was directed at transporting the maximum current through an expensive induction core which requires a powerful pulser, circa 100MW per module, to supply the magnetizing current and drive the beam. The drift tube, on the other hand, is essentially a capacitor of a few hundred pf and the beam currents for HEDP are low, so the pulser is different and in most respects easier to make. In the induction core case, doubling the current through a given core halves the pulse duration, allowing the core radial build to be halved and the core volume to be more than halved, thus reducing the cost of the core and pulser. With the drift tube there is little incentive to making its diameter small, with much of the cost of making a small accelerator being associated with the number of parts rather than their size and weight. Electrically, driving a 1m diameter drift tube within a 1.5m vacuum tank is similar to driving a 2m tube in a 3m tank as far as capacitance is concerned, but the beam current would quadruple. The strategy thus is to use as many beams as necessary to get the desired beam power, overlapping the beams only at the focal spot.

The drift tube functions by hiding the beam bunch within a cylindrical metal enclosure while its voltage is switched. The beam is accelerated exactly as by a sequence of DC accelerating gaps, except that the voltage of the drift tubes stays around the 1MV level while the beam energy accumulates at the rate of about 1MV



BBC 803-3655A

Figure 2

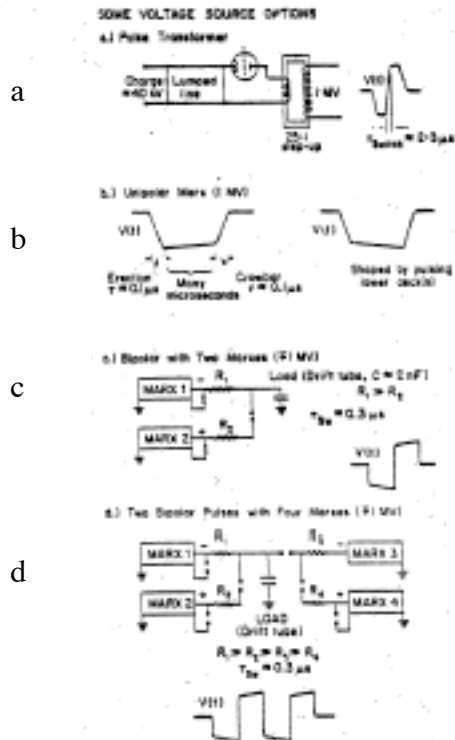


Figure 3 Some pulse modulator choices:
 (A) Thyatron and pulse-transformer.
 (B) Unipolar Marx generator, (C) Bipolar Marx generator combination, (D) Double pulsing (Bipolar) Marx Generator Combination.
 The natural RC droop of the Marx pulse can be removed and a positive ramp created by pulsing the lower decks.

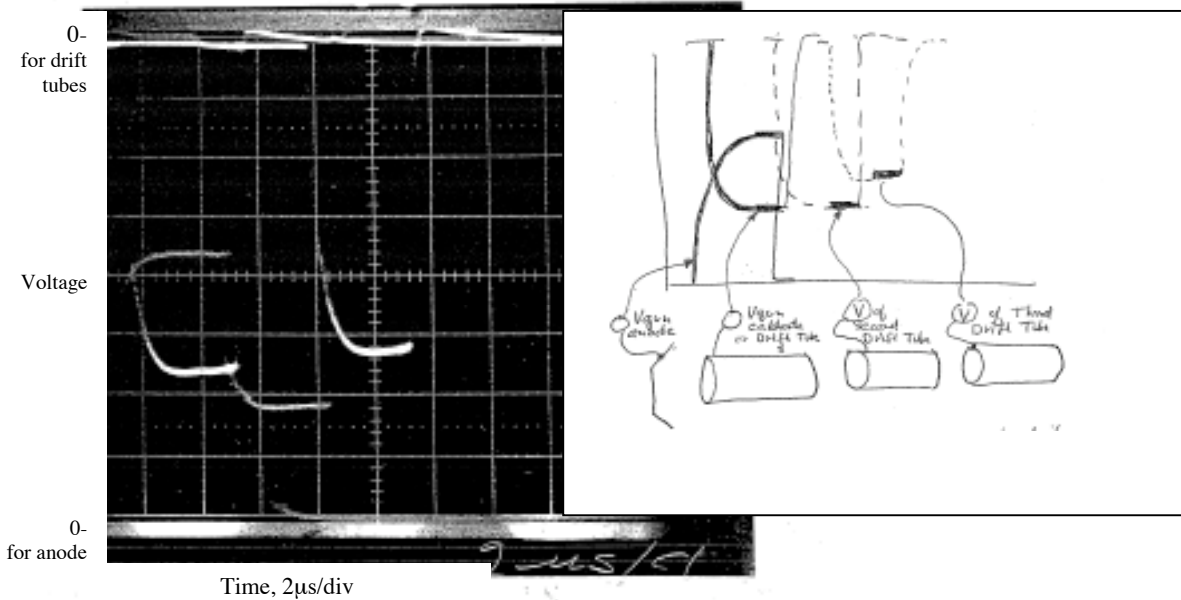
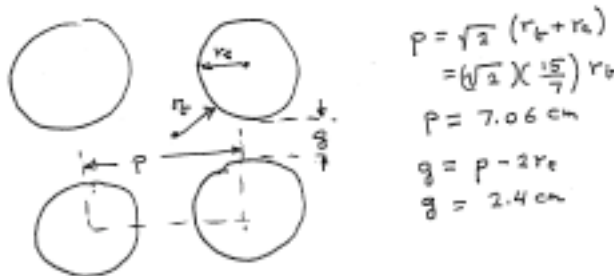


Figure 4

Figure 5. The four Marx generator plus crowbar voltages used to drive the gun, positively, and the three drift tubes negatively and delayed by the beam time of flight. Horizontal sweep $2\mu\text{s}/\text{div}$. Voltage is from capacitive dividers each of which has its own calibration. Voltages were held to about 1% tolerance at a typical operating level of 400 kV. The parts of the waveforms when beam is present are darkened, at the right, v . The gun and each drift tube had its own Marx generator and crowbar. The portions of the waveform used in accelerating beam are shown with heavy lines on the right.

The Drift Tube

Taking the recently “standard” electric quadrupole geometry as in HCX, the electrode radius is $\frac{8}{7}$ of the aperture radius of 2.33cm.



This geometry eliminates the next higher allowed multi-pole, $n=6$, can transport $0.25\mu\text{C}/\text{m}$ at electrode voltages of $\pm 75\text{kV}$, and shields the beams from each other. A surrounding o potential shell requires a spacing of at least $0.5g$. A 4×4 array thus fits into a drift tube of diameter

$$D = 4\sqrt{2P} + 2R_e + g$$

$$D_{16} = 48\text{cm} \quad (D_{12} = 40\text{cm})$$

The length of the drift tube is the sum of the bunch flat top, bunch rise and fall distances, the switching time multiplied by beam speed, and the field penetration distance into the drift tube ends.

$$L_{DT} = 2r_g + (tr + tp + tf)v_g + t_{sw}v_g$$



For a bunch with 50ns rise, 100ns flattop, 50ns fall and a switching time of 100ns,

$$L_{DT} = 50 + (50 + 50 + 100 + 100)(3\text{mn}/\text{ns}) = 1200\text{mm}$$

Doubling the useful portion to 200ns adds 300mm, for $L_{DT} \rightarrow 1500\text{mm}$

Adding room to hold off 1.5MV increases the accelerator length per drift tube to $L_{DT} = 140\text{cm}$ for the 100ns-flat bunch and 170cm for the 200ns-flat bunch.

The drift tube capacitance is

$$C = \frac{2\pi\epsilon_0\ell}{\ln\frac{6}{a}} = \frac{(2\pi)(8.854)(1.4)}{\ln(1.5)} = 200\text{ pf (radially)}$$

$$C_{stem} \cong 20\text{ pf/ft} \rightarrow 50\text{ pf}$$

$$C_{ends} = \frac{2\epsilon_0 A}{d} \rightarrow 15\text{ pf}$$

$$\Sigma C = 265\text{ pf for "100ns" and 300pf for "200ns"}$$

The energy in the fields is

$$V_{DR} = \frac{1}{2} CV^2 = \left(\frac{1}{2}\right)(300 \times 10^{-12}) \left(\frac{3^2}{4^2} \times 10^{12}\right) = 84\text{ joules}$$

The beam takes out 2 joules on each end, when the bunch enters and when it leaves.

If these beam sizes are scaled up in order to better match an injector, the above values stay the same.

As the bunch accelerates, the physical lengths of the bunch are kept fixed, but the portion of the drift tube length attributable to switching time lengthens as velocity: (100ns) (3m/ μ sec) at injection \rightarrow (100ns)[9m/ns or 18m/ns] for a lengthening of 60cm or 1.5m for the 10MeV or 40MeV cases respectively.

The bunch fall time portion is carried along to act as a buffer for the "good parts" of the pulse. The ends have the space charge and longitudinal ear fields in addition to acceleration and bunching fields and hence get more heated up longitudinally and mismatched transversely than the body of the bunch.

The 10MeV Design

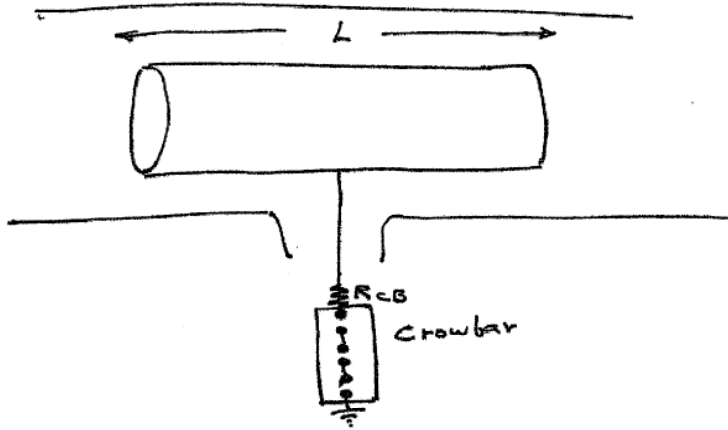
The 10MeV designs basically assumes the appearance of a matched, small beam at the entrance of the first drift tube, at an energy of about 1.8MeV, 750keV from the drift tube, ~1MeV from the gun. During the rest of the acceleration the beam gains 1.5MeV every time it crosses a gap. The lengths of the drift tubes are adjusted as required to match the focusing lattice, and diagnostics, correctors, and focusing arrays are placed between drift tubes as required.

The K^+ focusing periods are about 40cm at injection and increase to

$$\left(\sqrt{\frac{10}{1.8}}\right)(40) = 94\text{ cm at the end. Therefore, the first few drift tubes have } \sim 6 \text{ arrays and the}$$

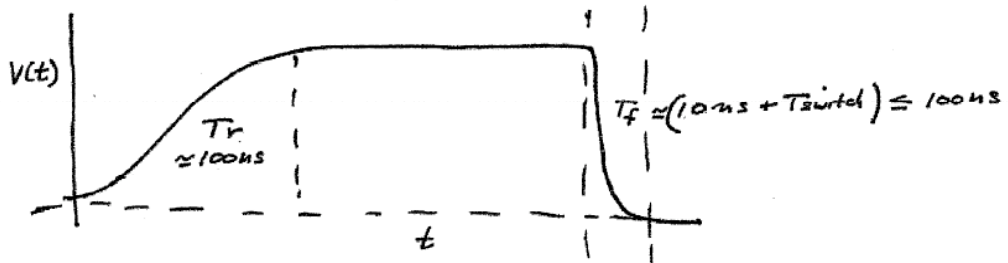
last ones ~ 4 arrays. The quads and drift tubes both lengthen with velocity, the quads linearly and the drift tubes somewhat less rapidly as discussed above. The drift tube lengths must also be adjusted to contain full half-periods.

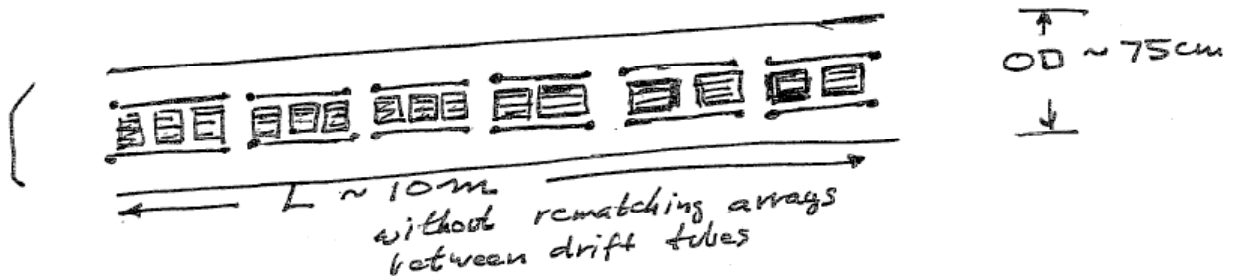
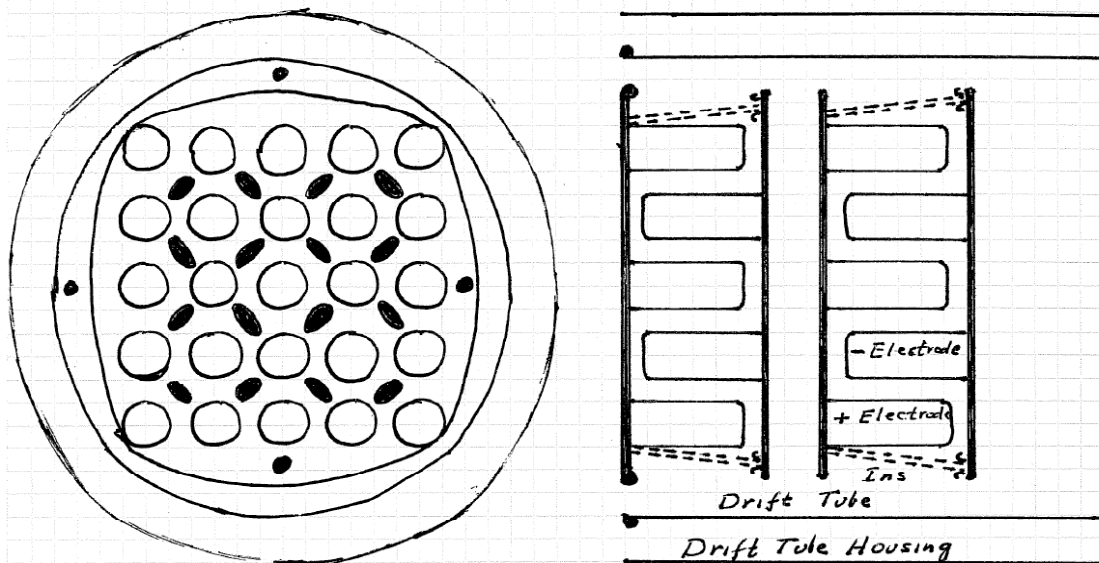
$$L_{DT} = v(T_{\text{beam flat part}} + T_{\text{beam rise \& fall}}) + vT_{\text{switch}} + (G + 2a)$$



If $R = \frac{Z_0 DT}{2}$

$$T_{f \min} \approx \frac{L}{c} \sim 10 \text{ ns} + T_{\text{switch}}$$





If the last gap provides the tilt, $\frac{\Delta E}{E} \sim \frac{.75}{10}$, $\frac{\Delta v}{v} \sim \frac{.75}{20} \sim 4\%$ and 25 bunch lengths are needed for the drift line. Here, since the beam is going into plasma, only the flat part of the pulse needs to be tilted, so 25 times 30cm = 7.5m. Applying tilt at the entrance and exit of the last drift tube could roughly halve the drift distance.

The 40 MeV Design with a Stripper and Charge Separator at 4 MeV

The desire is to increase the acceleration rate by using a high charge state q of the ion, obtained by passing the beam through a thin jet or ribbon of gas, followed by a magnetic dipole in a short neutralized region which is long enough to allow a separation of 1 beam "diameter" per charge state. Among all the possible gases and stripping energies, there must be optimum pairs for every desired charge state. Here we simply assume that near 4MeV the yield is 25% into charge state 4. With further work, some other nearby charge state and energy may turn out superior.

Starting with the nominal $\frac{1}{4} \mu C/m$, after stripping the electrical charge is $\frac{1}{4} \mu C/m$ and the particle number is $\frac{1}{16} p \mu C/m$. With the same acceleration system, the

1.5MV/drift tube becomes 6 MeV/drift tube. Adding 36MeV thus requires 6 more drift tubes. The focusing is still at the limit of its capabilities, but the lattice has to be rearranged to match the higher charge state and faster acceleration schedule. The bunch maintains its length.

The beam entering a neutralized region just before the stripper would focus to a smaller size that with space charge, in one plane, reducing the required bend for charge separation. All of this takes place between drift tubes, with some focusing and re-matching arrays in that elongated space.

End containment

The end focusing ears, which counteract the space charge defocusing fields, are calculated below for assumed bunch ends of 15 cm each. The required voltage of about 25 kV per drift tube is modest compared to the acceleration voltage of 750 kV, but the 50 ns long triangular voltage pulse and the means by which it is superimposed on the drift tube may require a more powerful independent pulser and combining circuit. Such circuits using inductive adding were used on SBTE, for a short pulse, and on MBE-4 for a long pulse for tilt control. The waveform tolerance for accelerator pulsers has usually been in the range of 1% for the flat portion, and it is possible that some of the main pulser ripple or rise times could be of use for end containment.

$$\lambda = \frac{1}{4} \mu C/m$$

$$\Phi \cong 2.5kV$$

$$Tr_f T_f = 50ns = 15cm$$

$$Eq = \frac{2.5}{.15} = 16.7 kV/m$$

$$V_q \cong 25 kV/dt$$

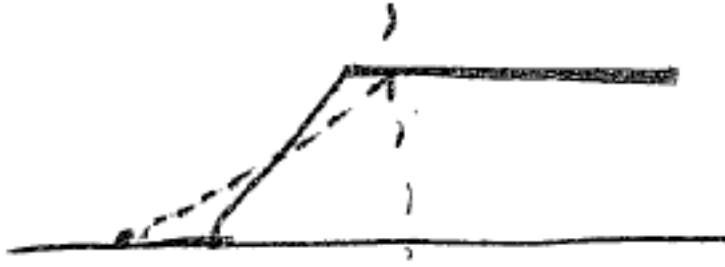
Between pulsers, the ends elongate with the space charge wave speed λ inwards and about twice the wave speed outwards. $v_\lambda = \sqrt{\frac{\Phi_G}{m/e}}$ is the space charge wave speed and the end erosion is approximately thrice that.

$$v\lambda = 7.9 cm/\mu s$$

$$v_{end\ erosion} \cong 24 cm/\mu s$$

$$\text{Travel time through } 1DT \sim \frac{1.5m}{3m/\mu s} = \frac{1}{2} \mu s$$

\therefore End motion \sim 12 cm in first DT
 \sim 4 cm in, 8 cm out



So even here we need a pulser to restore the end or a longer end, which is sacrificial.

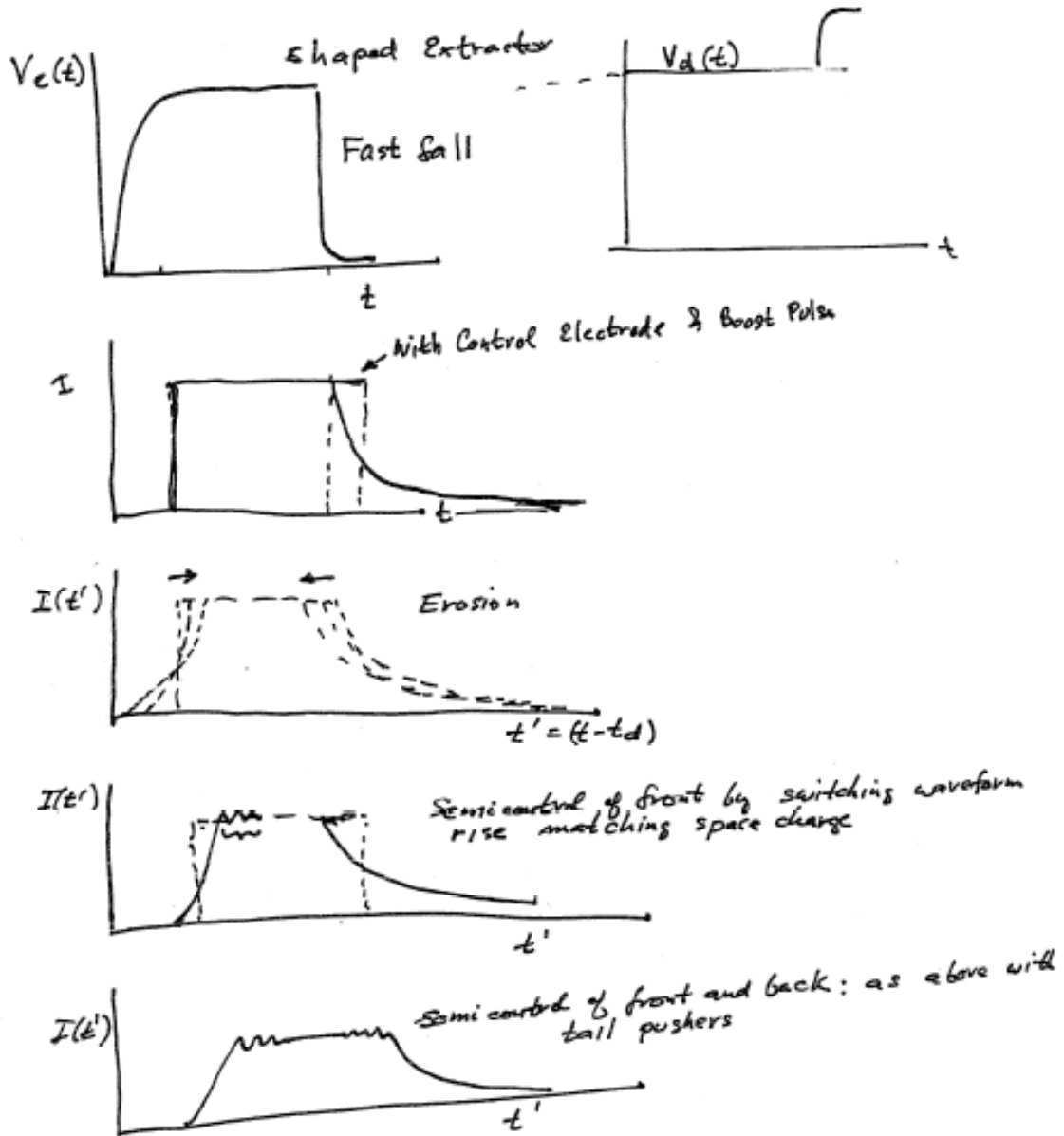
Through the entire accelerator the transit time is $\sim 3 \mu\text{sec}$ leading to 6 times longer erosion distances on the bunch.

$\rightarrow \frac{(6)(24)}{2} = \frac{144\text{cm}}{2} = 72 \text{ cm}$ of which the inward wave is 24 cm and outward motion is 48 cm.



One choice is to approximately double the pulse length to get enough sacrificial beam. A more complete calculation of the end dynamics would have to have the current rise time and energy distribution of the bunch ends when the bunch leaves the injector.

Bunch Length Control

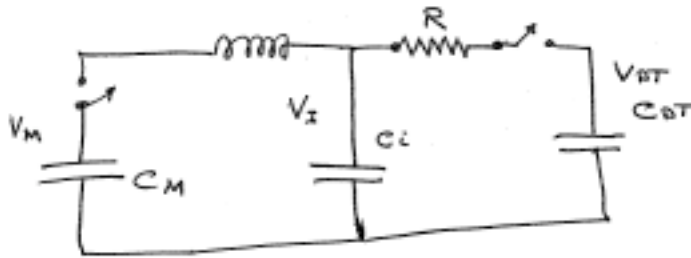


The Pulser Circuit

The drift tubes may be charged up on any convenient time scale, using a Marx generator or a pulse transformer. The original experiment used Marx generators, but the choice was influenced by availability of some of the parts and a design base; pulsed transformers were looked at briefly, and one choice to look at would be a 30kV thyratron capacitor discharge into a 25:1 step up transformer for establishing the initial voltages before beam enters the drift tube. The Marx generators that were constructed had many meters of wire connecting the capacitors and spark gaps inside them so the voltage rise time, determined essentially by the wire inductance and the

capacity to ground along the Marx and in the high-voltage terminal, was about 100ns. For beam dynamics reasons the rise time was slowed to 1 μ s with a series resistor to the emitter. The fall time, on the other hand, should be made short, and this was accomplished in the original experiment by a crowbar spark gap and a damping resistor. The resulting voltage pulses, representative of what could be achieved today with modest effort are shown in Fig. 4. The attained rise times of 100ns for a single polarity Marx and crowbar spark gap, and the estimated 300ns switching time for a bipolar drift tube were all acceptable when the beam pulse was several μ s long. For HEDP, because the beam duration is only circa 100ns, it is desirable to shorten the switching time with a different circuit.

The causes of the slow Marx switching time are the stray and load capacities of the Marx driven through the Marx inductance. It is certainly possible to construct a lower inductance Marx, but the charging time varies only as $T_{sw} \propto \sqrt{L_s C}$, so that the internal inductance must be reduced by a large factor to see a significantly shorter rise time. A more attractive solution is to use the Marx (or pulse transformer) to resonantly charge on intermediate low inductance capacitor, and use that capacitor, which is an inherently low inductance element, to rapidly charge the drift tube. The full circuit and important relations are shown in Fig. 5.



$$V_I = \left(\frac{2C_M}{C_M + C_i} \right) V_M$$

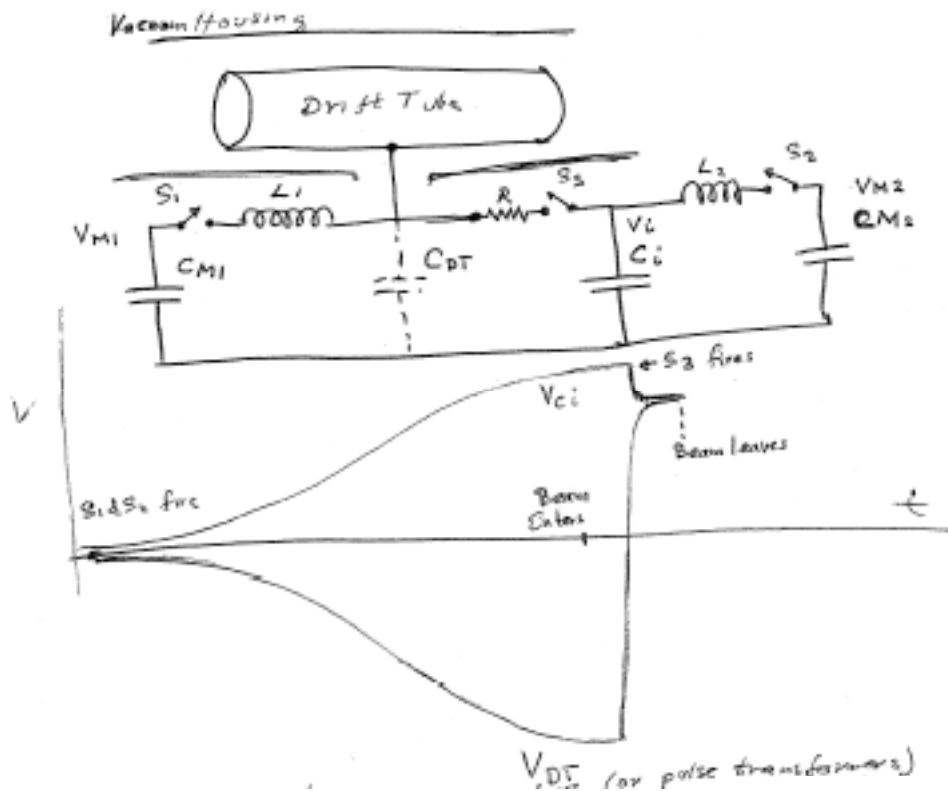
$$V_{DT} = \frac{C_i}{C_i + C_{DT}} V_i$$

$$V_{DT} = \left(\frac{C_i}{C_i + C_{DT}} \right) \left(\frac{2C_M}{C_M + C_i} \right) V_M$$

$$\tau = \frac{(R)(C_{DT} C_i)}{(C_{DT} + C_i)}$$

Figure 5. Circuit for pulsing a drift tube, incorporating an intermediate capacitor.

Bipolar Pulsing Circuit



A slow charging circuit is used to charge up the intermediate capacitor C_2 , and this is switched to the drift tube through a low resistance R .

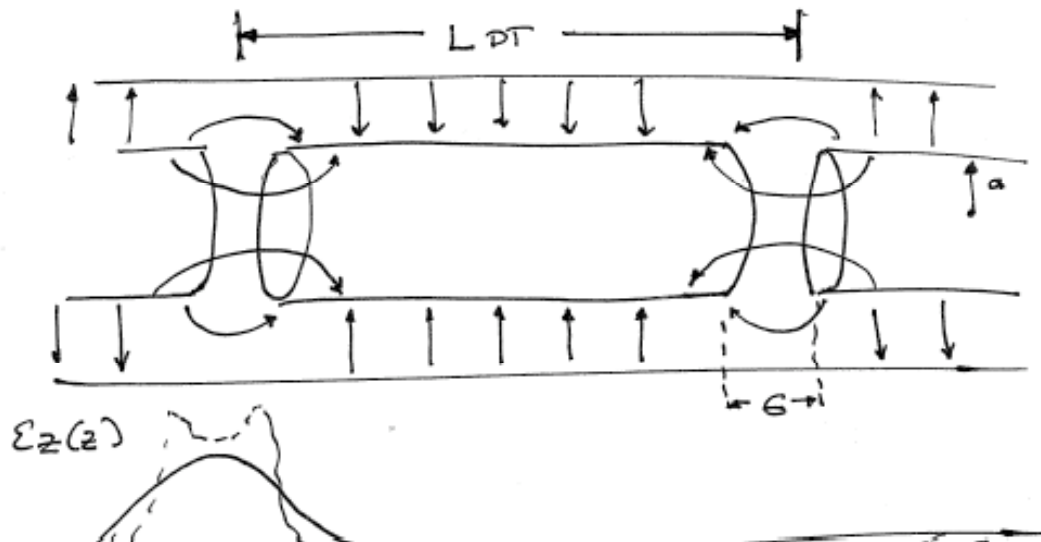
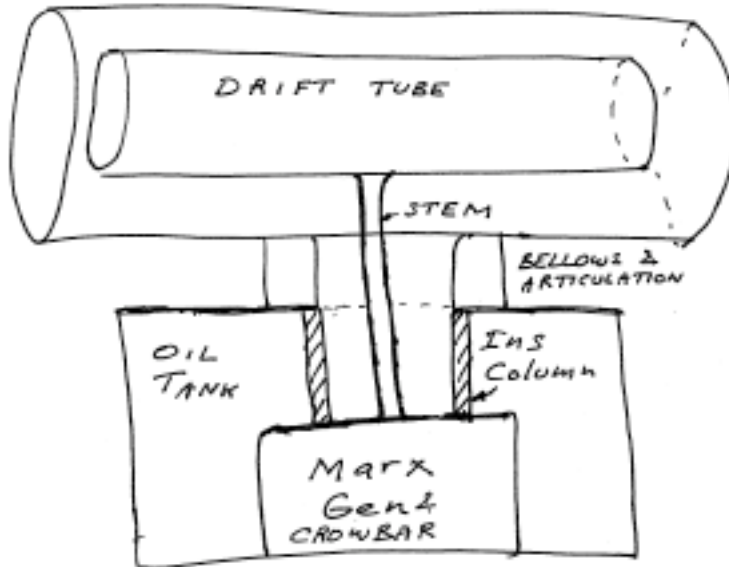
This circuit uses two Marx generators (or pulse transformers) with capacitances C_{M1} , C_{M2} . C_{M1} slowly and resonantly charges up the drift tube capacity C_{DT} through L_1 . C_{M2} slowly and resonantly charges up the low inductance intermediate capacitor C_i . C_i then resistively charges the drift tube to a positive voltage.

$$\text{Initially, } V_{dt} = \frac{2C_{M1}}{C_{M1} + C_{DT}} V_{M1}, V_1 = \frac{2C_{M2}}{C_{M2} + C_i} V_{M2} \text{ after resonant charge.}$$

After S_3 is closed, current flows through the small resistor R , with negligible current through the inductors, with

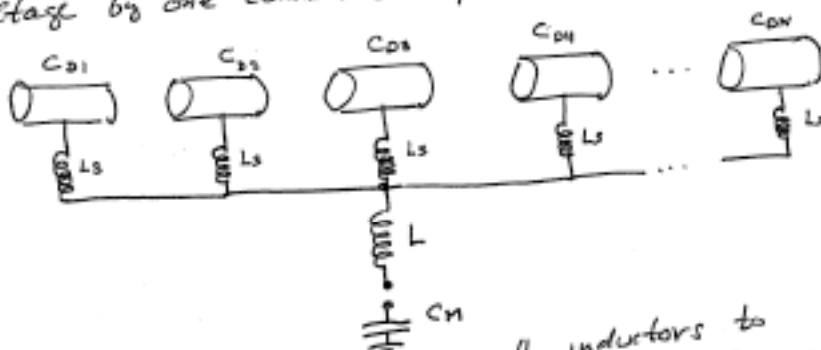
$$V_{dt} = \frac{C_i}{C_i + C_{dt}} V_i \approx \left(\frac{C_i}{C_i + C_{dt}} \right) \left(\frac{2C_{M2}}{C_{M2} + C_i} \right) V_{M2}$$

The resonant charging steps are efficient and may be used to increase the Marx voltages by about 50% at the drift tube and at the intermediate capacitor.

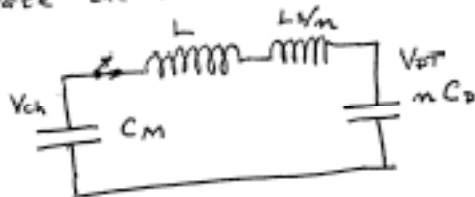


Initial Charging of the Drift Tubes

The drift tubes are all charged to a high negative voltage by one common slow pulser

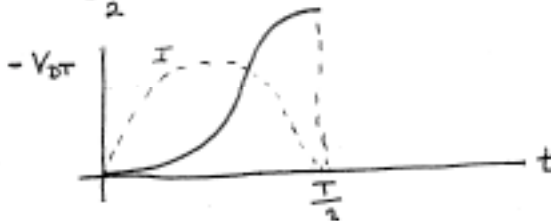


The L_s are relatively small inductors to isolate the drift tubes after switching. Neglecting C_0 variation,



$$V_{DT} = V_{ch} \left(\frac{2C_M}{C_M + nC_D} \right)$$

$$\frac{T}{2} = \text{half cycle charging time} = \pi \sqrt{\left(L + \frac{L_s}{n} \right) \left(\frac{C_M n C_D}{C_M + n C_D} \right)}$$



η = efficiency of energy transfer

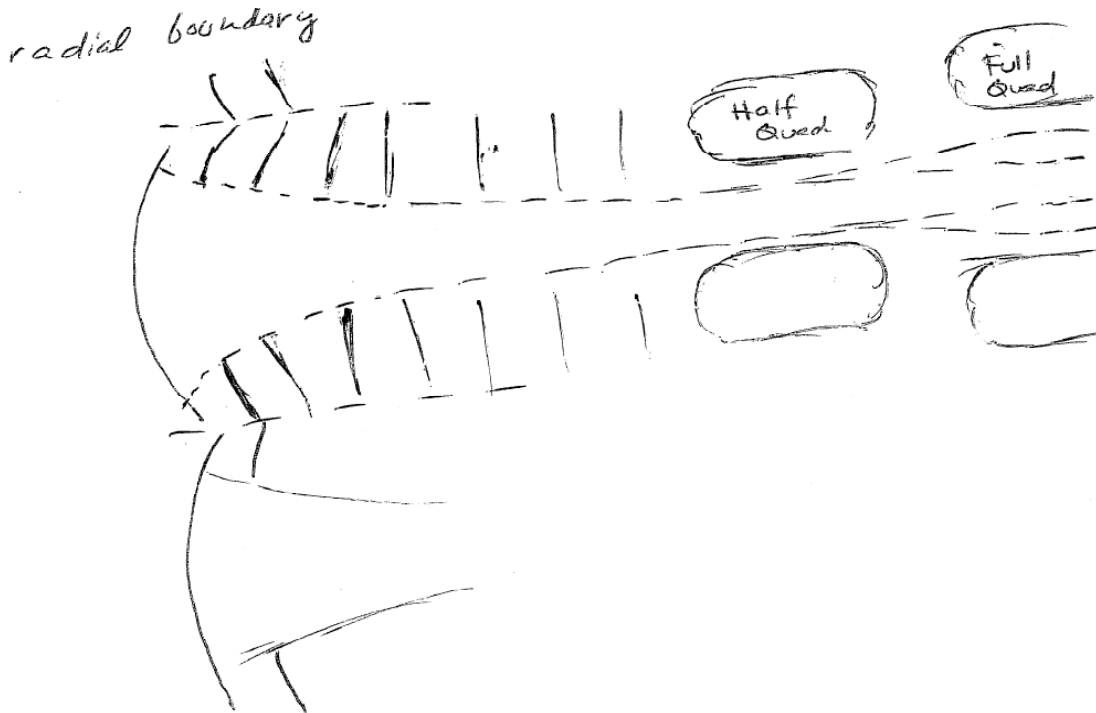
$$\eta = \frac{4C_1 C_2}{(C_1 + C_2)^2} \quad \text{where } C_1 \text{ is } C_{Mn} \text{ and } C_2 \text{ is } nC_D \text{ plus the cable capacity.}$$

Voltage waveforms of the anode emitter and the three drift tubes through capacitive dividers each of which has its own division ratio making the traces unequal. Actual voltages were controlled to equal each other to within 1%.

Sources

If the new multi-beam sources work out as expected, then the standard HCX lattice will be adequate, with a cell size of 7cm. If, however, they are delayed, then the existing ~10cm sources could be matched directly into a double size lattice of 14cm, especially if a converging beam enters the first “half quad”. The larger quads, with voltage scaling as $\sqrt{d_g}$, would transport $0.35\mu\text{C}/\text{m}$ later on, so a beam tilt can be started in the first drift tube to arrive at the higher λ later downstream.

— A gun geometry with a Pierce column or graded radial boundary is sketched below:



One of the problems in a multi-beam source array, especially at low energies where the space charge is high, is beam-beam interaction. This can be reduced to any level by providing a conducting boundary between the beams, with the potential distribution along this boundary matched to the distribution it would have in a converging spherical geometry. The design task is to find a small number of electrodes that satisfactorily approximate this.

Drift Compression and Final Focus

Drift compression and final focus have not been the major concerns of this note, only the accelerator. These would be similar to those of some of the other concepts. Of the

several strategies possible at the end, the major choices are whether the energy tilt required for bunching is left on the beam or removed, whether the steering angles are left on the beams or removed, and whether the beam is focused or not in the drift region. If the beam were kept neutralized, then a long drift distance would enable compression with small tilt and small convergence angles. Because of the low particle energy the beams can be independently steered and the first order chromatic aberrations can be compensated with pulsed dipoles and quads working upstream of the final focus, when the pulse duration is some tens of ns. The biggest unknown is how much the transverse and longitudinal emittances grow during acceleration and beam manipulations. The data on the emittances of the beam at the end of the electrically focused section of HCX, which uses similar currents and technology are encouraging.

Conclusion

In the two major options discussed there are numerous choices, such as outlined in Fig. 6. Closely spaced sources of the existing type but with a Pierce column type of boundary could be designed and built on a short time scale, followed by matching and transport in a lattice with quads which are about twice as large as currently used, all at low risk. The currently developmental multibeamlet sources would shrink the matching section and array sizes, and presumably lower cost. Advantage could be taken of the short accelerator length and the short bunch duration to increase the filling factor; such a system optimizes at a smaller quad size than currently used. The large sources and quads could taper down to a smaller size along the length of the machine, if desired. Choices such as these would be partly clarified by cost estimates of the various options and contrasted with the risks involved. The option of using a stripper to raise charge state to get a higher acceleration rate needs more preliminary work. The full system is shown in Fig. 7. The full HCX beam could be stripped and charge separated at 1 and 2 MeV to get valuable experience, which would point towards the optimum stripping energy and yield. Modest development could also be devoted to the drift tube insulator stack and the pulsers, at low cost, because some of the original Marx generators and crowbar spark gaps exist and can operate in the interesting voltage and pulse duration regions. The switching speed limits and the bunch end containment which also depends on pulsers account for about one half of the length of the drift tubes for HEDP, and consequently about half of the total cost. This is why pulsers have a large part in the note and why pulser development could have a high payoff.

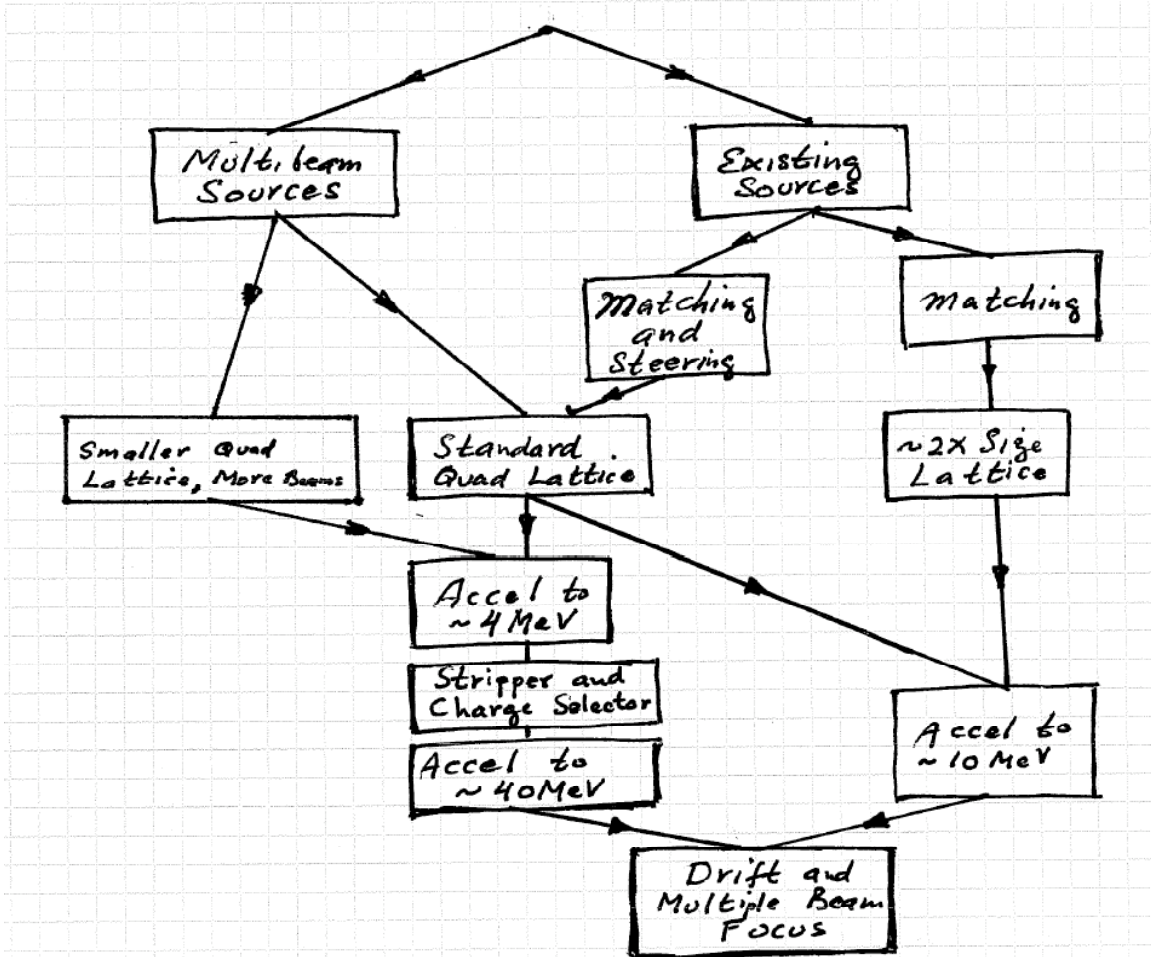
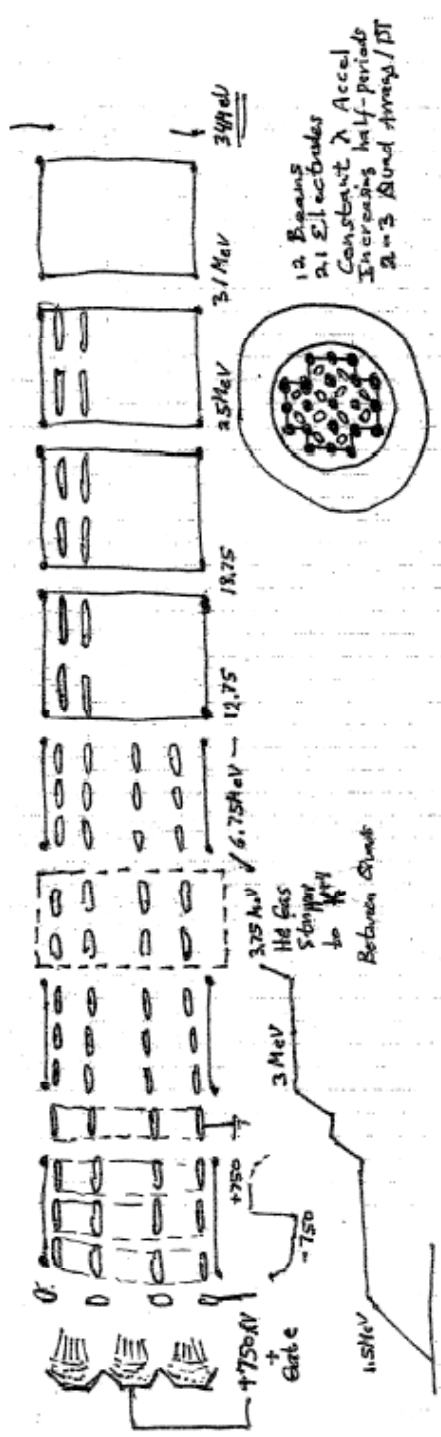


Fig. 6. Various accelerator choices using standard size, larger and smaller quadrupole lattices.



Estimate $\frac{1}{4}$ of Beam goes to $+4$
 $R_0 = \frac{1}{4} \text{AC/m} \times 12 \text{ Beams} \times \frac{1}{3} \text{ in Flat-top} = 1 \text{ AC}$
 Front & back temper ends $\rightarrow 1 \text{ AC}$
 $\phi = 10 \text{ kV/AC} \times \frac{1}{4} \text{ AC/m} = 2.5 \text{ kV}$
 $E_z = \frac{2.5 \text{ kV}}{\frac{1}{8} \text{ m}} = 7.5 \text{ kV/m}$
 Focusing and bending at end easy because of high $\frac{E}{m}$
 Acceleration and focusing tailored for $+4$ after stripper
 ed Cluster outer diam $\sim 40 \text{ cm}$, Beam cluster outer diam $\sim 2.5 \text{ cm}$
 Drift tube diam $\sim 40 \text{ cm}$, Outer Container $\sim 80 \text{ cm}$
 Drift tube length $\sim 1 \text{ meter}$
 Total length $\sim 8 \text{ meters}$, $\langle E \rangle \approx 4 \text{ MeV/m}$
 1 pulser for all the -750 kV slow rise pulses
 7 Independent fast pulses for the $+750 \text{ kV}$ and Shaping
 Inter-drift tube grounds as needed for HV, remaking
 Hope

Figure 7. Drift tube accelerator including a stripper at 4 MeV, to reach higher particle energies.

References

- [1] Ion Induction Linac, 500 Joule Test Bed, PUB-5031, Sept., 1979, LBL.
- [2] Ion Induction Linac Test Bed, PUB-5039, Ap. 1980, LBL
- [3] Proceedings of the Heavy Ion Fusion Workshop, BNL 50769, Oct. 1977

Issues

1. Putting on a bunch-maintenance tilt, which is too big and too abrupt, leads to mismatch.
 Slow and gentle leads to adiabatic
2. Putting on a large energy increase, in the early gaps, with a beam, and an abrupt lattice change also leads to mismatch

How big and bad are these mismatches
Is pulsed rematching required between Dt's

Replacing Dt's with Il gives smaller, more frequent energy gains and allows any pulse duration; as before, accel rate is low from cost, but this may be desirable from beam dynamics.

3. Trade between beam spacing, number of shielding and potential grading electrodes
4. Fill factor for short pulse, short length machine
5. Magnetic lenses in neutralized stripping section
 Pulsed plasma region and question of nearly HV

Salvage valve in arrays, correctors, multi-beam source array

Not much value in DT's, but could explore $\frac{\Delta E/gap}{E}$ issue

Phase-Space Considerations

Roger Bangerter

Historically phase-space considerations have been among the factors that determine the parameters and characteristics of accelerators for fusion. Targets and focusing systems constrain all six dimensions of phase space and therefore place limits on both the transverse and longitudinal emittance of the beam(s) emerging from the accelerator. Although it is, in principle, possible to reduce emittance, the techniques for doing so are difficult to apply to inertial fusion. In general, emittance is expected to increase as the beam is accelerated.

The requirements for HEDP are similar to those of fusion. In both cases the focussed intensity and the specific energy deposition are the fundamental quantities; but, in fusion, the requirement on the rho-r product of the fuel sets a minimum scale size for total energy that is not necessarily applicable to HEDP. The quantities that are important for HEDP and fusion are also important for WDMP but the requirements for WDMP are significantly less stringent. Nevertheless, phase-space considerations are also of fundamental importance for WDMP.

There are a number of effects that can, under some circumstances, produce emittance or lead to its growth. For longitudinal emittance these effects include:

1. The longitudinal “temperature” of the source.
2. Coupling of transverse temperature to the longitudinal direction. This coupling is expected to be rapid. The longitudinal temperature rises to a value that is comparable to, but less than, the transverse temperature. In most accelerators that have been designed, the beam is compressed transversely after it leaves the source so the transverse temperature of the beam can be higher than the source temperature, even without transverse emittance growth.
3. Scattering and charge exchange in the source.
4. Longitudinal energy variations or wiggles on the beam emerging from the source. Although there is a 1-D analytic extraction waveform that gives a monoenergetic beam, these wiggles have always been seen in experiments and in simulations, for example, in the simulations shown by Enrique Henestrosza at this workshop. It is not known if a perfect waveform exists in 3-D.
5. Electrons. Fields produced by electrons are often unpredictable. They can produce nonlinear fields that lead to effective emittance growth.
6. Waveform errors in the injector and accelerator -- and in any final ramp used to compress the beam longitudinally.
7. Nonlinear or nonuniform self fields.
8. Mismatches between self and applied fields.
9. Instabilities, waves, etc. in the injector, accelerator, and final compression section.
10. Virtual anode effects.
11. Inductive effects.

12. Rapid transitions between accelerator sections. Steve Lund has recently shown that rapid transitions can have a significant effect on transverse phase space. It is likely that there will be longitudinal analogs of these effects.

These effects can be quite constraining. Consider, for example, some recent modular-solenoid driver cases presented at the 2004 HIF Symposium. These systems were designed to deliver about 6.7 MJ of energy -- appropriate for the hybrid target. Economic considerations limit the number of modules. The cases presented at the Symposium used about 24 modules. Each module accelerated two pulses of neon ions to about 210 MeV. The initial duration of each pulse was approximately 20 ns. There are important technical issues associated with double pulsing; but, for now, assume that double pulsing works and that the bunches can be combined longitudinally as they approach the target. Thus there are 12 beam lines on each side of the target.

Consider first a single beam line. MRC has simulated a 1-beam compression and focusing system based on neutralized drift compression with solenoidal focusing into an adiabatic plasma lens, followed by a 5 mm, 50 kA channel. The results were presented at the VNL PAC meeting in August 2004. The 5-mm channel is appropriate for the hybrid target. Other parameters are an initial beam current of 3.35 kA of singly charged neon, an initial beam radius of 10 cm, a normalized transverse emittance of 8 mm·mr, 147 kJ of beam energy, and an initial pulse duration of 210 ns. These numbers give an average kinetic energy of approximately 210 MeV, an ion velocity of 0.15 c, a line charge density of 75 nC/m, and a charge per pulse of 0.7 mC. A total of 24, 147-kJ beams would give 3.5 MJ, so the simulations rigorously apply to only one of the two pulses in each beam line (with a few percent safety factor). The simulations show a remarkably large tolerance to energy spread, a total of 20% head-to-tail corresponding to a half width of 21 MeV. With this energy spread, slightly over 90% of the beam falls within a 5-mm spot at the end of the channel. The duration of the final pulse for a 7-MJ target is of the order of 10 ns, but it must have a special shape and a rapid fall time to avoid wasting energy. It appears reasonable to believe that one could synthesize the pulse by appropriate timing of a number of individual pulses having rounded pulse shapes with a width of 5 ns or a half width of 2.5 ns. Combining 2.5 ns and 21 MeV, we get a longitudinal admittance of 0.0525 eV·s.

For comparison, consider the longitudinal emittance produced by a typical ion source. Simulation numbers are available for the multi-aperture ion source recently designed by Joe Kwan and Dave Grote. The simulated performance of this source is comparable in brightness to the measured properties of typical thermionic sources for potassium. For lighter ions such as neon (or sodium), the multi-aperture sources will likely be superior.

Grote's simulations give 0.57 A of 40-amu ions at 1 MeV. After beamlet merging, the mean radius of the elliptical beam is 1.55 cm and the normalized emittance is 0.9 mm·mr. One can estimate the transverse beam temperature using the familiar formula,

$$\sigma = m (0.5\gamma a)^2 \quad (1)$$

where ϵ is temperature (eV), m is ion mass (eV), and ϵ and a are respectively normalized emittance and beam radius in consistent units (m·rad and m). Using Grote's numbers one obtains $\epsilon = 30.6$ eV. If one scales these sources to different current by changing the number of beamlets, one would expect the temperature to remain invariant since the electrostatic energy of a single beamlet is invariant. Similarly, the temperature should not depend strongly on ion mass because the line-charge density doesn't depend on ion mass.

By what factor must the source be scaled? Obtaining the required 0.7 mC of charge in 20 μ s requires a current of 35 A. For neon, the source would produce 1.4 times as much current as for potassium, or 0.806 A. The source must therefore be scaled up a factor of $35/0.806 = 43.4$ in transverse area or 6.59 in radius. Remarkably, this scaling factor gives a beam radius of 10.2 cm which is essentially consistent with the radius chosen by MRC. (The line-charge density and therefore the radius are more or less invariant in a solenoidal system. Note also that the normalized transverse emittance given by equation (1) would be 8.3 mm·mr.) Anyway, no additional expansion or compression of the beam is needed so 30.6 eV remains a good estimate of the transverse temperature. Assume that one half this temperature is transferred to the longitudinal direction. Transformed to the laboratory, a longitudinal beam temperature ϵ gives a longitudinal energy spread $\Delta T = \pm 2(2\epsilon T)^{1/2}$ where T is kinetic energy. The initial factor of two comes from multiplying the rms velocity spread by 2 to convert to a value suitable for calculating 'edge' emittance. Using the source voltage of 1 MV, one obtains $\Delta T = \pm 11.1$ keV. Multiplying by one half the initial pulse duration (10 μ s) to get longitudinal emittance, one obtains 0.11 eV·s which is slightly more than twice the admittance of the focusing system. Note that this emittance comes only from effect 2 in the list given above.

Now consider double pulsing. If one could combine two pulses perfectly in the longitudinal direction, the longitudinal emittance would double. If the interpulse time is equal to the pulse duration (reset time equal to pulse duration) the longitudinal emittance would increase by a factor of 3 – actually more than a factor of three because of non-negligible rise and fall times. Such a strategy would already have a significant effect on accelerator efficiency because the core losses during reset would equal the core losses during one of the pulses. With a single pulse, the reset losses are much lower because the reset is done slowly.

In summary, based on a consideration of only one of the many sources of longitudinal emittance, and on a specific type of ion source and final focusing system, the estimate just described fails to give an acceptable answer by at least a factor of 4.

Is the estimate just described likely to be optimistic or pessimistic? By working on target design, one might be able to use a rounded pulse shape that is natural to produce. Maybe one could hope to increase 2.5 ns to nearly 5 ns. Or perhaps less than half the transverse temperature might be transferred to the longitudinal direction. On the other hand, the current calculations appear to be optimistic in a number of ways. The neglect of all sources of longitudinal emittance except the second has already been mentioned. It appears to this author, that some of these effects could easily give contributions to

longitudinal emittance that are comparable to or larger than the effect considered. Also, the MRC simulations may be quite optimistic. The initial beam size is assumed to be 10 cm; but, according to equation (2) of Lee and Briggs (LBNL-40774), the rms on-axis solenoidal field would have to be 10.6 T to transport the assumed 75 C/m. Therefore the peak field would have to be greater than 10.6 T, particularly if one considers the substantial gaps and dead-space needed for a high-gradient machine. This problem is exacerbated if one includes the relatively large rise and fall times needed to keep the ‘ear’ fields within acceptable bounds. In the ‘all-ears’ limit (a parabolic pulse) one would have to either increase the peak line-charge density by 50% or increase the pulse length by 50%. Also, since only one of the two pulse was considered, the line-charge density after compression would have to be increased by an additional factor of two to make the simulations realistic for 24 beams. Furthermore, the simulations assumed unphysical magnetic fields for the electron barrier and they assumed a perfectly linear adiabatic lens and a perfectly linear channel. Effects of stripping and recombination were ignored except at the beginning of the adiabatic lens where stripping to +10 was assumed to be instantaneous and complete. Moreover, the longitudinal admittance of such a system decreases as transverse emittance increases. The initial transverse emittance of the example ion source already exceeds the emittance assumed in the simulation but we have assumed that some of the transverse emittance is coupled to the longitudinal direction. Regarding transverse emittance, it would be necessary to combine 12 beams transversely into a single channel. Even if the distance between beam centers were only 3 beam radii, the transverse emittance in the channel would have to increase by a factor of about 5 relative to the 1-beam case. Finally, there is one effect that remains largely unstudied. At the target, it is necessary to provide return-current channels to carry the current away from the target. These would presumably be perpendicular to the beam channels. The angles of the ions relative to the channel axis are large enough (of the order of 100 mr) that a small distortion or expansion of the beam channels by the target and/or the return-current channels (for example, a 1 mm expansion 1 cm from the target) could cause significant beam loss. Parenthetically, channel expansion is another effect that should be investigated. In an MHD model, the transverse beam pressure greatly exceeds the magnetic pressure.

There are also a number of effects that must be considered regarding transverse emittance. These include:

1. The temperature of the source. Presumably some of this temperature could be transferred to the longitudinal direction if the longitudinal temperature is sufficiently low. The transfer of longitudinal energy to the transverse direction is expected to be slow.
2. Mismatches and transitions.
3. Errors, nonlinearities, and imperfections in the focusing elements.
4. Instabilities
5. Electrons
6. Misalignments

As in the longitudinal case, these considerations can place important limits on

performance. For example, one can easily show that the normalized transverse admittance of the 5-mm, 50-kA channel described above is approximately 75 mm·mr. If the transverse emittance were to increase by even a factor of two in the machine, to say 15 mm·mr, 12 combined beams would completely fill the transverse admittance of the channel, reducing the longitudinal admittance, in this approximation, to zero. In summary, it appears that the example case fails to satisfy the phase-space constraints – probably by a substantial factor.

What can be done to improve the situation? As noted above, improvements in targets could help. In addition there appears to be some room for design improvements and further optimization of the compression and focussing system. One could also hope for brighter ion sources, although this strategy would work only if the source is the dominant source of emittance. One might also try to use a different final focusing system where transverse combination into a single channel is not required.

Consider a system that utilizes neutralized ballistic focusing. If one considers only transverse emittance and chromatic aberrations, one can easily derive the usual equation for the minimal focal spot radius $r = (2\chi/f\Delta)^{1/2}$ where χ is a chromatic factor ($\chi = 1$ for a simple solenoidal system) and f and Δ are respectively the standoff between the final lens and the target and the fractional energy spread (half width). If one puts in the estimates of emittance and energy spread obtained from the example case, the focal spot is too large by a substantial factor if f is greater than about 1 m.

Of course, one could design a modular-solenoid system that meets the phase space requirements by increasing the kinetic energy and ion mass and/or using more, smaller beams (modules). The question is whether such a system can have reasonable economics and efficiency.

As noted above, the requirements are relaxed significantly for WDMP. Some preliminary estimates at the Workshop suggested that phase-space volume, based on only a few of the considerations listed above, might be okay, but not by a large margin, for some of the WDMP systems. More work is required to do the calculations accurately and to include all the important effects.

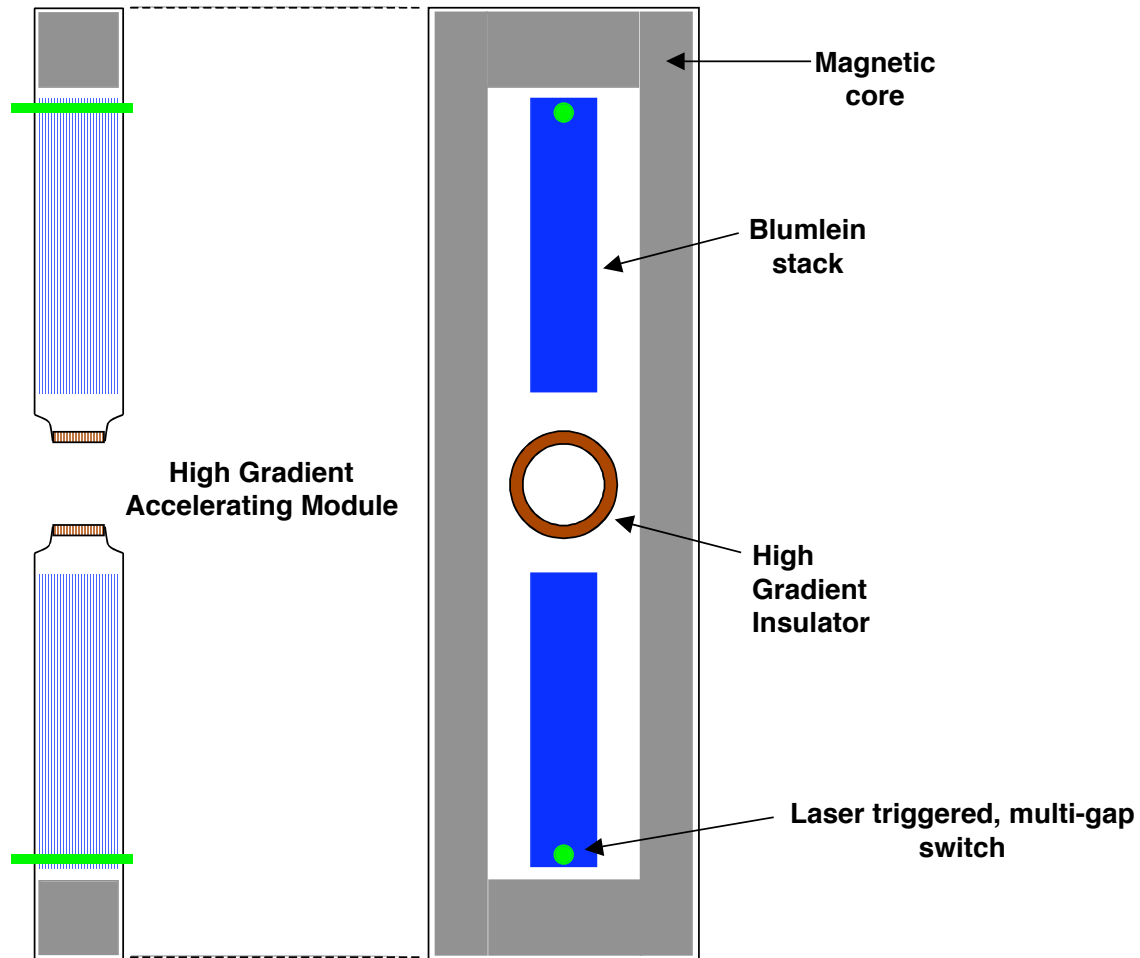
In conclusion, phase-space considerations are important. Many accelerator options for WDMP and HEDP have been suggested but only a very small number can be pursued. It is likely that careful consideration of phase-space requirements will eliminate a number of the options – particularly if the ability to extrapolate from WDMP to HEDP and/or fusion is believed to be an important consideration.

High Gradient Induction Cell

G. J. Caporaso
Lawrence Livermore National Laboratory

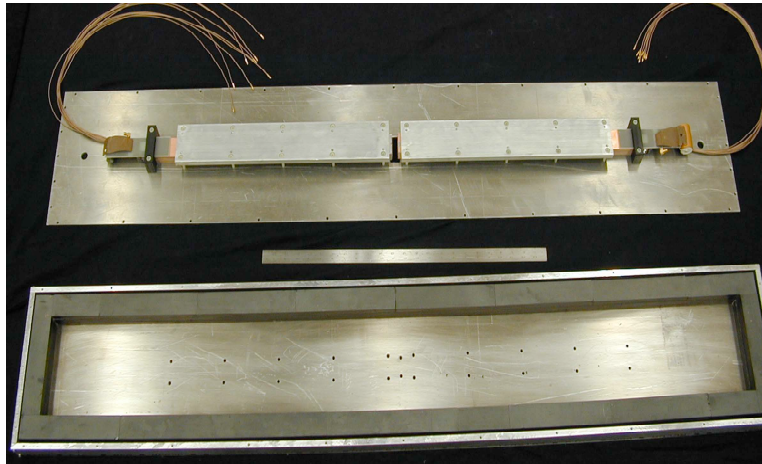
A concept being developed for high current electron beams may have application to HEDP and is described here. It involves the use of planar Blumlein stacks placed inside an induction cell. The output end of the Blumlein stack is applied across a high gradient insulator (HGI)¹. These insulators have been used successfully in the presence of kilo Ampere-level electron beam currents for tens of nanoseconds at gradients of 20 MV/meter.

At the switch end of the Blumlein (the end opposite the output end) a voltage erects upon closure of the switches. A magnetic core material is used to prevent the discharge of the lines from the switch end. The system under active development uses a laser-triggered, multi-gap gas switch. An illustration of the concept is shown below.



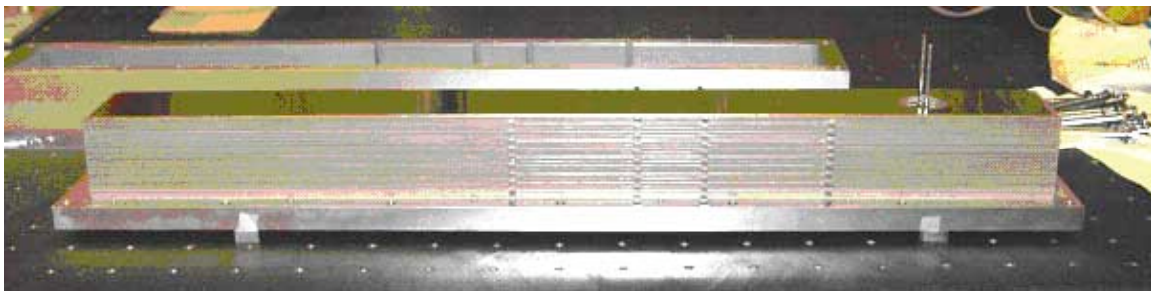
Proposed high gradient induction module shown from the side (left) and from the top (right). The high gradient insulator is deliberately made shorter than the cell in order to provide room for a short magnetic focusing element.

This goal for this cell is an average accelerating gradient of 3-5 MV/meter. The concept shown above employs two Blumlein stacks and a ferrite core for isolation. The cell architecture has been verified by constructing a low voltage model that uses avalanche transistors as switches and a material called RT-Duroid (a commercially printed circuit board laminate that has a relative dielectric constant of 10.2 and is available in large sheets) for the Blumleins. The working model is shown below.



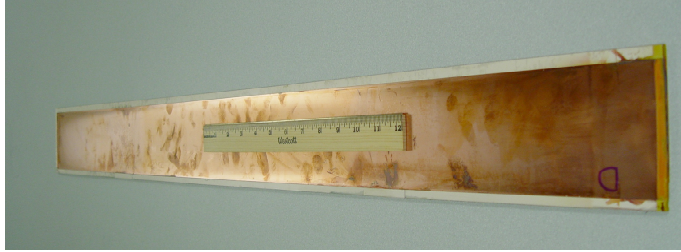
The scale cell model shown with the top metal cover removed. The ferrite isolation in the form of “bricks” can be seen in the bottom portion of the picture while the two Duroid Blumlein stacks can be seen in the upper half of the picture. This cell produced an output pulse of 10 ns.

At the present time a high voltage test is underway using a Duroid stack of 20 Blumleins and the multi-gap laser triggered switches. The stack should produce a 20 ns wide output pulse.



A Duroid stack of 20 Blumleins approximately one meter in length and 11.5 cm high (with end plates). The individual lines are charged from 20 – 30 kV.

We have been developing a castable dielectric material with a relative dielectric constant of about 40 that has large bulk breakdown strength. We were recently able to cast a large size stripline using this material. Use of this material should permit a factor of two reduction in the lateral size of the induction cells. The material is a suspension of high dielectric constant material in a plastic-like binder and can be cast into almost any desired shape.



A one-meter long stripline of the castable dielectric. This line has a relative dielectric constant of about 40 and is relatively flexible.

This cell concept has the potential to increase the average accelerating gradient of electron induction machines by about an order of magnitude but has several disadvantages. In contrast to the usual induction cell, the pulsed power drive is internal to the cell and is fixed by the stripline and core geometry; it cannot be adjusted externally. This disadvantage can be somewhat offset by tapering the Blumleins to arrive at a desirable output pulse shape. Also, the core volume tends to be rather large, as it must surround the Blumleins.

Because the core is not driven uniformly magnetic flux does not symmetrically flow in the core; some of the flux leaves the core and closes through the stripline leading to a reduction in core impedance over what would be the case for symmetric drive. In the scale model, the output pulse into a matched load was approximately two thirds of the charge voltage due to the loading of the lines by the core. This problem can be reduced by the use of higher dielectric stripline material.

In order to preserve as high an accelerating gradient as possible relatively little space is available for focusing elements. This space is made available by increasing the gradient on the HGI as compared to the cell interior. The length of the HGI may be made smaller than the cell length by a factor of 2 to 4 leaving over the half of the beamline available for focusing elements. While this appears adequate for electron beam applications it may not be enough space for HEDP.

References:

1. Sampayan, S., Vitello, P., Krough, M., and Elizondo, J., IEEE Trans. Dielectrics and Electrical Insulation 7 (3): 334-339 June 2000.

Final Focus and Drift Compression Working Group Overview

Edward Lee

The Final Focus and Drift Compression group examined a wide variety of issues and several system scenarios, with the general objective of bringing beams from an accelerator to an experiment. The typical final pulse duration ($t_f \approx 1.0\text{ns}$) and spot radius ($r_s \approx 1.0\text{mm}$) present a challenging task that involves a number of innovations, to be outlined below. Short reports covering many aspects of a compression/focus system follow this overview. A typical parameter set, considered by the entire workshop, is as follows:

ion = Ne^+ (or Ne^{++})
kinetic energy = 19 MeV
 $\beta = .045$
ion number = 1.4×10^{13}
Total energy = 43J
Total charge = $2.2\mu\text{C}$ (or $15\mu\text{C}$)

At the end of acceleration the pulse duration is about 100-200ns and it is to be compressed to 1.0ns by the imposition of a velocity tilt. This is a head-to-tail linear ramp of velocity (with only minimal errors allowed) such that the pulse tail nearly overtakes the pulse head at the experimental target. Pulse length in meters decreases from 1.35m to 1.35cm in x100 compression, and line charge density increases by the same factor. For charge state +1 the final density is $160\mu\text{C}/\text{m}$, and the self-force would be enormous if this were done in vacuum – center to edge potential of 1.4MV! So it is assumed that the beam pulse may be neutralized by plasma or injected electrons, and the self-electric and self-magnetic fields are nearly eliminated. A residual potential of order 500 volts is expected since electrons must be accelerated to at least a fraction of the beam speed. The excess of electrons also neutralizes the space charge field in the longitudinal direction. Plasma should be “over-dense” to accomplish this condition, i.e. $n_e > 10 n_b$ in charge state +1. However this is not such a high density of plasma that scattering and stripping of the beam ions is expected to be appreciable, except very close to the target if extra plasma is created there; this is an issue for additional research.

The velocity tilt that is imposed at the start of drift compression is not removed by the space charge force near the final focus (as it is in the standard Heavy Ion Fusion approach) because the field is neutralized. Therefore the beam pulse must be focused with a large variation of momentum still present, and the resulting chromatic aberration must be considered. If a single, short focal length, solenoid is used to focus the beam, then tilts as large as $\pm 5\%$ seem to be manageable, i.e. $\Delta\beta/\beta \approx 0.10$. Such a tilt limit places a lower bound on drift distance.

$$\text{drift distance} = \frac{\text{initial pulse length}}{\text{tilt}}.$$

So for the example of x100 compression, a full tilt of $\pm .5\%$ has drift distance $= 1.35 \times 10 = 13.5\text{m}$. Roughly speaking, the deviations from linearity in the tilt waveform must be smaller than the inverse of compression, so for compression by x100 with tilt

$\pm 5\%$, the random velocity variations must be less than .1% times the beam velocity. This is a very significant restriction on accelerator design and technology.

Although it received relatively little attention at the workshop, an HEDP facility should be able to serve multiple users, say $N=5$, but not necessarily provide beam to more than one user at a time. This consideration implies N separate beam lines and a switchyard. The separate beam lines must be spaced far enough apart so that experiments are physically separated by at least a few meters, so the switching is through angles of order 20 radians or more. Chromatic problems must again be considered in switchyard design. It will be very helpful in this regard if beam trajectory bending by magnetic dipoles can be carried out inside the neutralizing plasma rather than upstream in the accelerator vacuum.

Beam transport during compression is generally assumed to use nearly continuous solenoid magnets of moderate strength ($B \approx 1.0T$), whose purpose is to both guide the beam centroid and confine the beam's transverse thermal pressure. For a given emittance (edge unnormalized value = ϵ) and beam radius a , we need

$$\epsilon \approx \frac{2(\epsilon_0 \epsilon) \epsilon}{a^2},$$

where $(\epsilon_0 \epsilon) = \epsilon mc/q$ is the ion's magnetic rigidity. For the 19MeV N_e^{+1} , we get $(\epsilon_0 \epsilon) = 2.8$ T-m. For $\epsilon = 10^{-5}$ (ϵ) m-r and $a = .02m$, we need only $B = 2 \times 2.8 \times 10^{-5} / (.02)^2 = .14T$. However, the final focus lens may require a high field ($B \approx 15T$) to produce a desired short focal length ($f \approx .4m$). The short focus is needed to overcome the finite emittance, since the spot radius is limited to

$$r_s \geq \frac{\epsilon}{\theta}$$

where θ is the convergence cone half angle to the target. For the relatively large $\epsilon = 50mr$, and $\theta = 10^{0.5} mr$, we have $r_s \geq 10^{0.5} / .05 = .2mm$. This would be excellent, but the chromatic aberration is expected to considerable increase this value, as would a larger emittance.

At this stage we may summarize the situation as follows:

- HEDP with accelerated ion beams
- ϵ large space charge force ϵ must neutralize
- ϵ magnets must work in plasma and focal design be insensitive to tilt

Some broad physical issues are apparent:

- How large are deviations from charge and current neutralization?
- Is the beam-plasma interaction stable?
- What are the effects of stripping, scattering and energy lose?
- What is the tilt limit?
- Does the neutralizing flow of electrons get significantly impeded by magnetic dipoles and quadrupoles?
- On what time scale can a magnet be pulsed inside a neutralizing plasma (if needed)?

Further considerations of beam dynamics for design include:

Strip to high charge state advisable?
 Matching of the beam envelope from the accelerator to the neutralized beam line
 Mechanism for emittance growth during transport
 Flexibility of final focus for experimenter
 Achromatic switchyard
 Flexibility of major parameters - ion mass, energy, current, pulse duration.

In designing a compression and focusing system various “tools” or “tricks” are available that can be invoked to match the beam from the accelerator to the requirements of the HEDP experiment. Several of these have been mentioned before, but here we wish to emphasize that there are varying levels of uncertainty, risk, and need for development. In fact the present VNL program is now largely oriented to their experimental and computational investigation.

A fundamental concern is the effect of a transverse magnetic field on neutralization by electrons. Suppose B_y is a dipole field of (say) 1.0 kG strength. We may reasonably assume electrons flow across the beam path along field lines to achieve a high level of charge neutrality. However current neutrality, which is also desired, is impeded. If current is also neutralized, the longitudinal drift speed of the electrons is

$$v_e = v_b \frac{n_b}{n_e},$$

and the induced electric field transverse to the beam is

$$E_x = v_e B_y = v_b \frac{n_b}{n_e} B_y.$$

This force acts to oppose the intended bend force ($= q v_b B_y$), such that the total force on the beam is now

$$F = q v_b B_y \left[1 - \frac{n_b}{n_e} \right].$$

This may be “ok” if n_e and n_b are steady and predictable, or the force reduction may be made negligible by making n_e large with locally dense preformed plasma. The simulation code LSP was used to investigate the correctness of this simple model, with a surprising result: net bending force was close to that with no plasma. This is not understood.

Another simulation result is the predicted suppression of the two-stream instability by the application of a solenoidal field, which effectively eliminates fast growing transverse modes.

Stripping was estimated to be a marginal problem. The estimated cross section for 19MeV $Ne^+ \rightarrow Ne^{++}$ on Hydrogen atoms is $\sigma = 3 \times 10^{17} \text{ cm}^2$. Suppose the pressure is as high as 1.0 mT. Then the stripping distance is $(n_H \sigma)^{-1} \approx 1000 \text{ cm}$. For H pressure much, much less than 1.0mT (the usual situation) we may assume that the beam remains in charge state +1.

It may be desired to pre-strip the beam to $q \approx +7$, which is the equilibrium state (± 1). This lowers the rigidity by a factor of 7 and reduces the required strength of the

final focussing magnet by the same factor. However about half of the beam ions would be lost in the stripping process.

An incomplete but illustrative list of tools and tricks includes:

- Neutralized drift compression
- Strong solenoid lens for final focus ($\sim 15\text{T}$)
- Magnetic dipoles for:
 - Stopping upstream electron flow
 - Achromatic switchyard
 - Achromatic multiple beam illumination of target
- Instability suppression by solenoids
- Pulsed lenses to compensate chromatic aberrations
- Adiabatic funnel close to experiment

Conceptual system layouts were considered for a single beam accelerator and multiple (18) beam and (12) beam rf accelerators.

Case 1

The single beam system is relatively straight forward, with bends only in the upstream switchyard. However there are two general versions for the drift section, as shown in the following sequences (fig. 1)

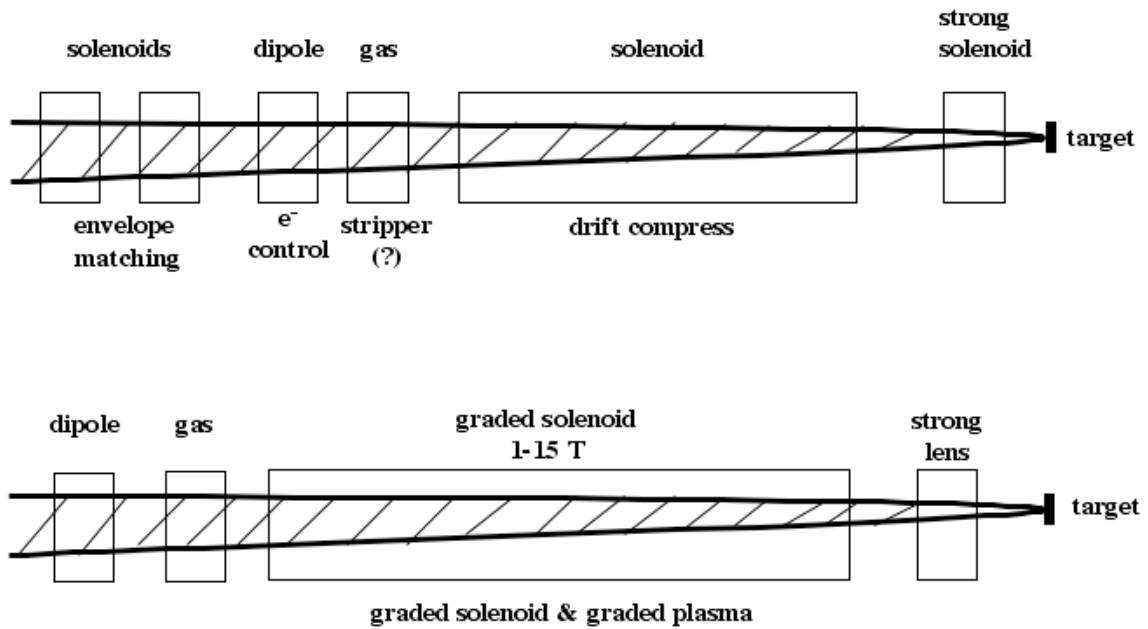


Figure 1

The idea behind the graded solenoid is to make an adiabatic match of the beam to drift system equilibrium conditions. This avoids the complications of upstream matching.

Case 2
rf acceleration – scheme 1

This presents 18 beams in a ring pattern, with tilt = $\pm .035$, and x200 total compression. The compression distance is therefore $2.7\text{m}/.07 = 39\text{m}$. The accelerator system is expected to produce the large value of emittance = $3\text{ }\mu\text{m-mr}$ (rms-normalized) so the unnoralized edge value is $4\sigma_x/\sigma_x = 2.7(\text{ }\mu\text{m}) \times 10^{-4} \text{ m-r}$.

Drift compression is in 18 separated lines, which are brought together a few meters from final focus using achromatic bend systems of a standard type using weak quadrupoles (see fig. 2). A special bend is inserted in each line to disperse the beam proportional to tilt in a way that compensates the chromatic effect at final focus. That is, a first order achromat for beam position is created. A strong, multibeam final lens (15 T solenoid) brings the spot radius to a 1.0 cm, followed by an adiabatic lens to produce a 1.0 mm final spot on target. This last element is described in a short note in the proceedings (see S.S Yu, "Adiabatic Plasma Lens -- A Current Density Booster"), and is an extrapolation by a factor 3 from what is achievable at present.

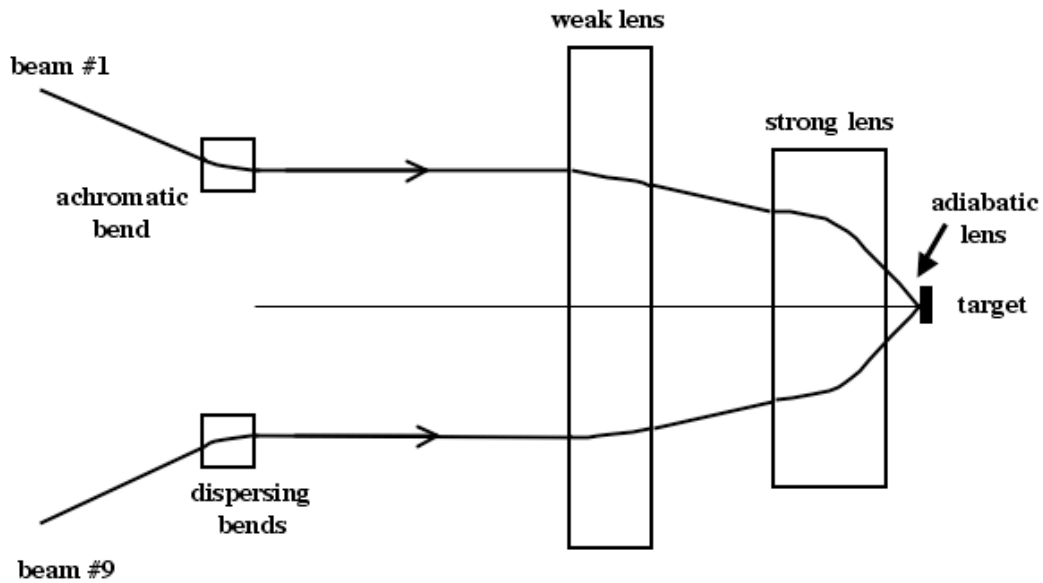


Figure 2

Case 3
rf accelerator – scheme 2

Here we merge 12 beams into one, and emittance is assumed to blow up to $\sim 3 \times 10^{-3}$ (m-rad). To achieve small spot radius on target ($r_s \approx 1.0 \text{ mm}$) measures are taken upstream, with the use of pulsed lenses (in vacuum) to compensate chromatic effects (see fig. 3). All beams are focused at once in a large strong lens with large cone angle ($\approx 200 \text{ mr}$). This takes the collective radius down to 1.0 cm. A further decrease to 1.0 mm is achieved with the (hypothetical) adiabatic lens. In this scheme the tilt is $\pm 5\%$ and the beam radius drops from 30cm to 1.0 cm in only 3.0m distance. It is expected that a significant halo will be produced, but a “good” pulse core will be available for experiments.

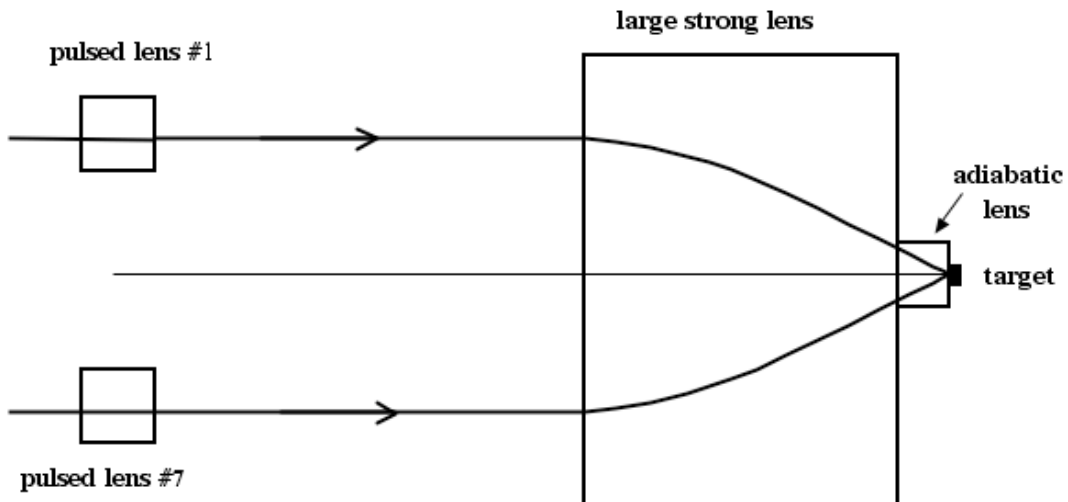


Figure 3

Strong Solenoidal Final Focus Lens for HEDP

Edward Lee

Ion driven HEDP experiments require small focal radii for beam pulses that have very large momentum variations. This is because the plasma that neutralizes the beam's space charge also eliminates the longitudinal electric field, which could remove the velocity tilt prior to final focus. A typical assumed momentum variation is around $\pm 5-10\%$, applied to compress the pulse by a factor of 200 in duration. This range is well beyond the maximum $\pm 1\%$ that is typical of high-energy accelerators. The complicated combinations of bends and sextupoles that are used to produce an achromatic focus for small momentum spread appear unattractive and probably mal-functional in the present context due to their large higher order aberrations. An alternative, which is proposed here, is to live with the (second order) chromatic aberration of a linear lens system, and design the final focus to make the effect no worse than that of the natural focal spot blowup due to finite emittance. This is done by using a single strong lens (a short solenoid) that acts on a relatively small initial pulse radius in parallel-to-point focal optics. The focal length of the lens is made as short as possible in order to minimize the spot radius due to emittance. A third important consideration is that the physical length of the lens be less than its focal length so that the HEDP experiment does not get placed inside the magnet bore.

The competing desires for the focal system would not be very difficult to accommodate if the "magnetic rigidity" of beam ions (momentum/charge) was less than about .5 T-m. However, for the typical HEDP example of 20MeV Ne^+ , the rigidity is $[B\rho]=2.88$ T-m. Suppose the focal length is $f=.5$ m and the length of the magnet's wire layer is $\ell=.25$ m. The high rigidity requires peak solenoid field of about

$$B = \frac{2[B\rho]}{\sqrt{\ell f}} = \frac{2 \times 2.88}{\sqrt{.25 \times .5}} = 16.3T$$

Fortunately solenoids with fields this high are now available commercially, built with NbSn wire cooled to 4.2K.

We can now compute the approximate focal radius for a concrete example:

$$\text{Ion} = 20\text{Mev } Ne^+ \quad \begin{cases} q = 1 \\ m = 20\text{amu} \end{cases}$$

$$\text{normalized edge emittance } \epsilon_t = 10^{16}(\text{m}) \quad m \text{ } r$$

$$\text{momentum variation } \frac{\Delta P}{P} = \pm .05$$

$$\beta = \sqrt{\frac{2E}{Mc^2}} = .0463$$

$$\text{emittance } \epsilon = \frac{\epsilon_t}{\beta} = 2.16 \times 10^{15}(\text{m}) \quad m \text{ } r$$

$$\text{initial radius } a_0 = .015m$$

Peak Magnetic Field $\square = 16.3T$

Wire layer length $\ell = .25m$

$$\text{Rigidity } [\square \square] = \square \frac{Mc}{qe} = 2.88T \square m$$

$$\text{Focal Length } f = \frac{4[\square \square]^2}{\square^2 \ell} = .50m$$

$$\text{Convergence half angle } \square = \frac{a_0}{f} = .03\text{radian}$$

$$\text{Natural spot radius from emittance } r_e = \frac{\square}{\square} = .72mm$$

$$\text{Chromatic aberration radius from } \square P/P \quad r_c = a_0 \frac{\square P}{P} = .75mm$$

$$\text{effective spot radius } r_s = \sqrt{r_e^2 + r_c^2} = \underline{\underline{1.04mm}}$$

The above case (which does achieve an effective spot radius of about 1.0mm) also displays the tradeoff among variables. For example, a larger initial radius a_0 would increase \square and therefore decrease r_e . But larger a_0 would also increase r_c . Shorter f would be helpful because we could then increase \square at constant a_0 or decrease a_0 at constant \square . But shorter f requires even higher \square than the already impressive 16.3T that was assumed. Another idea is to strip the neon ions to a higher charge state, say +7, at some point prior to final focus. This has penalties such as loss of ~50% of the beam pulse and probable emittance growth.

Issues for Neutralized Drift Compression and Focusing of Heavy Ion Beams for HEDP

D. R. Welch, ATK Mission Research, Albuquerque, NM

Introduction

In order to study high energy density physics (HEDP) with heavy ion beams, the beam radius must be focused to < 1 mm and the pulselength must be compressed to < 1 ns. The typical scheme for temporal pulse compression makes use of an increasing ion velocity to compress the beam as it drifts and beam space charge to stagnate the compression before final focus. Shown schematically in Figure 1, beam compression in a neutralizing plasma does not require stagnation of the compression enabling a more robust method.¹ The final pulse duration can be minimized at the HEDP target can be programmed via an applied velocity tilt and theoretically is limited only by the longitudinal emittance. In the schematic for solenoidal focusing, the beam must transition from Brillouin flow equilibrium in vacuum into a plasma region with only weak solenoidal fields. The neutralizing plasma allows the high perveance beam to compress nearly ballistically before being transversely focused by a strong solenoid and discharge channel. In this section, several issues relevant to neutralized drift compression (NDC) are investigated mainly with the particle-in-cell code LSP.² The sensitivity of the compression and focusing to beam momentum spread, plasma, and magnetic field conditions is studied.

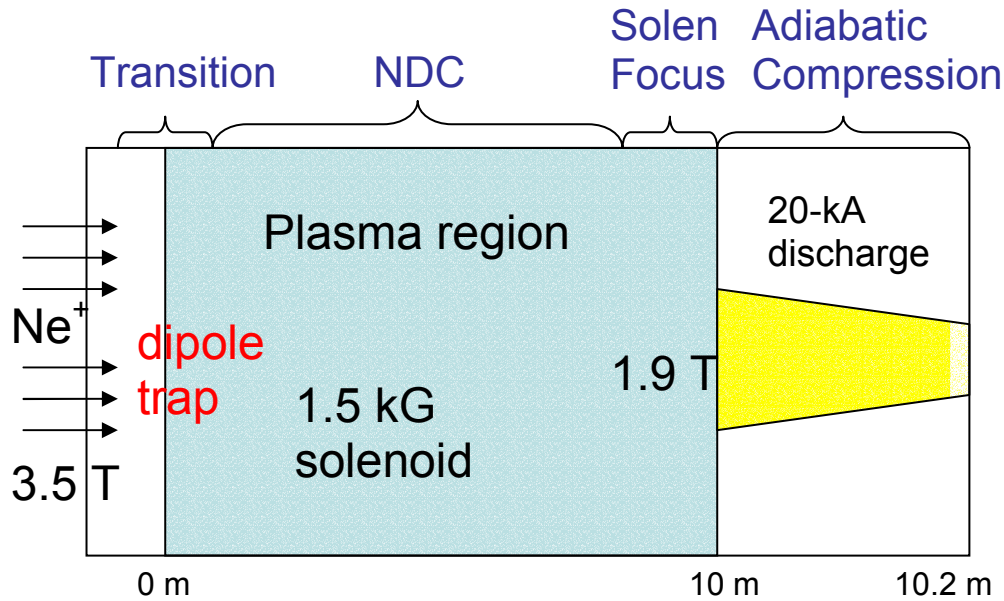


Figure 1 A schematic of a possible beam transport and final focus design using neutralized drift compression for HEDP is shown. The beam enters at the left in Brillouin flow equilibrium with a 5-10% velocity tilt, transitions to a NDC region, is focused by a strong solenoid, captured in an APT discharge channel and guided to the target.

Feasibility of achromatic beam focusing via a time-dependent solenoidal field

A major issue concerning NDC involves the final transverse focusing of the beam just before striking an HIF target or entering an adiabatic section of the discharge channel for further focusing. This focusing must accommodate a large energy spread (10--20%) for the 5--20-m drift length and hit a 1-mm radius. From the immersed envelope equation, we solve for the energy acceptance of the neutralized solenoidal focusing assuming small energy variation ΔE about E . With small beam emittance, $K=0$, and constant Ω_L , the entire beam is captured within some final radius given

$$\frac{\Delta E}{E} < \frac{8}{\pi r},$$

with r being the ratio of the initial-to-final radius. Practically, the beam emittance ultimately limits the maximum tolerable focal length.

The above criterion sets a limit on the maximum energy variation of a beam coupling to a fusion target directly or with an intermediate step to discharge channel. Given the goal of a 1-mm

radius spot at the target and assuming a 2-cm radius beam, the accepted energy variation is roughly 13%. Coupling into a discharge channel of 2-cm radius increases the accepted spread to 26%. An adiabatic discharge channel with a 4-mm initial and 1-mm final radius can then compresses the beam to the 1-mm radius.

There have been two proposed schemes³ to improve the energy acceptance which involve time-dependent solenoidal or static dipole fields. Although time-dependent solenoidal correction in vacuum looks feasible, it has been suggested that, given the long drift length, time-dependent correction in the plasma region would be easier. Of course the major issue here is the penetration of field into a highly conductive low-beta plasma.

We set up a quick 2D cylindrical LSP simulation of the idea with a solenoidal field ramping up from 0.15 to 1.5 kG in 100 ns. The solenoid extends 40 cm in length with a 14-cm inner radius. For convenience the coils are made up a purely azimuthal time-dependent current in vacuum. The 3-eV, 10^{11} cm^{-3} density C^+ plasma (the plasma beta increases to roughly 10^{-5}) is centered in the 15-cm radius drift tube with a 10-cm outer radius. At this point, the resemblance of the configuration to a theta pinch is uncomfortably evident. The response of the plasma is shown in Figure 2. Note that field does not readily penetrate the plasma but compresses it on axis resulting in a highly non-uniform field and plasma structure. Obviously, this brute force technique in a plasma is not appropriate.

The second technique is to use a series of dipole bends in a plasma to yield a first-order achromatic system. The problem is that the beam must cross these field lines while still maintaining adequate current and charge neutrality. The more gently varying fields of a solenoid are still mainly the direction of the beam and do not appear to present any problem. A simple quasi-neutral assumption for the plasma electron demands that the plasma electron transition to $\mathbf{E} \times \mathbf{B}$ drift in the dipole region, i. e. $v_{ze} = E_x / B_y$ where B_y is the applied field. For a given plasma and beam density (n_p and n_b), the

induced transverse electric field $E_x = v_b B_y n_b/n_p$. The force from this field acts to resist the dipole field deflection of the beam; however, if the force is uniform, it can be compensated for. The necessary uniformity would set constraints on the uniformity of the plasma, but decreases with plasma density.

Once again, we test the concept with a series of LSP simulations. To best calculate the plasma response, the 10-cm wide beam is injected with a large mass (100x Ne), charge state +1, $7 \times 10^{10} \text{ cm}^{-3}$ density (50 A/cm² current density) and $0.15c$ velocity. The beam will not be noticeably offset spatially, but the impact on transverse phase space can be assessed. The plasma density is varied from $n_p = 1, 4, 10, 40 n_b$. The induced electric field well within the beam generally scales with that predicted, however as seen in Figure 4, the induced self magnetic has a similar scaling. This field decreases linearly with n_b/n_p . The net Lorentz self force on the beam is actually fairly small because the electric and magnetic components nearly cancel. This type of cancellation has long been observed in beam transport in an initially field free plasma as well. As seen in Figure 4, the self fields decrease and become increasing smooth as the plasma density increases. The transition to uniform fields is thicker both axially and radially for the lower densities. Some work in this regime has already been done with field distortion attributed to electron advection.⁴ The impact on the beam transverse velocity is seen in Figure 5 where the beam velocity v_x as it propagates through the lens is plotted for the $n_p = n_b$ and $40 n_b$ simulations. Note the width of the velocity spread increases markedly with the lower density case but in the high density case, the distribution is simply offset as desired without additional spread. Thus, these simulations suggest that dipole field will not disrupt beam NDC as long as the plasma density is 10-100x that of the beam.

Beam Two-Stream Instability

A possible obstacle to beam compression is caused by the relative velocity of the beam ions and background plasma electrons. The electrostatic beam-plasma electron two-stream or Buneman instability has a 1D dispersion relation given by

$$\frac{\omega_b^2}{(\omega - kv_b)^2} + \frac{\omega_p^2}{\omega^2} = 1,$$

where ω_b is the beam-plasma frequency. The key parameters to evaluate the instability growth are then for transport distance $\zeta = z\omega_b/v_b$ and for beam pulse duration $\tau = t\omega_p$. Changing beam and plasma frequencies, as well as 2D effects, have a stabilizing influence on the instability. The instability can result in modulation of the beam longitudinal and transverse emittance which ultimately limits the final pulse time and spot. Previous LSP simulations have shown that the effect of the growth in the longitudinal emittance is weak, however, two dimension effect could degrade the beam transverse emittance as well.

In the worst case scenario, a uniform $3 \times 10^{11} \text{ cm}^{-3}$ density, sharp-edged beam is injected into a uniform plasma in a 2D cylindrical LSP simulation. The Ne^+ beam has a 15-kA current, 220 MeV energy, and a 10-cm uniform density. A nominal 500-G uniform solenoidal field permeates the drift tube. We should see strong growth of the instability in this case. With $v_b/\omega_b = 50 \text{ cm}$ and 10-m propagation length $\zeta_{max} = 20$ and for the 100 ns pulse, $\tau_{max} = 3000$. In the entirely uniform density simulation, the transverse normalized emittance grows 10x from $2 \times 10^{-4} \text{ pi-cm-rad}$ to $2 \times 10^{-3} \text{ pi-cm-rad}$ as seen in Figure 6. Note that the emittance growth saturates by the 8 m position. We attempt to reduce the growth in three subsequent simulations varying one parameter at a time. For the axially varying plasma density simulation, the plasma density is given a variation from 1.5×10^{11} to $6 \times 10^{11} \text{ cm}^{-3}$ with a 8 m wavelength. In this case, the saturated emittance grew to $1.5 \times 10^{-3} \text{ pi-cm-rad}$. In the third simulation, the plasma was given a gaussian radial variation from $6 \times 10^{11} \text{ cm}^{-3}$ on-

axis to $1.5 \times 10^{11} \text{ cm}^{-3}$ at the beam edge. Here, the beam emittance growth was smallest with a growth to $1.1 \times 10^{-3} \text{ pi-cm-rad}$. Finally, we give the beam a gaussian profile out to an e-fold keeping the current constant. Again seen in Figure 6, the saturated beam emittance grew to $1.2 \times 10^{-3} \text{ pi-cm-rad}$. We also looked at increasing the applied solenoidal field 500 G to 2 kG with uniform densities. This had only a modest positive effect reducing the emittance growth roughly 10%. These results are encouraging since we have identified at least three different mechanisms to reduce saturated growth that could possibly be additive and yield a more manageable emittance growth.

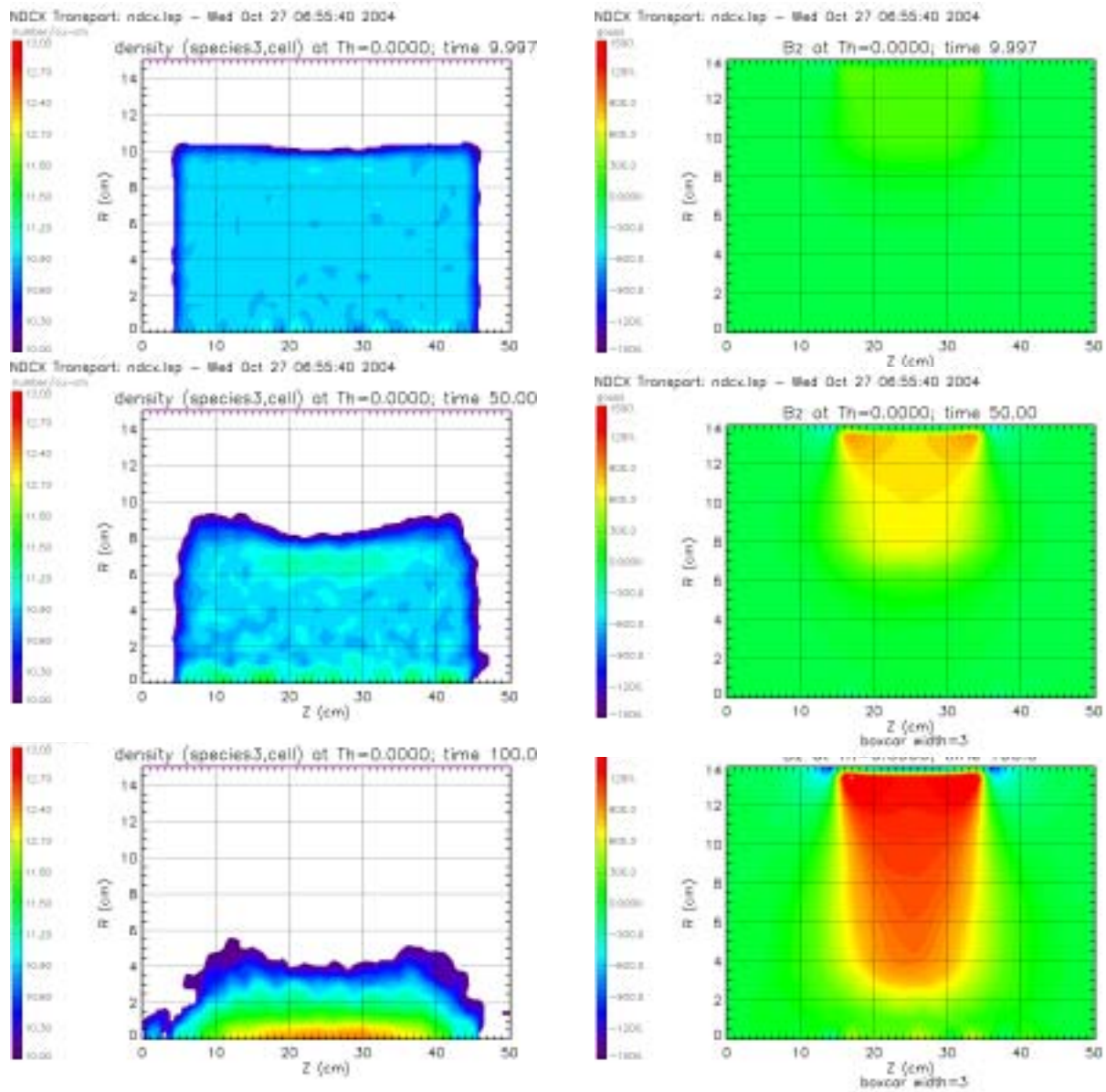


Figure 2 The plasma density (left) and axial magnetic field (right) evolution are shown at 10, 50 and 100 ns. The solenoidal current ramps up in 100 ns ($z=15$ to 35 cm with a 14-cm inner bore) in the 2D cylindrical LSP simulation.

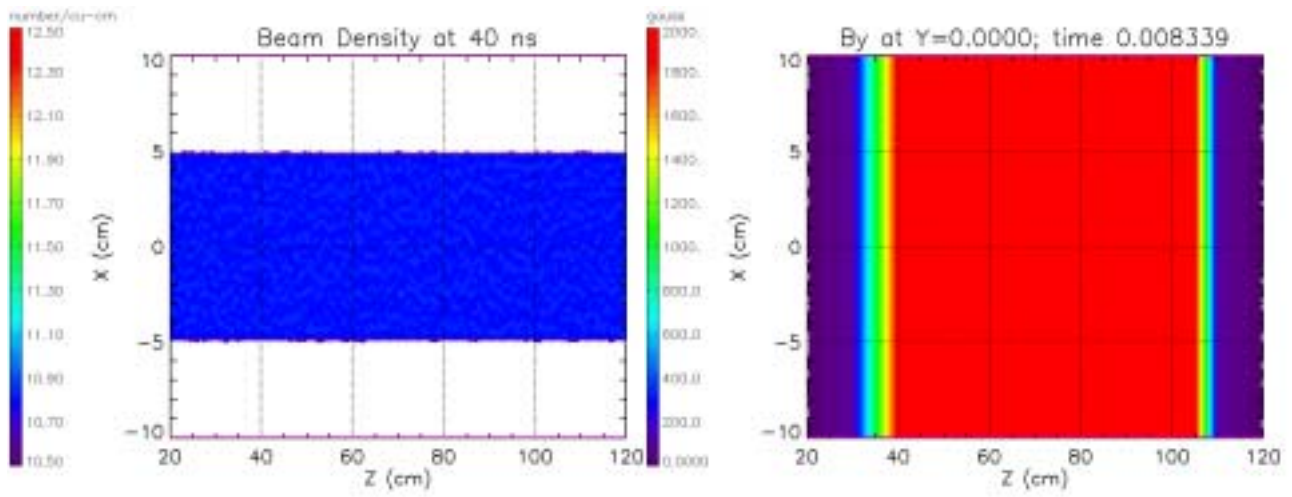


Figure 3 The beam density (left) and dipole magnetic field (right) are plotted for the series of LSP dipole field plasma neutralization simulations. The beam density is 10^{11} cm^{-3} with a $0.15c$ velocity (50 A/cm^2). The dipole field strength is 2 kG and extend from $z = 35\text{-}105 \text{ cm}$.

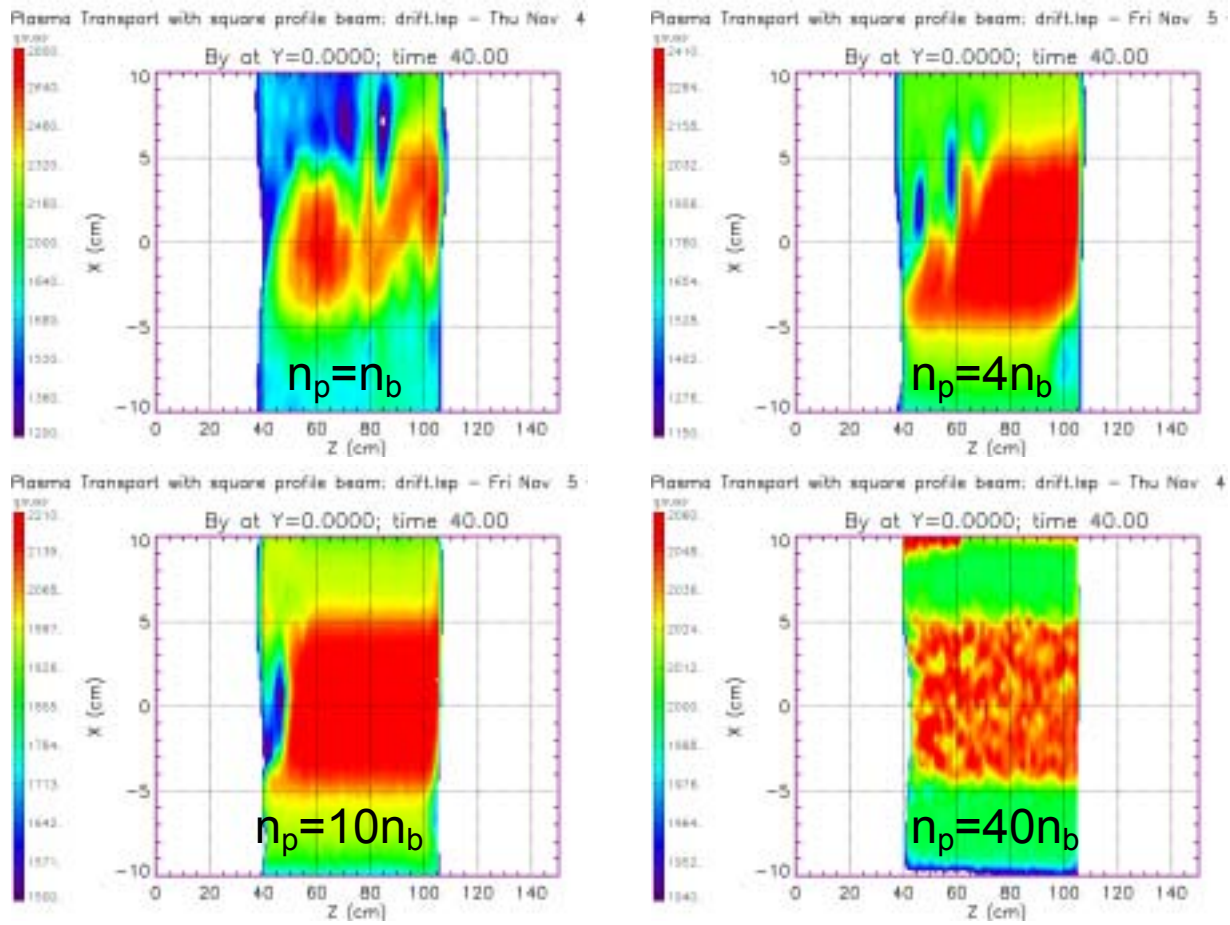


Figure 4 The (self + applied) dipole magnetic field is plotted after 40 ns into the LSP simulation with plasma densities of 1, 4, 10 and $40n_b$. The applied dipole field magnitude is 2 kG.

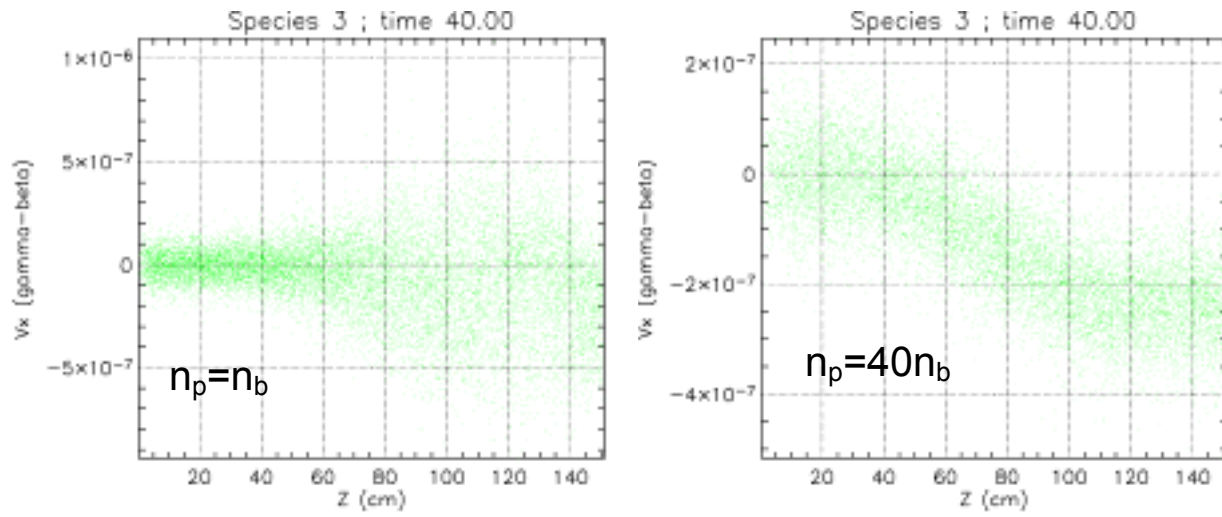


Figure 5 The beam transverse velocity v_x is plotted versus z for the simulations with plasma density equal and 40x the beam density.

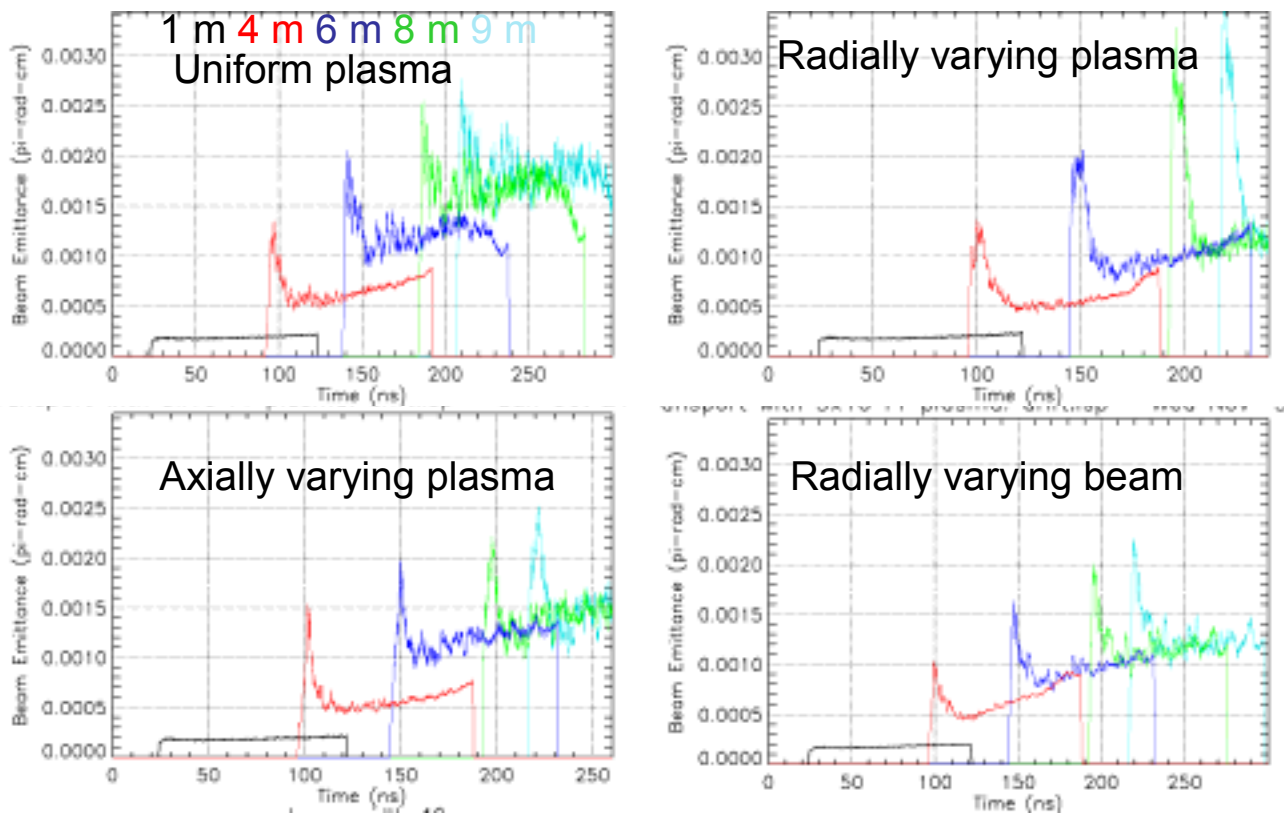


Figure 6 The transverse emittance for a 15-kA 100-ns 220 MeV Ne^+ beam is plotted at $z = 1, 4, 6, 8,$ and 9 m downstream from injection. The plasma had a nominal $3 \times 10^{11} \text{ cm}^{-3}$ density. The 4 simulations had uniform, axially varying plasma, radially varying plasma and radially varying beam densities.

¹ D. R. Welch, D. V. Rose, T. C. Genoni, S. S. Yu, and J. Barnard, proceeding of the 2004 HIF Symposium (2004).

² D. R. Welch, D. V. Rose, B. V. Oliver, and R. E. Clark, Nucl. Instrum. Meth. Phys. Res. A **464**, 134 (2001); LSP is a software product of Mission Research Corporation (<http://www.mrcabq.com>).

³ E. Lee, private communication (2004).

⁴ B. V. Oliver and R. N. Sudan, Phys. Plasmas **3**, 4730 (1996).

Ne Charge State Distributions In Gaseous And Solid Targets

Igor Kaganovich, PPPL, VNL

Ne charge state distributions were measured in Ref.1 in Zapon foils (solution of celluloid in fusel oil) for ion energy >30 MeV. For energy 30 MeV Ne charge distribution is shown in Fig.1.

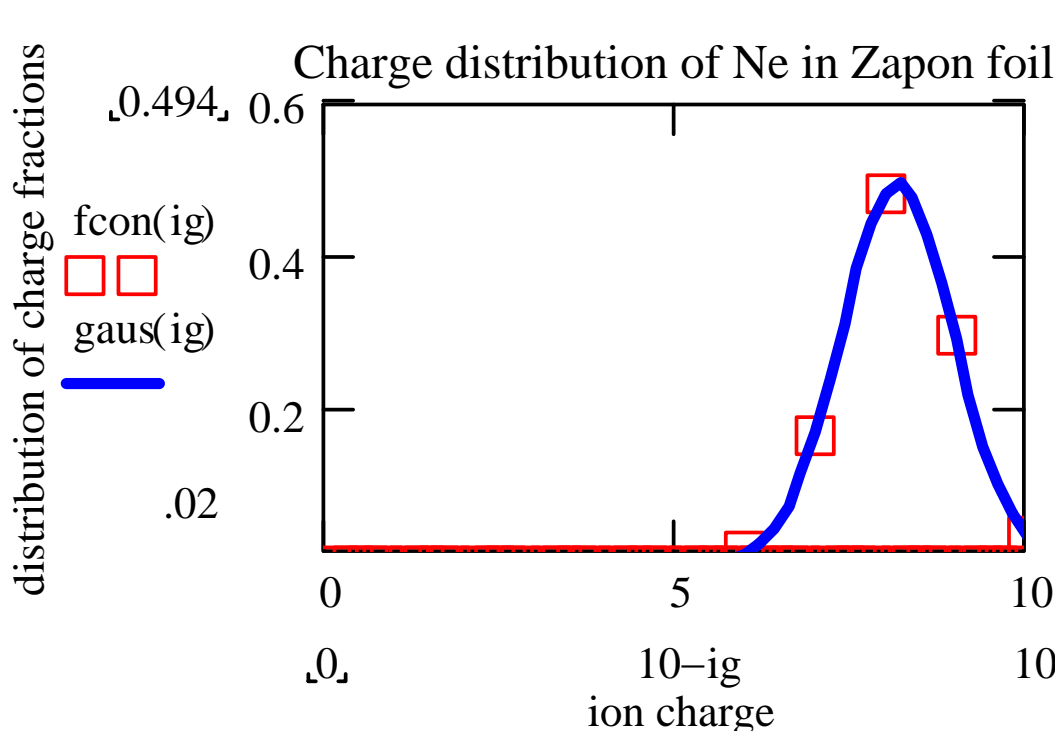


Fig.1 Experimental data on distribution of Ne ions on charge state in Zapon films. Symbols show the experimental data, line – the approximation with a Gaussian function.

This distribution is well described by a Gaussian distribution with

$$f(i) = \frac{1}{\sqrt{\pi} s} \exp\left[-\frac{(i - \langle i \rangle)^2}{s^2}\right],$$

for 30 MeV Ne ions in solid target

$$\langle i \rangle = 8.71 \text{ and } s = 1.14,$$

where $\langle i \rangle$ is the average charge and s is the dispersion of charge.

For gaseous targets the average charge should be lower than in solid targets. I could not find data for our velocity range, but judging from the data for heavier projectile ions presented in Betz review [2] on page 506, the average charge is one charge lower in gaseous target than in solids. Therefore, we can expect

for 30 MeV Ne ions in gaseous targets

$$\langle i \rangle \approx 7.7 \text{ and } s \approx 1.$$

For 20 MeV also comparing with Betz review data for S ions we can expect average charge low for 1.1 charge, thus yielding

for 20Mev Ne ions in gaseous target:

$$\langle i \rangle \approx 6.5 \text{ and } s \approx 1.$$

This result well corresponds to Lamb's rule [2] as the ion velocity in atomic units is 6.3. which is roughly equal to the average charge $\langle i \rangle \approx 6.5$. (This is equivalent to original Lamb's principle: that the kinetic energy of the target electron in the frame of projectile ion is equals to the ionization energy of the electron left on the ion in equilibrium charge state.)

For a fully ionized plasma targets, the average charge can be close to the equilibrium charge in solid targets, as the dominant process for charge transfer in gaseous targets - charge exchange from neutral atoms is impossible in plasmas and solid targets.

The only way to have fully stripped Ne ions is to increase Ne energy by factor of 2. This will decrease stopping power only by factor of 50% but can make focusing scheme much easier!

The charge exchange cross section for Ne^+ ions was measured in Ref.3 for energy range up to 500keV. It is roughly proportional to the target atom cross section for these low energies and ranges from $8 \cdot 10^{-17} \text{cm}^2/\text{atom}$ for H to $5 \cdot 10^{16} \text{cm}^2/\text{atom}$ for Kr gaseous targets. That should set residual gas pressure limit for vacuum requirement in accelerator.

References:

- [1] Heckman et al, Phys. Rev, **129**, N3 1240 (1963).
- [2] H.D. Betz, Rev. Modern Phys., **44**, N3, 465 (1972).
- [3] A.B. Wittkower and H.B. Gilbody, Proc. Phys. Soc., **90**, 353, (1967).

Constraint on Longitudinal Velocity Spread for Beams Undergoing Longitudinal Compression

William Sharp, LLNL

The initial longitudinal temperature of a beam imposes an important limit on the minimum beam length that can be achieved by neutralized compression. Before compression, the initial longitudinal phase-space of an idealized beam might look like the left sketch in Fig. 1, with an initial length L_i and a linear head-to-tail variation Δv_z in the locally averaged longitudinal velocity. At any point z along the beam, there will be some velocity spread δv_z about the average value due to the finite longitudinal temperature of the beam.

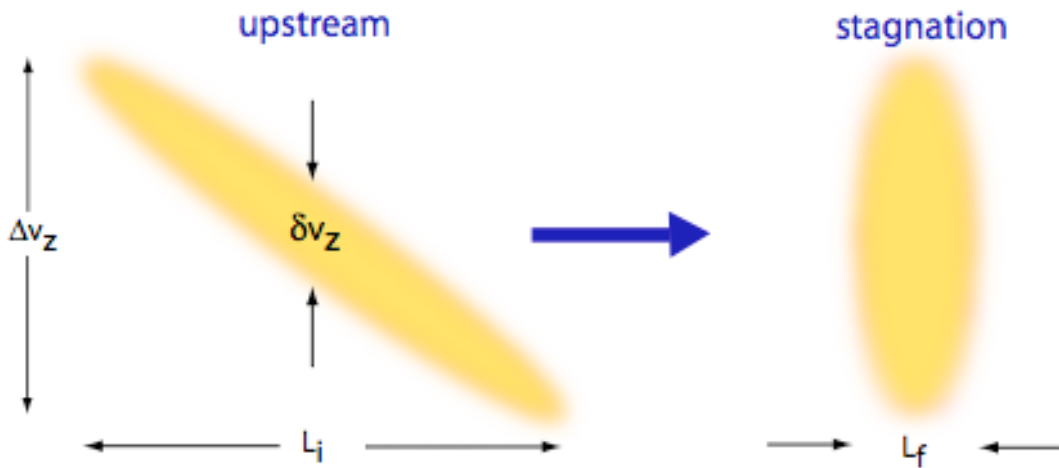


Figure 1: Sketch of a beam longitudinal phase-space to illustrate neutralized compression.

If we assume complete neutralization of the beam space charge and an absence of collisions and external electric fields, the beam phase-space dynamics becomes very simple. Under these conditions, the longitudinal velocity v_z of a beam ion remains constant during compression. Consequently, ions with the same v_z but different longitudinal positions, given by their coordinate z , will move together as the beam propagates through the transport lattice but shift in z relative to particles with different v_z values. If one pictures the beam as a stack of horizontal slices, each with constant v_z , then it is obvious that the phase-space area of the beam, and hence the longitudinal emittance, is constant during compression. It is also evident that the minimum length is just the longitudinal extent of the slice traveling at the average velocity of the whole

beam, $\langle v_z \rangle$. When $\Delta v_z \ll \langle v_z \rangle$, this minimum length L_f is well-approximated by noting that Δv_z bears the same relation to $\langle v_z \rangle$ as L_f does to L_i , giving the approximate relation

$$L_f \approx L_i \Delta v_z / \langle v_z \rangle. \quad (1)$$

A more careful calculation, assuming that the beam phase-space distribution is initially ellipsoidal in the $z - v_z$ plane, gives the relation

$$(L_i / L_f) - 1 \approx (\Delta v_z / \langle v_z \rangle). \quad (2)$$

When Δv_z goes to zero, Eq. (2) gives the correct result, $L_f \sim L_i$, and the expression reduces to Eq. (1) when $\Delta v_z \ll \langle v_z \rangle$. For 100:1 compression and $\Delta v_z / \langle v_z \rangle = 0.1$, Eq. (2) indicates that $\Delta v_z / \langle v_z \rangle$ must be 0.001 or less. For a 20-MeV beam, this constraint would limit longitudinal temperature to less than 40 keV. Since we expect a longitudinal temperature after injection on the order of 10 eV, a 40-keV limit before compression leaves a comfortable margin for heating during acceleration.

We should point out that Eq. (2) ignores several effects that could undermine neutralized compression. Any residual electrostatic charge will resist compression and, if the fields are nonlinear, may increase the longitudinal temperature. Scattering due to collisions with the background plasma will increase the temperature by transferring longitudinal energy to the transverse direction, and beam stripping from these collisions will increase the beam charge, possibly requiring a higher plasma density for effective neutralization. Also, the L_f expression assumes that transport is stable during compression. These effects should be analyzed and, if necessary, simulated before we accept Eq. (2) as a plausible estimate of neutralized compression.

Using Pulsed Lens to Compensate Tilt
 Yu-Juan Chen
 Lawrence Livermore National Laboratory
 January 12, 2005

We have mentioned the possibility of using a pulsed lens upstream of the neutralizing plasma channel to compensate the energy tilt (dP/P) of the 2-kA, 19-MeV, 30 mm-mrad (un-normalized) Ne⁺ beam at the HEDP workshop. In this report, the needed pulsed magnetic field and the beam envelope and its final spot size are discussed. Figure 1 shows the magnetic tune for a simple beamline configuration. A constant solenoid field is used in this model to match the beam into the the plasma channel. Base on the needed field strength, ~ 77 T, a solenoid may not the best choice to focus a space charge dominated ion beam. However, using a solenoidal matching lens allows the beam remains round regardless of the energy tilt and the setting of the pulsed lens. A single loop 8-cm radius and 1-cm wide coil placed inside the matching solenoid so that it can either focus or defocus the beam depending on the polarity of the driving current. Roughly the fast coil needs to provide 2 - 3 Tesla of magnetic field change during the beam time in order to get the same beam spot at the target plan for $dP/P = \pm 5\%$. For a 20 - 30 ns long beam pulse, dB/dt is about 1 kG/ns, which would be too large for a simple single-loop coil. Ten times of this fast coil field is also plotted in Fig. 1. LLNL's ETA-II target experiment's final focus lens' magnetic profile is used here for the final focus lens although LLNL's lens can only provide several kilogauss of magnetic fields. Two target plan locations ($z_f = 20$ cm and $z_f = 30$ cm) are studied.

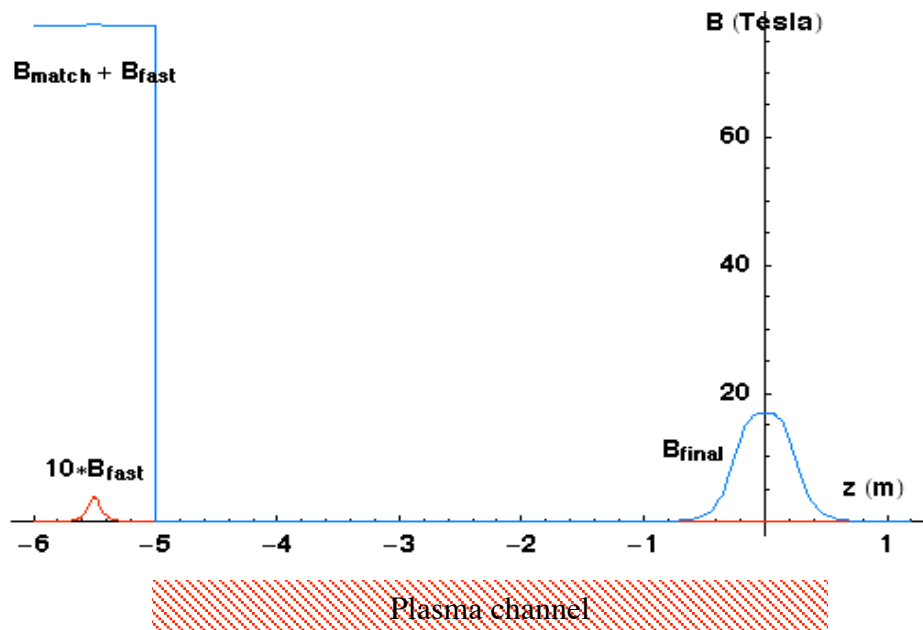


Fig. 1 The magnetic tune used in the envelope calculations

Figure 2 and 3 show the beam envelopes and compensated beam spots for $dP/P = \pm 5\%$, $\pm 2.5\%$, and 0 when the target plane is 30 cm downstream from the center of the final focus lens. The beam envelope parameters (radius and slope) are identical at the starting point, $z = -6$ m. Although the beam envelopes are quite different, the variation of the final spots is less than $\pm 1.5\%$. The corresponding fast coil's fields are given in Fig. 4.

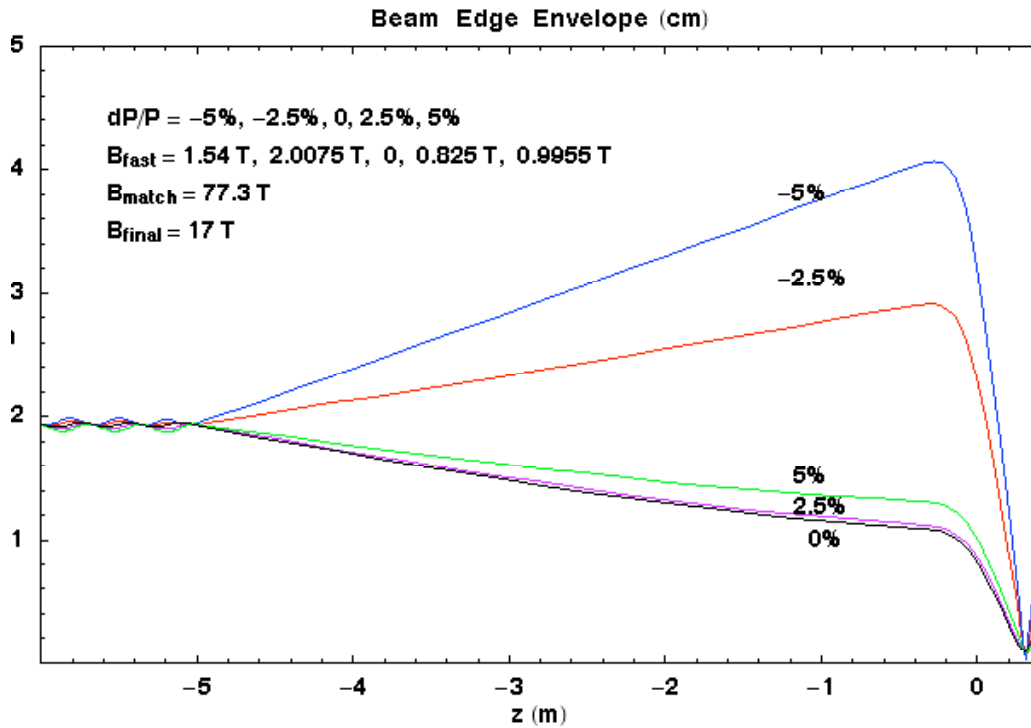


Fig. 2 Beam envelopes for the 2-kA, 19-MeV, 30 mm-mrad (un-normalized) Ne⁺ beam with various fast coil fields to compensate for final spot size variation introduced by energy tilt. The location of the focal point is at 30 cm.

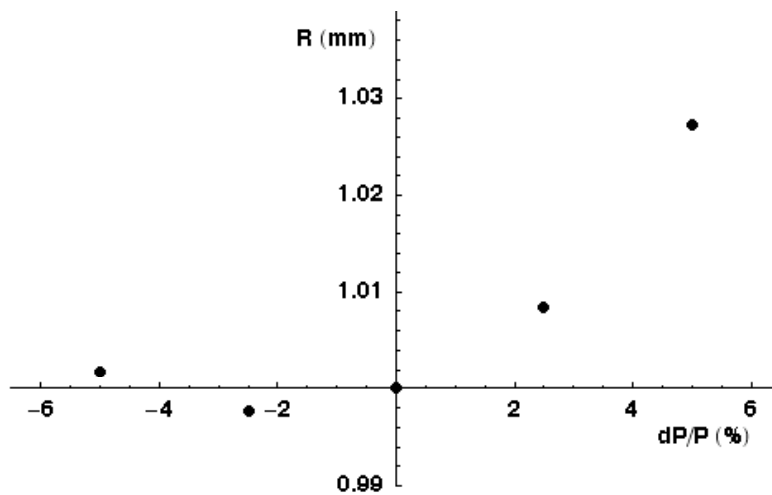


Fig. 3 Final beam radius at the focal point ($z = 30$ cm) as a function of energy tilt. The corresponding fast coil setting is given in Fig. 4.

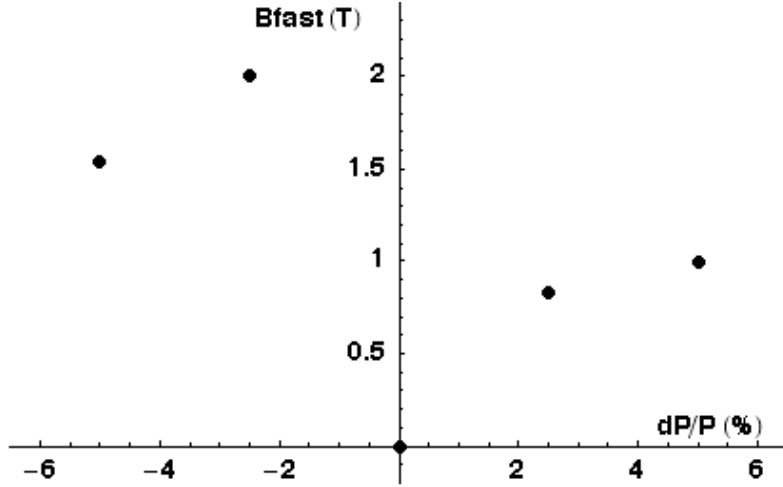


Fig. 4 The fast coil's magnetic fields used to maintain final spot size variation.

Figures 5, 6 and 7 show the beam envelope, spot size and the needed pulsed magnetic field when the focal point is located at $z = 20$ cm. These results are similar to the previous case.

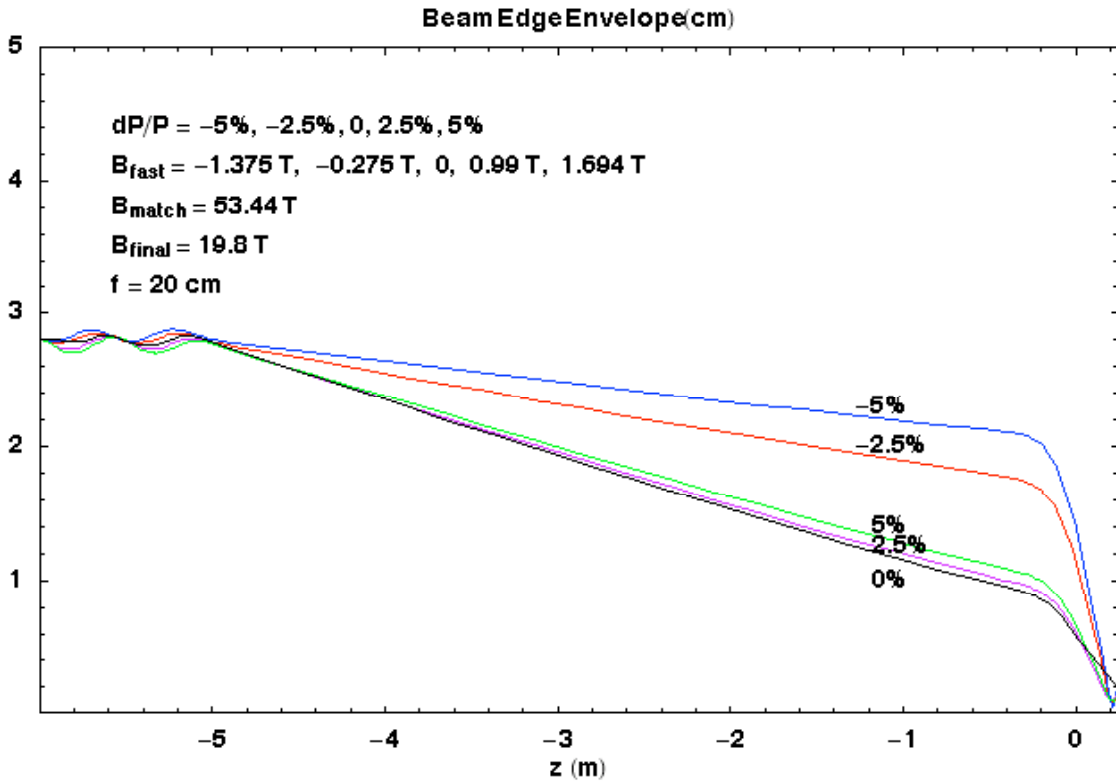


Fig. 5 Beam envelopes for the 2-kA, 19-MeV, 30 mm-mrad (un-normalized) Ne+ beam with various fast coil fields to compensate for final spot size variation introduced by energy tilt. The location of the focal point is at 20 cm.

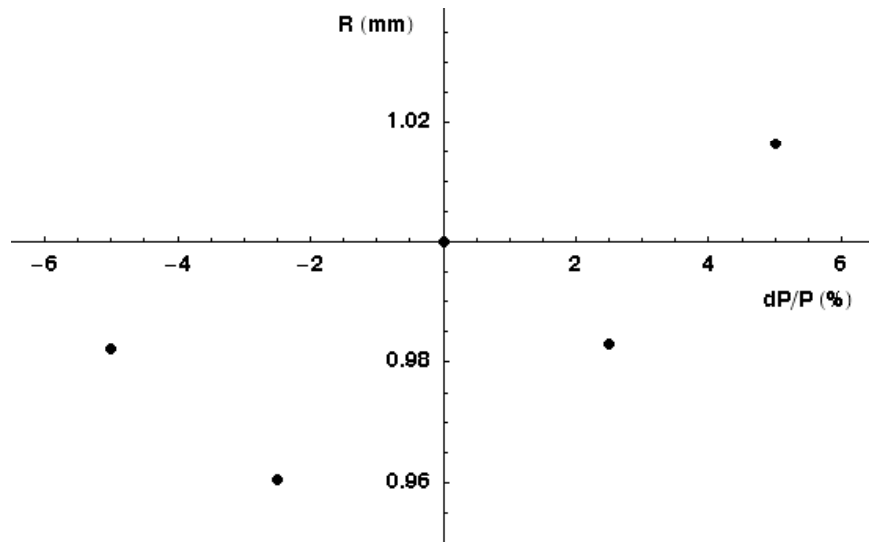


Fig. 6 Final beam radius at the focal point ($z = 20$ cm) as a function of energy tilt. The corresponding fast coil setting is given in Fig. 7.

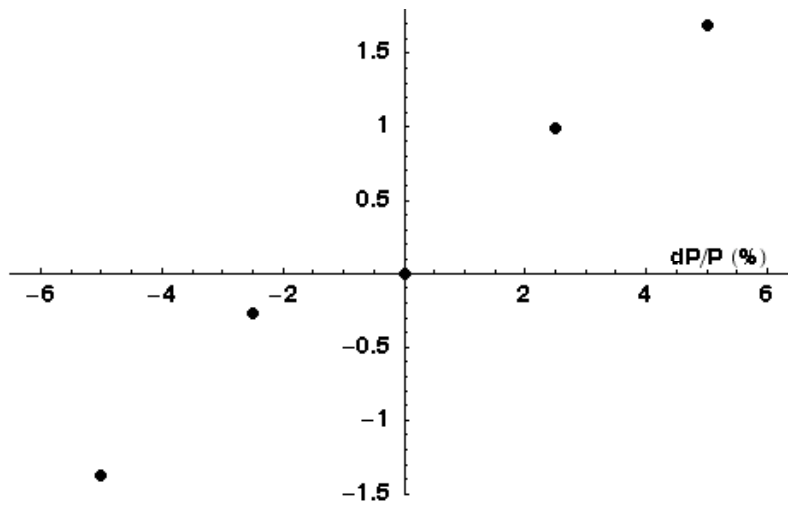


Fig. 7 The fast coil's magnetic fields used to maintain final spot size variation. ($f = 20$ cm)

ADIABATIC PLASMA LENS – A CURRENT DENSITY BOOSTER

Simon Yu

The adiabatic plasma lens provides a mechanism for increasing the current density at target by up to a factor of 10. The physical setup consists of a tapered insulating tube filled with a gas at ~ 1 torr density. An external discharge (~ 10 kV) initiates a current (~ 50 kA) along the length of the tapered tube. The adiabatically increasing azimuthal magnetic field confines and further reduces the beam size as it traverses down the tube. This tapered tube is located at the downstream end of a high-field focusing solenoid, and immediately upstream of the target.

In this note, we describe the basic physics of the plasma lens, and present an HEDP relevant numerical example at the end.

Charge and current neutralization

The fundamental premise of an adiabatic plasma lens is that the highly conducting medium of the current-carrying channel provides total charge and current neutralizing for the incoming ion beam. The particle dynamics therefore reduces to simple single particle orbits in an azimuthal magnetic field. A typical example would be a fully ionized channel with a temperature of 7 eV. The conductivity is $\sigma \sim 10^{14} \text{ sec}^{-1}$ [units in cgs]. Charge neutralization takes place in a time exceedingly short relative to the pulse length

$$\tau_e = \frac{1}{4\sigma} \sim 10^{15} \text{ sec}$$

In this environment, the magnetic field changes slowly. The magnetic decay time is

$$\tau_m \sim \frac{4\pi a^2}{c^2}$$

For a typical millimeter-sized beam for HEDP, $\tau_m \sim 12 \text{ ns}$, which is much longer than the beam pulse length ($\sim 1 \text{ ns}$). Hence over the pulse duration full charge and current neutralization is a good approximation.

Particle dynamics in adiabatic discharge channel

Since the ions do not see any of the beam space charge, the particle dynamics reduces to single particles in an external \vec{B} field, given by

$$\frac{d^2 x}{dz^2} = k^2 x$$

where $k^2 = \frac{2I}{a^2 (\gamma M c^3 / Ze)}$

where x , γ , M , and Z are the transverse position, ion speed (normalized to speed of light c), the mass, and charge of the ion respectively, and a discharge current I flows in a channel of radius a . This formula assumes a radially uniform current density. The generalization to non-uniform distribution is straightforward.

The betatron wave number k can vary with z , due to continuous stripping $Z(z)$, as well as channel tapering $a(z)$. The solution to the Hill's Equation

$$\frac{d^2x}{dz^2} = -k^2(z)x$$

is easily obtained in the adiabatic approximation

$$\frac{1}{k^2} \frac{dk}{dz} \ll 1$$

and is given by

$$x = \frac{c}{k^{1/2}} e^{i \int k dz}$$

In practice, the adiabaticity condition can be met as long as the length of the channel L_c is of the order of the betatron period at entrance $L_i = \frac{2\pi}{k_i}$.

It is important to note that the amplitude of x is proportional to $k^{-1/2}$. As the channel tapers, k increases and x is reduced. The beam envelope, R , which is the ensemble average of the ions, will similarly decrease as it goes down the tapered tube.

Characteristics of beam transport in adiabatic channel

The picture of single particle transport in Z -pinch leads immediately to some general conclusions:

1. The beam envelope within the channel is very insensitive to beam energy spread, since

$$\frac{\Delta k}{x} \approx \frac{1}{2} \frac{\Delta k}{k} \approx \frac{1}{4} \frac{\Delta Z}{Z} \approx \frac{1}{8} \frac{\Delta E}{E}$$

Hence 40 % energy spread leads only to 5% variation in beam envelope.

2. Beam transport is insensitive to spread in ion charge state

$$\frac{\Delta k}{x} \sim \frac{1}{4} \frac{\Delta Z}{Z}$$

3. The reduction of beam size, from initial beam radius R_i to final beam radius R_f , is proportional to the square root of the taper ratio $\frac{a_i}{a_f}$ where a is the channel radius

$$\frac{R_i}{R_f} = \frac{a_i}{a_f} \left(\frac{R_i}{R_f} \right)^{1/2}$$

4. Finally, the channel can accommodate large emittances with sufficient channel current. Assuming that the beam is in quasi-equilibrium at target, we have

$$\frac{\epsilon_f^2}{R_f^2} = \frac{2I}{\epsilon M c^3 / Ze}$$

The final emittance ϵ_f at target may be slightly higher than the beam emittance ϵ at entry into the discharge channel, depending on details of the channel current radial distribution. If the distribution is uniform, then the emittance is preserved $\epsilon = \epsilon_f$

A numerical example

For Ne at $\epsilon = 0.045$ and $Z=7$, we can reduce a beam radius from 1mm to 0.5mm if the tapered tube has an initial radius of 2mm and final radius of 0.5mm. Assuming beam un-normalized edge emittance of 5×10^{-5} m-rad, the current required is 20kA. The length of the tapered tube is 12 cm.

A Unique U.S. Approach for Accelerator-Driven Warm Dense Matter Research--Preliminary Report

Grant Logan, Ron Davidson, John Barnard, Richard Lee

Preliminary version September 28, 2004

This first preliminary white paper will be updated periodically as we learn more from further analysis, and to take into account input we get from various workshops, such as the one on HEDP planned at LBNL on Oct. 26-29, 2004.

I. Introduction

The warm density matter regime of high energy density physics [1, 2, 3] has a high scientific discovery potential for the properties of plasmas at high densities and pressures and at moderate temperatures (kT) in which the Coulomb interaction energy between plasma particles exceed kT . This leads to correlations in the plasma characterized by the dimensionless “coupling” parameter $\Gamma > 1$, where Γ is defined by

$$\Gamma = \frac{q^2 n^{1/3}}{kT}$$

Here q is the effective ion charge and n the ion density. Strongly-coupled plasmas with $\Gamma > 1$ are difficult to study analytically and by numerical simulation. Many astrophysical systems (e.g., brown dwarfs, and giant planets) and inertial fusion plasmas in the beginning stages of compression fall into this regime. There is an opportunity to develop improved understanding and models through accurate measurements of properties in the large parameter space of temperature and density where data is currently limited or non-existent. X-ray free-electron lasers (Fourth generation light sources), ultra-short pulse and high energy optical lasers, pulsed-power z-pinch x-ray sources, and high explosives are all capable of producing warm dense matter conditions at various temperatures, pressures, and sample sizes. Therefore, the challenge is not how to create warm dense matter conditions, but to create it so that it’s fundamental properties can be best studied. The goal is to advance this field of science through a variety of complementary facilities and methods which offer several combinations of desirable attributes:

- Precise control and uniformity of energy deposition;
- Large sample sizes compared to diagnostic resolution volumes;
- A benign environment for diagnostics (low debris and radiation background);
- High shot rates (10/hour to 1/second) and multiple beamlines/target chambers;
- Sites with easy access for broad participation by university scientists and students; and with the technical support for designing and fielding targets for qualified experiments.

Dedicated, modest energy facilities are needed for developing new experimental techniques and diagnostics as well as the largest facilities for the most demanding target requirements. The recent report [4] of the National Task Force on High Energy Density Physics notes: “...a range of facilities is essential to perform experiments at increasing energy/current in order to develop experimental and diagnostic techniques before carrying out experiments on the

larger facilities such as the National Ignition Facility (NIF) or the Z/ZR facility, where operating costs are high.” Because of the high costs and limited number of shots available to external users on the large facilities, modest scale facilities, as the one described in this white paper, will be crucial “to validate simulation capabilities, to gather physical insight, and to develop target fabrication expertise, that will ensure success of the limited number of experiments possible on the largest facilities.”

A recent white paper [5] for DOE Science Director Ray Orbach describes the general scientific motivation for high energy density physics, and how LBNL could contribute to selected key scientific questions in a variety of ways, including the use of heavy-ion beam accelerators. That white paper described the physics motivation for considering the use of heavy ions to heat warm dense matter:

“Intense ion beams, if compressed to short enough pulses and delivered to small enough focal spots, could provide an important new tool for exploring high energy density plasmas (HEDP) in a different, complementary way to using lasers. This is because of the unique energy deposition property of ion beams, namely, that in very dense plasmas compared to the beam ion density, ions are observed to slow down in straight-line trajectories due to classical processes. At high energies, the ion range can be large compared to the optical mean-free-paths in solid-density plasmas, allowing ion energy deposition at the Bragg peak to be well-inside targets that would be opaque to laser light or soft-x-ray radiation. In contrast, lasers deposit their energy at plasma critical densities \ll solid densities, where $\omega_{\text{laser}} \ll \omega_p$. Here, ω_p is the plasma frequency. The deep penetration of high-energy ion beam heating allows more flexibility in some types of targets that can be used for dense plasma science.”

Recent research in the heavy-ion fusion program describes how the use of heavy-ion beams with energies just above the Bragg peak in dE/dx (ion energy loss per unit range) can maximize heavy ion deposition power density and uniformity simultaneously [6]. As a guiding principle we believe this method will provide a unique and affordable approach for a U.S. heavy-ion driven HEDP user facility.

The purpose of the present white paper is to address more specifically the opportunities and plans to develop a US accelerator-driven HEDP user facility, namely:

- (1) How modest-cost U.S heavy-ion accelerators and experimental target areas can best be designed to meet the needs of HEDP users (Section II), and compare with the HEDP-use potential of other accelerators particularly, GSI-SIS18/100.
- (2) Describe how certain types of targets and diagnostics can be well matched to heavy-ion drivers to explore warm dense matter where data is most needed to test strongly-coupled plasma models and determine equations of state (Section III)

The above-mentioned favorable deposition properties of heavy ions, and a German government decision to upgrade a heavy-ion linac and storage ring at GSI in part for warm dense matter studies, provides motivation for an intended collaboration called High Energy Density Matter Generated by Heavy Ion Beams (HEDgeHOB) [7], including U.S. participation under the auspices of a DOE-German government agreement for collaboration in dense plasma science [8].

During the next 8 to 10 years that it will take before the GSI upgrade is productive, the GSI group will be testing diagnostics using less intense heavy ion pulses from their present machine, and there is opportunity for the U.S heavy-ion driven HED program to benefit from this collaboration. In particular, the Germans will be learning how to use transmission, energy loss, and charge state measurements of the heavy-ion beam itself as a probe for warm dense matter, and there will also be the application of an intense short-pulse laser to image dense heavy-ion beam targets [7]. However, international collaboration will not benefit the U.S. science program without U.S. state-of-the-art ion beam facilities to contribute to the underlying science through a strong domestic research program in high energy density physics.

This white paper is laid out as follows: Section II describes how U.S. accelerators with low cost, moderate energy ions can provide a unique approach to heating warm dense matter that would complement the GSI capability and greatly enrich the mutual collaboration. Section III describes opportunities and plans for targets, chambers and diagnostics which will provide an excellent match for US accelerator capabilities to advance HEDP science. Conclusions are given in Section IV.

II. U.S. approach proposed with moderate energy ion accelerators

Maximizing desirable attributes for advancing warm dense matter science

The principal goal is a dedicated, modest energy facility, such as recommended by the National HEDP Task Force, which could advance the warm dense matter regime of HEDP science in the U.S. by allowing many users to explore new experimental techniques at low cost and with many shots, which could later lead to qualified experiments on high energy NNSA-funded facilities. As discussed in the introduction, there are several candidate drivers for such facilities, so the strategy is to develop an approach which can maximize the five desirable attributes for scientific productivity described in the introduction, and at minimum cost. Appendix 1 contains excerpts from the National HEDP Task Force Report [4] on the top-level scientific question regarding the prerequisite heavy ion beam compression and focusing required for the U.S. accelerator-driven HEDP approach described in this white paper, and also describes a ten-year research plan with intermediate milestones to address the principal beam physics questions. The intense beam-plasma regimes in the accelerator and in the longitudinal drift compression region are themselves interesting “extreme states of matter” to study as well as the warm dense matter target physics. Building upon the National Task Force report described in Appendix 1, this white paper provides additional description of the plans, issues and opportunities for the experimental targets, diagnostics and facility operation so as to optimize the scientific productivity and utility of this approach for warm dense matter research. In parallel with the accelerator/beam compression experiments, we plan to explore candidate experimental target and chamber designs that can best utilize the ion beams as they progress up in intensity at each stage. We also plan to gradually develop an appropriate suite of diagnostics, starting with existing ion and laser beams in other facilities, so as to be able to field initial HEDP user experiments beginning in about 5 years.

Maximizing precision control of energy deposition

To maximize precision control of the energy deposition profile, it is proposed to use ion beams with predictable deposition physics [5]. The energy loss and charge state of the transmitted ions can also be used as a diagnostic for warm density matter energy density and temperature. Multi-stage accelerators with agile voltage waveform control will be used to precisely tailor the longitudinal energy distribution of the ion beams, and therefore manipulate the energy deposition and pressure profiles in the targets. Fast ions (fast compared to average target electron velocities) deposit energy by slowing down on target electrons at a rate dE/dx that increases as the ions slow down until the ion speed drops below the average electron velocity (bound electron velocities for cold target materials, or electron thermal velocity in fully ionized targets). At such a point, sometimes referred to the Bragg peak, dE/dx reaches a maximum and then declines to zero as the ion stops. Figure 1 plots a typical curve of dE/dx as a function of penetration depth in a target for a fast heavy ion with an initial kinetic energy starting well above the peak in dE/dx , such as the case in multi-GeV heavy ions in RF linac/storage ring accelerators for nuclear physics studies at GSI [7]. As a complementary approach to the GSI program, it is proposed to use ion beams entering the targets at moderate kinetic energies just above the energy where the ion deposition rate dE/dx is maximum for a given ion species and target condition, to maximize both the rate and uniformity of energy deposition [6]. The moderate ion energies required for heating at the peak in dE/dx , in the range of a few MeV, allows this U.S. approach to use moderate accelerator voltages, lengths, and cost.

Table 1 lists ion ranges in solid cold titanium foils for selected light ions at various initial energies, and the corresponding ion energies at the dE/dx peak. The proposed use of ions just above the peak in dE/dx minimizes the accelerator length and cost, but requires more ions to deliver a given energy to the target compared to using ions at much higher energies. The current density of ions at the moderate energies required to heat targets to several eV temperature, when also compressed to sufficiently short pulses that the target conditions remain uniform for measurements, leads to the necessity to compress and focus the ion bunches within a background plasma in order to neutralize the beam space charge between the accelerator and the target [4, 9, 10].

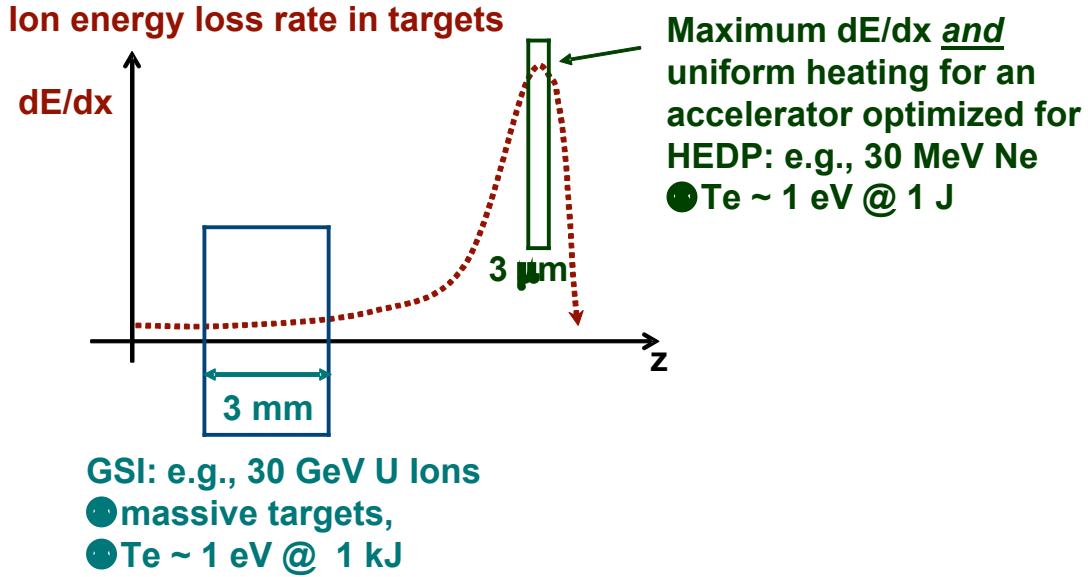


Figure 1 A typical curve of ion energy loss rate versus depth z into a target. It is proposed to inject ions at moderate kinetic energies just above the energy of peak dE/dx , such that the peak in dE/dx occurs in the center of the target for maximum uniformity. The targets should still be less than the total ion range, to allow the energy loss of transmitted ions to be used as a diagnostic for energy deposition, and the charge state of the transmitted ions for target temperature.

Beam ion	Initial energy (MeV)	Range in solid titanium (microns)	Energy at dE/dx peak (MeV)
H	1	11.4	0.11
He	1	3.1	0.7
N	10	5.8	7.7
Ne	16	6.3	15

Table 1 Nominal ion ranges and energies at dE/dx peaks in cold titanium target foils for a few selected light ions for a moderate energy and cost accelerator for HEDP studies (from Ref. 6). Exact ranges and energies at the dE/dx peak depend on the temperature and degree of ionization of the target.

Large sample sizes compared to diagnostic resolution scales

Typically, ion focal spot radii of approximately 1 mm are expected, which is large enough in the radial direction that the beam heating can be uniform radially within a few hundred microns of the axis where local target properties can be measured. For solid target foils with thicknesses less than the few-micron ion ranges shown in Table 1, hundred-picosecond-scale ion pulses are desired to limit the effects of hydrodynamic expansion during the measurements. A few years will be required before the beam compression research described in Appendix 1 would

evaluate the potential to achieve sub-nanosecond pulses, and it is planned to drive targets of 10's to 100's of micron thicknesses that could work with longer, nominally 1 ns, ion pulses. In addition, such minimum thicknesses will make it easier for diagnostics to resolve central portions of the target sample. However, thicker targets at solid density imply longer ion ranges, higher ion kinetic energy and mass at peak dE/dx , and thus greater accelerator length and cost. Therefore, it is planned to start warm dense matter experiments with low average density foam or wire-array targets which can be 10 to 100 times thicker for the same ion range and pulse energy, and with corresponding longer hydro-expansion times, assuming the ion heating homogenizes the resulting plasma. Similarly, it may be possible to make dense gas jets at low temperatures where small clusters or droplets form within the jets (two-phase flows), resulting in uniform sub-solid density plasmas after isochoric beam heating for equation of state studies. Fig. III.x in Section III illustrates how plasma densities lower than solid, densities down to 0.01 x solid density or lower, can still provide discriminating data to test equation-of-state models, and so use of low density foams or gas jets can keep the initial accelerator pulse energy requirements and costs low. A key design issue is how fast and how uniformly the interstitial voids in such initially heterogeneous targets fill in with ion beam heating. Hydrocodes with Advanced Mesh Refinement are available to evaluate this issue. Use of low-density foam targets will allow us to begin warm density matter research with pulses initially as low as 1 J and then upgrade the accelerator pulse energy in steps up to about 100 J. This is a prudent way to manage the investment cost and technical risk while developing experimental techniques at each stage.

Benign environment for diagnostics and personnel safety

Moderate energy ion pulses at peak dE/dx as indicated in Table 1 should not generate significant hazards or facility activation from neutrons or gammas produced by the ion beams themselves. (In contrast, at multi-GeV energies, heavy ions create neutrons and radioactive nuclear fragments, which can lead to significant facility shielding expenses). In experiments needing a short-pulse laser for x-ray diagnostics, multi-MeV electrons can be produced which can require some gamma shielding, but not likely neutron shielding to prevent activation. Also, with the modest pulse energies envisioned here, only about ten micrograms of target material are vaporized each shot, making target debris from a large number of shots and rapid bursts of shots tolerable before diagnostic windows likely need to be cleaned or replaced.

High shot rates/multiple experimental chambers/dedicated site

As in conventional accelerators serving multiple experimental areas for multiple users, we envision an ion beam deflector using dipole magnets, or equivalent rapid switching, to support three or more experimental target chambers with one accelerator. As long as pulsed energy charging supply currents are designed for high shot rates, accelerators of the type envisioned here have been demonstrated to sustain 1 Hz pulse rates, and can likely be designed for 10 Hz with the low time-average duty factors for the required beam loading. Thus accelerator constraints will likely support pulse rates as high as experimental data acquisition rates require, even for more than one chamber. For solid targets mounted on in-vacuum target wheels containing 100 or more targets, 100-pulse trains at 10 shots per minute rates might productively be used, and pulse rates of 1 Hz might be useful with gas jet targets, as long as diagnostic data acquisition rates are designed to keep up with such rates. If such high shot rates

were available, advantage would be taken of statistical averaging to reduce the measurement error bars wherever possible. The data rates required to optimize scientific productivity will not be known until experiments are carried out. Since it doesn't add much cost to design accelerators for high shot rates, the goal is to provide high-shot-rate capability in nominal 100-shot bursts of 0.1 to 1 Hz.

As pointed out in the National HEDP Task Force [4], and discussed further in Section III, university users need considerable on-site assistance with designing, fabricating, and fielding their experimental targets, and with diagnostic setup and data acquisition around the experimental chambers. This user support will work best if the funding for the facility and on-site support is dedicated to the warm dense matter science program as the primary mission. A non-weapons lab site can also facilitate access for university users and students.

Figure 2 shows a conceptual example of an accelerator-driven HEDP user facility, with a single ion beam linac supplying several target chambers through a beam director (three chambers are shown in this example). The beam intensities after acceleration are high enough that beam space charge must be neutralized in low density ($\sim 10^{12} \text{ cm}^{-3}$) pre-formed plasma from the exit of the accelerator up to each target. Each type of experimental target is expected to require an integrated design for the target holder, plasma source, diagnostics, final focus, and plasma filled drift compression line, as illustrated in Fig 2. The beam director may contain one or more variable dipole magnets to provide beam deflection on demand into any chamber, and to provide first-order chromatic correction for optimal beam focus. In addition, the accelerator is short enough (<3 meters) to allow the option to have the linac pivot around the beam director, eliminating or reducing the bend angles required for each chamber. (Numerous experimental diagnostics would make moving the target chambers instead very time-consuming).

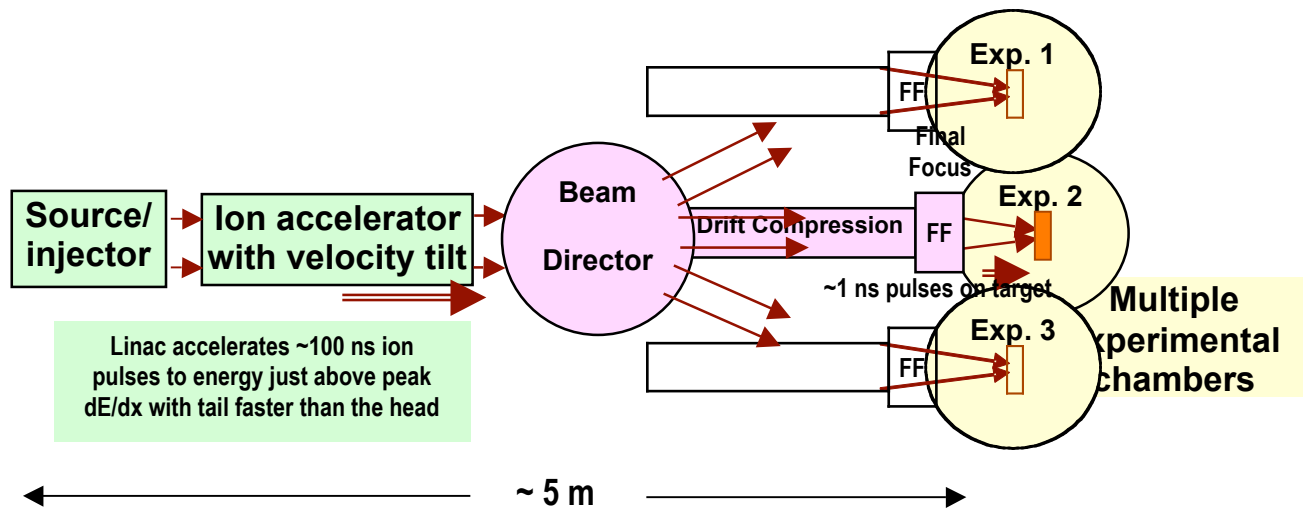


Fig. 2: Schematic of a modest size ion linac driving multiple HEDP experimental chambers with ions at a few MeV near the peak in dE/dx . Ion pulses are longitudinally drift compressed and focused within low density background plasma between the accelerator and the targets.

The ion accelerator section depicted in Fig. 2 takes the beam from the injection energy up to two-thirds or more of the desired energy above the peak in dE/dx for a chosen ion species, with the remaining energy for the velocity tilt added by a special induction module. The induction module with agile waveform control provides a rising voltage pulse for the subsequent longitudinal beam compression in the plasma-filled drift lines to each target. For the first (uniform) part of the beam acceleration after injection, several types of accelerators are being considered, including multi-stage induction, helical pulse lines, and RF. There is also a single voltage gap version of induction, called the Induction Voltage Adders (IVA). All of these options will be assessed in a workshop for accelerator-driven HEDP in October 2004. All of these options will require neutralized beam pulse compression and final focusing to meet desired HEDP conditions as described above, and any option would go through incremental stages of experiments for neutralized pulse compression as described above and in Appendix 1. One example of a sequence of three accelerator and beam compression experiments based on induction, called Neutralized Drift Compression Experiments (NDCX series) is shown in Figure 3. In these sketches, only one target chamber is shown because they illustrate beam compression experiments. In the middle step labeled NDCX IIb and the last step NDCX-III, warm dense matter experiments would utilize several target chambers as illustrated in Fig. 2.

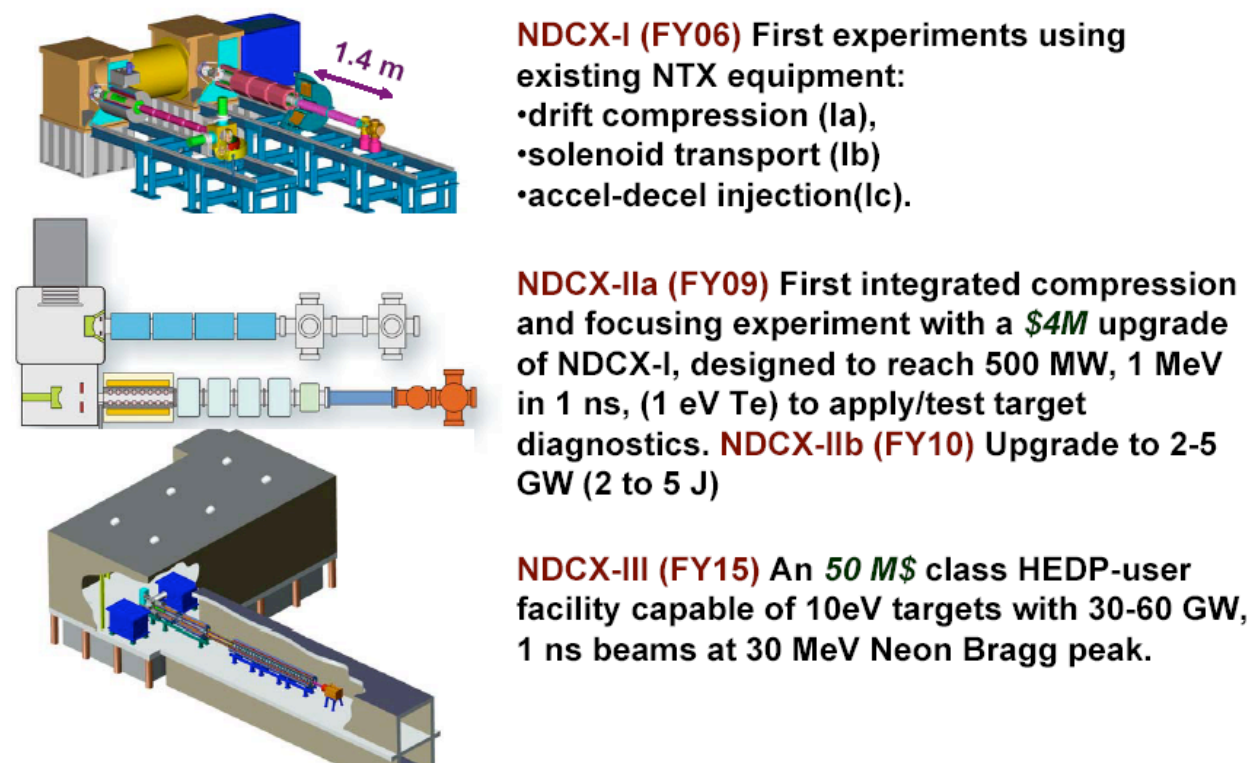


Figure 3: A sequence of neutralized drift compression experiments with increasing capability for warm dense matter experiments. The steps labeled NDCX-IIb and NDCX-III would be configured with multiple experimental chambers (only one chamber shown) for warm dense matter studies as in Fig. 2.

The capability of NDCX drivers for warm dense matter studies approximately parallels the capability of GSI: the Germans are now working on upgrading the linac injection and vacuum system in the present SIS 18 ring with a goal to store ~ 10 X more ions, which may take several more years, if the recent rate of progress is maintained. If successful, the SIS18 should then deliver roughly a kilojoule of 300 MeV/u heavy ions compressed to ~ 100 ns, which they calculate should be sufficient to reach 1 eV average target temperatures in isochoric heating experiments. The German government has approved construction of a larger upgrade, called SIS-100, which should be delivering 40 kJ beams of higher energy 0.5 -1 GeV/u heavy ions to targets approximately 7-8 years after construction funding starts, hopefully beginning next year. The SIS-100 is estimated to be able to achieve 20 eV in isochoric heating experiments [7]. The reason achievable target temperatures are expected to be similar between SIS-18 and NDCX-II-Ib, and between NDCX-II and SIS-100, despite the fact that the corresponding GSI beam pulse energies are almost 1000 X higher, is because the GSI ion ranges are also 1000 X longer than in the NDCX machine using lower energies where dE/dx peaks (see Fig. 1). SIS is intended to be a multi-user facility, so that the warm density matter group at GSI has to share the beam time, and this is also why they have to accept the constraints of the higher beam energies optimized for nuclear physics [7].

Contributions of NDC beam compression and focusing research to basic beam/plasma physics

A very important aspect of the ion driven HEDP and the heavy ion fusion program is its strong synergism with other areas of physics research with high discovery potential. Prominent among these areas of connection are: advanced nonlinear dynamics (collective interaction processes, chaos); high energy and nuclear physics (accelerator physics); non-equilibrium statistical mechanics of charged particle systems; nonneutral plasma physics (space-charge effects, theoretical techniques); magnetic fusion plasma physics (beam-plasma interactions, diagnostic techniques); advanced computing (algorithms, massively parallel computations); and atomic physics (ionization and stripping cross sections). Very importantly, the detailed theoretical and experimental investigations of the intense charged particle beams carried out in the ion-driven HEDP program contribute significantly to the foundations of accelerator physics that find applications in other areas of research, including high energy and nuclear physics. Areas of common scientific interest include: halo particle production and control; the effects of intense space-charge fields; electron cloud effects; the use of background plasma to focus intense ion beams; and beam manipulation and compression, to mention a few examples. The high space-charge fields associated with the intense ion beams encountered in ion driven HEDP and heavy ion fusion assure that the scientific challenges associated with collective excitations, electron cloud effects, beam-plasma interactions, etc., have high intellectual challenge and impact potential in other important areas of beam science research.

III. Opportunities to optimize targets, chambers and diagnostics for warm dense matter studies using moderate energy ion accelerators.

The interest in the warm dense matter regime arises because in dense plasmas the atoms and/or ions will start to behave in a manner that is intrinsically coupled to the plasma. That is, the plasma starts to exhibit long- and short-range order due to the correlating effects of the

atoms/ions. This intriguing regime where the plasma can no longer be considered a thermal bath and the atoms are no longer well described by their isolated atom behavior provides a tremendous challenge to researchers. In the limit of dense cool plasmas one obviously arrives at the threshold of condensed matter. Here the problem has changed from a perturbative approach to ground-state methods where complete renormalization of the atom/ion and its environment is essential.

From the perspective of plasma studies the defining quantity is the coupling parameter Γ , *i.e.*, the ratio of the inter-atomic potential energy to the thermal energy given by the equation:

$$\Gamma = \frac{Z^2 e^2}{r_0 k T} \quad \text{with } r_0 = \left(\frac{3Z}{4n_e} \right)^{1/3}$$

where Z is the ion charge and r_0 is the interparticle spacing given in terms of the electron density n_e .

The regions of interest span the density-temperature phase space going from modestly coupled ($\Gamma \leq 1$) to strongly coupled ($\Gamma > 1$), while bridging the transition regimes between solid to liquid to plasma.

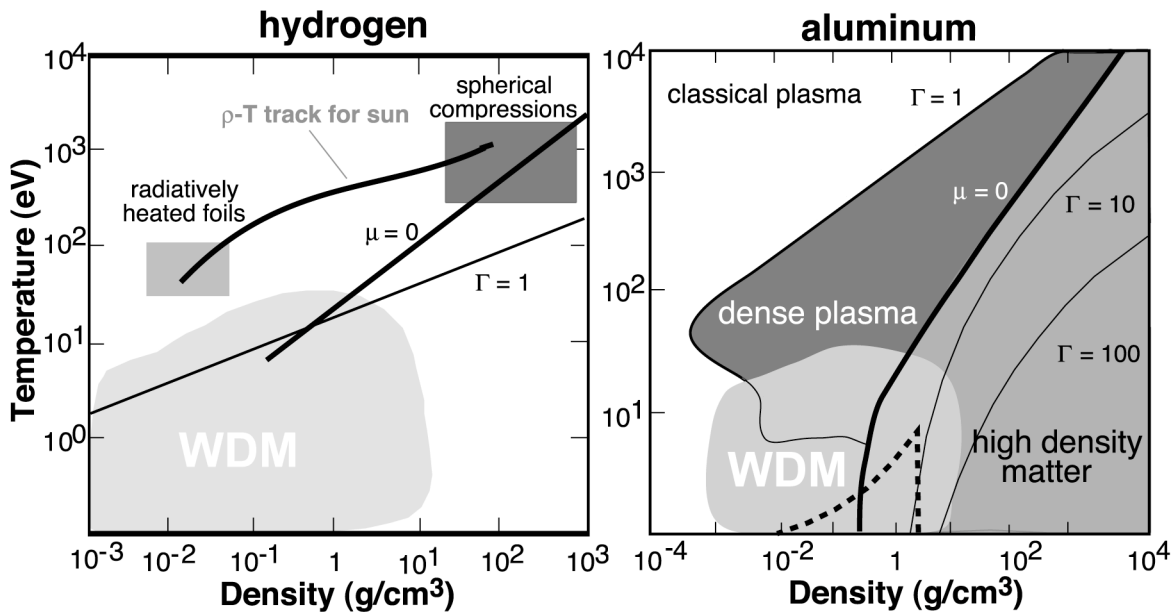


Figure 4. The temperature-density phase diagram for hydrogen on the left and aluminum on the right. The relevant regimes are noted, as are the various values of the coupling Γ . The regions of greatest uncertainty are roughly noted by the light gray areas. Also indicated is the region where degeneracy will become important: it is the region to the right of the line where the chemical potential $\mu = 0$. The hydrogen data is taken from a compilation of data from the NRL Plasma Formulary [22] while the aluminum data is derived from the QEOS formalism [23].

In figure 4 above we show the region of the temperature-density plane where warm dense matter studies are important. Here we show the temperature (T) in eV versus the density (ρ) in g/cm^3 both for hydrogen, a low Z element, and aluminum, a moderate Z element. The region where the theoretical uncertainties are largest are those where the standard theoretical approaches fail and

experiments are exceedingly difficult. The difficulty arises theoretically from the fact that this is a regime where there are no obvious expansion parameters, as the usual perturbation expansions in small parameters used in plasma phase theories are no longer valid. Further, there becomes an increased importance on density-dependent effects, *e.g.*, pressure ionization, as the surroundings starts to impinge on the internal structure of the ion or atom. Experimentally the study of warm dense matter is difficult, as the isolation of samples in this regime is complicated. Indeed, although the plasma evolution of *every* P - T path that starts from the solid phase goes through this regime and plays an important role in its evolution, trying to isolate warm dense matter remains a major challenge.

It has been exceedingly difficult to perform experiments in the warm dense matter regime, which is, simply, why we know so little about it. As a first step, one must create a well-characterized warm dense matter state; the second is to gain information on the state through experiments. The first step has been the problem: warm dense matter is not a limiting case of matter, *e.g.*, high- or low-temperature. When created in a laboratory environment, it does not tend to remain in a specified thermodynamic state for very long, making characterization difficult.

This WDM regime is accessed in all laboratory experiments where one creates a plasma from solid or near solid density targets; however, it is difficult to study this part of the plasma creation process in isolation. Rapid temporal variations, steep spatial gradients, and uncertain energy sources lead to indecipherable complexity. Indeed, although there has been much interest in this regime, witnessed by the literature on strongly coupled plasmas, there has been little progress. The interest generated in laboratory experiments is mirrored in the astrophysical literature where the warm dense matter regime is found, for example, in the structural formation of large planets and brown dwarfs. See ref. [13] for information on effects at 1 Mbar for hydrogen-bearing astrophysical objects; refs. [14-17], for information on Jovian planets; ref. [18] for extrasolar giant planets; refs. [19] and [20] for information on brown dwarfs; and ref. [21] for information on low mass stars.

The fact that the Heavy Ion beam source will allow the creation and probing of the warm dense matter regime in the laboratory, as discussed briefly below, will provide a set of data that will spark the field. The idea is simple but the impact may be vast, as the data obtained in the generation of the warm dense matter along an isochore, *i.e.*, a track of constant density, with subsequent probing along the release isentrope, *i.e.*, a track of constant entropy, will be unique and critically important for progress in the field. The importance of this data derives from the fact that to date the only possible method of generating warm dense matter is by shocking the material. The shock method provides information along the principal Hugoniot, that is, the locus of points in the pressure-density space that are accessed by a single shock – one point for each shock. Although this has been quite useful, it is a very limited set of data providing little information on the general behavior in the warm dense matter regime. Indeed, the amount of data that is currently available is so limited that one finds insufficient constraints on theoretical development. This can be illustrated by the curves in figure 2 where several predictions for an isochore of aluminum is presented in the temperature and pressure phase-space. Note that the four theories shown in the figure *all* predict theoretical Hugoniots that fit the experimentally determined Hugoniots, but all differ rather dramatically along the isochore. As aluminum is the most studied material, figure 2 can be interpreted as the minimum degree of uncertainty in this field of research and makes obvious the need for experimental data in this regime [24].

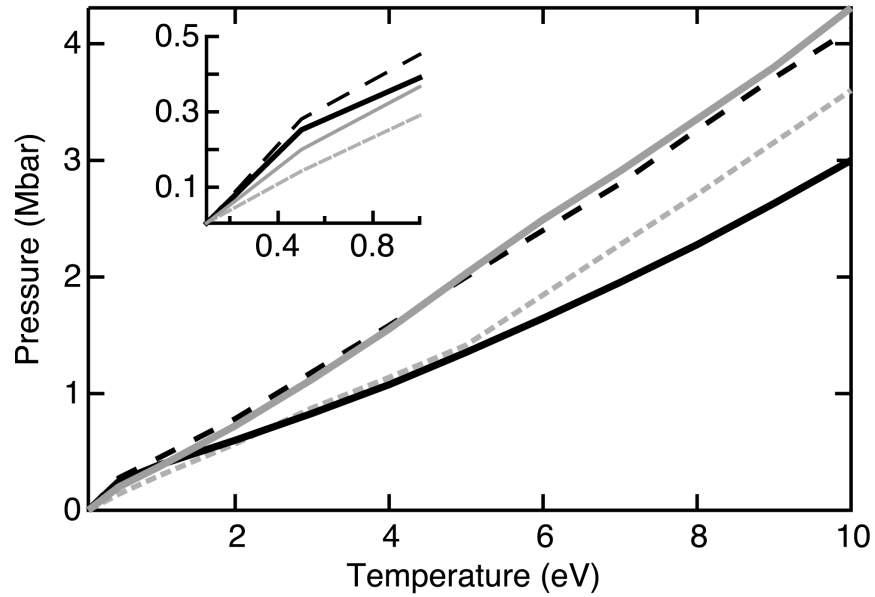


Figure 5. The isochore for aluminum in the warm dense matter regime for four theoretical models that all provide predictions consistent with the experimental points along the principal Hugoniot. The inset shows the low pressure low temperature region expanded. Data derived from heavy ion beam generated sources will assist in motivating theoretical developments for this important regime.

Further, one can illustrate the level of uncertainty in the equation of states by comparing models that are considered valid for simulations by virtue of the fact that where the data exist, i.e., along the principal Hugoniot, the models agree with experiment. In figure 6 we show two such examples. Here we have plot of the differences in the predicted pressure over a range of the temperature-density phase space that covers the warm dense matter regime for two elements, Al and Cu. The choice of Al and Cu is pertinent as these are two of the most studied materials for shock-generated equations of state. In figure 3 the first thing to note is that there are substantial region within the warm dense matter phase-space where differences $> 80\%$ in the pressure are common. Second, we note that there are regions where the differences between the models are quite small and these correspond to those areas where the principal Hugoniot measurements have provided data to guide the theoretical development. Another way of saying this is that the measurements are essential for guidance and, indeed, this is what the heavy ion beam experimental capability will provide.

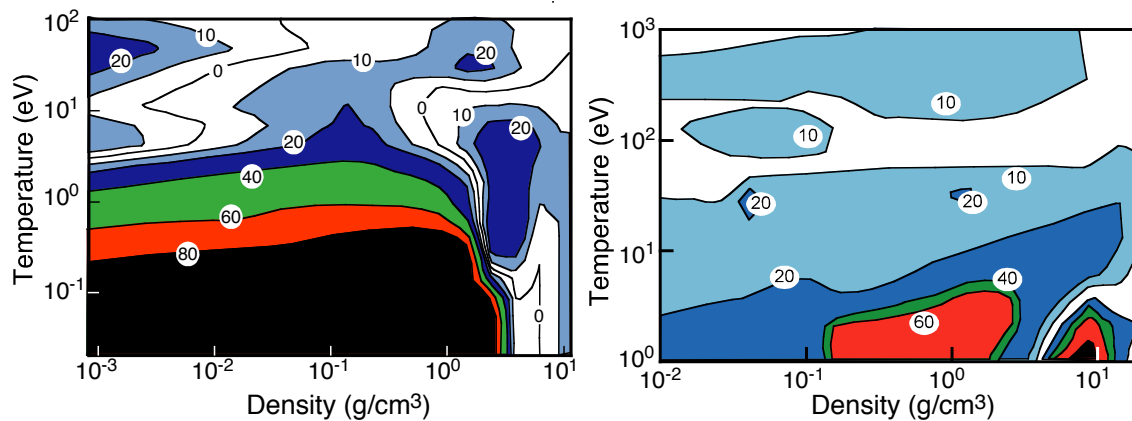


Figure 6. Comparison of the variation in pressure between two equations of state models commonly used, in the density-temperature phase space. Note that differences are greatest in the Warm Dense Matter regime.

Targets and experiments for WDM studies:

The design of the target will ultimately follow from the physics to be investigated. Some of the fundamental areas to be investigated include measurements of equation of state, thermal and electrical conductivity, and opacity. Other measurements will look at the transition of wire arrays or foams from the solid to the plasma state, examining the persistence of granularity and inhomogeneities in the system.

A number of types of measurements and diagnostics will be needed to obtain physical data on the state of the warm dense matter. These include:

1. Time dependent measurement of rarefaction waves and hydrodynamic expansion of the heated material, by imaging the emission.
2. Measurement of shock wave velocities, by imaging of emission and/or backlighting with x-rays, for those configurations in which shock waves are generated.
3. Measurement of the final charge state and energy of the ions after passing through the target. One can measure both total energy of the beam to determine the deposition and also the energy of the ions to further ensure that one understands the deposition mechanisms.
4. Measurement of the emission spectra of the heated target (in the WDM regime the temperatures are sufficiently low that at best VUV spectroscopy is needed – it is one of the charms of the regime that the medium is dense and there is little observable emission).
5. Measurement of the absorption spectra of the heated target being backlit by a laser-produced x-ray source.
6. Electrical resistivity measurements by applying a voltage across the target and observing the current response as the pulse is heated.

The targets themselves will have a variety of configurations. A simple planar target has been the basis for many of the calculations used for determining accelerator parameters. Typically,

focal spot radii will be of order 1 mm, and the range of medium mass ions in solid material in the few to tens of MeV energy range will be of order a few microns. So the aspect ratio of beam radius to target thickness will be ~ 100 to 1, (i.e the targets will be flat and planar). This is in contrast to the experiments at GSI, where much larger ion energies (~ 100 's of MeV/amu) are achieved with much lower currents ($\sim 10^{10}$ ions/bunch, ~ 200 ns pulse length), and so the target geometries tend to be long (~ 1 cm) and cylindrical relative to the radius of (~ 1 mm). The planar targets will tend to expand primarily longitudinally, in contrast to the predominantly radial expansion of cylindrical targets.

For lower density targets (ρ as low as 0.01 times solid density) for the same ion range the physical length is inversely proportional to ρ so for the few to tens of MeV ions, the range can be 100's of μ m up to a mm. In this case, the geometry of the heated region varies from thin up through the regime of near equality between longitudinal and transverse scales. Metal foams have been proposed for use on the National Ignition Facility (NIF) and for Inertial Fusion Energy (IFE) targets, so material testing of these components would be of benefit to both the Inertial Confinement Fusion (ICF) and IFE programs. Similarly, the evolution of wire arrays (as are being used on Sandia's Z-pinch machines) can be studied, and the transition from solid state to plasma state can be explored.

Other targets such as compressed gas targets, gas and liquid jets, and metal and other foams can be used to vary the density of the target over a wide range, so that a large fraction of the ρ - T plane can be explored using ion beam driven WDM.

The form of the experiments can be outlined simply. For example, the heavy ion beam can heat a sample isochorically. Then with measurements of the deposited energy, radiography of the heated volume, and *in situ* probes provided by high-energy laser generated x-rays one can determine the local volumetric expansion and temperatures. Thus the equation of state can be determined. Note in figure one that the area of phase space covered by a single experiment, although it maps out the points along the isentrope as expansion occurs, does not cover the entire space. Indeed, to cover the entire space one needs to make samples of less than solid density, e.g., underdense foams. In this manner one can span a large part of the interesting phase-space with changes of samples but with similar measurement techniques.

Finally, we note that although the experiment mentioned appears simple it is quite complex. First, the simultaneous measurement of a set of physical parameters in an experiment where all the data must be obtained on each shot necessitates the implementation of a number of diagnostics. This implementation, in turn, requires that the samples be constructed and have metrology performed to ensure that each diagnostic instrument (spectrometers, beam deposition, time resolved radiography, *in situ* scatter and/or absorption measurements) can obtain uncompromised data. This will, in turn, necessitate that shielding of the various components be ensured. Second, the accuracy required for equation of state measurements is highly dependent on the measurement of, for example, the expansion velocities that in turn is dependent on accurate distance versus time diagnostics. In those cases where one uses x-radiography to measure the expansion uniformity of the sample, alignment and diagnostic calibration (e.g., in a streak camera uncertainty in the sweep speed and its linearity) combine to make 10% accuracies difficult to attain. Third, the variation of the heavy ion beam focus, the variation in beam total energy, and the variation in the beam spectrum (here we mean velocity profile) requires that one have a series of reproducible experiments to evaluate a single data point in the EOS. Fourth, the need for reproducibility requires additional pulses. So repetition rates of order minutes or even

seconds will be needed to account for the experiment preparations, calibrations, and accelerator variability.

Estimating accelerator requirements

In order to set the requirements on an ion accelerator for heating a target to Warm Dense Matter conditions, an understanding of the scaling of the energy loss rate dE/dX is needed, where E is the ion energy and $X = \int dz$ is the integrated range of the ion. This quantity has been displayed graphically for a number of different ions, in ref [B1], and scaling to other target materials is also given.

For heating solid aluminum (at room temperature) over a range of ion mass from 4 amu (Helium) to 126 amu (Iodine), the energy loss at the peak of the dE/dX curve (dE/dX_{max}) may be parameterized approximately as:

$$(1/Z^2)dE/dX_{max} \approx 1.09 (\text{MeVcm}^2/\text{mg}) A^{-0.82} \quad (1)$$

where Z and A are the ion nuclear charge and atomic mass, respectively. Expressing dE/dX_{max} as a function of A only yields:

$$dE/dX_{max} \approx 0.35 (\text{MeVcm}^2/\text{mg}) A^{1.07}. \quad (2)$$

Thus, the peak energy loss rate increases (nearly linearly) with ion atomic mass.

Similarly, the energy at the peak increases with ion nearly quadratically with A :

$$E (\text{at } dE/dX_{max}) \approx 0.052 \text{ MeV } A^{1.803}. \quad (3)$$

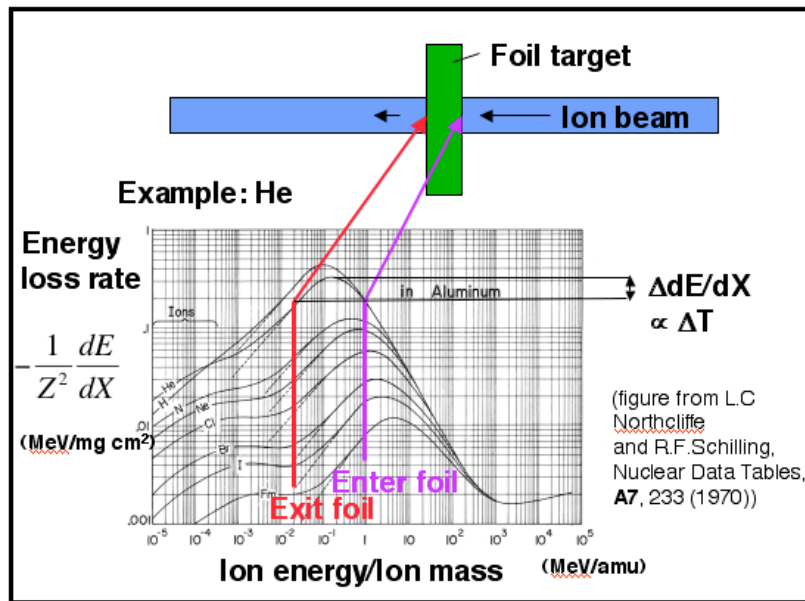


Figure 7. Temperature variations in an ion-beam heated foil can be minimized by choosing an ion and energy such that the peak in dE/dX occurs in the center of the foil (ref. [B2]).

Target uniformity is another important consideration. In ref. [6] it was pointed out that target temperature uniformity can be maximized in simple planar targets if the particle energy reaches the maximum in the energy loss rate dE/dX when the particle has reached the center of the foil (see figure 7). For any specified fractional deviation in target temperature (assuming the energy is deposited in a time short so that no hydrodynamic, radiative, or other cooling has occurred) one can determine the energy at which the ion must enter and exit the foil. From the dE/dX curves of ref. [26] we find that for the entrance and exit energies to have a 5% lower energy loss rate relative to the peak in dE/dX , $\Delta E/E \approx 1.2$, where ΔE is the difference in ion energy between entering and exiting the foil, and E is the energy at which dE/dX is maximum. Note the large (>1) fractional range in energy relative to peak energy is expected for a broad peak in a log-log representation. The spatial width of the foil Z , for a 5% temperature non-uniformity is then given by:

$$Z = \Delta E / (\Delta dE/dX) \approx 0.77 \rho_{al}^{-0.733} (A/\rho_{al}) \quad (4)$$

Here we have used $\rho_{al} = 2.7 \text{ g/cm}^3$ to convert the range into a physical distance. So by using materials of low density such as metallic foams, for example, the width of the foil can be large, which can be advantageous as will be shown. The total energy density U , calculated from the total energy deposited over the course of the pulse and neglecting losses is thus:

$$U = N_{ions} E / \rho_{al}^2 Z = 3.7 \times 10^9 \text{ (J/m}^3\text{)} (N_{ions}/10^{12}) (1 \text{ mm}/r)^2 (A/\rho_{al}) A^{1.07} \quad (5)$$

Here N_{ions} is the number of ions in the pulse, and r is the equivalent radius of the focal spot, defined such that the beam is assumed to have uniform density within r , and has zero intensity outside of r . So to achieve high energy density, large particle number, small spot radius, and higher target densities must be attained. In addition, to realize the energy density given by eq. (5), the hydrodynamic expansion timescale Z/c_s must be much shorter than the pulse duration Δt .

Hydrodynamic disassembly time:

The sound speed c_s is given by $c_s = (P/\rho)^{1/2} = (\gamma P/\rho)^{1/2}$. Here γ is the ratio of specific heats, P is the pressure and ρ is the mass density. For estimating purposes, we take γ to be 5/3, although more refined estimates below will relax this assumption. For a ‘‘shock tube,’’ that at a finite longitudinal distance z , has a discontinuous drop to zero pressure at some initial time, an analytical solution exists (ref. [27]; see fig. 8) in which a rarefaction wave propagates inward at speed c_s , and a plasma front flows outward at $2 c_s$. For the case of isochoric heating, when the pulse duration $\Delta t \ll \Delta z / c_s$, where Δz is the width of the foil, the dynamics will be the same as the shock tube solution. For times $\Delta t \sim \Delta z / c_s$, we expect that, since the sound speed is increasing over the course of the pulse, the position of the rarefaction wave z_r will be somewhat less than would be expected if calculated on the basis of the final heated plasma:

$$z_r = \int_0^{\Delta t} c_s dt = \frac{2}{3} c_{s*} \Delta t \left(\frac{\Delta t}{\Delta t} \right)^{3/2}. \quad (6)$$

Here $c_{s*} = c_s(T_*)$ and we assume $\frac{T}{T_*} = \frac{t}{\Delta t}$, where T_* is the temperature achieved at the end of the ion pulse; we also assume $c_s \propto T^{1/2}$.

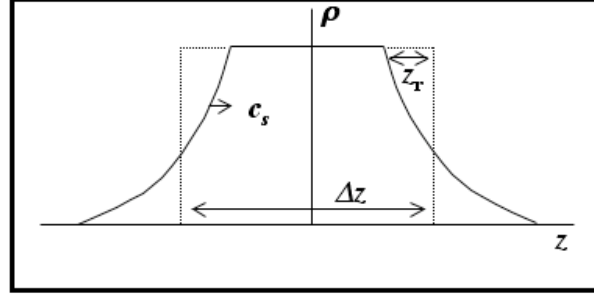


Figure 8. Schematic representation of rarefaction wave propagating inward at sound speed c_s , and plasma front moving outward at speed c_s . As material is heated over course of pulse c_s increases. The original density distribution of the foil is indicated by dotted line, and location of the rarefaction wave by z_r .

We envision isochorically heating a target foil, and taking measurements with various optical or beam diagnostics. If our diagnostic is unable to resolve a volume smaller than the volume heated by the ion beam, and if we want to distinguish equations of state with 5% accuracy, then the sample volume cannot consist mostly of blow off material (i.e. material that is part of the rarefaction wave). If we demand that the blow off material is less than 5% of the total mass, that implies $2z_r/\Delta z < 0.05$, or

$$\Delta t < 3\Delta z/(80 c_s^*). \quad (7)$$

If on the other hand, the diagnostic has resolution z_{\min} such that it can sample a fraction of the target ($z_{\min} < \Delta z$), then, as long as the central part of the target has not been "contaminated" by the rarefaction wave, useful data can be obtained by just observing the central (heated) part of the foil. In this latter case, the pulse duration must satisfy

$$\Delta t < 3(\Delta z - z_{\min})/(4 c_s^*). \quad (8)$$

If $\Delta z \gg z_{\min}$, this can be a significantly longer time, but in any case, the longer of the two timescales above (eq. 7 and eq. 8) should be taken. For our examples to be discussed below, we have used z_{\min} to be 40 μ , which may be achievable using a K- α diagnostic generated by a short pulse laser.

In order to calculate more accurately the sound speed, one needs to understand the response of the target to the energy deposited by the ion beam. In particular, the pressure and temperature will depend on the ionization state of the plasma. For our estimating purposes, we use a model developed by Zeldovich and Raizer and summarized in ref. [28]. The basic idea of the model is to calculate the average ionization state Z^* by approximately solving the Saha equation and accounting for the ionization energy of each ion in the energy density U (where $U = (3/2)nkT + Q(Z^*)\rho/Am_h$), and to include contributions to the pressure P (where $P = nkT = kT(Z^* + 1)\rho/Am_h$) from the electrons and partially ionized target atoms. Here $Q(Z^*) = \sum_{i=1}^{Z^*} I_i$, where I_i is the (known) ionization energy of the i^{th} level of the target material, n is the total number density of ions, atoms, and electrons, and ρ is the mass density. Other more detailed equation of state models, including degenerate effects, correlation effects, and more exact treatment of the Saha equation, may have an impact on various transport and thermodynamic properties. These details are not to be minimized; after all that is why there is an experimental interest in this regime. For our purposes, however, the Zelodovich-Raizer equation of state allows approximate calculation of Z^* (see fig. 9), T , and the coupling parameter Γ_{ii} .

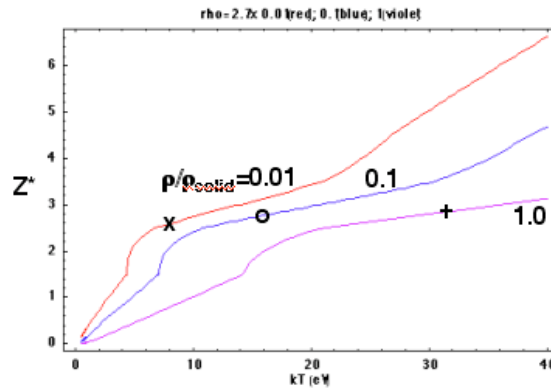


Figure 9. Calculation of ionization state, as a function of temperature for three different densities, using Zeldovich-Raizer equation of state. The x, o, and + would correspond to the conditions of reached in accelerator described by the central column of each of the 1%, 10%, and 100% solid density cases in Table 2.

Examples of accelerator requirements:

Using the model described in the previous section for ion beam stopping, the time scale for hydrodynamic expansion and the equation of state we are able to make estimates of the required beam parameters for exploring the Warm Dense Matter regime. Tables 2 and 3 give examples of requirements for two different ion energy and mass, Neon⁺¹ ($A=20.17$) at foil entrance energy (E_{\max}) of 19 MeV, and Chlorine⁺¹ ($A=35.453$) at $E_{\max}=52.4$ MeV. The energy at the center of the foil (E_{center}) and the energy at the exit of the foil (E_{\min}) are listed in the captions to the tables. For each ion, three different mass densities of Aluminum target are given: Solid density (2.7 g/cm^3) and 10% and 1% of solid, which can be produced by making an aluminum "foam." In turn for each target density, three target temperatures are shown. Both tables are based on a minimum diagnosable length scale Z_{\min} of 40λ . It is clear from the tables that solid density, although resulting in the highest energy density, requires vary short pulse durations, because the foil width is smaller than Z_{\min} and so only a small rarefaction wave propagation distance is allowed. But for the 1% and 10% cases, the foil is larger than Z_{\min} , so that the rarefaction wave propagation distance can be 10's or 100's of microns, with concomitantly longer pulse duration times. In all cases the plasma temperature is in the few to tens of eV, and the required number of particles is in the order of 10^{12} to 10^{13} particles, for equivalent focal spot radii of 1 mm.

$\rho(\text{g/cm}^3)(\% \text{solid})$	0.027 (1%)			0.27 (10%)			2.7 (100%)		
Foil length (m)	700			70			7		
kT (eV)	3.5	7.9	15	4.5	15	20	7.1	31	38
Z^*	1.2	2.6	3.1	0.95	2.7	3	0.69	2.8	3.1
$\square_{\text{li}}=Z^{*2}e^2n_i^{1/3}/kT$	0.51	1	0.92	0.53	1.3	1.2	0.38	1.5	1.4
$N_{\text{ions}}/(r_{\text{spot}}/1\text{mm})^2 / 10^{12}$	2.24	7.96	22.4	2.24	14	22.4	2.24	22.4	30
$\square t$ (ns)	56	30	18	2.5	1	0.8	0.03	0.01	0.008
$U (\text{J/m}^3)/10^{11}$	0.021	0.073	0.21	0.21	1.27	2.1	2.1	21	28

Table 2. Neon beam: $Z=10$, $A=20.17$, $E_{\min}=4.4$ MeV, $E_{\text{center}}=11.7$ MeV, $E_{\max}=19$ MeV, and $\square z_{\min}=40 \lambda$

ρ (g/cm ³)(%solid)	0.027 (1%)			0.27 (10%)			2.7 (100%)		
Foil length (m)	1050			105			10.5		
kT (eV)	3.5	7.9	15	4.6	15	20	7.1	31	38
Z*	1.2	2.6	3.1	0.96	2.7	3	0.69	2.8	3.1
$\rho_{li}=Z^*e^2n_i^{1/3}/kT$	0.51	1	0.76	0.53	1.3	1.1	0.38	1.5	1.4
$N_{ions}/(r_{spot}/1mm)^2 /10^{12}$	1.24	4.3	12.4	1.24	8	12.4	1.24	12.4	16
ρt (ns)	87	46	27	5.6	2.2	1.8	0.045	0.014	0.012
U (J/m ³)/10 ¹¹	0.021	0.073	0.21	0.21	1.35	2.1	2.1	21	28

Table 3. Chlorine beam: $Z=17$, $A=35.453$, $E_{min}=12.3$ MeV, $E_{center}=32.4$ MeV, $E_{max}=52.4$ MeV, and $\rho_{Zmin}=40$.

Tolerance on Velocity Spread:

Several different types of accelerators are being considered to produce the very short (<~ ns) pulses required for HEDP studies. But one common thread in all of the approaches, has been the need to invoke neutralized drift compression, to overcome the limit imposed by space-charge. Neutralized drift compression is a departure from the more traditional approach of non-neutral drift compression that allows the longitudinal space charge to cause the beam velocity to "stagnate," thereby removing the velocity tilt, just as the beam is passing through the final focusing magnets, thus minimizing any potential chromatic aberrations that arise in the final focusing process. Using neutralized drift compressions achieves shorter pulses, but the various longitudinal parts of the beam that have different longitudinal velocities maintain those velocities through to the end, including the final focus. So, not only do the final focusing optics have to be tolerant of velocity spread, but target heating uniformity must be maintained as different parts of the beam (with different longitudinal velocities) will have different stopping powers (dE/dX) and which in principal lead to a temperature variation larger than that of a single particle near the Bragg peak.

To investigate the effect of velocity spread we integrated the dE/dX curves of ref. [26]. As an example we investigated the evolution of a He ion beam propagating through 1 μ foil of aluminum (see figs. 10 and 11). To represent the effect of a velocity spread we chose a number of different ion energies and averaged the energy loss rate at each point in the foil (corresponding to a energy distribution that is uniform between an lower and upper energy cutoff), and then calculated the maximum change in energy loss rate and normalized to the average energy loss rate in the foil ($= \Delta T/T$). In the 1 μ foil case, for Helium with energy centered about 0.8 MeV and with zero energy spread, there was a 1.8% fractional spread in dE/dX through the foil. (So $\Delta T/T=0.018$ for this example, and is defined as the difference between the maximum and minimum energy loss rate divided by the average energy loss rate). As we increased the energy spread of the He beam, the calculated $\Delta T/T$ did not significantly increase until the velocity spread $\Delta v_{spread}/v=(1/2)\Delta E_{spread}/E$ is of order the fractional energy change of a single particle through the foil $\Delta E_{single_particle}/E$. Here ΔE_{spread} is the half width of the uniform particle distribution in energy and Δv_{spread} is the corresponding velocity spread. The general conclusion, would appear to be that if $\Delta E_{spread} \ll \Delta E_{single_particle}$ then there is no appreciable degradation of the uniformity. On the other hand, there does not appear to be a significant advantage in a small but finite energy spread. Both statements need to be verified over a broad range of foil thickness and particle energy spreads, and the dependence on particle distribution function needs to be explored. If confirmed the temperature uniformity variations in the target may not be the most severe

limitation to the allowed energy spread from velocity tilt, but more likely final optics considerations.

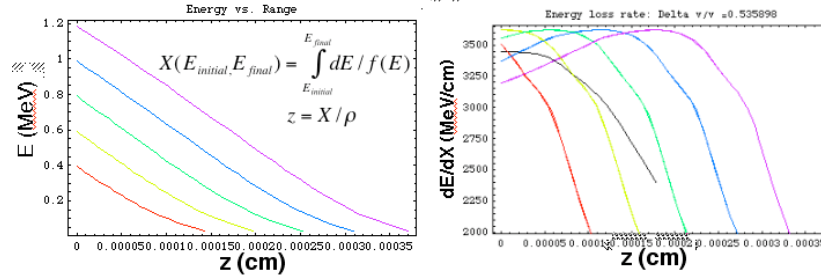


Figure 10. Energy vs. distance and dE/dX vs distance, for a He ion propagating in cold aluminum, for five different energies ranging from 0.4 to 1.2 MeV. The black curve in the right hand figure is the average of the five colored curves and represents the total average energy loss rate for an ion distribution function that is uniform in energy.

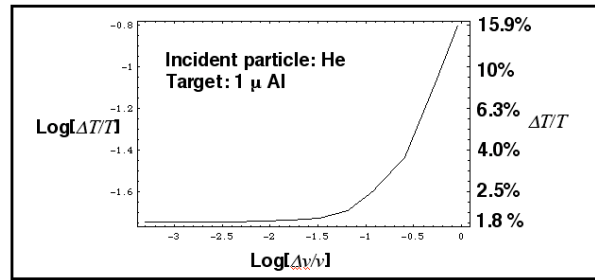


Figure 11. Temperature uniformity vs. velocity spread, for a He beam with central energy 0.8 MeV, propagating through a 1 μ cold aluminum foil.

Not only do HEDP experiments require uniform deposition but they also require high intensity, which means both short pulse and small beam radius. We may make simple estimates for the contribution to the spot size from chromatic effects (i.e. for the effects of a velocity spread) from a number of optical systems. For example, for a "thick" solenoidal lens in which a beam enters a solenoid with zero convergence angle and focuses to a spot within the solenoid, it can be shown to have a radius from emittance and chromatic effects r_{spot} to be approximately:

$$r_{\text{spot}}^2 \approx \left(\frac{f}{2}\right)^2 \left(\frac{\Delta v_{\text{spread}}}{v}\right)^2 + \left(\frac{2f}{r_0}\right)^2 \quad (9)$$

where r_0 is the radius of the beam at the entrance to the solenoid, f is the focal length, i.e., the distance from the entrance of the solenoid to the focal spot, and f is the beam emittance. The quantity r_{spot} is minimum when $r_0^2 = (2/f) \epsilon / (\Delta v_{\text{spread}}/v)$ and has the value

$$r_{\text{spot}}^2 = 2f \epsilon \Delta v_{\text{spread}}/v \quad (10)$$

At minimum pulse duration the velocity tilt is converted to a velocity spread, so achieving high beam intensity will limit the velocity tilt. A system which is less sensitive to velocity tilt has also been proposed, such as the adiabatic plasma lens, but the dynamic range of these types of lens are generally limited to a reduction in spot size to a factor of around 2 or less, so these will most

likely be used as a final "after burner" optic, with the bulk of the focusing being carried out by a conventional, solenoid optic, for which equations (9) and (10) provide limits.

IV. Conclusions

Accelerator-produced heavy ion beams offer unique capabilities to drive matter to the densities and temperatures known as the High Energy Density Physics regime (and particularly that part of the parameter space known as the Warm Dense Matter regime). Considerations of the precise control and uniformity of energy deposition, relatively large sample sizes, a benign diagnostic environment, high shot rates with multiple beamlines, and the possibility of easy access by a broad range of investigators all point to a useful and unique role for heavy ion accelerators to play in exploring the physics of this regime. Further, a plan of near term accelerator research studying a new method of reaching high intensity, i.e. neutralized drift compression followed by neutralized focusing, is the enabling physics that would lead to a user facility within a 10-year timescale. We are beginning to lay the ground work for the optimization of such a facility, by considering a range of options (ion mass and energy, acceleration method, target and diagnostic configurations). This work has just begun but it is our conviction that the scientific discovery potential of such a facility would be high, and if the facility were built it could be the "spark" that ignites the field.

Acknowledgements

The authors would like to thank Dick Briggs, Debbie Callahan, Chris Celata, Andy Faltens, Alex Friedman, Larry Grisham, Enrique Henestroza, Ed Lee, Jay Marx, Lou Reginato, Dave Rose, Andy Sessler, John Staples, Max Tabak, Will Waldron, Dale Welch, Jonathan Wurtele, Simon Yu for their ideas, discussions, calculations and simulations that have contributed to our current understanding of ion-driven HEDP.

References

1. M Turner, et.al., *Connecting Quarks with the Cosmos: Eleven Science Questions for The New Century* (National Academies Press, 2003).
2. R. C. Davidson, et. al., *Frontiers in High Energy Density Physics - The X-Games of Contemporary Science* (National Academies Press, 2003).
3. *The Science and Applications of Ultrafast, Ultraintense Lasers: Opportunities in Science and Technology Using the Brightest Light Known to Man* (Report on the SAUUL Workshop, June 17-19, 2002).
4. R. C. Davidson, et. al., *Frontiers for Discovery in High Energy Density Physics*, (prepared by the National Task Force on High Energy Density Physics July 7, 2004)
5. *An Integrated High Energy Density Physics Program at LBNL Based in the Office of Science* LBNL White Paper sent by LBNL Director Charles Shanks to DOE Science Director Ray Orbach September 1, 2003
6. L. R. Grisham, *Moderate Energy Ions for High Energy Density Physics Experiments*, Physics of Plasmas, in press (2004).
7. D. Varentsov, editor, "Studies on High Energy Density Matter with Intense Heavy Ion and Laser Beams a GSI" (HEDgeHOB), a white paper on proposed collaboration in warm dense matter research at GSI April 13, 2004

8. "Implementing Agreement between the Department of Energy of the United States of America and the Federal Ministry of Education and Research of the Federal Republic of Germany on Collaboration in the Field of Dense Plasma Physics" (DOE Office of Fusion Energy Science, September 2001)
9. S.S. Yu, et al., Nuclear Instruments and Methods in Physics Research A, in press (2004).
10. D.R. Welch, et al., Nuclear Instruments and Methods in Physics Research A, in press (2004).
11. M. Leitner, et al., Nuclear Instruments and Methods in Physics Research A, in press (2004).
12. N. Tahir, et al., Nuclear Instruments and Methods in Physics Research A, in press (2004).
13. Van Horn, H. M. (1991). *Science* **252**, 384-389.
14. Smoluchowski, R. (1967). *Nature* **215**, 691-695.
15. Hubbard, W. B. (1981). *Science* **214**, 145-149.
16. Chabrier, G., Saumon, D. Hubbard, W. B. & Lunine, J. I. (1992). *Ap. J.* **391**, 817-826.
17. Nellis, W. J., Ross, M. & Holmes, N. C. (1995). *Science* **269**, 1249-1252.

18. Saumon, D., Hubbard, W. B., Burrows, A., Guillot, T., Lunine, J. I. & G. Chabrier (1996) *Ap. J.* **460**, 993-1018.
19. Saumon, D., Hubbard, W. B., Chabrier, G. & Van Horn, H. M. (1992). *Ap. J.* **391**, 827-831.

20. Hubbard, W. B., Guillot, T., Lunine, J. I., Burrows, A., Saumon, D., Marley, M. S. & Freedman, R. S. (1997). *Phys. Plasmas* **4**, 2011-2015.
21. Chabrier, G. & Baraffe, I. (1997). *Astron. Astrophys.* **327**, 1039-1053
22. Huba, J. D. (2000). *NRL Plasma Formulary* (Office of Naval Research. Washington. DC) <http://wwwppd.nrl.navy.mil/nrlformulary/nrlformulary.html>.
23. More, R. M., Warren, K.H., Young, D.A. & Zimmerman, G.B. (1988). *Phys. Fluids*, **31**, 3059-3078.
24. Rogers, F. J. & Young, D. A. (1997). *Phys. Rev. E* **56**, 5876-5883.
25. Rogers, F. J. (2000). *Phys. of Plasmas* **7**, 51-5.
26. I.C. Northcliffe and R. F. Schilling, "Range and Stopping Power Tables for Heavy Ions," Nuclear Data Tables, **A7** 233-463 (1970).
27. L.D. Landau and E.M. Lifshitz, Fluid Mechanics, [Pergamon Press, Oxford], Chapter 10, Section 92, problem 2. (1959).
28. R. J. Harrach and F.J. Rogers, *J. Appl. Phys.* **52**, 5592 (1981).

3.2 Heavy-Ion-Driven High Energy Density Physics and Fusion

Accelerators producing appropriately tailored energies of intense heavy ion beams can provide a useful tool for creating uniform high energy density matter to study the strongly-coupled plasma physics of warm dense matter in the near term, and for inertial fusion in the longer term. Both fusion and high energy density physics applications of heavy ion beams require understanding the fundamental physics limits to the compression of ion beams in both space and time before they reach the target, as well as a basic understanding of collective beam-plasma interaction processes and beam energy deposition profiles within the dense plasma targets. This thrust area focuses on the beam and target physics knowledge base needed over the next ten years for future heavy ion beam applications to high energy density physics and fusion. The emphasis during the first five years is on determining the physics limits to heavy ion beam longitudinal compression and transverse focusing upstream of the target, and during the second five year period, an increased effort is planned for beam-target interaction physics and target diagnostic development for high energy density physics. This heavy ion high energy density physics thrust would also make significant contributions towards heavy-ion-driven inertial fusion.

3.2.1 Motivating Intellectual Question

How can heavy ion beams be compressed to the high intensities required for creating high energy density matter and fusion ignition conditions?

Heavy ion beams have a number of advantages as drivers of targets for high energy density physics and fusion. First, heavy ions have a range exceeding the mean-free-path of thermal x-rays, so that they can penetrate and deposit most of their energy deep inside the targets. Second, the range of heavy ion beams in dense plasma targets is determined primarily by Coulomb collisions with the target electrons. The ions slow down with minimal side-scattering, and their energy deposition has a pronounced peak in the rate of energy loss dE/dx that increases with the beam ion charge state Z . These properties make heavy ions an excellent candidate for high energy density physics studies, where thin target plasmas would be uniformly heated by locating the deposition peak near the target center. The primary scientific challenge in exploiting these desirable properties in the creation of high energy density matter and fusion ignition conditions in the laboratory is to compress the beam in time (by 1000 times overall, requiring 10-100 times more longitudinal bunch compression than present state-of-the-art) to a pulse length that is short compared to the target disassembly time, while also compressing the beam in the transverse direction (by 10 times) to a small focal spot size for high local deposition energy density. Proposed new experiments compressing intense ion beams within neutralizing plasma would significantly extend the beam current into high-intensity regimes where the beam would not otherwise propagate in the absence of background plasma, and where beam-plasma collective effects with longitudinal and azimuthal magnetic focusing fields have not been previously explored.

A basic understanding of the collective processes and nonlinear dynamics of intense, high-brightness, heavy ion beams, and a determination of how best to create, accelerate, transport, compress and focus these beams to a small spot size are critical to achieving the scientific objectives of heavy ion fusion and ion-beam-driven studies of warm dense matter. Most of the kinetic energy of heavy-ion beams is in the directed motion of the beam particles, but a small fraction is in random kinetic energy, characterized by the effective temperature of the beam particles. Plasma electrons can be used to neutralize much of the repulsive space charge that resists the beam compression in time and space, but the beam temperature ultimately limits the smallest achievable spot size and pulse duration after the space charge forces are removed from the beam inside plasmas. To minimize the beam temperature, and thereby maximize the energy deposition in the target, the beam dynamics must be controlled with high precision throughout the entire dynamical trajectory, using accurately positioned and tuned confining magnets, carefully tailored accelerating fields, and final charge neutralization techniques that do not degrade the beam quality.

There are key synergistic relationships of the research on intense heavy ion beams to understanding the nonlinear dynamics of intense charged particle beams for high energy and nuclear physics applications, including minimization of the deleterious effects of collective processes such as the two-stream (electron cloud) instability, and the use of a charge-neutralizing background plasma to assist in focusing intense beams to a small focal spot size (plasma lens effect).

3.2.2 Research Opportunities

Target and Accelerator Requirements: A recent sub-panel of the Fusion Energy Sciences Advisory Committee [1] reports *“Inertial fusion energy capabilities [laser, accelerator and z-pinch drivers for fusion energy] have the potential for significantly contributing to high energy density physics and other areas of science. For example, isochoric heating of substantial volumes to uniform, elevated temperatures should be achievable using heavy ion beams...Moreover, the rapid turnaround capabilities envisioned for inertial fusion energy drivers could accelerate progress in HEDP science by enabling a wide community of users to conduct “shot-on-demand” experiments with data rates and volumes far exceeding those obtained on large systems that currently require long times between shots.”* As indicated by the scientific question and supporting narrative for heavy-ion-driven high energy density physics and fusion, the primary scientific challenge is to compress intense ion beams in time and space sufficiently to heat targets to the desired temperatures with pulse durations of order or less than the target hydrodynamic expansion time. For low energy ions (in the few to tens of MeV range), requirements to study strongly-coupled plasma properties in the warm dense matter regime are: target foils of thickness a few to tens of microns, 1 to 20 Joules (in a single beam), 0.5 to 10 eV temperature, 0.2 to 2 nanosecond final pulse duration, and 0.5 to 2 mm-diameter focal spot size. Target diagnostics for high energy density physics studies should have spatial resolution small compared to the focal spot size, temporal resolution small compared to the target hydrodynamic expansion time after heating, and energy deposition measurement accuracy better than 3%. For x-ray production in inside indirect-drive fusion targets, ion beams must heat foam layers 1-100% that of solid-density with 50 to 200 kJ per beam (many beams), 200 eV target radiation temperature, 5 to 10 nanosecond final pulse duration, and 4 to 10 mm-diameter focal spot size. For high energy density physics studies, ranges of ions with 0.2 to 1 MeV/u should be larger than the target thickness, with the deposition peak centered in the target

in order to achieve maximum uniformity inside the target for accurate measurements of the heated plasma properties, and to allow analysis of transmitted ion energies and charge states as a diagnostic. Hydrodynamic codes with a capability for calculating energy deposition from a distribution of incident ion energies and angles should evaluate changes in observable target properties for different equation-of-state models. For fusion, radiation transport is a key additional target code capability that is required. Ion ranges with 10 to 20 MeV/u should be less than the target radiator thickness, but larger than the mean free path of the target x-rays so that the peak ion deposition can occur inside the radiation case (hohlraum) surrounding the fusion fuel capsule.

The minimum pulse length and focal spot radius depend on the final longitudinal and transverse effective temperatures, respectively, accumulated from all non-ideal effects experienced by the ion beam as it travels from the source through the accelerator, and through longitudinal compression and final focus onto the target. Accelerators for both high energy density physics and fusion must initially inject sufficiently bright (low temperature) beams, accelerate the heavy ions to the desired energy range, and then longitudinally compress and radially focus the beams onto the target with minimal growth in the longitudinal beam temperature (much less than a factor of 10 to allow overall axial bunch compression by a factor of 100 or more), and with minimum transverse temperature growth (much less than a factor of 10 to allow radial focusing by more than a factor of 10).

Scientific Objectives and Milestones: Advances over the past several years include: (i) high current ion sources and injectors (0.1 to 1 A of potassium) have been shown to have adequate initial beam brightness (sufficiently low transverse and parallel temperatures) to meet the above requirements at injection; (ii) negligible beam brightness degradation has been observed in transport of 200 mA potassium ion beams through electric quadrupole focusing magnets; and (iii) more than 95% of potassium beam space charge has been neutralized with pre-formed plasma over ~ 1 meter lengths without deleterious beam-plasma instabilities. Over the next five years, before beam-on-target experiments begin, the research will address the key remaining beam physics issues necessary to meet the accelerator requirements described above. These fall into four scientific areas:

- (1) ***High brightness heavy ion beam transport*** in magnets, particularly to understand limits on beam-channel wall clearance (aperture fill) imposed by gas and electron cloud effects, together with beam matching and magnet non-linearities.
- (2) ***Longitudinal compression of intense ion beams***, particularly to understand limits on longitudinal compression within neutralizing background plasma, and the effects of potential beam-plasma instabilities over distances longer than 1 meter.
- (3) ***Transverse focusing onto targets***, particularly to understand limits on focal spot size set by chromatic aberrations due to uncompensated velocity spreads from upstream longitudinal compression, and beam temperature growth from imperfect charge neutralization.
- (4) ***Advanced beam theory and simulation***, particularly developing, optimizing and validating multi-species beam transport codes that can predict self-consistently the beam loss with gas and electron clouds, and developing integrated beam simulation models required to analyze source-to-target beam brightness (temperature) evolution.

After the beam physics issues identified above are favorably addressed over the next five years, emphasis will be placed on the fifth scientific thrust area:

- (5) **Beam-target interactions**, particularly to understand beam deposition profiles within thin foil targets and the potential uniformity of isochoric heating, accounting for target and beam ion charge state conditions, including development of accurate beam deposition and laser-generated x-ray target diagnostics, and extension of integrated beam simulation models from source *through* target.

These scientific areas will be pursued with an overall 10-year objective of providing the beam and target physics knowledge base for a future ~\$50M-class heavy-ion accelerator-based high energy density physics facility for achieving 1-10 eV solid-density plasmas by isochoric ion heating with uniformity and diagnostic resolution adequate to discriminate the predictions of various *ab initio* theories for strongly-coupled plasmas. Successful achievement of this objective will address the Office of Management and Budget/Office of Fusion Energy Sciences 10-year measure for inertial fusion energy/high energy density physics: “*With the help of experimentally validated theoretical and computer models, determine the physics limits that constrain the use of inertial fusion energy drivers in future key integrated experiments needed to resolve the scientific issues for inertial fusion energy and high energy density physics*”. In addition, such an accelerator-driven high energy density physics facility would represent an important step towards the long-term objective of heavy-ion-driven inertial fusion.

Research Tools, Facility Requirements, and Milestones: Several specific facility requirements with intermediate two-year and five-year milestones (for experiments and modeling) are required to measure progress towards the 10-year objective. These include:

Two-Year Science Goals (FY06):

A2: Intermediate experiments to assess the physics limits of neutralized ion beam compression to short pulses. Measure the parallel and transverse temperature of a high perveance ion beam (space-charge potential / kinetic energy larger than 10^4) before and after longitudinal compression by a factor of ten in neutralizing background plasma, and before and after pre-bunching of initially non-neutral ion beam in an acceleration-deceleration system. This series of experiments and modeling is needed to design integrated experiments combining neutralized drift compression and final focusing.

B2: Intermediate experiments to develop a predictive capability for gas and electron effects. Compare measured and calculated effects of gas and electron clouds on beam temperature as a function of beam aperture fill factors initially in transport lines with four magnets (quadrupoles and solenoids). This series of experiments and modeling will provide the scientific basis for future experimental upgrades.

Five-Year Science Goals (FY09):

A5: Integrated beam experiments on neutralized compression and focusing onto targets. Compare the measured and simulated focal spot beam intensity profiles in integrated experiments with beam current and energy upgraded from that used in A2, with a goal of 1 eV temperature in targets (a temperature corresponding to the high energy density threshold level of 10^{11} J/m³ at solid density). This series of experiments and modeling of compression and

focusing will provide the physics basis for a future heavy-ion high energy density physics facility.

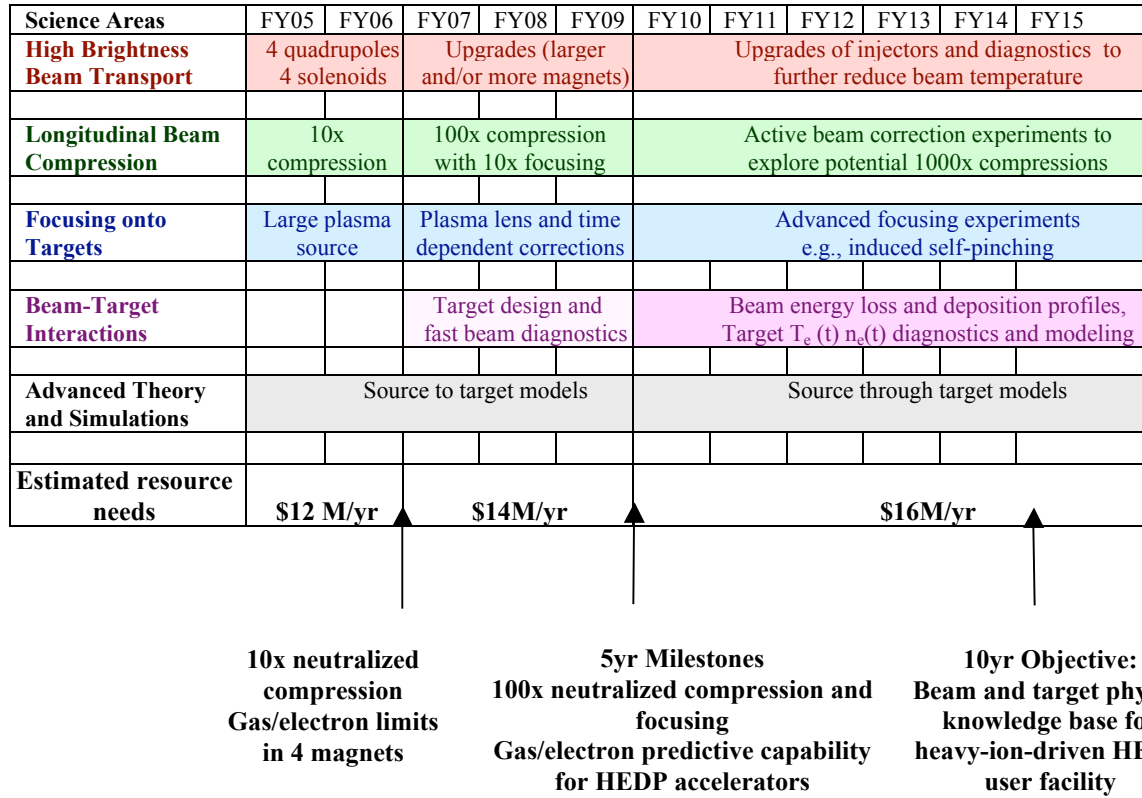
B5: Demonstrate predictive capability for gas and electron effects for a heavy-ion high energy density physics facility. Compare measured and calculated effects of gas and electron clouds, in combination with beam matching and magnet errors, assuming B2 results warrant an upgrade to longer lattice transport experiments. This series of experiments and modeling is essential to determine the magnet apertures of quadrupole and solenoid transport options for a future heavy-ion high energy density physics facility.

Figure 3.1 gives a timeline with milestones and resource requirements.

Opportunities for Interagency Cooperation: Several opportunities exist for scientific cooperation between the heavy-ion-driven high energy density physics/fusion thrust area sponsored by the Office of Fusion Energy Sciences (OFES) and other federal agencies. These include:

1. Office of Basic Energy Sciences (OBES), with the Spallation Neutron Source (SNS) at the Oak Ridge National Laboratory, in common areas of need for data on wall secondary electron production and gas desorption induced by beam loss [2], and in multi-species particle-in-cell simulation models of the impact of gas and electron clouds on the beam, including two stream instabilities [3, 4]. This area may be critical to the achievement of full average beam power and neutron production in the SNS.
2. National Nuclear Security Agency (NNSA), with the Proton Storage Ring (PSR) and Dual Axis Radiographic Hydro Test facility (DARHT) at the Los Alamos National Laboratory [3, 4], in common areas of modeling multi-species gas/electron effects including two-stream instabilities (PSR), and in efficient computational techniques with multi-species modeling of electron beam neutralization from gas and ions backstreaming from the targets (DARHT).
3. Collaborations with the high energy and nuclear physics accelerator communities on joint development of advanced computational tools are important to predict and control electron cloud effects, beam halo production and associated losses, including use of Adaptive Mesh Refinement techniques [5] and nonlinear perturbative (□f) particle simulation techniques [3] developed for modeling heavy ion experiments. Sharing these computational tools can greatly increase the range of intense beam physics problems that can be modeled for a variety of scientific applications.
4. Within strongly-coupled plasma regimes of high energy density physics, scientific progress would benefit from comparisons of equation of state and constitutive properties data obtained using heavy ion isochoric heating with similar data obtained using other future high energy density physics drivers, including lasers, Z-pinches, and X-ray free electron lasers (XFELs)[6].

Figure 3.1: Timeline and Resource Requirements for Heavy-Ion Driven HEDP/fusion



References

[1] "A Review of the Inertial Fusion Energy Program" Final Report to FESAC, March 29, 2004
 [2] A.W. Molvik, et al., "Electron effects in intense, ion beam linacs theory and experimental planning for HCX", to be published in *Laser and Particle Beam* **20** (4), 2002.
 [3] H. Qin, E. A. Startsev and R. C. Davidson, "Nonlinear Perturbative Particle Simulation Studies of the Electron-Proton Two-Stream Instability in High-Intensity Proton Beams", *Phys. Rev. Special Topics on Accelerators and Beams* **6**, 014401 (2003).
 [4] T.-S. Wang, P. J. Channell, R. J. Macek and R. C. Davidson, "Centroid Theory of Transverse Electron-Proton Two-Stream Instability in a Long Proton Bunch" *Phys. Rev. Special Topics Accelerators and Beams* **6**, 014204 (03).
 [5] J. L. Vay, et. al.. "Mesh Refinement for Particle-In-Cell Plasma Simulations: applications to and benefits for Heavy Ion Fusion, to be published in Proc. of 14th Int. Symp. Heavy Ion Inertial Fusion. (Laser and Particle Beams).
 [6] *Frontiers in High Energy Density Physic -The X-Games of Contemporary Science* (Nat Academies Press, 2003).

Agenda: Workshop on
Accelerator Driven High Energy Density Physics
Held October 26-29, 2004
Lawrence Berkeley National Laboratory

Tuesday, October 26, 2004 (Building 71 Conference Room)

8:30 Coffee and donuts

9:00 Welcome, Logistics, and Working Group Membership -- Ed Lee

9:20 Motivation -- Grant Logan

9:50 Experiments, Science, and User Requirements -- Dick Lee
(35 min talk + 5 min discussion)

10:30 Coffee Break

10:50 Accelerator and Final Requirements -- John Barnard
(25 min talk + 5 min discussion)

11:20 Source Issues -- Joe Kwan (25 min talk + 5 min discussion)

12:00 Lunch at meeting place

1:00 rf - status and working group plan -- John Staples
(35 min talk + 5 min discussion)

1:40 multi-gap accelerator - status and working group plan -- Dick Briggs
(35 min talk + 5 min discussion)

2:20 single-gap accelerator - status and working group plan -- Craig Olson/
Paul Ottinger (35 min talk + 5 min discussion)

3:00 Coffee Break

3:20 Final focus/drift compression concepts -- Ed Lee
(35 min talk + 5 min discussion)

4:00 Initial working group break out meetings

5:30 End of day

Wednesday, October 27, 2004

9:00 Working group meetings

10:30 Coffee break/intergroup discussions

11:00 Resume working group meetings

12:00 Lunch/intergroup discussions

1:00 Resume working group meetings

3:30 Coffee break/intergroup discussions

4:00 Status report: Experiments

4:15 Status report: rf

4:30 Status report: multi-gap

4:45 Status report: single-gap

5:00 Status report: final focus/drift comp

5:15 End of Day

Thursday, October 28, 2004

9:00 Working group meetings

10:40 Coffee break/intergroup discussions

11:00 Resume working group meetings

12:00 Lunch

1:00 Resume working group meetings

3:30 Coffee break/intergroup discussions

4:00 Resume working group meetings

5:30 End of day

Friday, October 29, 2004

9:00 "Overview of the National Task Force Review on High Energy Density Physics"-- Ron Davidson

9:40 Status report/assignments: Experiments

10:10 Status report/assignments: rf

10:40 Coffee break

11:00 Status report/assignments: multi-gap

11:30 Status report/assignments: single-gap

12:00 Status report/assignments: final focus/drift comp

12:30 Final discussion

1:00 Meeting ends/ lunch on your own

**Attendees List for HEDP Workshop
October 2004**

Last Name	First Name	Group Number	Institution	Email
Albritton	James	1	LLNL	albritton1@llnl.gov
Alonso	Jose	1,2	LBNL	JRAlonso@lbl.gov
Bailey	David	1	LLNL	dsb@icf.llnl.gov
Bangerter	Roger	2,3	LBNL	robangerter@lbl.gov
Barnard	John	1, 4	LLNL	jjbarnard@lbl.gov
Bernal	Santiago	3	Maryland	sabern@umd.edu
Bieniosek	Frank	1,2,3,4	LBNL	fbieniosek@lbl.gov
Birdsall	Ned	3	UCB	birdsall@eecs.berkeley.edu
Briggs	Dick	3	SAIC	richard.j.briggs@saic.com
Callahan	Debbie	1	LLNL	callahan1@llnl.gov
Caporaso	George	1,3	LLNL	caporaso1@llnl.gov
Celata	Christine	1,2,3,4	LBNL	cmcelata@lbl.gov
Chen	Yu-Jiuan	3, 4	LLNL	jychen@llnl.gov
Chou	Wieren	2	Fermi	chou@fnal.gov
Corlett	John	2	LBNL	JNCorlett@lbl.gov
Cowan	Tom	1	U. Nevada	cowan@physics.unr.edu
Davidson	Ron	1,2,3,4	PPPL	rdavidson@pppl.gov
Esarey	Eric	1	LBNL	EHEsarey@lbl.gov
Falcone	Roger	-	UCB	rwf@physics.berkeley.edu
Faltens	Andy	3	LBNL	A_Faltens@lbl.gov
Fawley	Bill	1,4	LBNL	WMFawley@lbl.gov
Friedman	Alex	3	LLNL	friedman1@llnl.gov
Gough	Rick	-	LBNL	RAGough@lbl.gov
Grisham	Larry	1	PPPL	lgrisham@pppl.gov
Grote	Dave	3	LLNL	grote1@llnl.gov
Hammel	Bruce	1	LLNL	hammel1@llnl.gov
Herrmannsfeldt	Bill	1,2,3,4	SLAC	wbhap@slac.stanford.edu
Kaganovich	Igor	4	PPPL	ikaganov@pppl.gov
Keller	Rod	2,3	LBNL	r_keller@lbl.gov
Kwan	Joe	2,3	LBNL	jwkwan@lbl.gov
Lambertson	Glen	2	LBNL	grlambertson@lbl.gov
Lee	Edward	4	LBNL	eplee@lbl.gov
Lee	Dick	1	UBC	lee32@llnl.gov
Leemans	Wim	1	LBNL	wpleemans@lbl.gov
Leitner	Matthaeus	1,2,3,4	LBNL	mleitner@lbl.gov
Libby	Steve	1	LLNL	libby1@llnl.gov
Logan	Grant	1,2,3,4	LBNL	bglogan@lbl.gov
Lund	Steve	3	LLNL	lund3@llnl.gov
Marx	Jay	1,2,3,4	LBNL	jnmarx@lbl.gov
Meier	Wayne	-	LLNL	meier5@llnl.gov
More	Dick	1	LLNL	more@nifs.ac.jp
Olson	Craig	3	Sandia	clolson@sandia.gov
Ostroumov	Peter	2	ANL	ostroumov@phy.anl.gov
Ottinger	Paul	3	Naval Research	ottinger@suzie.nrl.navy.mil
Penn	Greg	1,2		gpenn@socrates.berkeley.edu
Qin	Hong	4	PPPL	hqin@pppl.gov
Raparia	Deepak	2, 4	BNL	raparia@bnl.gov
Reginato	Lou	3	LBNL	lreginato@lbl.gov

**Attendees List for HEDP Workshop
October 2004**

Renk	Tim	3	Sandia	tjrenk@sandia.gov
Roy	Prabir	4	LBL	pkroy@lbl.gov
Schoessow	Paul	4	Tech X Corp	pvsetxcorp.com
Sharp	Bill	4	LBL	wmsharp@ll.gov
Seidl	Peter	3	LBL	paseidl@lbl.gov
Sessler	Andy	2	LBL	amsessler@lbl.gov
Staples	John	2 (2 chair)	LBL	jwstaples@lbl.gov
Stoltz	Peter	1	tech-x	pstoltz@txcorp.com
Tabak	Max	1	LLNL	tabak1@llnl.gov
Thio	Francis	1,2,3,4	DOE	francis.thio@science.doe.gov
Yu	Simon	4	LBL	ssyu@lbl.gov
Vay	Jean-Luc	4	LBL	jlvay@lbl.gov
Waldron	Will	3	LBL	wwaldron@lbl.gov
Welch	Dale	4	MRC	drwelch@mrcabq.com
Wurtele	Jonathan	1,2	LBL	jswurtele@lbl.gov
Zholents	Sasha	2	LBL	aazholents@lbl.gov
Westenskow	Glen	2,3	LLNL	westenskow1@llnl.gov
Vanacek	Sam			chvanecek@lbl.gov
Groups	1= experiments / diagnostics	2= rf acceleration		
	3= pulsed power acceleration (multi-gap and diode)	4= final focus / compression		

Recent studies of the possibility of Warm Dense Matter (WDM)/High Energy Density Physics (HEDP) science driven by ion accelerators have indicated that relatively large regions with homogeneous conditions can be created in a target by using ions at the Bragg peak. The ion driver and focusing system must supply a beam that is sufficiently compressed in time and space to achieve the required intensity and with a sufficient uniformity and sufficiently small velocity spread to assure a target with minimal variations in temperature and density. These goals are challenging, but do not seem unobtainable. The workshop will examine three concepts already under consideration and consider the requirements for an integrated scientific exploration of HEDP using such a driver.

The broad objectives of this workshop are to:

1. Explore options and possibilities for a staged experimental program in WDM/HEDP that utilizes ion accelerator sources as they become available, from early machines that can be developed at modest cost beginning with existing equipment, to later machines that reach well into the HEDP regime. Define physics regimes and scientific objectives to be explored, requirements for targets and diagnostics, and the scientific program that can be carried out using the ion beam drivers under consideration.
2. Study various approaches, including conceptual designs of three types of accelerators: pulse-power-driven single-stage diodes; pulse-power-driven multi-stage accelerators; and rf-accelerators. In addition, study options for pulse compression and final focus.

Important issues to be considered in developing a program for ion driven HEDP science are:

- Precise control and uniformity of energy deposition;
- Large sample sizes compared to diagnostic resolution volumes;
- A benign environment for diagnostics (low debris and radiation background);
- High shot rates (10/hour to 1/second) and multiple beamlines/target chambers;
- Sites with easy access for broad participation by university scientists and students; and with the technical support for designing and fielding targets for qualified experiments.
- Low cost
- State of technological readiness

As a starting point we will aim for target characteristics that fall within a broad range in temperature and density, (these properties are to be defined

more precisely by the HEDP experiments working group): Temperature between 0.1 and 30 eV, density between 10^{-3} to 30 g/cm^3 .

The temperature must be constant over a hydrodynamic expansion time, and the volume must be sufficiently large to be able to diagnose the state of the properties with minimal ($< \sim 5\%$) variations over the volume being diagnosed. Additionally, the energy deposition over the volume must result in similarly small ($< 5\%$) variation in the volume being diagnosed. As a specific example, consider a Ne+1 beam, entering a 70 micron thick Aluminum foam target (mass density $\rho = 0.1$ solid density), with ion central energy entering the foam at 19 MeV, and exiting at 4.4 MeV. The combination $N_{\text{ions}} / (r_{\text{spot}} / 1 \text{ mm})^2 > 1.4 \cdot 10^{13}$, where N_{ions} is the number of ions in the pulse and r_{spot} is the equivalent pulse radius if the intensity were uniformly distributed over a circle of radius equal to r_{spot} . If the pulse duration is less than 1 ns, this should result in a 15 eV plasma, with mean ionization state of 2.7, and mean energy density $1.3 \cdot 10^{11} \text{ J/m}^3$.

